ELECTROCHEMICAL ASSESSMENT AND SERVICE-LIFE PREDICTION OF MECHANICALLY STABILIZED EARTH WALLS BACKFILLED WITH CRUSHED CONCRETE AND RECYCLED ASPHALT PAVEMENT

A Thesis

by

MICHAEL WATTS ESFELLER, JR.

Submitted to the Office of Graduate Studies of
Texas A&M University
in partial fulfillment of the requirements for the degree of

MASTER OF SCIENCE

August 2006

Major Subject: Civil Engineering

ELECTROCHEMICAL ASSESSMENT AND SERVICE-LIFE PREDICTION OF MECHANICALLY STABILIZED EARTH WALLS BACKFILLED WITH CRUSHED CONCRETE AND RECYCLED ASPHALT PAVEMENT

A Thesis

by

MICHAEL WATTS ESFELLER, JR.

Submitted to the Office of Graduate Studies of
Texas A&M University
in partial fulfillment of the requirements for the degree of

MASTER OF SCIENCE

Approved by:

Chair of Committee,	David Trejo
Committee Members,	Daren B.H. Cline
	Richard B. Griffin
	Ken Reinschmidt
Head of Department,	David V. Rosowsky

August 2006

Major Subject: Civil Engineering

ABSTRACT

Electrochemical Assessment and Service-life Prediction of
Mechanically Stabilized Earth Walls
Backfilled with Crushed Concrete and Recycled Asphalt Pavement.
(August 2006)
Michael Watts Esfeller Jr., B.S., University of South Alabama
Chair of Advisory Committee: Dr. David Trejo

A Mechanically Stabilized Earth (MSE) wall is a vertical grade separation that uses earth reinforcement extending laterally from the wall to take advantage of earth pressure to reduce the required design strength of the wall. MSE wall systems are often prefabricated to reduce construction time, thus improving constructability when compared with conventionally cast-in-place reinforced wall systems. However, there is a lack of knowledge for predicting the service-life of MSE retaining wall systems when recycled backfill materials such as Recycled Asphalt Pavement (RAP) and Crushed Concrete (CC) are used instead of Conventional Fill Material (CFM). The specific knowledge missing is how these recycled materials, when used as backfill in MSE wall systems, affects the corrosion rate of the reinforcing strips. This work addresses this knowledge gap by providing recommendations for MSE wall systems backfilled with CC or RAP, and provides a guide to predict the service-life based on corrosion rate test data obtained from embedding steel and galvanized-steel earth reinforcing strips embedded in MSE wall systems backfilled with CC, RAP, and CFM. Experimental data from samples emulating MSE wall systems with steel and galvanized-steel reinforcing strips embedded in CC and RAP were compared to samples with strips embedded in CFM. The results of the testing provide data and methodologies that may, depending on the environmental exposure conditions, justify the use of RAP and CC for the construction of MSE walls. If these backfill materials are obtained from the construction site, this could provide a significant cost savings during construction.

DEDICATION

The author dedicates this thesis to his wife Emilie Evans Esfeller whose love, patience, and constant support have been extraordinary.

Most of all *Deo gratias*.

ACKNOWLEDGEMENTS

The author takes this opportunity to acknowledge the guidance, sponsorship, and academic leadership provided by Dr. David Trejo. The support provided by committee members Dr. Daren B.H. Cline, Dr. Richard B. Griffin, and Dr. Ken Reinschmidt are appreciated.

The sponsorship of research project 0-4177 by the Texas Department of Transportation (TxDOT) is gratefully acknowledged. Special thanks to the TxDOT 0-4177 project team members: Dr. David Trejo, Dr. Ellen M. Rathje, Dr. Alan F. Rauch, Dr. Kevin J. Folliard, Dr. Dallas Little, Moses A. Ogolla, and Chirayus Viyanant.

The help and friendship of those who performed research under the guidance of Dr. Trejo with the author is greatly appreciated, especially Radhakrishna Pillai Gopalakrishnan, Dr. Ceki Halmen, and Dr. Francisco Aguiniga. The assistance of Scott Cronauer, Materials Lab Coordinator and Mike Linger, Geotechnical Lab Coordinator were especially valuable to the research effort.

The encouragement of Kirk Powell while the author was writing was very beneficial. The assistance of Tony Vasquez with detailing to produce the views and section details of the forms for the long-term tesing is appreciated.

The author cherishes the guidance and financial aid provided by his parents Michael W. Esfeller, Sr. and Patricia W. Esfeller. The steadfastness required for execution and completion originated from the prime example of work ethic provided by the author's father. Encouragement from the author's brother David W. Esfeller and other family members is appreciated.

TABLE OF CONTENTS

Page

Page

Page

Page

LIST OF FIGURES

Page

Page

Page

Page

LIST OF TABLES

Page

Page

Page

1. INTRODUCTION

1.1 PROBLEM STATEMENT

The use of recycled materials such as Crushed Concrete (CC) and Recycled Asphalt Pavement (RAP) has become an increasingly important issue in society. One possible use for CC and RAP is for backfill of mechanically stabilized earth (MSE) walls. The appropriateness of CC and RAP as backfill for MSE walls depends on long-term corrosion performance of these systems. Service-life prediction methods specifically for MSE walls are currently being developed, and the particular influence of using recycled materials as backfill instead of a Conventional Fill Material (CFM) such as quarried stone for MSE walls has not been studied. A determination of the effect of CC and RAP on the service-life of MSE walls would enable engineers to make judgments on the appropriateness of using these materials instead of CFM for these walls.

1.1.1 Recycled Materials as an Alternative Backfill

Transportation infrastructure upgrades are more prevalent today than new construction. Due to this prevalence, it is not uncommon that contractors accumulate materials from the demolition of roadways, such as CC and RAP. Finding appropriate uses for these recycled materials as backfill can be economically advantageous for State Highway Agencies (SHAs). The use of CC and RAP materials may result in a cost savings in the case that these materials are competitively priced and provide similar or longer service-life than MSE walls backfilled with CFM. The use of recycled materials onsite as a replacement for CFM backfill also has the potential to reduce construction costs because the recycled material would not have to be hauled offsite and select backfill materials would not have to be hauled to the job site.

This thesis follows the style of *ASCE Journal of Materials in Civil Engineering*.

1.1.2 Recycled Backfill Materials Use for MSE Walls

The use of recycled materials as backfill for retaining walls is being explored by SHAs. One popular method of building retaining walls uses the concept of MSE walls. A MSE wall is a vertical grade separation that uses earth reinforcement extending laterally from the wall to take advantage of earth pressure to reduce the required design strength of the wall. MSE wall systems are often prefabricated to reduce construction time, thus improving constructability when compared with conventionally cast-in-place reinforced wall systems. The precast panels that make-up the facing units of the MSE wall system also allow for many types of finished surfaces that are aesthetically pleasing, making these systems appealing. MSE walls can be used to reinforce the earth that supports a ramp approach to a bridge that serves as an overpass. These wall types are often designed and constructed for highway overpasses where the right-of-way space is limited. Major highways and limited right-of-way space is most frequently encountered in urban landscapes. In urban landscapes, it is possible that recycled materials will be competitive with CFM for MSE walls because extensive urban development often signifies depleted aggregate supplies. Also, the source of the recycled materials, existing roadways, are often near the area where MSE walls are built. This combination of factors can make recycled materials a more viable backfill alternative for SHAs, particularly for MSE walls.

1.1.2.1 Challenges

There are challenges with using recycled materials as backfill for MSE walls. Defining the service-life of MSE walls backfilled with recycled materials is a difficult challenge for SHAs. Currently, it is difficult to predict the service-life of MSE walls due to the limited historical data available on these systems. Frondistou-Yannas (1985) reported that MSE walls were first introduced in the United States in 1969 and removed from the Federal Highway Administration experimental status in 1974. It is important that the service-life of an MSE wall be predicted based on the type of backfill material,

reinforcing strip type, environment, and other conditions. The challenge to predict the service-life of MSE walls is complicated further when recycled backfill materials are used. It is difficult to predict the behavior of recycled materials because they are more difficult to characterize and classify than conventional aggregates. CC and RAP are made of an agglomeration of several different materials. More than one type of aggregate is often used in concrete and asphalt mixtures. The challenge of estimating service-life is also difficult because there is limited infrastructure built using recycled materials and studies on the performance of systems containing these materials are scarce. Specifically, the influence of using recycled materials instead of CFM for MSE walls has not been thoroughly investigated. Service-life prediction methods specifically for MSE wall systems are just recently being developed.

1.1.3 Service-life and Life-cycle Costing of MSE Walls Backfilled with Recycled Backfill Materials

The issue of using recycled materials as backfill has impacts on the domain of service-life and life-cycle cost. Life-cycle cost is the cost associated with original construction, maintenance, and repairs until the structure has reached the end of its service-life and requires replacement. Examination of the life-cycle cost is important because it can be used to establish optimal repair and replacement plans. Life-cycle cost cannot be properly estimated for MSE walls without knowing the service-life. Therefore, it is necessary to determine how recycled backfill materials affect the service-life of MSE walls. Once a service-life estimation procedure for MSE walls backfilled with recycled materials versus MSE walls backfilled with CFM is developed, SHAs can use this procedure to determine the cost-effectiveness of using recycled backfill for MSE walls.

1.2 THESIS ORGANIZATION

This thesis is comprised of six sections. Section 1 introduces the challenges associated with using recycled backfill materials for MSE walls.

Section 2 focuses on the challenges introduced in Section 1, formulates these challenges as specific problems, and provides background information on these problems through literature review.

Section 3 states the research objective and significance, provides justification for the experimental design, and describes the experimentation procedures in detail.

Section 4 presents the results of the experimentation to provide an assessment of backfill corrosivity. The prominence of backfill corrosivity indicators based on the experimentation is presented. The results are based on a statistical analysis of the collected experimental data.

Section 5 presents backfill corrosivity and service-life estimation results. Current industry service-life models are used with the collected experimental data as input. The results from the service-life models are then presented and discussed.

Section 6 presents a summary of the research and provides conclusions and recommendations for future research.

2. BACKGROUND AND PROBLEM DESCRIPTION

2.1 MSE WALL SYSTEMS

MSE wall systems are structural composites and consist of four elements (Elias 1990, Frondistou-Yannas 1985):

- reinforcing elements,
- connections between facing units and reinforcing elements,
- facing units, and
- select granular backfill.

MSE wall systems are often employed to construct vertical or steep slopes. MSE wall systems were first introduced to construct road embankments in France, and were first introduced in the United States in 1969 (Frondistou-Yannas 1985). Before MSE walls, conventional retaining wall systems were typically rigid concrete, such as cantilever and gravity retaining wall systems. The rigid wall systems confined the soil and resisted the forces acting on the wall. MSE wall systems use reinforcing elements to strengthen the soil and reduce the forces acting on the wall face. The reinforcing elements develop a tensile strength in the backfill from the frictional forces developed along the length of the reinforcing elements (Frondistou-Yannas 1985).

MSE wall systems can provide an initial cost savings of 20 to 60 percent compared to conventional rigid walls (Morris and Delphia 1999). In addition to the initial cost savings, MSE walls have the following advantages when compared to conventional systems: use of prefabricated wall units, relative ease of construction, high load carrying capacity, little site preparation, and aesthetically pleasing appearances (Morris and Delphia 1999).

Several types of reinforcing elements can be used for MSE walls: metallic strips, metal grids or mesh, nonmetallic strips, or nonmetallic geogrid (Morris and Delphia 1999). This thesis focuses on the service-life of MSE walls reinforced with metallic reinforcing strips.

2.2 MSE WALLS AND CORROSION

2.2.1 Metallic Reinforcing Strip Corrosion

The predominant factor that causes MSE wall failure, resulting in service-life reduction, is the corrosion of the metallic reinforcing strips (Elias 1990). With regard to metal structures such as reinforcement, the service-life can be defined as "the time it takes for corrosion to reduce metal thickness to a point where a metal structure no longer has the mechanical strength needed to continue the service for which it is designed" (Tait 1994). As such, the potential effect of using recycled backfill materials on the corrosion of MSE wall reinforcing strips needs to be researched.

2.2.2 High Chloride Ion Concentrations and Corrosion

Salting of roadways and bridge decks with sand/salt mixtures occurs in many parts of the United States when de-icing and anti-icing applications are required. High chloride concentrations often exist in backfills adjacent to roadways that have been frequently salted. Frondistou-Yannas (1985) identified a gap in the existing knowledge of the corrosion susceptibility of internally reinforced soil retaining structures when he found that data are lacking on the effect of high chloride concentrations on the corrosion of metal reinforcement typically used in MSE walls. Chloride and sulfate ions have been associated with high corrosivity (Rabeler 1989). The suggested limits for the presence of these two ions in the backfill are 100 ppm and 200 ppm for chlorides and sulfates respectively (Elias 1990).

Chloride concentration may be of greater concern in the case of recycled backfill materials than CFM because the previous application of the recycled backfill material may have been exposed to these corrosive ions. High chloride contents could exist in the recycled CC, depending on the service and location of the concrete structure from which the CC was obtained. For example, if the recycled CC to be used as backfill was previously used as concrete pavement on a bridge or adjoining a bridge in a region

exposed to freezing, the CC is likely to have elevated chloride concentrations. The pavement in the region exposed to freezing often requires salting during its service-life. The applied salt can become soluble when the ice melts, and chlorides can be transported into the concrete pavement. Similar transport of chlorides can also occur in RAP. The likelihood of the presence of chloride ions in recycled materials is often greater than that of CFM because the recycled materials often come from a structure that requires repair or replacement due to accelerated deterioration. Many of these structures required repair or replacement due to corrosion degradation resulting from chloride ion ingress. Thus, the affect of high chloride concentrations on the corrosion of reinforcement commonly used in MSE walls needs further study.

2.3 BACKFILL CORROSIVITY

Backfill material for MSE walls should have the following characteristics: be easily compacted, be free draining, have high frictional strength, have low creep susceptibility, and have low corrosiveness (Morris and Delphia 1999). The interaction of the backfill material with the reinforcement should not promote corrosion of the reinforcement. Morris and Delphia (1999) recommended that the following soil tests be required for backfill for MSE retaining wall systems:

- Sampling,
- Grain Size Distribution,
- Atterberg Limits,
- Classification,
- pH,
- Resistivity,
- Relative Density, and
- In-Place Density.

The following soil tests are listed as optional for identifying problem backfill soils for MSE walls (Morris and Delphia 1999):

- Shear Strength,
- Permeability,
- Collapse Potential, and
- Specific Gravity.

Another soil test that should be required for backfill for MSE walls is the determination of chloride, sulfate, and sulfide concentrations. Chloride ions, sulfate ions, and sulfide ions have been identified as promoting corrosion (Romanoff 1957) and are important elements in determining backfill corrosivity (Elias 1990). Elias (1990) groups chloride, sulfate, and sulfide under the term of soluble salts with other salts such as carbonate. Carbonate forms a scale on most metals and can act as a corrosion inhibitor (Elias 1990). The soluble salts noted with the most significant impact on the corrosion of metallic reinforcement in soils are chloride ions, sulfate ions, and sulfide ions (Elias 1990).

The oxidation-reduction (redox) potential of a soil can also provide information on the type of corrosion mechanism, i.e., aerobic or anaerobic (Elias 1990). Other countries such as the United Kingdom and Germany use the soil redox potential as one of the test criterion for the suitability of select backfill material used in conjunction with galvanized-steel earth reinforcement (Elias 1990).

The particle shape and surface characteristics of soil should also be studied because along with the grain size distribution, this information can provide an indication of the aeration level in a backfill material. Aeration affects the corrosion mechanism by creating aerobic or anaerobic conditions. The defining particle shape and surface properties are form, angularity, and texture. Each of these defining shapes and surface characteristics can be classified on a scale proposed by Al-Rousan et al. (2005). Morris and Delphia (1999) obtained results that indicate that particle shape is an important factor in the compaction of cohesionless soils. Their results indicated that the maximum dry unit weight increases with increasing roundness, while the grading of soil was shown to play a minor role in determining the compaction of cohesionless soils (Morris and

Delphia 1999). The compaction of a soil is defined as the elimination of air voids between the soil particles. Compaction directly affects aeration. Therefore, it is important to measure the particle shapes and surface characteristics and not just the grain size distribution.

The proportion of organic materials should also be measured because microbes can produce organic acids that can cause pitting corrosion of the metallic earth reinforcement (Elias 1990). If the organic material is unevenly distributed throughout the backfill material, pockets of soil can become anaerobic due to sulphate-reducing bacteria, resulting in severe pitting corrosion (Elias 1990).

There is a possibility that some types of recycled backfill materials do not promote corrosion of the metallic reinforcement, yet these materials are prohibited by the current specifications for MSE wall backfill. CC is crushed concrete that has been acquired from the demolition of a concrete structure. Concrete is a mixture of aggregate, cement, and water. Concrete typically has a high pH because of the calcium hydroxide in the hydrated cement paste. As the pH of the environment increases above approximately 10, the corrosion rate of iron decreases (Whitecavage 1990). Therefore, iron reinforcing strips embedded in CC could have a lower corrosion rate than reinforcing strips embedded in CFM or RAP under the same exposure conditions. Popova et. al. (1998) found that cement stabilized backfill or CC do not adversely effect backfill corrosivity toward steel and galvanized-steel reinforcement, compared to conventional backfill, if the cement concentration is 8 percent or higher.

2.3.1 Corrosivity Factors

Corrosion is a major concern for MSE walls incorporating metallic reinforcement. Accelerated or unanticipated corrosion of the metallic reinforcements could cause sudden and catastrophic failure of MSE structures, generally along a potential failure line of maximum tensile stresses in the reinforcements (Elias 1997). Backfill characteristics play a large role in the corrosion of metallic reinforcement or grids. A number of factors can influence the corrosion rate of embedded metal in soils. Due to the synergistic

effects of the various factors on corrosion, backfill materials must be well characterized to estimate the corrosion activity of embedded metal reinforcement. Some of the factors associated with the soil environment that have been reported to affect corrosion of metal elements embedded in soil include:

- Resistivity
- Texture
- pH
- Moisture content
- Water hardness
- Dissolved oxygen
- Soluble salts
- Organic content
- Redox potential
- Differential environment

Some of these above factors are often used as indicators for the corrosivity of backfill material. Backfill material for MSE walls is often restricted by specifications. Specifications for MSE wall backfill used in different countries for galvanized-steel reinforcement are shown in Table 2.1 (Elias 1990). Morris and Delphia (1999) proposed revisions to TxDOT specifications for MSE wall backfill, as shown in Table 2.2.

Table 2.1. Parameter Limits Imposed by Different Countries for Select Backfills Used in Conjunction with Galvanized-steel Earth Reinforcement (Elias 1990).

Property	U.S. FHWA	France	United Kingdom	Germany
Resistivity (ohm-cm)	> 3000	> 1000 dry, > 3000 wet	> 5000	> 3000
pH	> 5 & < 10	> 5 & < 10	> 6 & < 10	> 5 & < 9
Chloride Content (ppm)	< 200	< 200 dry, < 100 wet	< 500	< 50
Sulfate Content (ppm)	< 1000	< 500 dry, < 1000 wet	< 500	< 500
Sulfide Content (ppm)	---	< 300 dry, < 100 wet	---	---
Organic Content (ppm)	---	100 ppm	---	---
Biochemical Oxygen Need	---	Minimal	---	---
Redox Potential (+ mV)	---	---	200 - 400	100 - 200

Table 2.2. Recommended Electrochemical Requirements for MSE Wall Backfill for Revised TxDOT Specification (Morris and Delphia 1999).

Property	Recommended Requirement	Test Method
pH	> 5.5 & < 10	Tex-128-E
Resistivity (ohm-cm)	> 3000	Tex-129-E
The following applies if resistivity is between 1500 to 3000 ohm-cm:		
Chloride (ppm)	< 100	Tex-620-J
Sulfate (ppm)	< 200	

A brief description of the influencing factors reported to affect corrosion of metal elements embedded in soil is presented next.

2.3.1.1 Resistivity

Resistivity and the pH are the most commonly used methods for estimating corrosivity. Soil resistivity is often reported as the best indicator of a corrosive soil environment. Resistivity is a measurement of the difficulty of an electric current to flow through a material and is expressed in units of ohm-cm. Soil resistivity indicates the capability of the soil, as an electrolyte, to carry corrosion currents. As a result, a low resistivity value is indicative of high potential for corrosion, and conversely, a high resistivity value indicates a lower potential for a corrosive environment.

While resistivity is recognized as a key parameter for measuring corrosion potential in soils, there is considerable variability in the criteria for resistivity as a measurement of corrosivity. This variability in resistivity limits is illustrated by the different criteria adopted by different countries is shown in Table 2.1. An ideal backfill material is believed to have higher resistivity values although debate continues on the reliability for determining soil corrosivity using soil resistivity values.

Resistivity is related to several other factors. The resistivity value is influenced by the presence of soluble salts, moisture content, compaction and temperature (Eyre and Lewis 1987). High concentrations of soluble salts will decrease the resistivity of the material and affect the electrochemical reactions at the metal surface.

Caution should be used when using only resistivity values for determining soil corrosivity. Poor correlation between soil resistivity and observed corrosion rates has been documented (Escalante 1989). For example, a low redox potential can indicate a microbial induced highly corrosive environment in what would otherwise be a mildly corrosive environment based on soil resistivity data.

2.3.1.2 pH

It is well known that the pH of a solution can influence the corrosion of metal. Whitecavage (1990) showed a direct relationship between corrosion rate and pH values for various metals as shown in Figure 2.1. From this figure, it can be seen that high pH

values result in lower corrosion rates for iron. Yet, most criteria limit the pH to a value of approximately 10 for MSE wall backfill. Thus, for plain steel, higher pH values can provide more protection, and limiting the pH of these materials may not be desirable. As shown in Figure 2.1, lower pH values also significantly influence corrosion. Miller et al. (1981) found that almost without exception, a pH of 4 or less indicates high or very high soil corrosivity, and they speculate this is the case due to the acid environment dissolving mineral ions that induces relatively high salt concentrations. Soils with low pH values have been associated with generally higher corrosion rates for both galvanized-steel and plain-steel (Camitz and Vinka 1989). The influence of pH on corrosion rate has also been described by Bushman and Mehalick (1989). Below a pH value of 7, the corrosion rate for iron tends to increase with decreasing pH, while above a pH value of 10, corrosion rate tends to decrease with increasing pH (Bushman and Mehalick 1989).

Iron has a lower corrosion rate in alkaline solutions because the hydroxides of iron are essentially insoluble, forming a protective film on the metal surface (Whitecavage 1990). This phenomenon is displayed in potential - pH diagrams developed by Pourbaix (1966). The equilibrium reactions recorded by Pourbaix (1966) were for metal immersed in an aqueous electrolyte with hydroxyl ions, no other complexing or precipitating ions were present. Therefore the potential - pH diagrams can be used to provide an indication of the general effect of pH on the corrosion reactions of metals in aqueous solutions, but judgment should be exercised in applying these generalizations to corrosion in soil.

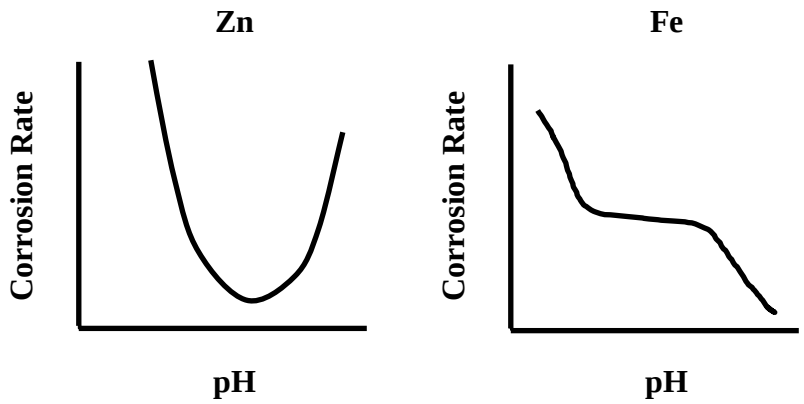

Figure 2.1. Influence of pH on the Corrosion Rates of Various Metals (after Whitecavage 1990).

For zinc (Zn), the corrosion rate increases rather sharply as the pH shifts from the near neutral pH value. Criteria for pH for backfill materials shown in Table 2.1 and Table 2.2 tend to limit the pH such that the corrosion activity of zinc is minimized. Because zinc is a sacrificial anode, the zinc on galvanized steel will eventually corrode away, leaving bare steel. The high pH has been responsible for high corrosion rates of zinc that did not decrease with time (Frondistou-Yannas 1985). Tomashov (1966) reported pH values that provide minimum corrosion for various metals. Variation of pH can occur from the addition of cement to soil, as shown in Table 2.3 (Popova et al. 1998). Small percentages of cement addition are enough to raise the pH value close to 12 (Popova et al. 1998).

More research is needed on the effects of a highly alkaline soil environment on buried metals. Steel in high pH solutions can exhibit low corrosion rates. Therefore, pH limits currently imposed need further investigation.

Table 2.3. Variation of pH with Cement Addition (Popova 1998).

Cement Concentration (Percent)	Measured Solution pH
0	7.0
1	11.3 to 11.4
4	11.8
8	11.9
13	12.0
25	12.1
100	13.0

2.3.1.3 Water Hardness

High water hardness, i.e., high concentrations of calcium carbonate, tends to decrease corrosion rates of steel (Moore and Hallmark 1987). Overall, this factor is believed to have a low impact on the corrosion performance of steel in soils or engineered backfill.

2.3.1.4 Soluble Salts

As the soluble salt content increases, soil resistivity generally decreases. This decrease in resistivity can affect the electrochemical reaction at the metal surface. While resistivity measurements can provide a measure of soluble salt concentration, the type of ion that reduces the resistivity is important. Certain ions have been associated with accelerated rates of corrosion. Particular ions that have been identified with high corrosivity include chloride ions and sulfate ions (Rabeler 1989). The presence of sulfide ions can be an indicator of sulfate reducing bacteria (Bushman and Mehalick 1989). These organisms thrive under anaerobic conditions and are most active for a pH near neutral. These bacteria grow in the pH range of 5.5 to 8.5 (Eyre and Lewis 1987). The

suggested limits for the presence of these ions in the backfill are 100 ppm and 200 ppm for chloride ions and sulfate ions respectively (Elias 1990). As already noted in Table 2.1, various limits exist throughout the world.

2.3.1.5 Redox Potential

The oxidation-reduction (redox) potential can provide information on the type of corrosion mechanism such as anaerobic bacterial corrosion. Elias (1990) reported that a low value of redox potential could indicate susceptibility to microbial attack, while a high value indicates the presence of oxygen-supported corrosion. Heavy clay soils pose the greatest risk of microbiological corrosion (King 1977). Anaerobic bacterial corrosion, as indicated by a low redox potential, has provided plausible explanations for corrosion problems in soils that would otherwise be considered mildly corrosive based on soil resistivity.

Redox potential may also indicate the presence of Ferro Bacteria. Ferro Bacteria oxidize ferrous ions to ferric ions, are typically aerobic, and often thrive in a neutral environment with algae (Eyre and Lewis 1987). The soluble iron content is directly related to redox potential and can be used to confirm soil aggressiveness (Booth et al. 1967). King (1977) labels soils containing more than 125 mg Fe/g as aggressive and soils containing less than 53 mg Fe/g as non-aggressive. Direct measurement of soluble iron is difficult to perform with confidence (King 1977).

While redox potential measurements can be readily performed, the resulting data are often highly scattered, as the measurements are very sensitive to local soil variability and disturbance. Consequently, correlations to corrosion rates can be of limited value. Limited research work has been performed in backfill applications on redox potential, especially when recycled materials are used as the backfill material.

2.3.1.6 Particle Size Distribution (Gradation)

A gradation with more fines will have a low hydraulic conductivity, which will raise the moisture content of the soil and increase the possibility of stagnation. Stagnated conditions promote microbiological activity that can significantly affect the corrosion rate. Gradations with coarser soil particles typically posses a higher hydraulic conductivity, thus providing better drainage and less aggressive conditions.

Soil gradation influences the air-water permeability of the soil. Therefore, soil gradation may be considered as an indirect measure of aeration in a soil. Coarse-grained sandy soils typically have higher air-water permeability values, capable of providing good aeration, while fine-grained clayey soils typically have poor aeration. Good aeration can allow for an increase in the initial corrosion rate; however, once corrosion products are formed in the soil, the corrosion products can form a protective barrier, resulting in lower corrosion activity. Localized corrosion, which is usually observed in unaerated soils (although, this is also a function of ion content), is significantly more damaging than a uniform corrosion process. Case histories (Camitz and Vinka 1989, Escalante 1989, Miller et al. 1981) appear to consistently indicate more severe corrosion problems in fine-grained clayey soils than in coarse-grained sandy soils, although in backfill applications, various results have been documented.

2.3.1.7 Moisture Content

Corrosion will not occur on metals in dry soil. Moisture is required for corrosion to occur. Soil resistivity decreases with increasing moisture content. Maximum corrosion rates often occur at intermediate moisture contents (65 percent saturation) (Briaud et al. 1998). At low moisture contents, there is insufficient water to support the corrosion process. At higher moisture contents, oxygen is excluded from the metal surface and corrosion rates are low. An example of this trend is given by Camitz and Vinka (1989) who report higher rates of corrosion in steels above the groundwater table, which has been attributed to the availability of oxygen to support the corrosion reactions.

Miller et al. (1981) reported high corrosivity values in soils with high moisture contents and soils below the groundwater table. Some of this observed behavior might have been due to corrosion mechanisms resulting from specific environmental conditions, such as microbial corrosion (Miller et al. 1981, Escalante 1989). An increase in soil moisture results in a lower presence of oxygen. The oxygen that is needed for the corrosion process must then be transferred by diffusion through the soil water. Some research indicates that below approximately 20 percent moisture content, the rate of oxygen transfer between the air and soil water can be quite high, and higher corrosion rates will occur (King 1977). Soil with a moisture content of 20 percent and greater can suffer from uniform corrosion (assuming no chloride or sulfate ions are present), while those below 20 percent are more likely to endure pitting corrosion (King 1977). The moisture content providing the maximum corrosion rate varies depending on other soil characteristics.

A number of parameters are possible for describing soil moisture. Moisture content is defined as the ratio, measured on a mass basis, of free water to solid material. Due to the significance of oxygen in corrosion, a moisture measure more relevant to corrosion studies may be the degree of saturation, defined as the percentage of void (non-solid) volume occupied by water.

2.3.1.8 Dissolved Oxygen

Metal components can be embedded in essentially undisturbed soil, disturbed soil, or recycled backfill materials (also disturbed). Studies by Romanoff (1957) indicate that corrosion is more severe in disturbed soils. This observation is supported by a number of investigators. Fischer and Bue (1981) reported that piles in undisturbed Norwegian sediments experienced very little corrosion, in spite of a low soil resistivity. Escalante (1989) postulated that the diffusion of oxygen in undisturbed soils, particularly in undisturbed soils beneath the groundwater table, is sufficiently low that the corrosion process is effectively stifled. This effect tends to override the effects of the usual indicators of corrosivity (resistivity, pH, etc.). Because oxygen availability is critical to

general corrosion, measurement of dissolved oxygen in the pore water could provide a meaningful parameter relevant to corrosivity.

2.3.1.9 Organic Content

Backfill materials should not contain large amounts of deleterious materials that could attack the reinforcement or cause some distresses to the material itself. This could be a significant issue with recycled materials and care must be taken to limit the organics in these materials.

2.3.1.10 Differential Environment

For the corrosion process to occur, an electrolyte must be present. A corroding metal has to be in an environment in which surrounding elements can act as the electrolyte. A differential environment or electrolyte can affect the corrosion rate because inhomogeneities in the electrolyte can cause potential differences on a metal surface. Examples of potential inhomogeneities reported by Escalante (1989) are differences in aeration, temperature, chemical composition, and dissimilar rates of flow.

Many situations can lead to the creation of a differential environment in MSE wall systems. Facing panels are an important component of MSE walls. These panels are often exposed to heat and radiation from the sun, and can experience frequent temperature changes. The soil behind an MSE wall is not subject to these frequent temperature changes. The temperature difference between the facing panels and the soil behind them could cause corrosion potential differences between the different parts of the reinforcement, which could result in elevated corrosion activity. In addition, soil behind the facing panels near the wall is normally compacted less than the soil away from the wall. Engineered backfill is typically used behind the wall. The engineered backfill is probably different from the existing soil, therefore a difference in corrosion potential could arise that may accelerate corrosion. The difference between the two soils may not be a significant factor if the soil reinforcement does not extend beyond the engineered

backfill into the existing soil. However, drainage from nearby roadways and natural soil water movement could carry salts into the backfill, creating different environments at the steel surface. Corrosion potential differences created by differential environments in MSE are difficult to measure and little is known on the magnitude of their contribution to the corrosion of MSE reinforcement. Thus, further investigations are required.

2.4 CORROSION OF METALS IN SOILS

As described earlier, many variables can affect the corrosion activity of metals embedded in soils. Corrosion activity in soils is dependent on parameters related to the metal and the soil environment. Soil environmental factors that can influence the corrosion rate of metals have already been described in 2.3.1, Corrosivity Factors. Metal parameters that can alter the corrosion performance include alloying elements, processing techniques, and dielectric coatings placed on the surface. Because these parameters can alter the corrosion mechanism, thus altering the rate of corrosion, a description of general corrosion mechanisms common to underground metal structures will be presented.

2.4.1 Corrosion Mechanisms

A constant, regular removal rate of metal from the overall surface of a metal is defined as uniform corrosion. This type of corrosion is the most common and costly corrosion mechanism and is often associated with atmospheric corrosion, but also occurs in underground corrosion. For uniform corrosion to occur, the metal must be metallurgically and compositionally uniform and the exposure conditions must be such that all surfaces are exposed to the same uniform environment. In underground environments, uniform corrosion is typically not as common as other corrosion mechanisms due to variations in water levels, non-uniformity of soils and/or backfill materials, varying oxygen contents, and other factors that promote other corrosion mechanisms. The uniform corrosion process is relatively predictable and correlation between the calculated and actual service-life can be determined.

To extend the life of the reinforcement in MSE walls, common practice is to galvanize the reinforcement. The use of coatings for MSE wall reinforcement is uncommon. Coatings are very susceptible to mechanical damage and usually require cathodic protection of the base metal to ensure coating sustenance (King 1977). Galvanization is typically zinc based. This galvanization acts as a sacrificial anode and the process is similar to galvanic corrosion. Galvanic corrosion generally results in uniform corrosion of the active metallic surface. If the thickness of the galvanization and the general corrosion rate is known, the length of extended service-life from the sacrificial coating obtained from galvanizing the steel can be predicted.

Localized corrosion is a mechanism that results in accelerated local attack on the metallic surface and is often referred to as pitting corrosion. These localized areas of attack often appear small, but can severely penetrate the metal and result in significant cross-section loss. Unlike uniform corrosion, pitting corrosion is unpredictable. The rate of this process is variable and depends on the migration of deleterious substances moving into and out of the corrosion pit. The localized corrosion mechanism is prevalent when the electrolyte contains chlorides, sulfates, or other salts.

Differential corrosion can occur when dissimilar alloys are coupled in the presence of a corrosive electrolyte. Each metal, alloy, and microstructural phase has unique corrosion potentials when immersed in corrosive electrolytes. Therefore, one of the alloys will favor corrosion in the electrolyte. When two different metals or alloys are connected while immersed in a corrosive electrolyte, the metal or alloy with the more active (more negative) corrosion potential, loses excess electrons to the less active (more positive) metal or alloy. In backfill applications, this differential corrosion mechanism is common where different backfill materials are present in the same general area.

2.4.2 Soil Corrosivity Assessment

An estimate of the corrosion activity of MSE wall reinforcing strips constructed using CC and RAP as backfill is necessary for service-life prediction. The corrosion activity of the MSE wall reinforcing strips can be assessed by examining the corrosivity

of the backfill. Examination of the backfill material is especially critical because of the diversity of backfill types. Each backfill can have unique characteristics, whereas the type of reinforcement used in MSE walls generally does not change. Approximately 95 percent of all reinforcing strips used in MSE walls, either in strip or grid configuration, have been galvanized-steel (Elias 1997). Aluminum alloys and stainless-steel reinforcement types have been used as reinforcement in MSE walls, but "their use has been discontinued due to extremely poor performance" (Elias 1997). An expanded knowledge of predominant corrosion mechanism parameters for CC and RAP on galvanized-steel and plain-steel reinforcement, and methods for MSE service-life estimation will help engineers design more economical MSE wall systems.

The design practice for soil reinforced structures places limits on measurable backfill characteristics thought to significantly influence the corrosion of the metallic reinforcement. The limits on various backfill parameters that have been adopted by different countries are shown in Table 2.1, which shows that there is no general consensus on quantitative backfill specifications for MSE walls.

Another method commonly used to assess the corrosivity of backfill materials is the American Water Works Association (AWWA) method. This method determines whether or not protective action (i.e., polyethylene encasement) should be implemented for ductile iron piping systems. The system evaluates the sum of weighted numbers called "points" that correlate to measures of resistivity, pH, redox potential, sulfides, and moisture levels to soil corrosivity (AWWA 1988). If these soil characteristics are known, points can be assigned for different characteristics, as shown in Table 2.4. If the sum of the points equals more than ten, the AWWA suggests that protective coatings be used. The Federal Highway Administration (FHWA) has adopted this procedure. The applicability of the AWWA method for assessing corrosivity with regard to recycled backfill materials should be evaluated, especially for recycled backfill materials. Currently, there is no generally agreed upon quantitative standard for assessing backfill corrosivity.

Table 2.4. AWWA Rating - Standard C105/A21.5-88 (1988).

Soil Characteristics				Points
RESISTIVITY - OHM-CM				
(based on single probe at pipe depth or water-saturated Miller soil box)				
			< 700	10
	700	to	1000	8
	1000	to	1200	5
	1200	to	1500	2
	1500	to	2000	1
			> 2000	0
pH				
	0.0	to	2.0	5
	2.0	to	4.0	3
	4.0	to	6.5	0
	6.5	to	7.5	0
	7.5	to	8.5	0
			> 8.5	3
REDOX POTENTIAL				
			> + 100 mV	0
	+ 50	to	+ 100 mV	3.5
	0	to	+ 50 mV	4
Negative				5
SULFIDES				
Positive				3.5
Trace				2
Negative				0
MOISTURE				
Poor drainage, continuously wet				2
Fair drainage, generally moist				1
Good drainage, generally dry				0

Methods also exist to determine the service-life of metallic reinforcement. One such statistical method proposed by Bushman and Mehalick (1989) could be used to predict the mean time to corrosion failure (MTCF). Their research found that considerable variance occurs in the measurement of corrosion inducing variables, and that the study of a single variable to predict MTCF would not be sufficient. To deal with this problem, a multiple regression analysis model was developed where the MTCF is impacted by each independent variable multiplied by a coefficient representing the relative contribution of the variable to MTCF. The general form of the multiple regression analysis model developed by Bushman and Mehalick (1989) is:

$$Y = B_o + B_1 X_1 + B_2 X_2 + \ldots B_k X_k + e \qquad (2.1)$$

where,

- Y = the dependent variable (for example, MTCF in years for each tested cast iron water pipeline location),
- $X_{1,2,\ldots,k}$ = each predictor variable which impacts the MTCF (for example, soil resistivity, moisture content, etc.),
- $B_{1,2,\ldots,k}$ = coefficient developed for each independent variable based on the relative contribution of each variable on the MTCF,
- B_o = constant or Y intercept, and
- e = random error possessing a normal probability distribution and having a mean equal to zero with a constant variance.

The difficulties in determining the coefficients for this method have limited its introduction into practice.

The American Association of State Highway and Transportation Officials (AASHTO) and the California Department of Transportation (CalTrans) currently have design guidelines for evaluating the service-life for galvanized-steel in soil applications. The AASHTO model requires a 75-year design life for permanent structures and provides parameters specifically for MSE structures (Elias 1997). The CalTrans (1993) method, California Test 643, estimates the service-life of 18 gage steel culvert with zinc coating weight of 2 oz/ft^2 (0.61 kg/m^2).

For MSE applications where the backfill meets the following criteria:

- Resistivity greater than 3000 ohm-cm,
- $5 < pH < 10$,
- Organic content is less than 1%,
- Chloride content is less than 100 ppm, and
- Sulfate content is less than 200 ppm;

AASHTO (Elias 1997) specifies that the maximum mass presumed to be lost per side is:

- 0.59 mil/yr (15 μm/yr) for the corrosion of the zinc coating during the first two years,
- 0.16 mil/yr (4 μm/yr) until the zinc coating is depleted, and then
- 0.47 mil/yr (12 μm/yr) for the remaining life of the steel.

A sacrificial thickness of 62.6 mil (1.59 mm) is calculated for a 75 year service-life assuming the standard galvanization thickness of 3.4 mil (86 μm). The sacrificial thickness to compensate for the effects of corrosion until the end of the service-life must be provided in addition to the required steel thickness for structural reinforcement. If the capacity of the remaining steel after 75 years is greater than the design requirements, the proposed system may be allowed. It should be noted that no reduction in tensile strength is used in the design procedure. Elias (1997) reasons that since the sacrificial thickness required is a maximum loss rate, the reduced minimum thickness should be assumed to be proportional to tensile strength, thereby requiring no further reduction in tensile strength. Research by Elias (1990) suggests that the loss of average tensile strength is related to average thickness due to corrosion loss by a factor of approximately two.

If the permanent structure is considered critical, a service-life of 100 years is generally considered appropriate (Reinforced Earth Company 1995). For years 75 to 100, the linear loss model specified by AASHTO becomes very conservative (Reinforced Earth Company 1995). A reduced loss rate of 0.28 mil (7 μm/yr) is recommended for carbon steel for years 75 to 100 (Reinforced Earth Company 1995).

The AASHTO model more accurately represents corrosion losses than the uniform model concept developed from the National Bureau of Standards (NBS) testing (Elias 1997). The following exponential equation was developed by Romanoff (1957) to predict the amount of general corrosion after burial:

$$X = Kt^n \tag{2.2}$$

where,

X is the loss of thickness or pit depth, in μm, in the metal at time t in years,

K and n are constants dependent on the soil

Elias (1997) suggested the predictive models shown in Table 2.5, which are based on corrosion in a wide range of soils and the generalized corrosion rate relationship developed by Romanoff (1957). It should be noted that the studies by Romanoff (1957) used to derive the predictive models do not present any data for soils with pH above 9.5.

Table 2.5. Generalized Soil Corrosion Predictive Models (Elias 1997 from data by Romanoff 1957).

Galvanized-steel		Carbon steel	
Average	**Maximum**	**Average**	**Maximum**
$X = 25t^{0.65}$	$X = 50t^{0.65}$	$X = 40t^{0.80}$	$X = 80t^{0.80}$

Elias (1997) found that the predictive models could considerably underestimate the corrosion of galvanization when compared to results from retrieval tests performed by other researchers. The empirical equations presented by Elias (1997) are based on data from a wide range of soils. Many of the soils do not meet the backfill requirements for MSE walls (Elias 1997). The Reinforced Earth Company (1995) found that the corrosion rate of galvanized-steel or carbon-steel reinforcement embedded in granular backfill meeting the requirements for MSE walls can be conservatively estimated by the equation to predict the average galvanized-steel corrosion rate presented in Table 2.5 based on data obtained from in-service structures during the Terre Armee Internationale (TAI) Corrosion Study. However, the TAI study did not encounter soils with high chloride concentrations. The maximum chloride concentration recorded for the in-service structures studied was 52 ppm (Reinforced Earth Company 1995). The study also found

that, "the rate of metal loss did not noticeably change during or after the transition from the zinc phase to the iron phase" (Reinforced Earth Company 1995).

CalTrans (1993) Test Method 643 determines the time of maintenance free service for galvanized steel culverts in soils with pH values less than 7.3 using the following equation:

$$Y = 13.79 \cdot \left[\mathrm{Log}_{10}R - \mathrm{Log}_{10}\left(2160 - 2490 \cdot \mathrm{Log}_{10}(\mathrm{pH})\right)\right] \quad (2.3)$$

where,

Y is the years to perforation for an 18 gage steel culvert, and

R is the minimum resistivity in ohm-cm.

For pH values greater than 7.3 the following equation is used:

$$Y = 1.47 \cdot R^{0.41} \quad (2.4)$$

Various factors can be applied to adjust the years to perforation for other pipe gauges. The gauges and respective factors are: 16 gage - 1.3, 14 gage - 1.6, 12 gage - 2.2, 10 gage - 2.8, and 8 gage - 3.4 (CalTrans 1993). The applicability of this service-life prediction method for galvanized-steel embedded in recycled backfill materials has not been assessed and research is needed.

Corrosion potential readings have also been used to assess soil corrosiveness. Corrosion potential measurements of metals in underground corrosion studies are typically measured in the field with a copper/copper sulfate ($Cu\text{-}Cu_2SO_4$) electrode. In general, for galvanized-steel, corrosion losses are greater if the corrosion potential is more positive (Elias 1990). A more negative corrosion potential reading on a metal implies greater chemical activity (Applegate 1960). Applegate (1960) states that very corrosive situations have resulted in readings of –600 mV or more negative for steel. Both Applegate (1960) and Elias (1990) state that corrosion potential readings do not provide an accurate assessment of the degree of corrosion or the corrosion rate. The corrosion potential can only be used to assess the composition of the exposed surface, in the case of galvanized-steel (Elias 1990). Typical corrosion potential values for

galvanization are in the range of –1100 to –800 mV and for carbon steel in the range of -700 to -400 mV measured with a Cu-Cu_2SO_4 electrode (Elias 1997). The transition stage from galvanized-steel to steel would yield intermediate values (Elias 1997). Applegate (1960) provides ranges of corrosion potential readings vs. Cu-Cu_2SO_4 for the corrosion of plain steel. These ranges are shown in Table 2.6.

Table 2.6. Probable Corrosiveness of Steel Using Potential Readings (Applegate 1960).

Potential vs. Cu-Cu_2SO_4 (mV)	Ratio of Min to Max Potential	Probable Corrosiveness
-150 or more positive	3 or more	Practically none
-150 to -300	2.0 to 3.0	Very mild
-300 to -450	1.5 to 2.0	Mild
-450 to -550	1.2 to 1.5	Moderate
-550 or more negative	1.2 or less	Severe

Eyre and Lewis (1987) provided a summary of soil corrosivity assessment techniques and backfill material criteria used in Britain, France, and Germany, in addition to the AWWA assessment technique. The British Department of Transport Technical Memorandum on Reinforced Earth is the only assessment technique that provides different criteria depending on reinforcement type. The German Gas Engineering Assessment Technique (Eyre and Lewis 1987) uses a point system similar to that of the AWWA method. Eyre and Lewis (1987) provide their own general soil corrosivity assessment technique. Their technique uses marks, essentially points, similar to the AWWA method to assess soil corrosivity. The methods presented by Eyre and Lewis (1987) are presented in Table 2.7. Eyre and Lewis (1987) also made suggestions to revise design standards for corrugated steel buried structures. Their recommendations were to perform the following assessments: soil classification, groundwater position, resistivity, pH, and presence of cinders and coke. If the soils receive marks within a particular range, then further testing for soluble sulfate, chloride ion, and sulphide should

also be performed (Eyre and Lewis 1987). In addition, Eyre and Lewis (1987) recommended that references to redox testing should be deleted. Eyre and Lewis (1987) tend to take a practical approach to testing by requiring further testing only for certain circumstances. Suggestions to the British Department of Transport Technical Memorandum on Reinforced Earth were also provided.

Table 2.7. Soil Corrosivity Assessment Techniques (after Eyre and Lewis 1987).

PARAMETER	BRITISH DEPARTMENT OF TRANSPORT TECHNICAL MEMORANDUM ON REINFORCED EARTH	FRENCH MINISTRY OF TRANSPORT SPECIFICATION FOR REINFORCED EARTH STRUCTURES	AWWA C105 ASSESSMENT TECHNIQUE	GERMAN GAS ENGINEERING ASSESSMENT TECHNIQUE	EYRE AND LEWIS
NATURE OF SOILS	The backfill material shall be frictional (FF) or cohesive frictional (CFF) fill and shall not contain unburnt colliery shale or pulverized fuel ash.	The backfill material can be either natural soils or materials of industrial origins. They should not contain any vegetative soil, any putrescible material, and any domestic waste.	Unspecified	Calcareous, marls, and sands +2 Loams, sandy loams, and sand clays 0 Clays and humus -2 Peat, thick loams, and marshy soils -4	BS 1377 test method shall be used for all plasticity index (PI testing) ● < 10% passing 63 μ BS sieve, and that passing 425 μ BS sieve, has PI < 2 +2 ● < 75% passing 63 μ BS sieve, < 10% passing 2 μ BS sieve, and that passing 425 μ BS sieve, has PI < 6 0 ● that passing 425 μ BS sieve, has PI < 15 -2 ● that passing 425 μ BS sieve, has PI ≥ 15 -4
RESISTIVITY	Min. (ohm-cm) Aluminum alloy 3000 Copper 2000 Galvanized-steel 5000 Stainless-steel 3000	Min. (ohm-cm) Structures outside water 1000 Structures in soft water 3000	<700 (ohm-cm) 10 700 to 1000 8 1000 to 2000 5 1200 to 1500 2 1500 to 2000 1 >2000 0	(ohm-cm) >10,000 0 10,000 to 3000 -1 3000 to 1000 -2 1000 to 100 -3 < 100 -4	(ohm-cm) ≥10,000 0 10,000 to 3000 -1 3000 to 1000 -2 1000 to 100 -3 ≤ 100 -4
REDOX POTENTIAL	FF (mV) CFF (mV) Aluminum alloy 400 430 Copper 250 250 Galvanized-steel 400 430 Stainless-steel 300 350	Not determined	(mV) > + 100 0 +50 to +100 3.5 0 to + 50 4 Negative 5	Not determined	(mV) ≥ + 400 +2 + 400 to + 200 0 + 200 to 0 -2 ≤ 0 -4
CHLORIDE ION CONCENTRATION	Max. [Cl^-] Aluminum alloy 0.05% Copper 0.05% Galvanized-steel 0.05% Stainless-steel 0.03%	Max. [Cl^-] Structures outside water 0.02% Structures in soft water 0.01%	Not determined	< 0.005% 0 0.005 to 0.025% -1 0.025 to 0.05% -2 > 0.05% -4	(ppm) ≤ 50 0 50 to 250 -1 250 to 500 -2 ≥ 500 -4
SULFATE ION CONCENTRATION	Max. [SO_4^{2-}] Aluminum alloy) Copper) 0.5% Galvanized-steel) Stainless-steel)	Max. [SO_4^{2-}] Structures outside water 0.1% Structures in soft water 0.05%	Not determined	< 0.02% 0 0.02 to 0.05 -1 0.05 to 0.1 -2 > 0.1 -3	Soluble sulfate (ppm) ≤ 200 200 to 500 500 to 1000 ≥ 1000
pH	Range Aluminum alloy 6 to 8 Copper 5 to 9 Galvanized-steel 6 to 9 Stainless-steel 5 to 10	Range 5 to 10	0.0 to 2.0 5 2.0 to 4.0 3 4.0 to 6.5 0 6.5 to 7.5 0 7.5 to 8.5 0 > 8.5 3	> 6 0 < 6 -2	≥ 6 0 < 6 -2
ORGANIC MATERIAL	Not determined	0.01% Max.	Not determined	Not determined	Organic content ≥ 0.2% -4

Table 2.7. CONTINUED.

PARAMETER	BRITISH DEPARTMENT OF TRANSPORT TECHNICAL MEMORANDUM ON REINFORCED EARTH	FRENCH MINISTRY OF TRANSPORT SPECIFICATION FOR REINFORCED EARTH STRUCTURES	AWWA C105 ASSESSMENT TECHNIQUE	GERMAN GAS ENGINEERING ASSESSMENT TECHNIQUE	EYRE AND LEWIS
SULFATE REDUCING BACTERIA (ACTIVITY INDEX)	Not determined	Structures soft water only B.O.D. 5 < 20 mg/kg max. bacteria population 10 per gm of soil	Not determined	< 5 0 5 to 7 -2 > 7 -4	Not determined
SULPHIDE	Not determined	Max. $[S^{4-}]$ Structures outside water 0.03% Structures in soft water 0.01%	Present 3.5 Trace 2 Not present 0	None 0 Trace -2 Present -3 High -4	None 0 Trace -2 Present -3 High -4
DRAINAGE	Not determined	Not determined	Poor drainage, continuously wet 2 Fair drainage, generally moist 1 Good drainage, generally dry 0	Not determined	With respect to groundwater level at buried position: Well drained area +1 Poorly drained area -1 Above foundation level of structure -4
MOISTURE CONTENT	Not determined	Not determined	Not determined	< 20% 0 > 20% -1	≤ 20% 0 > 20% -1
CARBONATE	Not determined	Not determined	Not determined	Copious +2 Present +1 Trace 0	Copious +2 Present +1 Trace 0
SOIL CONDITION	Not determined	Not determined	Not determined	Existing soil 0 Reclaimed ground -2 Same as excavated ground 0 Different from excavated ground -3	Cinder and coke or made ground: None 0 Exist -4
SCORING			10 points or more is corrosive to cast iron	0 Unlikely to be aggressive -1 to -4 Mildly aggressive -5 to -10 Aggressive < -10 Highly aggressive	≥ 0 Unlikely to be aggressive -1 to -4 Mildly aggressive -5 to -10 Aggressive ≤ -11 Highly aggressive

Although directly correlating resistivity values only with soil corrosivity is often not valid, Chaker (1981) provided a correlation of resistivity data to various mineral and soil materials and assessed soil corrosivity based on soil resistivity only, as summarized in Table 2.8. The use of the corrosivity assessment by Chaker (1981) is more applicable to field measurement of in-situ soils using the Wenner Four Electrode method as opposed to soils assessed on the basis of resistivity values obtained from aqueous solutions tested in a plexiglass soil box or obtained from conductivity measurement conversion.

Table 2.8. Soil Corrosivity Versus Soil Resistivity (Chaker 1981).

Soil Corrosivity	Soil Resistivity (ohm-cm)
Very corrosive	0 to 2000
Corrosive	2000 to 5000
Moderately corrosive	5000 to 10000
Mildly corrosive	10000 to 25000
Relatively less corrosive	25000 to 50000
Progressively noncorrosive	50000 to 100000

King (1977) evaluated the aggressiveness of soils based on resistivity and redox potential as shown in Table 2.9.

Table 2.9. Generally Accepted Parameters for Soil Aggressiveness (King 1977).

Aggressiveness	Resistivity (ohm-cm)	Redox Potential (corrected to pH = 7) Normal Hydrogen Electrode (mV)
Very corrosive	< 700	< 100
Corrosive	700 to 2000	100 to 200
Moderate corrosion	2000 to 5000	200 to 400
Mild or non-corrosive	> 5000	> 400 > 430 if clay soil

Popova et al. (1998) assessed the corrosivity of samples of steel and galvanized-steel in cement stabilized backfill saturated with distilled water and 4 percent sodium chloride solution. Samples of galvanized-steel were also tested in CC saturated with distilled water and with 4 percent sodium chloride solution. The galvanized-steel in CC was tested up to 470 days. For CC saturated with distilled water, the corrosion rates were in the range of 0.2 mpy (0.005 mm/yr) for 13 percent cement content and up to 0.79 mpy (0.02 mm/yr) for 4 percent cement content (Popova et al. 1998). For CC saturated with 4 percent sodium chloride, the corrosion rates were in the range of 1.6 to 5.9 mpy (0.04 to 0.15 mm/yr) for 4 to 13 percent cement content and 22.8 mpy (0.58 mm/yr) for samples with no cement (Popova et al. 1998). The galvanized-steel samples in CC with higher cement content exhibited lower corrosion rates for both solution types. The corrosivity of CC was marginally better than the cement stabilized soil for comparable conditions. Popova et al. (1998) concluded that corrosivity of CC appears to be comparable to, or slightly better than, conventional fill. The corrosion rates for galvanized-steel in CC found by Popova et al. (1998) provides values that can be used for comparison with other CC corrosivity assessment results.

2.4.3 Summary of Corrosivity Assessment Methods

There are many factors to be considered for assessing soil corrosivity. Several methods exist for assessing soil corrosivity, however the methods are generally inconsistent and acceptance criteria for backfill suitable for MSE walls varies between different agencies. Methods for assessing backfill corrosivity can be categorized into point systems, empirical equations (i.e. regression analysis), categorical systems, and specifications. Point systems corrosivity assessment techniques assign points to results from the testing of various parameters. These systems can be categorical in nature. Point systems are those by the AWWA Standard C105 (1988), German Gas Engineering (Eyre and Lewis 1997), and Eyre and Lewis (Eyre and Lewis 1997). Empirical equation assessment techniques are Regression Analysis Models (Bushman and Mehalick 1989), Generalized Soil Corrosion Predictive Model ([Romanoff 1957] and [Elias 1997]), and

CalTrans (1993) Test Method 643. Categorical assessment techniques use one or more factors to assess corrosivity and have several ranges of categories assigned to ranges of values for the particular factor(s). These techniques are an approach similar to point systems, however points are not tabulated. Categorical assessment techniques for corrosivity that are assigned are Probable Corrosiveness of Steel Using Potential Readings (Applegate 1960), Soil Corrosivity Using Soil Resistivity (Chaker 1981), and Soil Aggressiveness Using Resistivity and Redox Potential (King 1977). Specifications assess backfill corrosivity by providing acceptance criteria; backfill that does not meet the acceptance criteria is deemed unsuitable for MSE walls. Specification assessment techniques are FHWA, AASHTO, France, United Kingdom, Germany, and TxDOT.

It can be a challenge to know which of the corrosivity assessment techniques is the most suitable method to use. The number of differing techniques and different types of techniques complicates choosing the best assessment technique. Such is the case for the assessment of recycled backfill materials for MSE walls. New factors may need to be considered, such as cement concentration. The applicability of the assessment techniques to differing backfill types (i.e. differing gradations) should be clarified. Aspects of the current corrosivity assessment methods should be compared and evaluated to determine their applicability for assessing MSE wall backfill.

3. RESEARCH METHODOLOGY

3.1 EXPERIMENTAL PROGRAM OVERVIEW

Since previous studies have been limited on CC and RAP backfill materials, an experimental program investigating these recycled backfill materials was carried out to obtain data. The experimental program focused on three backfill materials: CFM, CC, and RAP.

The backfill materials were evaluated in reference to their effect on the corrosion of galvanized-steel and plain-steel earth reinforcing strips. Ribbed galvanized-steel and plain-steel earth reinforcing strips were investigated in this study. For this program, the plain-steel strips embedded in CFM are assumed to be the control samples.

The experimental program can be subdivided into two main tasks: materials characterization and corrosion testing. The corrosion testing is subdivided into short-term testing and long-term testing. The scope and justification of each task is briefly described next.

3.1.1 Materials Characterization Program

Characterization data were obtained for the CFM, CC, and RAP backfills and the galvanized-steel and steel earth reinforcing strips used in the research program. Characterization data for each of the backfills were determined from a series of tests. These tests included the following: grain size distribution, Atterberg limits, classification, specific gravity, relative density, adsorption, pH, resistivity, shape and surface characteristics, chloride content, sulfate content, sulfide content, oxidation-reduction potential, permeability, and evaluation for the presence of organics. These tests were deemed appropriate for evaluating the backfills after reviewing literature pertaining to MSE walls.

Characterization data for the reinforcing strips included size, shape, and chemical composition. Some of the backfill and reinforcing strip characterization data are not used directly in the results, but this information provides definition of the test conditions for this research.

3.1.2 Corrosion Testing Program

3.1.2.1 Short-term Testing

Because limited studies have been performed on correlating short-term corrosion test results with longer-term test results and because short-term testing (STT) is generally more cost-effective and applicable for the construction industry, STT was performed. These data were then compared with long-term test (LTT) data obtained in this experimental program. STT was performed to assess the corrosivity of the CFM, CC, and RAP backfill materials. The STT required that a solution be decanted from each of the backfill materials and used as an electrolyte in corrosion cells to test the corrosion of galvanized-steel and plain steel earth reinforcement. Three backfill materials, two reinforcement materials, and two environmental conditions were evaluated. Polarization resistance, mass loss, resistivity, pH, chloride content, sulfate content, sulfide content, and redox potential were evaluated.

3.1.2.2 Long-term Testing

LTT is generally more desirable to assess the corrosivity of backfill materials because it allows for more realistic evaluation procedures. For the LTT performed in this project, reinforcing strip samples were embedded in CFM, CC, and RAP. Plain-steel and galvanized-steel reinforcement samples were embedded in each backfill in an attempt to duplicate the reinforcement buried condition. For each combination (backfill and reinforcement type) samples were exposed to two exposure solutions: aqueous chloride solution and distilled water solution. Backfill material parameters were assessed to

correlate corrosivity with resistivity, pH, chloride content, sulfate content, and redox potential. Polarization resistance and open circuit potential (OCP) measurements were used to evaluate the corrosion performance of the embedded reinforcement samples. Mass loss testing was performed on the reinforcing strip samples at the end of test period to estimate the mean corrosion activity following ASTM G1 (1994 a), *Standard Practice for Preparing, Cleaning, and Evaluating Corrosion Test Specimen*. The corrosion activity data were then used to evaluate the service-life of each backfill and reinforcement material combination. The polarization resistance and OCP data were used to determine if these procedures could reliably be used to predict corrosion activity of the reinforcements embedded in the backfill materials. These results are presented in Sections 4 and 5.

3.2 MATERIALS CHARACTERIZATION DATA AND METHODS

The materials characterization methods are described in this subsection. In addition, the characterization data for the backfill materials and the earth reinforcing strips are presented. Numerous references are made to the "Results from the State-of-the-Art Review and Material Characterization" by Rathje et al. 2001, which was conducted prior to this experimental program and involved the characterization of the three backfill materials used in this study. The CFM, CC, and RAP characterized in the report by Rathje et al. (2001) were from the same sample stockpile used in this experimental program.

The three backfill materials were selected from suppliers in Texas. Galvanized-steel and plain-steel earth reinforcing strips were also obtained from a manufacturer in Texas. Although the backfill materials and earth reinforcement came from suppliers in Texas, the results from this study may be applicable to other agencies outside of the state that may want to use recycled materials for MSE wall construction.

3.2.1 Backfill

CFM, CC, and RAP backfill materials were characterized as part of this test program. The backfill materials were acquired from different sources, which were predetermined through a preliminary study (Rathje et al. 2001). One objective of the preliminary study was to identify producers of CC and RAP in Texas and to select sources for the materials that represent what is typically used in the state. The details of this selection process can be found in the first report by Rathje et al. (2001). Texas Crushed Stone from Georgetown, Texas was the chosen source for the CFM, Big City Crushed Concrete from Dallas, Texas was the source for the CC, and the TxDOT Corpus Christi District provided the RAP material (Rathje et al. 2001). The bulk material was hauled from the sources and stockpiled at the Pickle Research Center in Austin, Texas. To complete the experimental program, a portion of the bulk material was collected and transported to Texas A&M University in College Station, Texas.

Several laboratory tests were performed to characterize the engineering properties of the backfills. After reviewing the literature, it was decided that the CFM, CC, and RAP backfill materials used in this program would be characterized with the following tests:

- Grain size distribution,
- Atterberg limits,
- Classification,
- Specific gravity,
- Relative density,
- Adsorption
- pH,
- Resistivity,
- Chloride content,
- Sulfate content,
- Sulfide content,
- Redox potential,
- Shape and surface characteristics,
- Permeability, and
- Organics.

Upon visual inspection of the backfill materials, it was decided that testing for organics was not necessary. The backfill materials were free of any deleterious organics. Results and discussion from the shear strength testing is also not included. These tests were performed by others and are not discussed here because the results do not supply characteristics pertinent to the study of the corrosiveness of the backfill materials. The standardized test methods and any modifications used in this program to perform the above tests are presented in the following Subsections.

3.2.1.1 Grain Size Distribution (Gradation)

The grain size distribution was determined through a preliminary investigation on the CFM, CC, and RAP. The investigation concluded that the backfill materials should have a reference gradation as shown in Table 3.1 (Rathje et al. 2001). To determine the reference gradation, the grain size distribution was evaluated using sieve tests conducted in accordance with the ASTM D422 (1998 c), *Standard Test Method for Particle-Size Analysis of Soils*, on the three backfill materials. The grain size distributions of the backfill materials are shown in Table 3.1 along with the reference gradation. All CFM, CC, and RAP materials used in this experimental program were sieved and remixed to meet the reference gradation shown in Table 3.1. A single reference gradation was used in an attempt to eliminate the effect of grain size distribution on the test results, thereby allowing the experimental program to concentrate on the effects of the composition of the different backfill materials.

Table 3.1. Reference Gradation of CFM, CC, and RAP Backfill Materials (Rathje et al. 2001).

Sieve Size	Diameter (mm)	Percent Passing
2 inches	50.00	100.0
1 inch	25.00	88.0
1/2 inch	12.50	65.0
No. 4	4.75	35.0
No. 8	2.36	22.0
No. 16	1.18	15.0
No. 40	0.43	7.0
No. 100	0.15	1.5
No. 200	0.08	0.0

All of the "as received" CFM, CC, and RAP had to be processed to meet the reference gradation. The processing required drying, sieving, mixing, and adjusting the moisture content. The backfill materials were first dried. The CFM and CC were dried in an oven at a drying temperature of 230 $\pm$ 41^{o}F (110 $\pm$ 5^{o}C). The drying temperature is that recommended for drying soil in ASTM D2216 (1998 b), *Water Content Determination*. The CFM and CC were dried in the oven for a period of 12 to 24 hours and assumed to be at a constant mass state after the drying period. The RAP was not oven dried because the asphalt binding material can melt and change the size of the particles. The general drying practice required for the RAP in the experimental program was to air dry at room temperature for at least 24 hrs. However, since such a large quantity was needed for this program, the RAP was spread outdoors 2 inches $\pm$ 1 inch (51 mm $\pm$ 25 mm) thick layer on a clean concrete pavement to dry in the sun. The RAP was dried outdoors for more than three days with favorable weather (no rain), and was visually inspected for dryness before sieving.

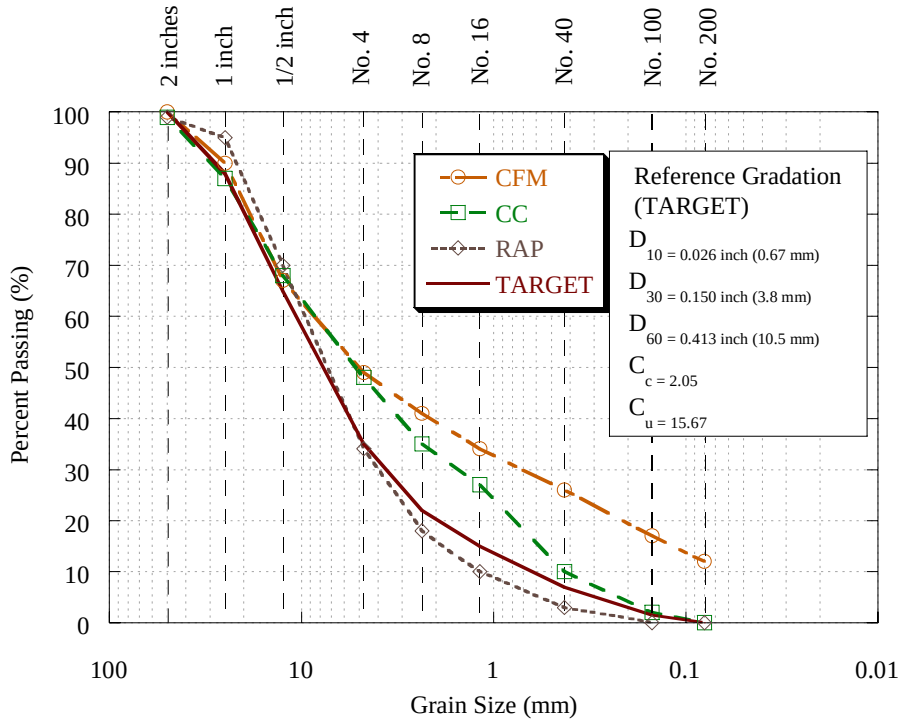

Figure 3.1. Reference Gradation for the Three Backfill Materials Used in the Experimental Program (Rathje et al. 2001).

The three backfill materials were mechanically sieved using a Gilson® TM5 and Gilson® CF1 sieve shakers. Before sieving the backfill materials, the time to shake the materials in the sieve machine had to be determined according to ASTM C136 (2001 c), *Standard Test Method for Sieve Analysis of Fine and Coarse Aggregates*. To determine the time to run the sieve shaker, a particle-size analysis was performed on a sample of material retained on each sieve size. It was determined that 13 minutes was the minimum time to run the sieve shaker. One inch (25mm), 1/2 inch (12.5 mm), No. 4 (4.75 mm), No. 8 (2.36 mm), No. 16 (1.18 mm), No. 40 (0.43 mm), No. 100 (0.15 mm), and No. 200 (0.08 mm) sieves were used.

After sieving all backfill materials required for the experimental program, the backfill materials retained on each sieve size were weighed in an appropriate proportion to build the reference gradation in Table 3.1. The weighed backfill material was added to

a concrete mixer for mixing 1 yd^3 (0.76 m^3). The mixed backfill material was stored dry in 55 gal (208 L) plastic drums until it was used in the experimental program.

3.2.1.2 Atterberg Limits

The Atterberg limits define the liquid and plastic limits of a soil. The limits are commonly used in the classification of soils. The liquid limit is defined as the "moisture content below which the soil behaves as a plastic material" (Bowles 1992). The plastic limit is defined as "the moisture content below which the soil is nonplastic (Bowles 1992)." The plastic limit test could not be performed because all three backfill materials were nonplastic. The determination of the liquid limit requires that a standard liquid limit device and grooving tool be used. The liquid limit is arbitrarily defined as the "water content at which a sample of soil placed in a brass cup, cut with a standard groove, and then dropped from a height of 0.39 inch (10 mm) will undergo a groove closure of 0.5 inch (12.7 mm) when the cup of soil is dropped 25 times at the rate of 120 drops/minute" (Bowles 1992). Ogolla (2002) performed the liquid limit test according to TxDOT method Tex-104-E *Determining Liquid Limits of Soils* and found an average liquid limit for the CC of 31 percent with a standard deviation of 4 percent. The average liquid limit of the RAP was 23 percent with a standard deviation of 3 percent (Ogolla 2002).

3.2.1.3 Classification

The backfill materials were classified according to the two classification systems most widely used, the Unified Soil Classification (USC) system and the AASHTO classification system. Both classification systems rely on the Atterberg limits, a sieve analysis, and a description of the soil. To classify the CFM, CC, and RAP according to these two systems, the liquid limit and gradation were used. A sieve analysis was not required because each of the backfills used in the experimental program were processed to the reference gradation shown in Table 3.1. Each of the graded backfill materials was classified as well-graded gravel (GW) by the USC, and as an A-1-a, gravelly with only a

small amount of fines, by the AASHTO classification system. The CFM is visually described as light brown limestone gravel, the CC as a gray crushed concrete gravel, and the RAP as a black recycled asphalt gravel. One drawback of the classification systems is that they are more applicable to the classification of soil than aggregate. A measurement or description of the particle shapes and surface textures of the aggregates are not required in these systems. Since the particle shape and surface texture of the aggregate could be important parameters for compaction, and thus corrosion performance, these tests were performed. Coarse aggregates with angular particle shapes will generally be more stable following compaction than a backfill with more rounded particle shapes.

3.2.1.4 Specific Gravity

The specific gravity (G_s) of any substance is defined as the density of the material divided by the density of water, which in terms of soil can be described as the ratio of the mass of a volume of soil particles to the mass of an equal volume of water. The specific gravity of the materials was determined by Rathje et al. (2001) using ASTM C127 (2001 a) *Apparent Specific Gravity of Coarse Materials* and ASTM D854 (2000 b) *Specific Gravity of Fine Materials*. Both methods were used and then a weighted average of the specific gravities measured by each method was calculated by Equation 3.1 (Rathje et al. 2001). This equation shows how the weighted average of the specific gravities was calculated. The average specific gravity was determined as follows:

$$(G_s)_{avg} = \frac{1}{\frac{P_1}{100G_1} + \frac{P_2}{100G_2}} \qquad (3.1)$$

where, P_n is the percentage by weight of each size fraction, and

G_n is the appropriate specific gravity of each size fraction.

The specific gravity obtained from ASTM C127 (2001 a), ASTM D854 (2000 b), and the weighted average for each backfill is presented in Table 3.2. The specific gravity of RAP is lower than typical soil. The smaller value of specific gravity for the RAP is probably due to the bituminous coating on the aggregate particles (Rathje et al. 2001).

Table 3.2. Specific Gravities of CFM, CC, and RAP (Rathje et al. 2001).

Material	Specific Gravity		
	> No. 4 sieve[a]	< No.4 sieve[b]	$(G_s)_{avg}$
CFM	2.64	2.69	2.66
CC	2.62	2.62	2.62
RAP	2.36	2.28	2.33

[a]From ASTM C127.
[b]From ASTM D854.

3.2.1.5 Relative-Density (Unit Weight)

The relative density was determined by Rathje et al. (2001) using Tex-113-E (2001) *Laboratory Compaction Characteristics and Moisture-Density Relationship of Base Materials*. To perform the test, a 10 lb (4.5 kg) modified compaction hammer with a drop height of 18 inches (46 mm) was used to compact soil in a 6 inch (152 mm) diameter by 8 inch (203 mm) high mold. A compaction energy of 22,900 ft-lb/ft^3 (1,096,460 J/m^3) is required by the test method, which translates to 50 blows of the hammer for a 2 inch (51 mm) layer within the compaction mold (four layers total). After compaction, the compacted material is weighed, extruded, dried in the oven, and re-weighed. The dry unit weight and water content were calculated and plotted against each other.

The backfill materials were compacted at various water contents to obtain a compaction curve. The compaction curves for the three backfill materials were used to determine the target dry density and corresponding moisture content. Table 3.3 shows the target moisture content and dry density for each backfill material (Rathje et al. 2001).

Table 3.3. Target Moisture Content and Dry Density for all Samples in the Experimental Program (Rathje et al. 2001).

Material	Moisture Content (%)	Dry Density (lb/ft^3)	Dry Density (kg/m^3)
CFM	10	125	2002
CC	10	119	1906
RAP	3	117	1874

When it was time to use the graded backfill materials for the experimental program, tap water was added to the graded material to achieve proper moisture contents (within $\pm$ 1 percent). Moisture content was determined using ASTM D4959 (1994 b), *Standard Test Method for Determination of Water (Moisture) Content of Soil By Direct Heating Method.*

3.2.1.6 Adsorption

The adsorption was determined for the backfills by following ASTM C127 (2001 a), *Standard Test Method for Density, Relative Density (Specific Gravity), and Absorption of Coarse Aggregate* and ASTM C128 (2001 b) *Standard Test Method for Density, Relative Density (Specific Gravity), and Absorption of Fine Aggregate*. The only deviation from the specification was that the RAP for the coarse and fine aggregate testing was not oven dried, but was dried at room temperature for at least 24 hours and inspected for a dry appearance. The samples for adsorption testing were obtained following ASTM D75 (1997 b), *Standard Practice for Sampling Aggregates*. The results of the adsorption test are shown in Table 3.4.

Table 3.4. Adsorption of Backfill Materials.

Material	Coarse Aggregate Adsorption (%)	Fine Aggregate Adsorption (%)
CFM	4.4	4.4
CC	4.1	4.3
RAP	1.0	1.3

3.2.1.7 Pore Solution pH

ASTM D4972 (1995 c), *Standard Test Method for pH of Soils*, was used to measure the pH of the pore solutions in the backfill materials. This method determines the solubility of soil minerals and the ion mobility. Another test method for measuring pH in soil, ASTM G51-95 (1995 b), *Standard Test Method for Measuring pH of Soil for Use in Corrosion Testing*, is also available. ASTM D4972 was chosen for testing the backfill materials because it was important that the pH be measured similar to the pH measurement requirements, *Method of Determining pH of Soil*, of the California Department of Transportation (Caltrans) California Test 643, *Method for Estimating the Service Life of Steel Culvert* (Caltrans 1993). Caltrans has a service-life prediction equation that relies on pH data acquired by testing according to their test procedure. It was important that the collected data be compatible with the service-life prediction equation so that this existing method of service-life prediction can be compared to any new models that are proposed as a result of this experimental program. The ASTM D4972 and Caltrans California Test 643 test methods use a sample of sieved material mixed in equal proportion with distilled water to form a soil-water slurry, and each requires a stabilization period of one hour. One difference between these two methods is that before the soil-water slurry is made, ASTM D4972 requires that the soil be "air dried," whereas the Caltrans California Test 643 does not specify a soil dryness requirement. ASTM G51 differs due to the requirement that the pH be measured without adding water to the soil. ASTM G51 states that water addition should not occur because

the added moisture can change the pH of poorly buffered soil. The amount of moisture present in the sample could significantly affect the pH reading. The characterization testing for pH found that CC has the highest pH of 11.8, followed by a pH of 8.6 for the CFM, and a pH value at 7.4 for the RAP.

3.2.1.8 Resistivity

Measurements of the minimum soil resistivity of each of the backfills were made according to the *Laboratory Method of Determining Minimum Resistivity* procedure outlined in Caltrans California Test 643 (Caltrans 1993). Resistivity was measured with a Miller Soil Box and Nilsson Soil Resistance Meter Model 400. The inside dimensions of the plexiglass soil box was 1.5 inches (39.37 mm) wide by 8.75 inches (222.3 mm) long by 1.25 inches (31.90 mm) deep. The dimensions of the soil box are such that the resistivity value can be directly obtained from the resistance meter. The soil box test setup is similar to that found in ASTM G57 (1995 a), *Standard Test Method for Field Measurement of Soil Resistivity Using the Wenner Four-Electrode Method*. This characterization testing found that CFM has the highest resistivity at 4400 ohm-cm, followed by RAP at 1700 ohm-cm, and CC at 410 ohm-cm.

3.2.1.9 Soluble Salts

The soluble salts that can promote corrosion are chlorides, sulfates, and sulfides (Elias 1990). ASTM D4327 (1997 c), *Chemically Suppressed Ion Chromotography*, was used for characterization of the backfill materials for chloride ions.

ASTM D4327, was also used to determine the concentration of sulfate ions in the backfill materials. This method was selected not only for its accuracy but also because it can quantify both chloride and sulfate ions in water in one test. Only water soluble sulfates, not total sulfates, are of concern for corrosion testing purposes (Eyre and Lewis 1987). The ASTM D4327 test method can detect seven common anions. The ion chromatography testing was done using a Dionex® DX-80 Ion Analyzer. The ion

chromatograph sample loop size was 0.000338 oz (10 µL). The analytical column used in the ion chromatograph was the Dionex® IonPac® AS14A. To analyze a sample, 0.0338 oz (1 ml) of the sample was injected into the ion chromatograph using a 0.0338 oz (1 ml) Becton Dickinson® sterile, single use syringe. The sample was injected through a 0.000007874 inch (0.20 µm) Corning® sterile syringe filter. The filter is required to avoid clogging the resin of the columns (ASTM D4327 1997 c).

Sulfides have typically been analyzed qualitatively for corrosion testing purposes (Eyre and Lewis 1987). However, quantitative measurement is possible. ASTM D4658 (1996), *Procedure for Sulfide Ion in Water,* is a quantitative test that was used to measure the sulfide concentration of the pore solutions from the different backfill materials. This method requires the use of an ion-selective electrode to determine the sulfide ion concentration in water.

Samples for chloride, sulfate, and sulfide analysis were collected and stored in a refrigerator at approximately 40^{o}F (4.4^{o}C) prior to testing. The samples collected for sulfide analysis were stored in a separate container because chemicals were added to preserve the sample. ASTM D4658 required that 2 molar zinc acetate and 6 molar sodium hydroxide be added to the samples collected for sulfide analysis. ASTM D4658 specifies that for a 3.38 oz (100 ml) bottle, 4 drops of 2 molar zinc acetate be added and 1 drop of 6 molar sodium hydroxide be added after the bottle is filled three-fourths of the way with the test sample. The samples collected for characterization were 4.22 oz (125 ml), therefore 5 drops of 2 molar zinc acetate were added along with 2 drops of 6 molar sodium hydroxide after the bottle was filled three-fourths of the way with the test sample.

ASTM D4658 requires that the bottle used to collect the sample should be stoppered and no air bubbles should be trapped beneath the stopper. This is required because trapped air can oxidize the sulfide and convert it to sulfate. The 4.23 oz (125 ml) Nalgene bottles were completely filled and capped off, and an effort was made to trap no air beneath the cap. The ion selective electrode used to find the sulfide concentration was an Orion® Silver/Sulfide Electrode Model 9616, which was calibrated using the solutions created by following ASTM D4658. A Denver® model 250 pH/ISE/conductivity meter was used to display the readings.

Soluble salt content characterization tests were performed on the decanted backfill solutions to determine if there was a significant change in the decanted solution due to the number of drainages. The solutions collected from the first drainage of distilled water through the backfills during the STT were used to characterize the backfill materials for chloride, sulfate, and sulfide. The concentration of chloride and sulfate ions was found following ASTM D4327 (1997 c). The chloride concentration for the backfill materials was 38 mg/L for CFM, 21 mg/L for CC, and 104 mg/L for RAP. The sulfate concentration for the backfill materials was 49 mg/L for CFM, 24 mg/L for CC, and 153 mg/L for RAP. The RAP had chloride and sulfate concentrations at least three times higher than the other backfill materials. No sulfides were detected in any of the backfill materials.

3.2.1.10 Oxidation-Reduction Potential

The solutions collected from the first drainage of distilled water through the backfills during the STT were used to characterize the backfill materials' redox potential. The redox potential was measured with a platinum electrode connected to a multimeter, which provided the capability of direct redox potential measurements that were pH adjusted. Currently, there is no ASTM standard for the measurement of redox potential. The redox potential of the backfill materials was 187 mV for CFM, -31 mV for CC, and 120 mV for RAP. Lower values indicate anaerobic conditions and increased susceptibility to microbial attack, while higher values indicate the presence of oxygen (Elias 1990).

3.2.1.11 Shape and Surface Characteristics

Current methods for analyzing shape and surface properties are subjective and relationships are lacking between shape and surface characterization data produced by these methods with performance parameters such as bonding, shear strength, and stiffness (Fletcher et al. 2002). Relationships are also lacking between shape and surface

properties and their influence on corrosion. The angularity and surface texture of coarse aggregate can be evaluated by counting the percentages of particles with one and with two or more crushed faces in a representative sample (Mamlouk 1999). This task can be laborious and subjective. Fine aggregate angularity and surface texture can be measured indirectly using the AASHTO TP33 Method A, *Test for Uncompacted Void Content of Fine Aggregate* (Mamlouk 1999).

Due to the limitations of current aggregate shape and surface characteristic measurement techniques, and because aggregate angularity and texture can influence corrosion, the backfill materials were evaluated using an innovative Aggregate Imaging System (AIMS) at Texas A&M University shown in Figure 3.2. Research by Al-Rousan et al. (2005) conducted with the AIMS developed an aggregate shape classification system shown in Table 3.5. The system was used to gather data on aggregate shape and surface characteristics, namely angularity, texture, and form of the backfill materials.

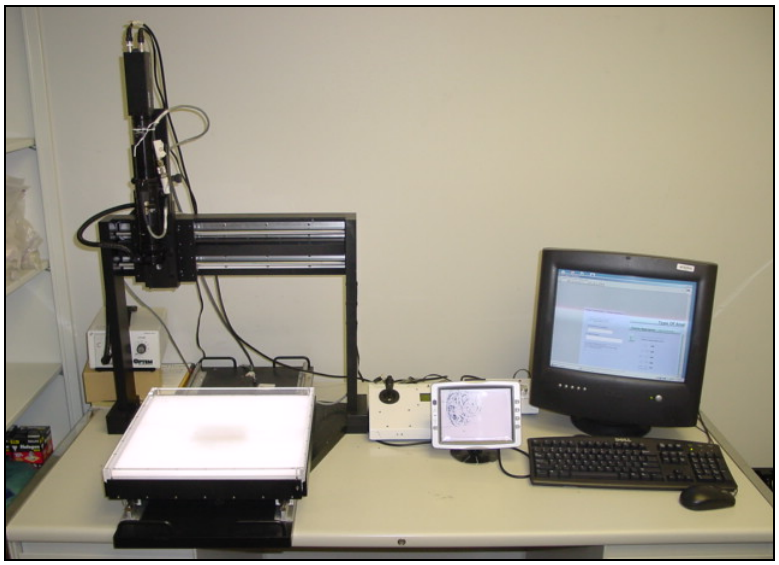

Figure 3.2. AIMS for Characterizing the Shape and Surface Characteristics of Fine and Coarse Aggregates.

The angularity was measured using gradient and radius methods for fine and coarse aggregate. The angularity gradient method measures the change in gradient along a particle boundary to quantify this parameter (Chandan et al. 2004). The angularity

radius method measures "the difference between the particle radius in a certain direction and that of an equivalent ellipse" in order to quantify angularity (Al-Rousan et al. 2005). Studies by Al-Rousan et al. (2005) suggested that the gradient method is more sensitive to angularity than the radius method. In the classification scale proposed by Al-Rousan et al. (2005), there are four angularity categories: angular, sub-angular, sub-rounded, and rounded.

The texture refers to the smoothness or roughness of the surface. AIMS measures texture by capturing images of the particle surface. The local variation in the pixel gray-intensity values from the captured image represents the texture (Fletcher et al. 2003). The image is processed and decomposed into a series of transformed images using wavelet analysis and then statistical parameters are computed from these images to quantify the texture (Chandan et al. 2004). The classification scale proposed by Al-Rousan et al. (2005) contains five texture categories: high roughness, moderate roughness, low roughness, smooth, and polished.

Al-Rousan et al. (2005) quantifies particle form based on two-dimensions (projection) or three-dimensions (sphericity). The form is found by measuring particle dimensions. If three dimensions are measured, the sphericity is found by using the longest dimension, the intermediate dimension, and the shortest dimension. The form measurement for projections is polar and is based on the magnitude of incremental differences in angles as measurements are made about different radii around the particle. The sphericity measurement relies on the two-dimensional projection and measurement of particle depth. The classification system has four categories for sphericity: high sphericity, moderate sphericity, low sphericity, and flat/elongated; and four categories for projection: circular, semi-circular, semi-elongated, and elongated. The aggregate shape classification system chart for angularity, texture, and form is shown in Table 3.5.

Table 3.5. Aggregate Shape Classification System Proposed by Al-Rousan et al. (2005).

Property	Scale				
Angularity	Angular	Sub-Angular	Sub-Rounded	Rounded	
	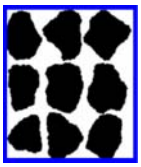	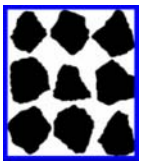		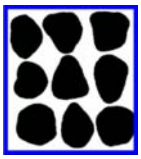	
Gradient[a]	> 4500	3000 - 4500	2000 - 3000	< 2000	
Radius[a]	> 10	7 - 10	5 - 7	< 5	
Texture[b]	High Roughness	Moderate Roughness	Low Roughness	Smooth	Polished
		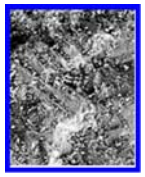	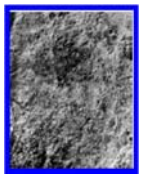	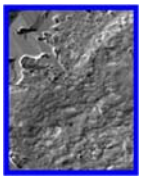	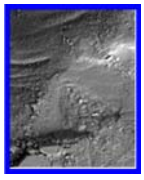
	> 750	550 - 750	350 - 550	200 - 350	< 200
Form					
Sphericity (3-D)[b]	High Sphericity	Moderate Sphericity	Low Sphericity	Flat/Elongated	
					
	> 0.8	0.6 - 0.8	0.5 - 0.6	< 0.5	
Projection (2-D)[a]	Circular	Semi-Circular	Semi-Elongated	Elongated	
					
	< 6	6 - 8	8 - 11	> 11	

[a]Measurement applicable to all sizes of aggregate.
[b]Measurement applicable to coarse aggregate.

Coarse and fine aggregate samples of each backfill material were measured using AIMS. The backfill materials were sampled according to ASTM D75 (1997 b). The aggregate samples were then sieved. After sieving, the coarse and fine aggregate samples were reduced to the size needed according to ASTM C702 Method A (1998 a), *Standard Practice for Reducing Samples of Aggregate to Testing Size, Method A - Mechanical Splitter*. Fifty-six particles of coarse aggregate were required for the measurement of angularity, texture, and sphericity for each backfill material. The coarse aggregate particles measured for the backfill materials were those that passed the 0.375 inch (9.50 mm) sieve and were retained on the No. 4 (4.75 mm) sieve. The coarse aggregate backfill material particles were rinsed with tap water and then air dried at room temperature for over 24 hours before measuring the particles with the AIMS. Measurements were made on all 56 of the coarse aggregate particles.

Approximately 0.165 lb (75 grams) of fine aggregate particles from each of the backfill materials was measured to quantify the angularity and form of the backfill materials. Sphericity measurements of the backfill materials' fine aggregate particles were not made because it is difficult to measure such small particles in three dimensions, and the sphericity had already been measured on the coarse aggregate. Texture measurements were not made on the fine aggregates because better images can be taken of the coarse aggregate. Al Rousan et al. (2005) found that changes in size for the same aggregate source did not have a noticeable affect on texture. Two sizes of fine aggregate particles were measured for the backfill materials; those that passed the No. 8 (2.36 mm) sieve and were retained on the No. 16 (1.18 mm) sieve; and those that passed the No. 16 (1.18 mm) sieve and were retained on the No. 30 (0.60 mm) sieve. The fine aggregate particles were not rinsed after sieving. AIMS made random measurements of these particles.

The results of the AIMS measurements for angularity are shown in Table 3.6. This table shows the percent of particles that fall within each angularity category. The CFM coarse aggregate has a higher percentage of rounded particles when compared to the CC and RAP. The RAP fine aggregate particles were found to be slightly more angular than the CFM and CC because for a given percent of particles, the RAP often has

a higher gradient and/or radius angularity than the CFM and CC. Graphs of the angularity, texture, and form measurements for the backfill materials are shown in Appendix A. Each graph in Appendix A shows the distribution of percent of particles versus one of the aggregate shape classification categories proposed by Al-Rousan et al. (2005). Morris and Delphia 1999 state that with respect to compaction, dry density should decrease with increasing angularity of particles. This statement holds true for the CFM, CC, and RAP.

Table 3.6. Angularity Classification of the Backfill Materials' Particles.

Property	**Percent of Particles**			
Angularity	Angular	Sub-Angular	Sub-Rounded	Rounded
Gradient				
No. 4 (4.75 mm)				
CFM, n = 56	21	27	27	25
CC, n = 56	21	36	28	15
RAP, n = 56	17	41	27	15
No. 16 (1.18 mm)				
CFM, n = 147	31	34	29	6
CC, n = 139	28	25	26	21
RAP, n = 119	36	39	17	8
No. 30 (0.60 mm)				
CFM, n = 207	27	35	27	11
CC, n = 246	27	37	24	12
RAP, n = 165	39	36	12	13
Radius				
No. 4 (4.75 mm)				
CFM, n = 56	11	26	41	22
CC, n = 56	11	35	32	22
RAP, n = 56	17	34	31	18
No. 16 (1.18 mm)				
CFM, n = 147	18	38	32	12
CC, n = 139	7	35	36	22
RAP, n = 115	15	38	34	13
No. 30 (0.60 mm)				
CFM, n = 193	12	41	33	14
CC, n = 226	14	30	32	24
RAP, n = 151	19	46	24	11

Note: n refers to the number of measurements made.

The results of the texture measurements are shown in Table 3.7. None of the backfill materials have a high roughness or polished texture. CFM has the roughest texture of the three backfill materials.

Table 3.7. Texture Classification of the Backfill Materials' Particles.

Property	**Percent of Particles**				
Texture	High Roughness	Moderate Roughness	Low Roughness	Smooth	Polished
No. 4 (4.75 mm)					
CFM, n = 56	0	37	61	2	0
CC, n = 56	0	10	79	11	0
RAP, n = 56	0	17	77	6	0

Note: n refers to the number of measurements made.

The results of the form measurements are shown in Table 3.8. The backfill materials had no flat/elongated coarse aggregate particles. The percentage of elongated fine aggregate particles was less than ten percent for each of the three backfill materials. The RAP fine aggregate particles had a slightly higher percentage of elongated particles when compared with the CFM and CC. A higher percentage of circular coarse aggregate particles were measured for the CC than those found in the CFM and RAP.

Table 3.8. Form Classification of the Backfill Materials' Particles.

Property	**Percent of Particles**			
Form				
Sphericity (3-D)	High Sphericity	Moderate Sphericity	Low Sphericity	Flat/Elongated
No. 4 (4.75 mm)				
CFM, n = 56	10	61	29	0
CC, n = 56	5	68	27	0
RAP, n = 56	7	84	9	0
Projection (2-D)	Circular	Semi-Circular	Semi-Elongated	Elongated
No. 4 (4.75 mm)				
CFM, n = 56	27	36	37	0
CC, n = 56	30	46	22	2
RAP, n = 56	24	44	32	0
No. 16 (1.18 mm)				
CFM, n = 147	13	48	30	9
CC, n = 139	20	44	28	8
RAP, n = 117	7	43	40	10
No. 30 (0.60 mm)				
CFM, n = 200	18	73	3	6
CC, n = 239	18	42	35	5
RAP, n = 151	13	37	40	10

Note: n refers to the number of measurements made.

In general, the backfill materials have similar angularity, texture, and form. The most notable differences identified between the backfill materials were:

- the CFM coarse aggregate has a higher percentage of rounded particles,
- the RAP fine aggregate is slightly more angular and elongated than the CFM and CC,
- the order of texture from higher roughness to lower roughness is CFM, RAP, and then CC, and
- a higher percentage of circular coarse aggregate particles were found in the CC when compared with the CFM and RAP.

It is unlikely that the small differences in shape and surface characteristics will influence the corrosion performance of the backfill materials.

3.2.1.12 Hydraulic Conductivity (Coefficient of Permeability)

Backfill for MSE walls should have a high level of permeability to minimize as much as possible the hydraulic pore pressure on the MSE wall. Gradation specifications for MSE walls often impose limits on the amount of fines allowed in a backfill in an effort to maintain a high level of permeability behind the MSE wall.

The backfill materials used in this experimental program were tested by Ogolla (2002) to determine the hydraulic conductivity by performing ASTM D2434 (2000 a), *Standard Method for Permeability of Granular Soils*. This test method specifies that any particles retained on the 3/4 inch (18.75 mm) sieve not be used in the permeability test specimens. Due to this requirement, Ogolla (2002) modified the reference gradation for the backfill materials to create a permeability gradation to be used for all the permeability tests with one exception - the as-received CC used in the experimental program included particles passing the No. 200 (0.08 mm) sieve. The exception was made for the CC to evaluate the reduction in permeability due to the presence of the fines (Ogolla 2002). The permeability gradations used by Ogolla (2002) are shown in Table 3.9.

Table 3.9. Permeability Test Gradations Used by Ogolla (2002).

Sieve Size	Diameter (mm)	Reference Gradation Percent Passing	Permeability Gradation Percent Passing	As-received CC Permeability Gradation Percent Passing
2 inches	50.00	100.0	100.0	100.0
1 inch	25.00	88.0	100.0	100.0
3/4 inch	18.75	76.5	100.0	100.0
1/2 inch	12.50	65.0	85.0	84.0
No. 4	4.75	35.0	45.7	53.6
No. 8	2.36	22.0	28.7	40.1
No. 16	1.18	15.0	19.5	29.3
No. 40	0.43	7.0	8.9	13.3
No. 200	0.08	0.0	0.0	1.6

One concern with using CC as backfill for MSE walls is whether unused portions of the cement binder within the CC will re-hydrate and reduce the permeability. Ogolla (2002) studied the effect of hydration of cement on the permeability of the CC. Samples for testing the hydration of cement on the permeability of the CC were prepared following a mix proportion estimated by using ACI 211, *Selecting Proportions for Normal, Heavyweight, and Mass Concrete* (Ogolla 2002). The laboratory created CC samples were crushed, sieved, and mixed to the permeability gradation shown in Table 3.9 (Ogolla 2002). Then the laboratory created CC samples were compacted into permeameters and the hydraulic conductivity was measured following ASTM D2434 test method (Ogolla 2002). Table 3.10 shows ranges of hydraulic conductivity of various materials for comparison with the measured values. The samples were compacted to meet the target dry density in Table 3.3 following Tex-113-E (Ogolla 2002). The laboratory created CC was crushed, prepared, and compacted at two different time periods, 4 days and 49 days after the concrete was mixed (Ogolla 2002). Permeability testing was done 3 days after compaction and 39 days after compaction to study the change in hydraulic conductivity due to hydration of unused cement binder in the laboratory created CC (Ogolla 2002). The results in Table 3.11 show that there was a 36 percent reduction in the average hydraulic conductivity between the laboratory created CC tested at 3 days and the samples tested at 39 days that was crushed, prepared, and compacted 4 days after mixing the concrete. This reduction in permeability indicates that hydration of the laboratory prepared CC likely occurred. However, there was no reduction in average hydraulic conductivity between the laboratory created CC tested at 3 days and the samples tested at 39 days that was crushed, prepared, and compacted 49 days after mixing the concrete. This could be because the additional curing time of the concrete used in the laboratory created CC samples allowed the cement binder to more fully hydrate. The data in Table 3.11 shows a 42 percent reduction in hydraulic conductivity between the CC tested with the permeability gradation and the CC with the as-received gradation. The as-received CC contains more fines, as shown by Table 3.9, which causes a significant reduction in permeability when compared to CC with particles finer than the No. 200 (0.08 mm) removed. The results show that the RAP has the

highest permeability, followed by the CFM, and then the CC. The higher permeability of RAP is likely due to the asphaltic coating over the particles. Since asphalt is hydrophobic, water tends to flow around the particles more easily. The results show RAP as five times more permeable than the CFM and six times more permeable than the CC. Ogolla (2002) noted that all three materials could be considered well-drained and the hydraulic conductivities for the backfill materials fall within the range of well-sorted sands as shown in Table 3.10. However, testing at Texas A&M University indicated that the CC samples may continue to hydrate after 39 days, further reducing the permeability.

Table 3.10. Hydraulic Conductivity Ranges for Unconsolidated Sediments (after Fetter 2001).

Material	Hydraulic Conductivity (in/sec)	(cm/sec)
Clay	4^{-10} to 4^{-7}	10^{-9} to 10^{-6}
Silt, sandy silts, clayey sands, till	4^{-7} to 4^{-5}	10^{-6} to 10^{-4}
Silty sands, fine sands	4^{-6} to 4^{-4}	10^{-5} to 10^{-3}
Well-sorted sands, glacial outwash	4^{-4} to 4^{-2}	10^{-3} to 10^{-1}
Well-sorted gravel	4^{-3} to 4^{-1}	10^{-2} to 1

Table 3.11. Hydraulic Conductivity Values for the Backfill Materials Reported by Ogolla (2002).

Material	Gradation Type	Time from Compaction to Test (Days)	Dry Density Average (lb/ft^3)	Dry Density Average (kg/m^3)	Dry Density Standard Deviation (lb/ft^3)	Dry Density Standard Deviation (kg/m^3)	Hydraulic Conductivity Average (in/sec)	Hydraulic Conductivity Average (cm/sec)	Hydraulic Conductivity Standard Deviation (in/sec)	Hydraulic Conductivity Standard Deviation (cm/sec)
Laboratory Created CC[a]	Permeability	3	120	1922	1.11	17.8	$3.9X10^{-3}$	$9.8X10^{-3}$	$1.5X10^{-3}$	$3.7X10^{-3}$
Laboratory Created CC[a]	Permeability	39	123	1970	0.64	10.3	$2.5X10^{-3}$	$6.3X10^{-3}$	$6.3X10^{-4}$	$1.6X10^{-3}$
Laboratory Created CC[b]	Permeability	3	122	1954	1.61	25.8	$3.5X10^{-3}$	$9.0X10^{-3}$	$8.3X10^{-4}$	$2.1X10^{-3}$
Laboratory Created CC[b]	Permeability	39	121	1938	0.87	13.9	$4.7X10^{-3}$	$1.2X10^{-2}$	$9.1X10^{-4}$	$2.3X10^{-3}$
CC	Permeability	39	125	2002	0.88	14.1	$5.1X10^{-4}$	$1.3X10^{-3}$	$9.4X10^{-5}$	$2.4X10^{-4}$
CC	As-received Permeability	39	124	1986	1.51	24.2	$3.0X10^{-4}$	$7.5X10^{-4}$	$1.5X10^{-4}$	$3.7X10^{-4}$
CFM	Permeability	Soon	133	2130	0.63	10.1	$6.7X10^{-4}$	$1.7X10^{-3}$	$3.9X10^{-5}$	$1.0X10^{-4}$
RAP	Permeability	Soon	117	1874	0.46	7.4	$3.4X10^{-3}$	$8.5X10^{-3}$	$3.5X10^{-4}$	$8.8X10^{-4}$

[a]Crushed/compacted 4 days after mixing
[b]Crushed/compacted 49 days after mixing

3.2.2 Earth Reinforcing Strips

Ribbed galvanized-steel and plain-steel earth reinforcing strips were characterized and used in the experimental program. The earth reinforcing strips were acquired from the Reinforced Earth Company. The earth reinforcing strips were characterized by size, shape, and composition.

3.2.2.1 Size

ASTM G162 (1999 a), *Standard Practice for Conducting and Evaluating Laboratory Corrosion Tests in Soils*, recommends that certain details of exposed specimen be reported. The items that should be reported are alloy and temper, metallurgical history, chemical composition, processing parameters for formed parts, coating chemistry, weight, and thickness. The plain-steel earth reinforcement used in this program had approximate dimensions of 1-15/16 inches wide (49 mm) x 78 inches (1980 mm) long by 0.16 inch (4 mm) thick. The galvanized-steel earth reinforcement strips were slightly wider and thicker; 2 inches (51 mm) wide and 0.19 inch (5 mm) thick. The strips also have a 9/16 inch (14 mm) diameter hole. The center of the hole is located 1-1/2 inch (38 mm) from the end of the strip.

The ribs on the plain-steel earth reinforcing strips were located on the top and bottom sides, and in a staggered configuration as shown in Figure 3.3. Two ribs, spaced 1-11/16 inches (43 mm) apart, were located approximately every 7 inches (178 mm) along the length of the plain-steel strips. Two ribs, spaced 1-13/16 inches (46 mm) apart were located approximately every 7-5/16 inches (186 mm) along the length of the galvanized-steel strips. The ribs in the earth reinforcing strips were approximately 0.04 inch (1mm) wide at the top, 0.2 inch (5 mm) wide at the base, and 0.08 inch (2 mm) tall.

These earth reinforcing strips were cut into smaller sample sizes using a band saw so that they could be embedded in the backfill materials for the long and short-term corrosion testing. The chemical composition of the base steel and the composition and

coating weight of the galvanization was determined through testing performed by Atlas Testing Laboratories, Los Angeles, California.

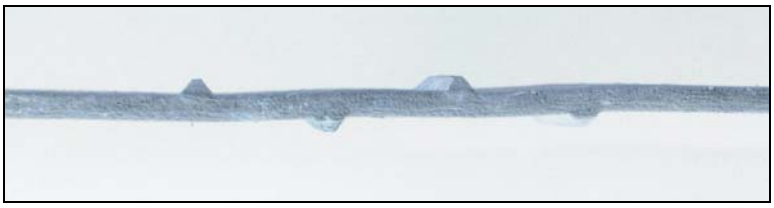

Figure 3.3. Side View of a Galvanized-steel Earth Reinforcing Strip Displaying the Ribs.

3.2.2.2 Chemical Composition

A plain-steel specimen 2 inches (50.8 mm) wide by 2 inches (50.8 mm) long was tested according to ASTM E415 (1999 e), *Standard Test Method for Optical Emission Vacuum Spectrometric Analysis of Carbon and Steel*, and identified the material as Society of Automotive Engineers - American Iron and Steel Institute (SAE-AISI) 1513 steel or Unified Numbering System for Metals and Alloys (UNS) G15130. The chemical composition limits for SAE-AISI 1513 are: 0.10 to 0.16 percent carbon, 1.10 to 1.40 percent manganese, 0.040 percent maximum phosphorus, and 0.050 percent maximum sulfur. The chemical analysis result used to identify the plain-steel material type is shown in Table 3.12.

Table 3.12. Chemical Analysis of Plain-steel Earth Reinforcing Strip Specimen.

Elements	Percent
Carbon	0.15
Chromium	0.10
Copper	0.42
Manganese	1.22
Molybendum	0.05
Nickel	0.27
Phosphorus	0.013
Silicon	0.16
Sulfur	0.021
Iron	Remainder

The steel can be categorized as a Group II SAE-AISI plain carbon steel because it contains 0.15 to less than 0.30 percent carbon. This plain-steel is not considered a mild steel because it contains greater than 0.75 percent manganese. Group II steels with less than approximately 0.75 percent manganese are commonly referred to as mild steels (Davis 1996). In general, carbon steels are best suited to galvanizing when alloying/impurities are less than the following levels: 0.25 percent carbon, 1.3 percent manganese, 0.05 percent phosphorus, and 0.05 percent silicon (Davis 1996).

Approximately 0.07 oz (2 grams) of galvanization was used to perform the wet chemical analysis to discover the chemical composition. ASTM E1097 (1997 a), *Standard Guide for Direct Current Plasma Emission Spectrometry Analysis*, was used to assess the composition of the galvanization and yielded the results shown in Table 3.13. These results show that the galvanized coating is composed of greater than 98 percent zinc.

3.2.2.3 Galvanization Coating Weight

A galvanized-steel specimen 2 inches (50.8 mm) wide by 3 inches (76.2 mm) long by 3/16 inch (4.75 mm) thick was tested to find the galvanization coating weight.

Test method ASTM A90 (2001 d), *Standard Test Method for Weight [Mass] of Coating on Iron and Steel Articles with Zinc Coatings* was performed. The coating weight for the specimen was 3.31 oz/ft^2 (1.01 kg/m^2) of sheet. This coating weight corresponds to an average galvanized coating thickness of 5.5 mil (140 μm), which surpasses the minimum sacrificial galvanized coating thickness for earth reinforcement required by the FHWA, which is 3.4 mil (86 μm) corresponding to a coating weight of 2 oz/ft^2 (0.61 kg/m^2).

Table 3.13. Chemical Composition of the Galvanized Coating on the Galvanized-steel Earth Reinforcing Strips.

Elements	Percent
Aluminum	<0.01
Boron	<0.01
Cadmium	0.03
Chromium	<0.01
Cobalt	<0.01
Copper	0.04
Iron	0.59
Lead	1.1
Magnesium	<0.01
Manganese	<0.01
Nickel	<0.01
Silicon	<0.01
Tin	0.04
Titanium	<0.01
Zinc	Remainder

The thickness of the galvanized-steel earth reinforcement was confirmed using an optical microscope. Two samples were selected at random and prepared for microscopic measurement of the galvanized coating thickness. Three microscopic measurements were randomly made of the galvanized coating on each sample. The average galvanized coating thickness determined by microscopic examination was approximately 6 mil (150 μm). Figure 3.4 shows the result of one of the microscopic measurements. These measurements confirmed the average coating weight found by using test method

ASTM A90 (2001 d). ASTM A90 is considered the more accurate method for determining the coating thickness.

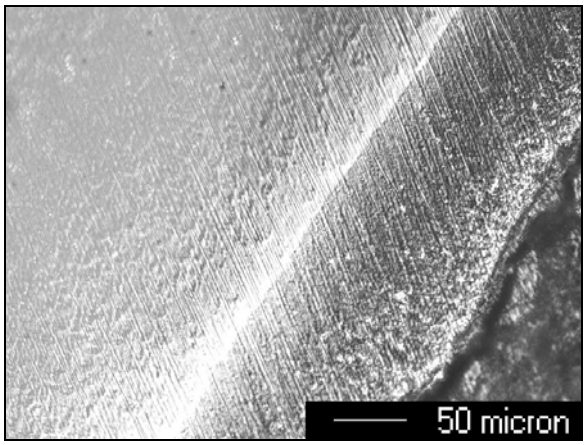

Figure 3.4. Typical Micrograph of the Galvanized Coating on a Galvanized-steel Earth Reinforcing Strip.

3.3 CORROSION TESTING METHODS

3.3.1 Short-term Corrosion Test Program

A description of the experimental design, test setup, and test procedure for the short-term testing program is provided in this subsection. The methods and materials used for performing the short-term testing are also described. The short-term testing consisted of placing samples in corrosion cells with a decanted solution from the backfill materials to monitor the corrosion with respect to time.

3.3.1.1 Experimental Design

The short-term testing consists of monitoring the corrosion of plain-steel and galvanized-steel samples in decanted solutions from the backfill materials. The parameter of interest is the backfill material corrosivity. Backfill material corrosivity

should be examined with regard to backfill type, reinforcement type, and exposure condition. Since backfill materials for MSE walls are repeatedly exposed to drainage cycles, it was thought that the pore solution of the backfill materials could change with time. Therefore, the number of drainages through the backfill was an additional variable that was examined. Since this variable has not been previously examined and its effects are uncertain, the pore solution from the backfill materials was evaluated after different drainage cycles. It should be noted that it might be difficult to determine the effect of the number of drainages on backfill corrosivity in the long-term testing because the condition of the reinforcement may change as a function of the number of drainages. Since the pore solution can have a significant impact on corrosion performance, short-term testing was performed using decanted pore solutions from the first drainage and the one-hundredth drainages.

For the short term testing, the backfill, reinforcement, chloride concentration, and pore solution drainage cycle were variables that could influence backfill corrosivity. These variables were controlled in the experiment. The three backfill materials (CFM, CC, and RAP), two reinforcement types (galvanized-steel [G] and plain steel [S]), two chloride concentrations (high chlorides [CL] and low chlorides [NCL]), and two pore solutions (first drainage [1] and one-hundredth drainage [100]) were examined. Thus, there are 24 levels to the experiment. The sample names were determined by the controlled variables in the short-term testing experiment as shown in Table 3.14.

The number of samples required for each level of the experiment was not calculated prior to the start of testing because preliminary test data with means and standard deviations on the data of interest (mass loss and current density) for this type of experiment were unavailable. Therefore, it was decided that three replicates should be made for each level. Three replicates would allow calculation of a standard deviation for the data obtained on each level. Since the need for statistical analysis of the data was anticipated, random number generation was used to match the backfill, chloride concentration, and drainage number to each reinforcement sample. Randomizing the experiment is important because it increases confidence that it was the difference in

treatments (observed conditions thought to influence a response) that resulted in a difference in response (Montgomery 1999).

Table 3.14. Determination of Level Names Based on the Controlled Variables for STT.

Backfill Type	Reinforcement Type	Chloride Concentration	Drainage Number	Level Name
CFM	G	CL	1	CFM_G_CL_1
			100	CFM_G_CL_100
		NCL	1	CFM_G_NCL_1
			100	CFM_G_NCL_100
	S	CL	1	CFM_S_CL_1
			100	CFM_S_CL_100
		NCL	1	CFM_S_NCL_1
			100	CFM_S_NCL_100
CC	G	CL	1	CC_G_CL_1
			100	CC_G_CL_100
		NCL	1	CC_G_NCL_1
			100	CC_G_NCL_100
	S	CL	1	CC_S_CL_1
			100	CC_S_CL_100
		NCL	1	CC_S_NCL_1
			100	CC_S_NCL_100
RAP	G	CL	1	RAP_G_CL_1
			100	RAP_G_CL_100
		NCL	1	RAP_G_NCL_1
			100	RAP_G_NCL_100
	S	CL	1	RAP_S_CL_1
			100	RAP_S_CL_100
		NCL	1	RAP_S_NCL_1
			100	RAP_S_NCL_100

Abbreviations: Conventional Fill Material (CFM), Crushed Concrete (CC), Recycled Asphalt Pavement (RAP), Galvanized-steel (G), Plain-steel (S), Chloride (CL), and Negligible Chloride (NCL)

The testing program consisted of performing characterization tests on the decanted backfill solution, electrochemical tests, and mass loss testing when the samples were removed from the corrosion cells. The characterization test program for the decanted backfill solutions is shown in Table 3.15. The objective of this test program was to determine if there was a significant change in the decanted solution due to the number of drainages. Descriptions of the characterization test methods on the decanted pore solutions from the different backfill materials were previously reported. The testing program for the corrosion cells is summarized in Table 3.16.

Table 3.15. Testing Program for Decanted Backfill Material Pore Solutions.

Characterization Test	ASTM Designation	Performed on Drainages
Resistivity	G57	1, 10, 20, 50, 100
pH	D4972	1, 10, 20, 50, 100
Redox potential	None	1, 10, 50, 100
Sulfate	D4327	1, 10, 100
Chloride	D4327	1, 10, 100
Sulfide	D4658	1, 10, 100

Polarization resistance and cyclic polarization testing were used to evaluate the corrosion activity of the samples in the corrosion cells. More frequent polarization resistance testing was required at the beginning of the test because the rate of change of the corrosion rate is often higher. Cyclic polarization testing was performed at the end of the testing period due to the destructive nature of the test.

Table 3.16. Testing Program for the Samples while in the Corrosion Cells.

Test Type	Target Test Time[a] (Days)	Target Test Time[a] (Hours)
Polarization Resistance	1	24
Polarization Resistance	2	48
Polarization Resistance	4	96
Polarization Resistance	7	168
Polarization Resistance	14	336
Polarization Resistance	21	504
Polarization Resistance	28	672
Cyclic Polarization	29	696

[a]The target test times are measured from the time that the samples were placed in the cells and the oxygen purging begun.

The final test performed on the reinforcement samples in this program was mass loss testing. The mass loss testing was performed according to ASTM G1 (1994 a).

3.3.1.2 Experimental Setup

3.3.1.2.1 Preparation of Samples

The earth reinforcing strips were cut into 1 inch (25 mm) by 1 inch (25 mm) samples. After the samples were cut to the required dimensions, all corners and edges of the sample were filed until rounded. This was done so that when the samples were epoxied, the epoxy would be more evenly distributed around the edges and corners and the likelihood of epoxy cracking would be reduced. After filing, all the edges, corners, and each surface of the sample that was cut was sanded with 320 grit sandpaper. Sanding was done to improve the bond between the epoxy and the sample. Care was taken to not damage the "as-received" surface condition of the reinforcing strip samples. After sanding, the samples were drilled and tapped to facilitate mechanical connection.

After drilling and tapping, the samples were cleaned in an ultrasonic cleaner with denatured ethyl alcohol. The cleaning time was 10 minutes for each sample. The plain-steel and galvanized-steel samples were cleaned in separate batches of ethyl alcohol.

After cleaning, the samples were allowed to dry, and each sample was then weighed to the nearest $3.5X10^{-6}$ oz (10^{-4} g). The weight was recorded as "weight before epoxy."

Sikadur® 35, high-modulus low-viscosity, high-strength, epoxy grouting/sealing/binder adhesive produced by Sika® corporation was used to coat the edges of the samples. The epoxy conforms to ASTM C881 (1999 c), *Standard Specification for Epoxy-Resin-Base Bonding Systems for Concrete*, Types I and II, Grade I, Class B and C, epoxy resin adhesive. The viscosity of the epoxy is approximately 375 cP. For comparison, water has a viscosity of 1 cP and 10W - 30 motor oil has a viscosity in the range of 150 - 200 cP. The epoxy was applied to the samples by hand with a camel hair brush. Care was taken so that epoxy did not run down over the exposed area of the samples. Two coats of epoxy were applied to each sample.

After the samples were epoxied, the samples were cleaned again in denatured ethyl alcohol in the ultrasonic cleaner for 10 minutes. After cleaning, the samples were re-weighed to the nearest $3.5X10^{-6}$ oz (10^{-4} g). The weight was recorded as "weight after epoxying." The samples were weighed twice (i.e., before and after epoxy application) because if the epoxy comes off during mass loss testing, the weight with no epoxy would be needed to calculate the mass loss. After weighing the samples, pictures of the front and back of each sample were taken. The samples were randomly assigned to the corrosion cells. The pictures of each sample were taken with its identification, which designates the exposure condition that the sample was randomly assigned. Figure 3.5. shows a photo of a sample that was used in one of the corrosion cells. The samples were then stored in plastic bags in a desiccator until the day they were to be placed into the corrosion cells for testing.

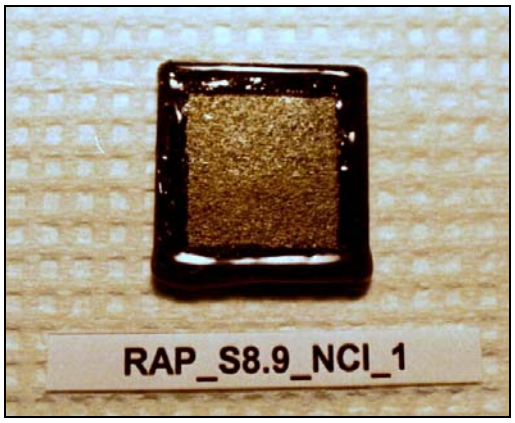

Figure 3.5. Typical Steel Sample Following Preparation for STT.

The counter electrodes for the corrosion measurements were 1 inch (25 mm) by 1 inch (25 mm) 52 mesh pure platinum wire gauze tack welded to an American Wire Gauge (AWG) 20 (0.81 mm) diameter 99.95 percent platinum wire 6 inches (152 mm) long. A counter electrode with a geometric area of at least twice the surface area of the working electrode, is often used for electrochemical corrosion testing to minimize current limitation by electrode area (Tait 1994). The total area of the wire mesh was determined to be 1.08 in^2 (0.0007 m^2). Therefore, approximately 0.5 in^2 (0.00032 m^2) would be an adequate surface area for the samples (working electrode). The exposed area of the samples used in the experimental program was 0.47 in^2 (0.00031 m^2), which corresponds to an 11/16 inch (17.5 mm) square. Another consideration in the determination of the area of the samples is the ratio of exposed area to the length of the exposed area/epoxy border. This is an important consideration because crevice corrosion can often occur along this border. One assumption that is made in the analysis of the data is that the samples corrode uniformly. Therefore, crevice corrosion can introduce error into the results. An attempt was made to minimize crevice corrosion by minimizing the ratio of the exposed area to exposed area/epoxy border and by using low viscosity epoxy, which has a smoother transition at the epoxy to steel interface when compared with high viscosity epoxy. The smoother the transition is between the epoxy and the exposed surface, the more likely that crevice corrosion will be reduced.

3.3.1.2.2 Preparation of Backfill Materials

The backfill materials were all prepared by sieving, mixing, and adjusting the moisture content as described in Subsection 3.2.1.1. The backfill materials were placed in 14.5 gal (55 L) Nalgene® carboys. A 6 inch (152 mm) by 8 inch (203 mm) piece of woven silt fabric was placed over the outlet on the inside of the container to limit the loss of fine particles through the outlet. Approximately 11.9 gal (45 L) of backfill material was placed in each container. A solution volume of 2.64 gal (10 L) was poured in with the backfill because at least 1.85 gal (7 L) was needed to perform the tests in the corrosion cells. The backfills were not compacted in the containers according to the recommended dry density in Table 3.3 due to the inability of the containers to support the stress.

3.3.1.2.3 Preparation of the Corrosion Cells

The corrosion cells used in the research were manufactured by EG&G Instruments, Inc., Princeton Applied Research (2000). The Model K47 corrosion cell system was used. This corrosion cell system consists of the following components: corrosion flask, specimen holder, counter electrode holder with counter electrode, reference electrode, bridge tube, purge and vent tube, and a ball and socket clamp. Figure 3.6. shows the corrosion cell system and components. Items that are not standard components of the model K47 that were used in the experiment are platinum counter electrodes and size 24/40 rubber septum stoppers. The reference electrode, specimen holder, and in general, the corrosion cell meet the specifications under the apparatus section of ASTM G5 (1999 b), *Standard Reference Test Method for Making Potentiostatic and Potentiodynamic Anodic Polarization Measurements*. The only difference between the polarization cell described in ASTM G5 and the corrosion cell used is that the corrosion cell did not have a thermometer inserted into the solution chamber. All cell components were properly cleaned prior to use and rinsed with water meeting ASTM D1193 (1999 d), *Standard Specification for Reagent Water*, ranging between Type I and Type II grade.

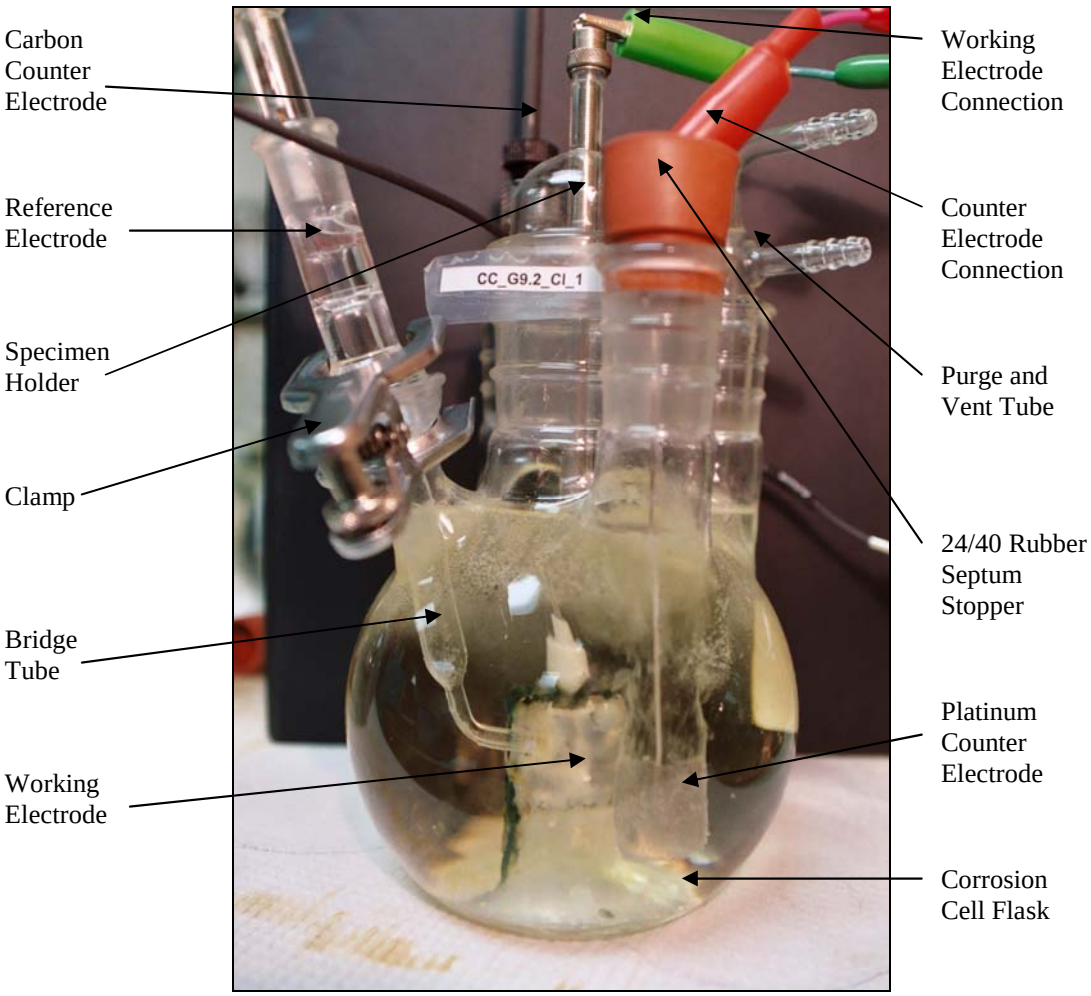

Figure 3.6. Corrosion Cell System and Components Used for the STT.

3.3.1.2.3.1 Corrosion Cell Assembly

After cleaning all the corrosion cell system components, the cells were assembled and randomly labeled. The plain-steel or galvanized-steel samples were attached to the specimen holder as shown in Figure 3.6. The ground-glass portions of the specimen holder, purge and vent tube, counter electrode holder, and reference electrode bridge tube were all greased with Lubriseal® stopcock grease. All of the components were then placed into the corrosion flask.

One graphite rod counter electrode was placed into each cell. The graphite counter electrode was lowered until it just cleared the bottom of the corrosion flask. The rubber septum holding the platinum counter electrode was inserted into the 24/40 joint. The platinum counter electrode was turned so that the 1 inch (25 mm) by 1 inch (25 mm) side faced the sample. The platinum counter electrode was positioned 1-1/2 inches (38 mm) $\pm$ 3/16 inch (5 mm) away from the working electrode.

The exposed area of the working electrode was aligned to face the platinum counter electrode. The end of the bridge tube was positioned so that the frit was approximately 0.04 inch (1 mm) away from the surface of the working electrode. The end of the bridge tube was also positioned so that it did not extend more than 0.04 inch (1 mm) beyond the edge of the epoxy-coated surface (out over the exposed area). Positioning the bridge tube in this way was important to prevent the shielding of current flow between the working electrode and platinum counter electrode. Figure 3.7. shows proper positioning of the bridge tube with reference to the working electrode.

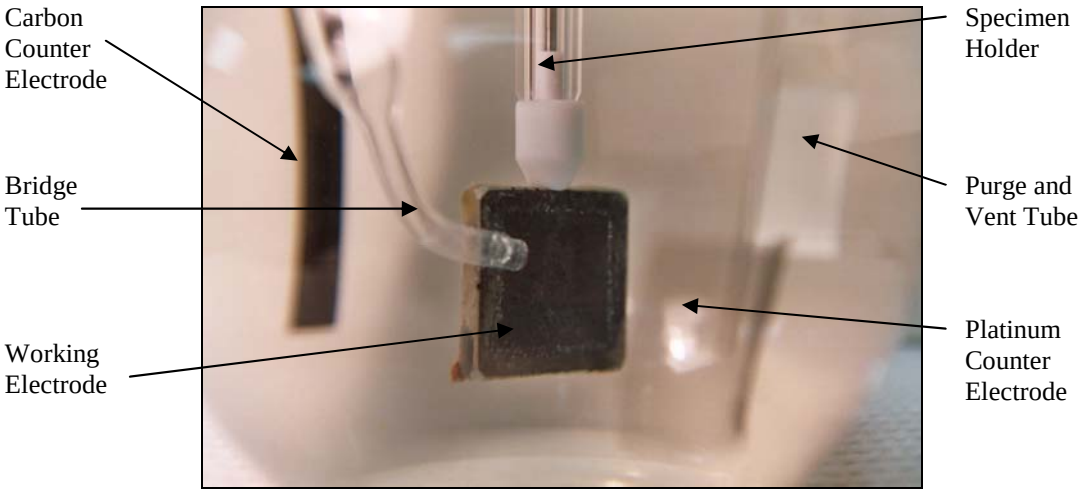

Figure 3.7. Close-up View of the Inside of a Typical STT Corrosion Cell.

The saturated calomel reference electrode was not placed in the bridge tube until the sample was to be tested. The same saturated calomel reference electrode was used throughout the experiment to promote consistency. This reference electrode was stored

with the tip in storage solution when not in use, and was periodically checked to ensure proper function.

3.3.1.2.3.2 Backfill Drainage Collection and Assessment

After the corrosion cells were properly assembled, the specimen holders with the samples were removed from the cells to allow for filling the cells with the decanted backfill solution.

A volume of 2.6 gal (10 L) was poured into the carboys over each backfill material. The volume of solution was determined by the amount of solution required for testing. Approximately 1.85 gal (7 L) of solution was required, 0.264 gal (1 L) per six corrosion cells and 0.264 gal (1 L) to perform characterization tests on the decanted pore solutions. These solutions were characterized for pH, resistivity, redox potential; and chloride, sulfate, and sulfide concentrations.

Figure 3.8. shows the system for collecting the pore solution from the backfill materials. Before collecting the pore solution for analysis, the solution was allowed to remain in the carboy for at least 24 hours. This was done so that the backfill constituents could have additional time to dissolve in the solution prior to drainage so that the drainage more accurately characterizes the actual field material. The solutions were analyzed after the first, 10^{th}, and 100^{th} drainages. Additional pH, resistivity and redox potential readings were obtained at the 20^{th} and 50^{th} drainages. All drainages between those being analyzed were allowed to remain in the container for at least 45 minutes. After 45 minutes, the containers were drained and then refilled for the next drainage. The solution was not left in the containers over 24 hours unless the drainage was to be analyzed. While performing the drainages, there was a considerable difference between the drainage times for the CFM and RAP compared to the CC. It took the solution approximately 30 minutes to drain through the CC, whereas it took approximately 15 minutes for the CFM and RAP. This behavior is in accordance with the permeability study that was performed to characterize the backfill materials referred to earlier. The CC is less permeable than the CFM and RAP. Due to the slower drainage time for the CC, the valve was left open and the solution was allowed to flow from the carboy

continuously for the testing program, except when the drainage needed to remain in the carboy for at least 24 hours. The filtered solutions were collected and then transferred into the corrosion cells (or used for characterization).

Figure 3.8. Drainage Collection from the Backfill Materials for the STT.

3.3.1.2.3.3 Purge System Setup

To ensure similar initial conditions, all cells were purged with oxygen. The backfill solutions in the cells were purged with 99.99 percent pure oxygen for 12 hours at the regulated rate of 0.2 SCFH (Standard Cubic Feet per Hour of equivalent air) (0.00566 m^3/h) after placing metallic samples in the cells. The corrosion cells are shown in Figure 3.9.

Figure 3.9. Purging of Corrosion Cells with Oxygen During the STT.

3.3.1.2.4 Potentiostat Settings

The potentiostat used for the STT program was a Verstat™ II manufactured by Perkin Elmer® Instruments. The potentiostat was controlled by the SoftCorr™ III user interface. The potentiostat settings for the linear polarization resistance testing were setup as shown in Appendix B. The potentiostat settings for the cyclic polarization testing are also shown in Appendix B.

3.3.2 Long-term Corrosion Test Program

The experimental design and setup descriptions for the LTT are provided in this Subsection.

3.3.2.1 Experimental Design

The LTT consists of monitoring the corrosion of plain-steel and galvanized-steel samples embedded in the three backfills. Similar to the STT, the factor of interest was the backfill corrosivity. This factor was examined with regard to backfill material type, reinforcement type, and exposure types. Table 3.17 shows the experimental program and sample identification system for the LTT samples. Eight replications were made at each

level for the measurement of potential readings and mass loss. Two replications were made at each level for the polarization and cyclic polarization resistance testing.

Table 3.17. Determination of Level Names Based on the Controlled Variables for Long-term Testing.

Backfill Type	Reinforcement Type	Chloride Concentration	Level Name
CFM	G	CL	CFM_G_CL
		NCL	CFM_G_NCL
	S	CL	CFM_S_CL
		NCL	CFM_S_NCL
CC	G	CL	CC_G_CL
		NCL	CC_G_NCL
	S	CL	CC_S_CL
		NCL	CC_S_NCL
RAP	G	CL	RAP_G_CL
		NCL	RAP_G_NCL
	S	CL	RAP_S_CL
		NCL	RAP_S_NCL

Abbreviations: Conventional Fill Material (CFM), Crushed Concrete (CC), Recycled Asphalt Pavement (RAP), Galvanized-steel (G), Plain-steel (S), Chloride (CL), and Negligible Chloride (NCL)

Data were collected during the LTT period using different measurements. OCP measurements were taken at predetermined intervals on all the samples to provide an indication of when the reinforcement began to actively corrode. These readings were taken before and after solution application because it was found that dryness of the backfill materials had a significant impact on the corrosion potential readings. The corrosion potential readings could also be useful in monitoring the degradation of the galvanized layer. An assessment of the galvanized layer degradation can be made by monitoring the OCP over time of the galvanized-steel samples and by comparing these readings to the OCP readings of steel samples under the same conditions. Elias (1990) recommended the use of OCP measurements with polarization resistance measurements to provide an effective monitoring scheme of the composition of the exposed surface.

Thus, some samples were equipped for measuring the polarization resistance, which can provide information on the corrosion activity. Polarization resistance measurements were often made both before and after solution application.

At the end of 336 days, the metallic reinforcement was removed from each of the cells and mass loss testing following ASTM G1 (1994 a) was performed. At the end of the LTT, measurements were also made on samples of the backfill materials to determine pH, resistivity, chloride, sulfate, sulfide, and redox potential.

3.3.2.2 Experimental Setup

3.3.2.2.1 Preparation of the Reinforcement Samples

The reinforcement strips were cut into samples using a large band saw. The plain-steel reinforcing strips were cut every 7 inches (178 mm) along the length of the strips to make samples. The galvanized-steel reinforcing strips were cut every 7-5/16 inches (186 mm) along the length of the strips to make samples. Samples were labeled with reference to their location on the reinforcing strip from which it was cut. The sample identifications were derived using this information (e.g., Sample S3.2 came from the second piece cut from the third steel reinforcing strip that was cut). The reinforcing strip edges were ground to round off the cut edges. A hole was drilled and tapped in the samples to accommodate insertion of a 4 inch (102 mm) long 5-40 threaded stainless-steel connection rod. The insertion of the threaded rod into each sample was necessary so that connection to the working electrode could be made for potential readings. The threaded rod protruded to the outside of the form so that a potential meter could be easily connected to take potential readings. After drilling and tapping, the samples were cleaned in an ultrasonic cleaner with denatured ethyl alcohol. The cleaning time was 10 minutes for each sample. The 5-40 threaded stainless steel rod was screwed into the sample after cleaning.

Sikadur® 35 epoxy was applied to all sides of the sample, except for the 1-15/16 inches wide (49 mm) by 4 inches (102 mm) long exposed area on the plain-steel strips and the 2 inches wide (51 mm) by 4 inches (102 mm) long exposed area on the

galvanized-steel strips. The epoxy was also applied to the 5-40 stainless steel rod except for the last 1-1/2 inches (38 mm) of the rod from the end opposite the connection. This section of the rod would protrude through the form. Only one-coat of epoxy was applied to each sample.

3.3.2.2.2 Preparation of the Backfill Forms

The dimensions of the backfill forms were determined by the maximum size aggregate. Since the maximum size aggregate is 1-1/2 inches (38 mm), a form that could accommodate this backfill material was designed. It was determined that the inside dimensions of the backfill form should be 6 inches (152 mm) wide by 10 inches (254 mm) long by 6 inches (152 mm) deep. A perspective view of a form with a plexiglass dam on the top for ponding is shown in Figure 3.10.

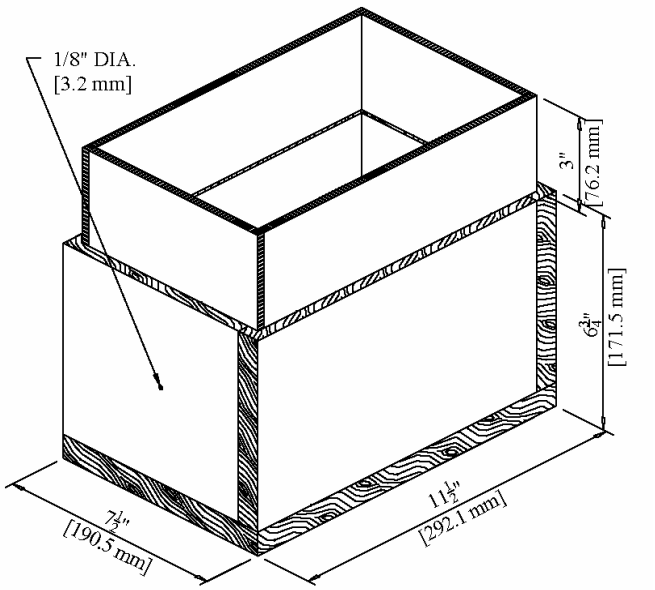

Figure 3.10. Perspective View of Form for Backfill Materials Used During LTT.

The backfill forms were fabricated with epoxied 3/4 inch (19 mm) thick plywood. Drilled into the bottom piece were fifteen 7/16 inch (11 mm) diameter holes spaced 2

inches (51 mm) apart on center, to allow the backfill material inside the backfill form to drain. Figure 3.11. shows the bottom view of the form. Before placing the backfill material in the backfill form, a 6 inch (152 mm) by 10 inch (254 mm) piece of woven silt fabric was placed in the bottom to cover these holes. This was necessary to prevent the loss of fine aggregate particles from the backfill form. A 3/16 inch (5 mm) hole was drilled through one of the end pieces for each backfill form. The hole center was located 3 inches (76 mm) from the inside bottom and top (centered) and 3 inches (76 mm) from the inside sides (centered) of the form. This hole was for the 5-40 threaded connection rod to protrude from the form.

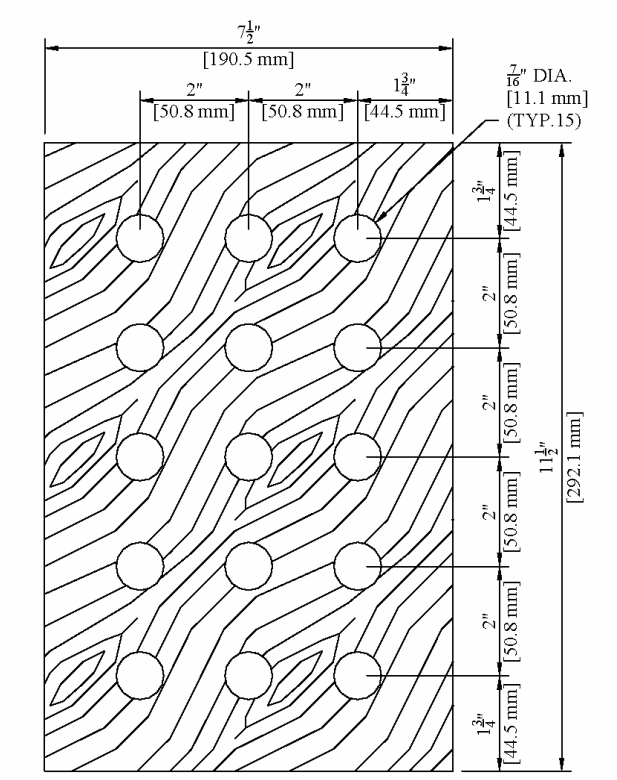

Figure 3.11. Bottom View of Form for Backfill Materials Used for LTT.

The samples to be tested by polarization resistance required slight modification of the forms. A detailed section view of the long-term test setup for performing electrochemical corrosion measurements is shown in Figure 3.12. . An additional

3/16 inch (5 mm) hole was drilled 1/2 inch (13 mm) above the other 3/16 inch (5 mm) hole (measured center to center). This hole was to allow a copper rod that was connected to the counter electrode to protrude from the form. A 3/4 inch (19 mm) diameter hole was drilled through the end piece. The hole center was located 3-1/4 inches (82 mm) from the inside bottom and 3 inches (76 mm) from the inside sides (centered) of the backfill form. This hole was to allow entry of the Luggin type probe.

3.3.2.2.3 Preparation of Probes

The Luggin type probes were made from the following:

- two 1/2 inch (13 mm) polyvinyl chloride (PVC) caps,
- one 1-1/4 inches (32 mm) long piece of 1/2 inch PVC pipe,
- one 2-3/4 inches (70 mm) long piece of 1/2 inch PVC pipe,
- one 1/2 inch-to-1/4 inch (13 mm-to-6.35 mm) PVC female threaded coupling,
- one Swagelok® teflon 1/4 inch (6.35 mm) male connector,
- one 4 inches (long piece of Swagelok® teflon 1/4 inch (6.35 mm) tubing,
- one Vycor® frit, and
- approximately 1.2 oz (35 ml) of 0.1 percent chloride solution.

A section view of the probe is shown in Figure 3.12. . After the probes were filled with the 0.1 percent chloride solution, the end of the probes were soaked in the same solution. The probe was then checked and any noticeable air bubbles were removed.

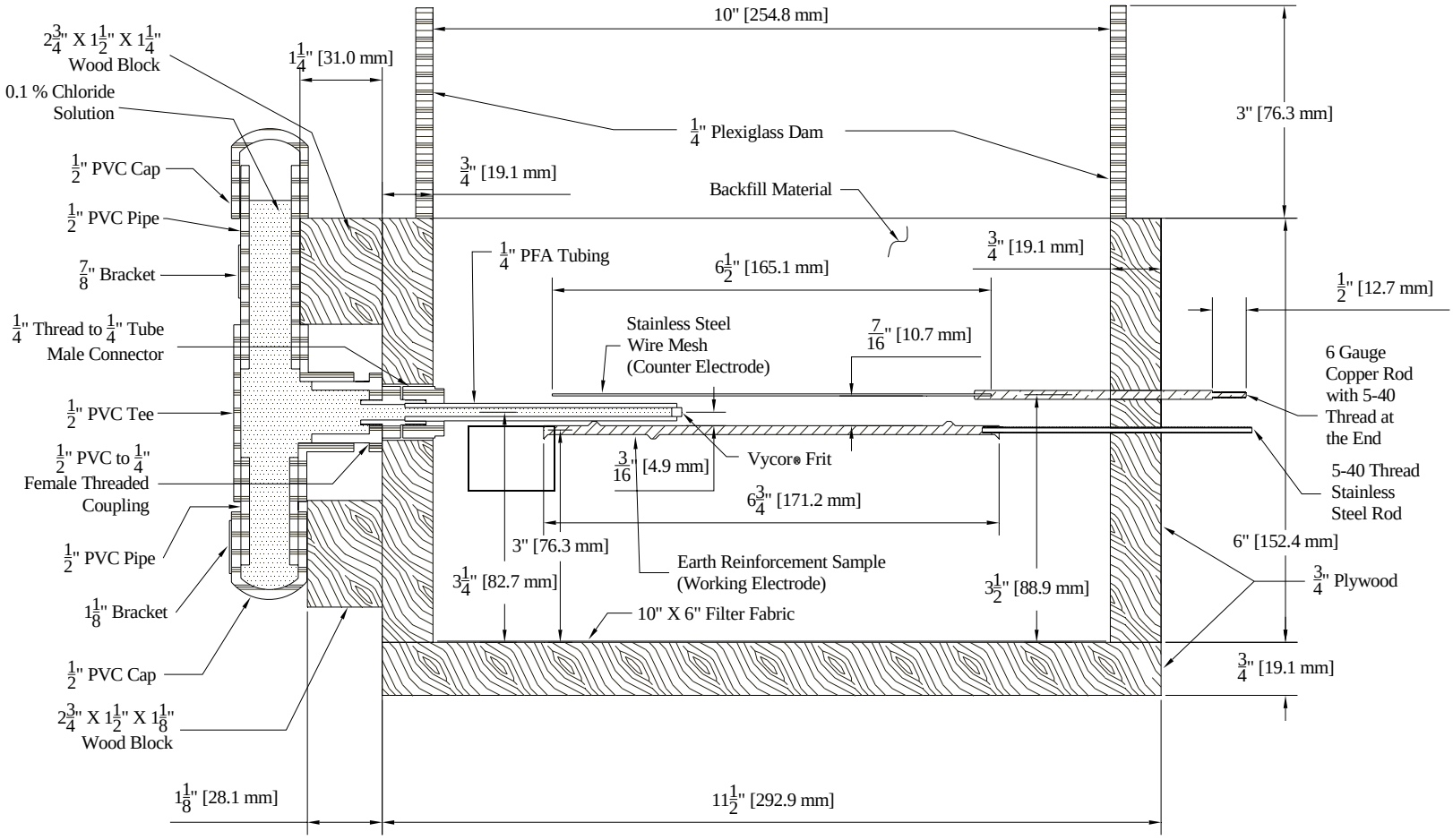

Figure 3.12. Section View of LTT Sample for Performing Corrosion Testing.

3.3.2.2.4 Preparation of Counter Electrodes

The counter electrode was made from a 3 inch (76 mm) by 6 inch (152 mm) stainless-steel wire gauze connected to an AWG 8 (3.26 mm) copper wire.

3.3.2.2.5 Corrosion Testing Sample Assembly

After the backfill forms were prepared and the woven silt fabric was placed in the bottom of the form, two layers of backfill material were compacted in the forms, the reinforcement sample was then inserted, and two more layers of backfill material were compacted in the forms for the long-term samples requiring only potential readings. For the LTT samples requiring polarization resistance testing the following occurred:

- two layers of backfill material were compacted,
- the reinforcement sample was inserted,
- the probe was inserted and secured to the form (see Figure 3.13.),
- some fines were placed around the tip of the probe,
- 1/2 inch (13 mm) of soil was added on top of the sample and probe,
- the counter electrode was inserted (see Figure 3.14.), and
- then the last two layers of backfill material were compacted.

The materials in the forms were compacted according to Tex-113E. The backfill materials placed in the forms for compaction were at the target moisture contents shown in Table 3.3. The LTT samples for polarization resistance testing were wired with connectors to facilitate connection for testing. For the LTT samples not requiring polarization resistance testing, the samples were prepared without probes, counter electrodes, or wiring.

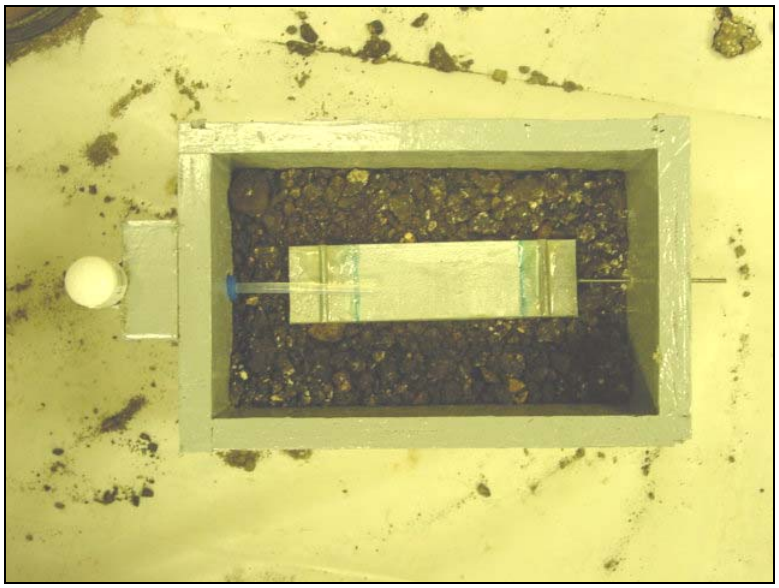

Figure 3.13. LTT Corrosion Testing Sample in Assembly after Probe Attachment.

Figure 3.14. LTT Corrosion Testing Sample in Assembly after Counter Electrode Placement.

Dams were added after the backfill material was compacted in the backfill forms. Dams were needed at the top of each backfill form to allow ponding of solution. The

dams were constructed of four pieces of plexiglass. Two pieces 10 $^{3}/_{8}$ inch (264 mm) by 3 inch (76 mm) and two pieces 6 $^{3}/_{8}$ inch (162 mm) by 3 inch (76 mm) were used to construct the dam. Figure 3.15. shows a top view of a form with its plexiglass dam installed. The perspective view in Figure 3.10. also shows the plexiglass dam. The plexiglass pieces for the dam were joined using silicone. Sealing with silicone was necessary to prevent leakage of solution from the backfill form.

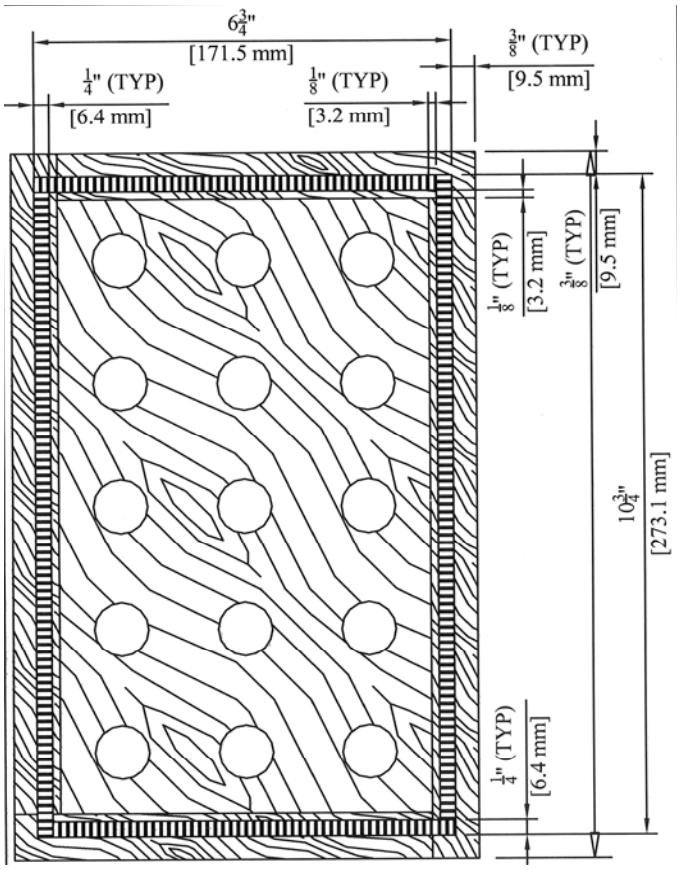

Figure 3.15. Top View of Form Used for Backfill Materials for LTT.

3.3.2.2.6 Backfill Sample Collection and Assessment

At the end of the LTT, samples of the backfill materials were collected for analysis. Approximately 1.1 lb (500 grams) of backfill materials just above the surface of

the reinforcement was evaluated for pH, resistivity, chloride ion concentration, sulfate ion concentration, sulfide concentration, and redox potential analysis.

Pore solution pH, sulfide, and redox potential testing were performed as described in Subsections 3.2.1.7, 3.2.1.9, and 3.2.1.10 respectively. Resistivity testing was performed using a conductivity meter and then converting the values from conductivity to resistivity.

Chloride and sulfate concentrations were measured using ion chromatography. ASTM D4327 (1997 c) was followed, however, this method is tailored for anions in aqueous solutions and does not provide a procedure for the preparation of samples obtained from soil pore solutions. AASHTO has adopted test standards for measuring the water soluble chloride ion in soil and the water soluble sulfate ion in soil, methods T-291-91 (AASHTO 2000) and T-290-91 (AASHTO 1999), respectively. These test methods do not list ion chromatography as an alternative method for measuring the water soluble chloride and sulfate ions in soil. These methods do however provide guidelines on how samples should be prepared before testing. Samples for examination by ion chromatography were prepared according to T-291-91, Part 22.

3.3.2.2.7 Potentiostat Settings for LTT

The potentiostat used for the LTT program was a Solartron™ 1287 and was controlled by the Corrware™ software interface. This potentiostat was used for all LTT polarization resistance measurements. The Verstat™ II potentiostat by Perkin Elmer® Instruments was used for all LTT cyclic polarization resistance measurements and was controlled by the SoftCorr™ III user interface. The potentiostat settings for the linear polarization resistance testing were setup as shown in Appendix B. The potentiostat settings for the cyclic polarization testing were setup as shown in Appendix B. The cyclic polarization was set to scan from -225 mV to +1000 mV and back to -225 mV with a scan rate of 1 mV/sec.

3.4 RESEARCH SUMMARY

The corrosivity of CC and RAP backfill materials were assessed in reference to galvanized-steel and plain-steel earth reinforcing strips commonly used in MSE walls. These assessments were compared with results from similar reinforcing strips embedded in CFM. Each backfill material was evaluated in the laboratory under similar environmental conditions. The performance of the materials exposure to very low and high chloride solutions were used to assess the corrosivity of the different backfill materials. Data were collected on the parameters that are typically measured for assessing backfill corrosivity. These results are presented in Section 4. A statistical analysis was performed on the results to detect any significant difference in the performance between these three materials. These results were used to evaluate the applicability of current service-life models for recycled backfill materials and if necessary, to propose a new model for predicting the service-life of MSE walls containing recycled backfill materials. A review of service-life models is discussed in Section 5. The service-life model for earth reinforcing strips aided the estimation of the life-cycle cost for different MSE wall systems.

3.5 RESEARCH SIGNIFICANCE

Results from this research are anticipated to assist engineers in correlating backfill material parameters with the corrosion activity, service-life prediction, and life-cycle cost for MSE walls. The findings of this research can be used to aid in making decisions regarding the use of CC and RAP. If it is determined that CC or RAP provides similar or longer service-life and lower life-cycle cost compared to that achieved when CFM is used, practitioners will have the opportunity to use these materials for MSE wall applications. Also, if the STT results correlate with those of the LTT, then it might be advantageous to use the STT procedure to assess backfill corrosivity to reduce research time.

4. RESULTS AND DISCUSSION

4.1 OVERVIEW

The STT and LTT corrosion results are presented in this section. The results of each testing program is presented independently and then compared. Based on the results, a general assessment of corrosivity was made for the backfill materials.

4.2 SHORT-TERM TESTING RESULTS

The STT results consist of measurements made on the metal (G or S) interaction with solution environment (CL or NCL) decanted through the backfill materials (CFM, CC, or RAP). This decanted solution is referred to as pore solution. Change in the pore solution with the number of drainages through the backfill materials was also investigated. STT results from mass loss and electrochemical testing are also presented in this section. The STT were performed so the results could be compared with the LTT results. If it is discovered that the STT could provide adequate insight into the corrosivity of the backfill materials, then the STT could be more economical for assessing the corrosivity of backfill materials. The test procedures for the STT were described in Subsection 3.3.1.

4.2.1 Pore Solution

Pore solution characteristics such as pH, resistivity, oxidation-reduction potential, chloride concentration, and sulfate concentration were measured as a function of the number of drainages through the backfill materials. These characteristics were measured for the first, 10^{th}, and 100^{th} drainages. Additional measurements on the 20^{th} and 50^{th} drainages were made for pH and resistivity. The measurements provide insight into the properties of the pore solution that results from the different backfill materials and how these properties change with the number of drainages.

4.2.1.1 pH

Figure 4.1 compares the change in pH with the number of drainages for each material-environment combination. For each material-environment grouping, it was found that the CC has the highest pH, followed by CFM, and then RAP. The change of the pH with the number of drainages differs depending on the environment. NCL solution (distilled water) tended to decrease the pH of each of the extracted pore solutions as the number of drainages increased. The pH of distilled water is approximately 7. Between the first and 100^{th} drainage, the pH of CC dropped from approximately 11.9 to 10.9, CFM decreased from approximately 8.5 to 7.8, and RAP remained nearly the same, at around 7.2. Thus, for the NCL drainages, the magnitude of the change in pH increased relative to how far away the initial pH of the pore solution was from the pH of distilled water.

For the CL drainages, Figure 4.1 shows that the pH of CC decreased slightly from approximately 12.1 to 11.8, whereas the pH of CFM increased from 8 to 9.7 and RAP increased from 7 to 9. It is unclear what causes the increases in pH for the CFM and RAP CL drainages. Although the pH does change with drainages, it is likely insignificant for CFM and RAP. However, the drop in pH of the CC could influence the potential corrosivity of this backfill material.

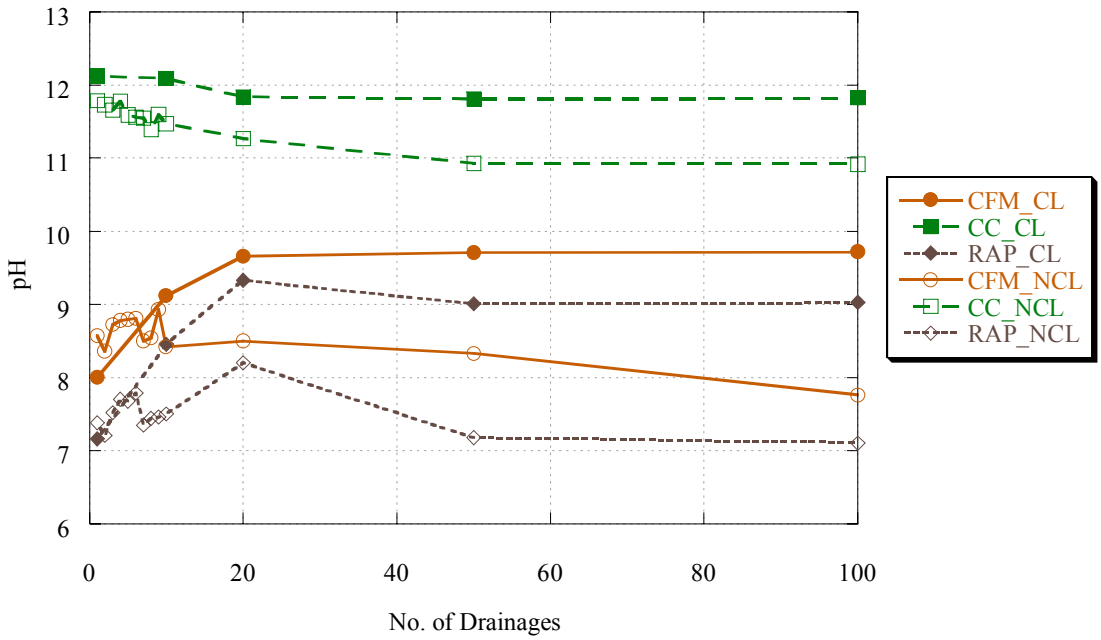

Figure 4.1. Pore Solution pH Versus the Number of Drainages through the Backfill Materials.

4.2.1.2 Resistivity

The pore solution resistivity results for drainages using CL solution are shown in Figure 4.2. Resistivity readings were taken for the first, 10th, 20th, 50th, and 100th drainages. The resistivity of the first CL drainages differs for each backfill material. CC has the highest resistivity at approximately 36 Ω-cm, followed by CFM at 28 Ω-cm, and RAP at 21 Ω-cm. The resistivity decreased by approximately 10 Ω-cm by the 20th CL drainage for each of the backfill materials. After 100 drainages, the resistivity had stabilized at around 19 Ω-cm for all three backfill materials.

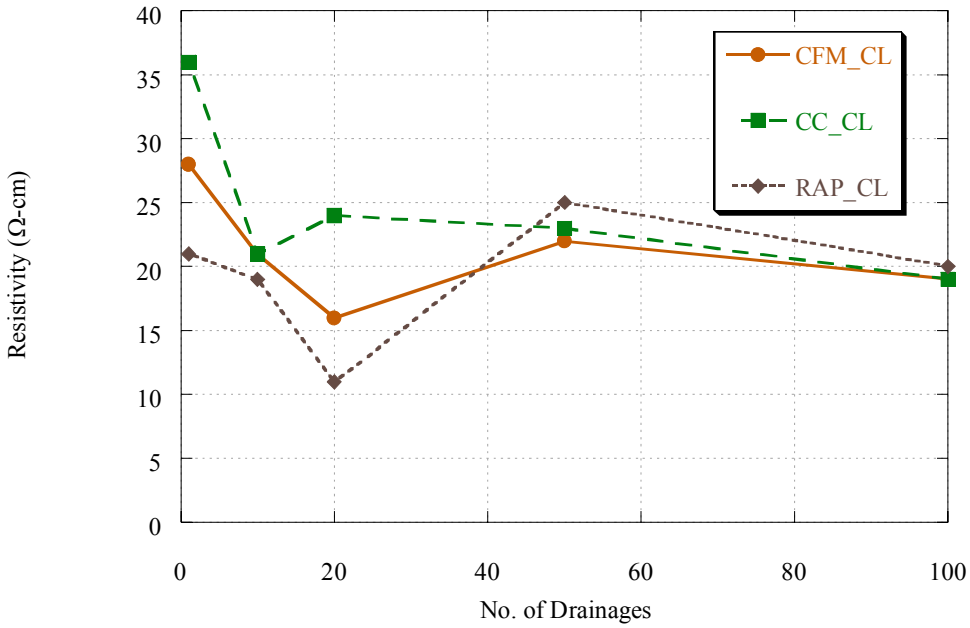

Figure 4.2. Pore Solution Resistivity for CL Drainages Versus the Number of Drainages through the Backfill Materials.

Figure 4.3 shows resistivity versus the number of NCL drainages through each backfill material. Resistivity readings were taken for the first through 10th, 20th, 50th, and 100th NCL drainages. CFM had the highest resistivity followed by RAP and CC. The CFM pore solution had the most variability in the resistivity readings. The resistivity of the first CFM drainage was approximately 4900 Ω-cm and had increased to 22,000 Ω-cm for the 10th NCL drainage and to 31,000 Ω-cm for the 50th NCL drainage. The resistivity of the CFM_NCL drainages then decreased to approximately 15,000 Ω-cm for the 100th NCL drainage. The resistivity of RAP_NCL drainages increased from 1700 Ω-cm for the first drainage to 4800 Ω-cm for the 10th NCL drainage and then remained fairly constant for the remaining readings, with a reading of 4900 Ω-cm for the 100th NCL drainage.

The pore solution resistivity readings for CC NCL drainages displayed less variability than the CFM and RAP readings. The resistivity of the first CC NCL drainage was 410 Ω-cm. The resistivity then increased to 1300 Ω-cm for the 20th NCL drainage and remained fairly constant for the remaining readings with a reading of 1200 Ω-cm for the 100th NCL drainage. The resistivity of the distilled water applied to the backfills was 5400 Ω-cm.

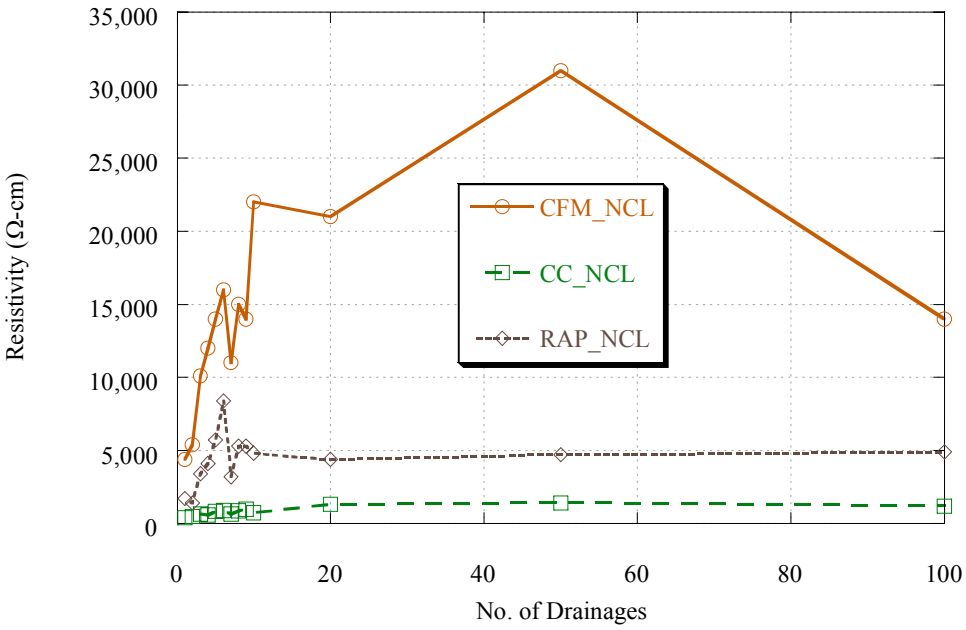

Figure 4.3. Pore Solution Resistivity for NCL Drainages Versus the Number of Drainages through the Backfill Materials.

4.2.1.3 Oxidation-Reduction Potential

The pore solution oxidation-reduction (redox) potential of the backfill materials was measured for the first, 10th, and 100th drainages. A plot of the readings is shown in

Figure 4.4. The pore solution redox potential of the CL drainages changed little with the number of drainages through the backfill materials. The redox potentials for the 100th CL drainage through CC, CFM, and RAP were -6 mV, 108 mV, and 205 mV respectively.

The pore solution redox potential of the NCL drainages had more variation than the CL drainages. The redox potential decreased from the first to the 10th NCL drainage for CFM and RAP pore solution NCL drainages, whereas the pore solution redox potential of CC increased slightly. From the 10th to the 100th NCL drainage, the pore solution redox potential of CC decreased slightly, whereas it increased for CFM and RAP. The redox potentials for the 100th NCL drainage through CC, CFM, and RAP were -20 mV, 119 mV, and 135 mV respectively. The pore solution redox potentials for CL drainages were higher than NCL drainages by approximately 70 to 130 mV for RAP and 20 to 40 mV for CC. For CFM, the pore solution redox potential of the first NCL drainage was higher than the first CL drainage by 75 mV, but for the 10th and 100th drainages, the NCL and CL pore solution redox potentials were separated by less than 11 mV. Lower values of redox potential indicate greater susceptibility to microbial attack. It appears that the number of drainages has little affect on the redox potential. The environment seems to have an impact on the redox potential for RAP pore solution, but not CFM and CC.

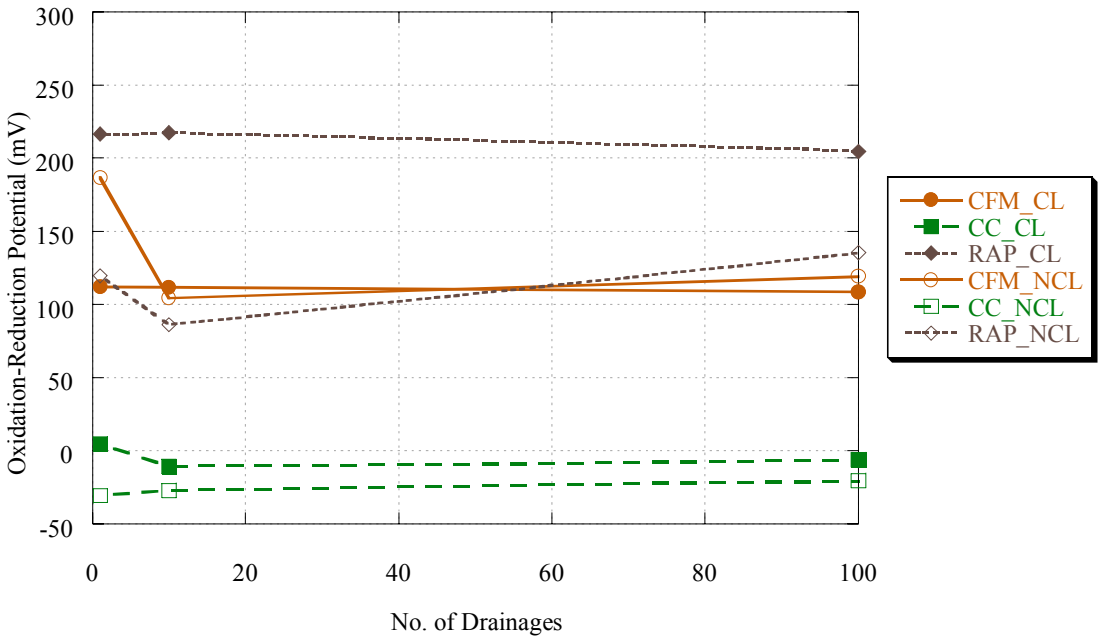

Figure 4.4. Pore Solution Oxidation-Reduction Potential Versus the Number of Drainages through the Backfill Materials.

4.2.1.4 Soluble Salts

The pore solution chloride concentration of the backfill materials was tested for the first, 10th, and 100th CL and NCL drainages. Figure 4.5 shows the pore solution chloride concentration for the CL drainages. Each of the backfill materials' pore solution had an increase in chloride concentration from the first to the 10th CL drainage. The chloride concentration increased by approximately 7700 mg/L, 6300 mg/L, and 3200 mg/L for CC, CFM, and RAP respectively. The pore solution chloride concentration for the 100th CL drainage for each of the backfill materials was approximately the same, 19,200 mg/L. Sometime between the 10th and 100th CL drainages, the pore solution

chloride concentration of the backfill materials stabilized to the chloride concentration of the applied 3 percent CL solution.

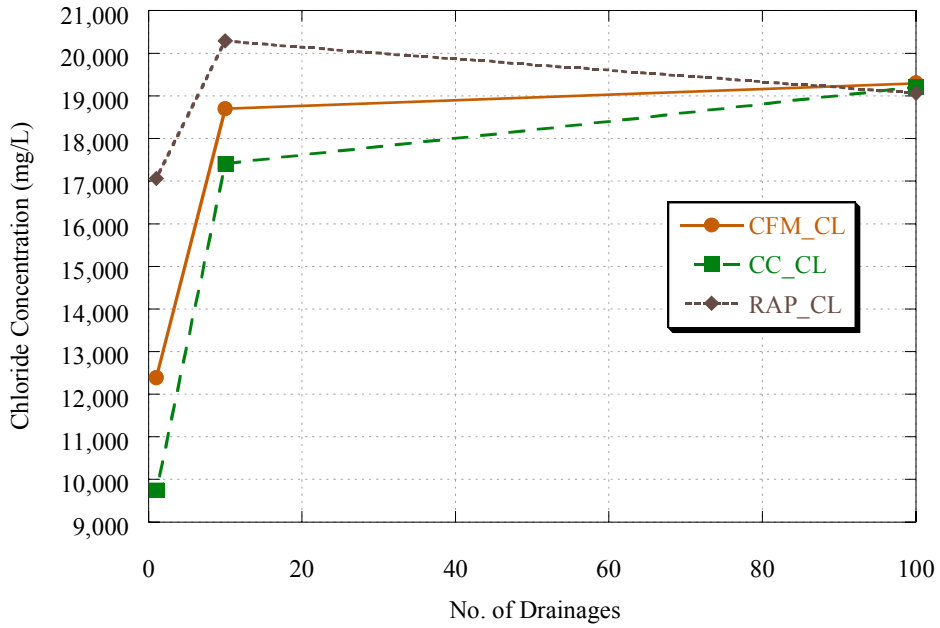

Figure 4.5. Pore Solution Chloride Concentration for CL Drainages Versus the Number of Drainages through the Backfill Materials.

Figure 4.6 shows the pore solution chloride concentration of the NCL drainages from the backfill materials. The pore solution chloride concentration was plotted on a logarithmic scale due to the large magnitude change in chloride concentrations over the measurements. The pore solution chloride concentration decreased from the first to the 10^{th} NCL drainage for each of the backfill materials. However, the pore solution chloride concentration for the CC did not decrease as much as the CFM and RAP over the testing period performed here. The CFM and RAP pore solution chloride concentration was

below 1 mg/L for the 10th NCL drainage, whereas the CC pore solution chloride concentration was 8 mg/L. For the 100th NCL drainage, the CFM and RAP pore solution chloride concentrations remained low, below 1 mg/L, and the CC pore solution chloride concentration decreased to 2 mg/L.

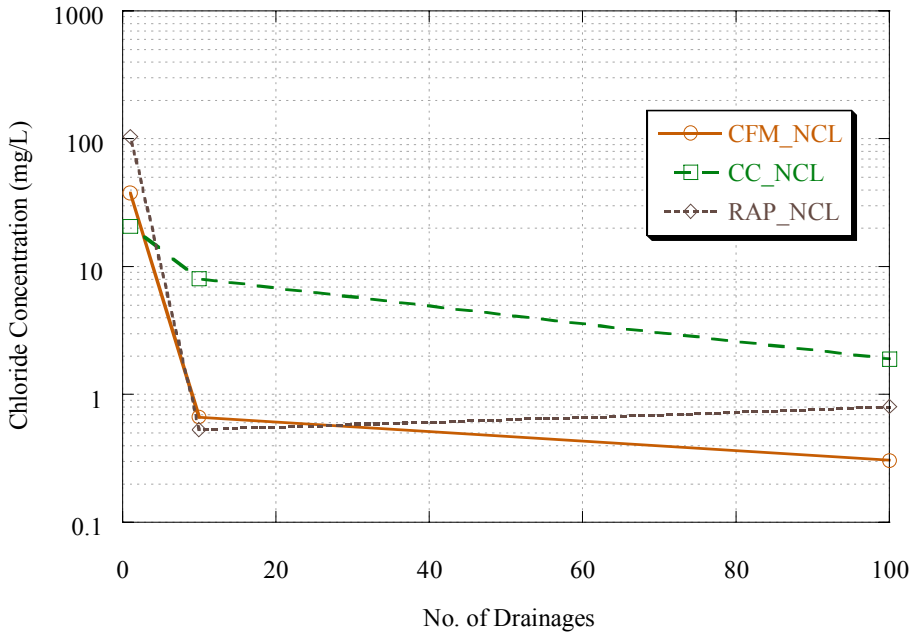

Figure 4.6. Pore Solution Chloride Concentration for NCL Drainages Versus the Number of Drainages through the Backfill Materials.

The pore solution sulfate concentration of the CL drainages from the backfill materials is shown in Figure 4.7. The pore solution sulfate concentration for the backfill materials was highest for CC, followed by RAP, and then CFM. The pore solution sulfate concentration of CC increased from approximately 770 mg/L at the first CL drainage to 830 mg/L for the 10th CL drainage, and remained at 830 mg/L. The RAP pore solution sulfate concentration remained constant from the first and 10th CL

drainages at approximately 470 mg/L and then decreased to 370 mg/L for the 100th CL drainage. Similar to CC, CFM showed an initial increase in pore solution sulfate concentration from the first to the 10th CL drainage. The sulfate concentration of CFM increased from 110 mg/L to 190 mg/L for the 10th drainage, which was followed by an increase to 270 mg/L for the 100th drainage.

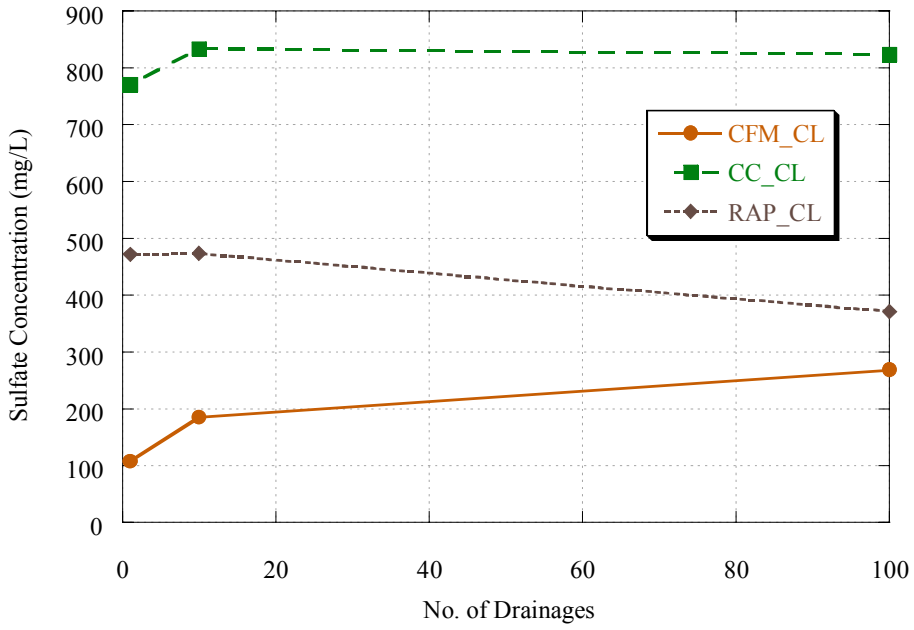

Figure 4.7. Pore Solution Sulfate Concentration for CL Drainages Versus the Number of Drainages through the Backfill Materials.

Figure 4.8 shows the pore solution sulfate concentration of the NCL drainages from the backfill materials. The pore solution sulfate concentration of the backfill materials for the first NCL drainage was approximately 150 mg/L for RAP, 50 mg/L for CFM, and 25 mg/L for CC. The pore solution sulfate concentration also quickly decreased for each of the backfill materials within the first 10 NCL drainages. This

indicates that drainages in the field may easily wash away sulfates, assuming sulfates are not in the source solution.

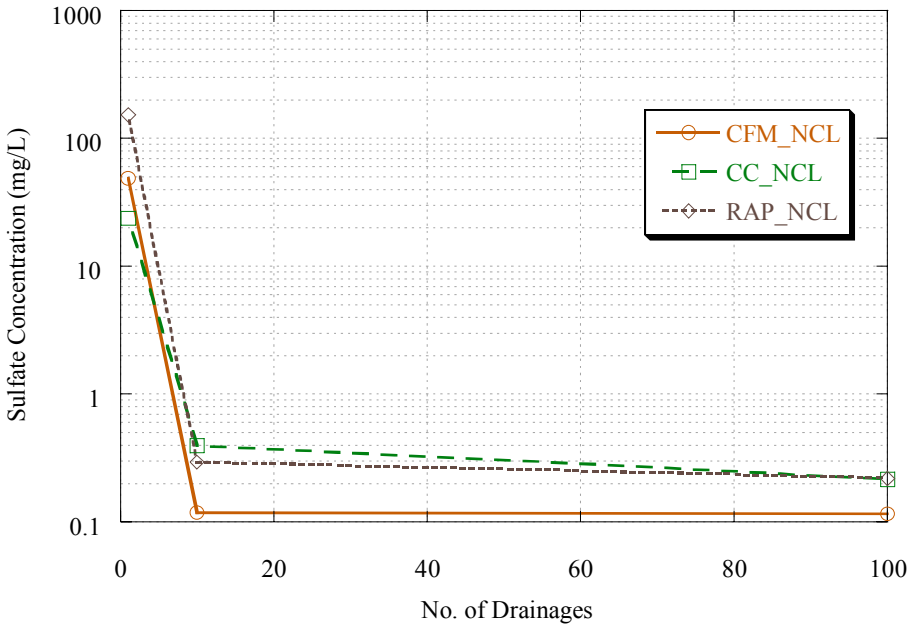

Figure 4.8. Pore Solution Sulfate Concentration for NCL Drainages Versus the Number of Drainages through the Backfill Materials.

4.2.2 Mass Loss and Corrosion Rates

The mass loss was measured for each STT sample. There were three samples within every STT group. The mass loss was used to determine the corrosion rates using Equation C.5 in Appendix C. Figure 4.9 shows the corrosion rates determined from the mass loss results for all STT CL groups. There are significant differences between G_CL and S_CL STT for each backfill material type. There is also a significant difference between G_CL_1 and G_CL_100, as well as S_CL_1 and S_CL_100 for each backfill

material type, with the exception of RAP_S_CL. The G_CL_1 has approximately 40 mils/yr (1016 μm/yr) higher corrosion rate compared to G_CL_100, whereas S_CL_1 compared to S_CL_100 has between 10 mils/yr (254 μm/yr) to 65 mils/yr (1651 μm/yr) lower corrosion rate. The lower corrosion rate for S_CL_1 compared to S_CL_100 is most likely due to the higher chloride concentration for the 100th drainage compared to the first drainage. It is unknown why the G_CL_1 corrosion rate is significantly higher than G_CL_100.

Within the G_CL_1 and G_CL_100 groups, there are no significant differences in corrosion rate between the backfill materials. Within the S_CL_1 and S_CL_100 groups, the corrosion rate for CFM is significantly higher than the corrosion rate for CC. However, this difference is slight in the S_CL_1 group, approximately 5 mils/yr (127 μm/yr). The difference in corrosion rate between CFM and CC is more pronounced for the S_CL_100 group, which is probably due to the large amount of variability in the CFM_S_CL_100 group. This group has the largest amount of variability in corrosion rate measurements of all others in the STT.

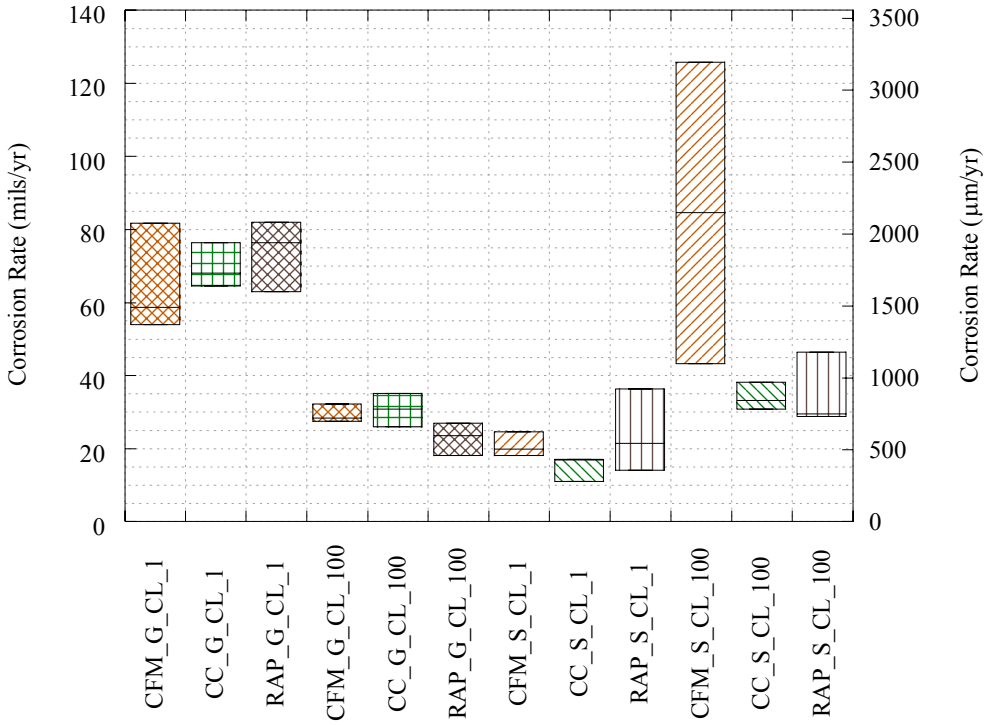

Figure 4.9. Boxplots of Corrosion Rates Calculated from Mass Loss Data for All STT CL Groups.

Figure 4.10 shows the corrosion rate results from the STT for all NCL groups. The boxplots show that all the corrosion rate results fall between 23 to 42 mils/yr (584 to 1067 µm/yr), and there are no significant differences between backfill materials within any of the groups. For the NCL samples, the testing period for the STT appears to be too short. More time is likely required to allow for more corrosion and the possibility of greater differences between the results.

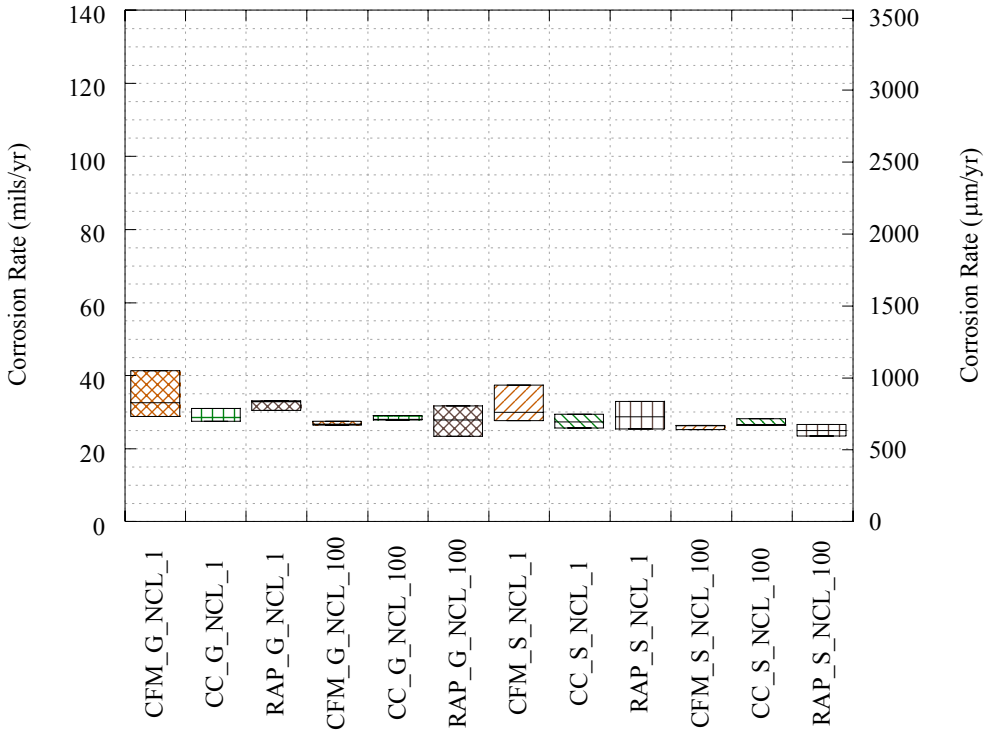

Figure 4.10 Boxplots of Corrosion Rates Calculated from Mass Loss Data for All STT NCL Groups.

The corrosion rates for all STT G groups are shown in Figure 4.11. The only significant difference between G_CL and G_NCL groups is between the G_CL_1 and all other groups. There is no significant difference between G_CL_100 and G_NCL_100. Although, it was expected that the G_CL_100 group would have higher corrosion rates than G_NCL_100, the corrosion susceptibility of the galvanized coating seems to be similar in both cases. Again, this likely indicates that the STT was too short to provide reasonable longer term corrosion performance data.

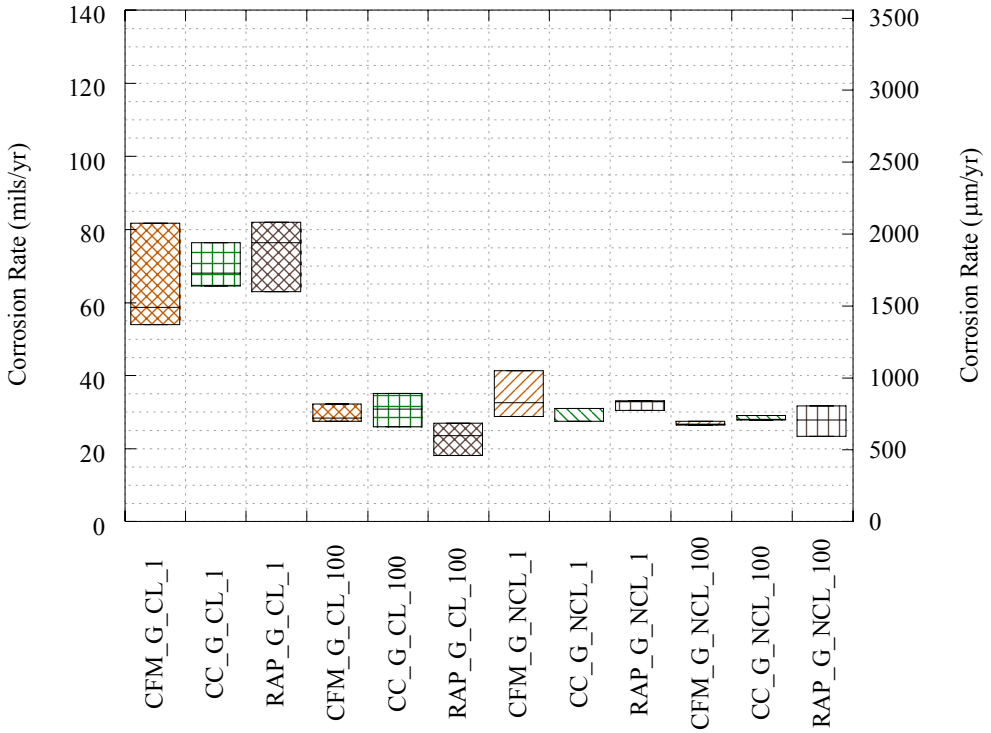

Figure 4.11. Boxplots of Corrosion Rates Calculated from Mass Loss Data for All STT G Groups.

Figure 4.12 shows the corrosion rate results for all STT steel groups. Results indicate that there is a significant difference between CFM_S_CL_1 and CC_S_CL_1. The corrosion rates for these groups are significantly less than all other groups, even the NCL groups, which is unusual. The explanation for the difference in these groups versus the others is unknown.

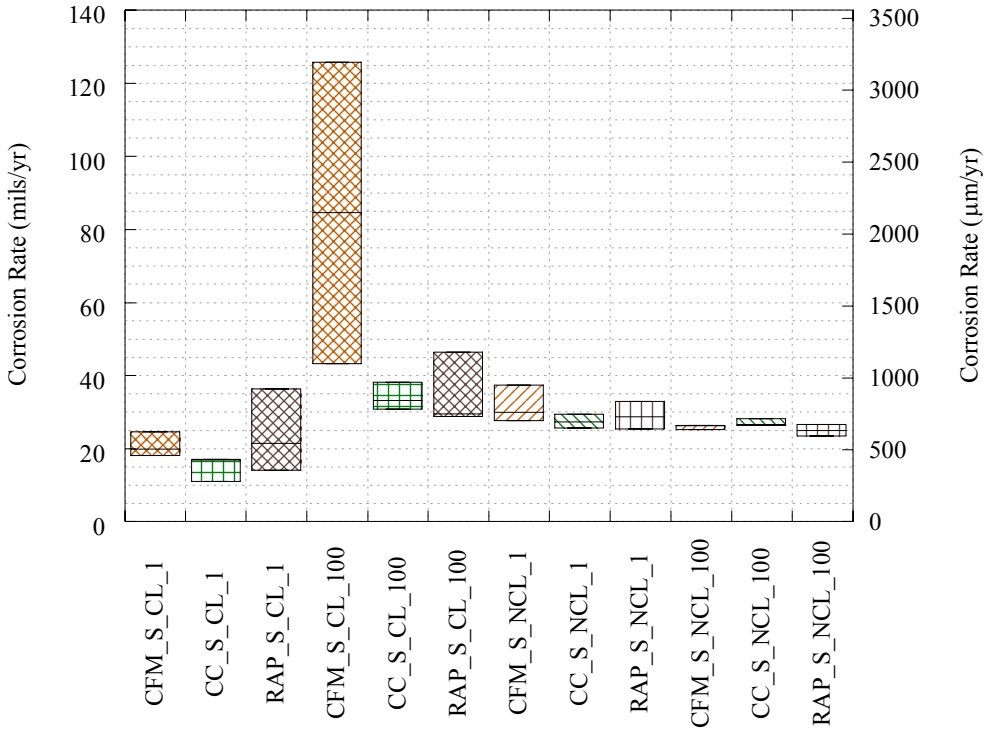

Figure 4.12. Boxplots of Corrosion Rates Calculated from Mass Loss Data for All STT S Groups.

4.2.3 Electrochemical Test Results

Electrochemical testing was performed on all STT samples. Non-destructive, linear polarization resistance testing was performed on these samples on a periodic basis. Destructive, cyclic polarization resistance testing was performed on these samples at the end of the STT.

4.2.3.1 Corrosion Rate Estimation

Data collected from linear polarization resistance and cyclic polarization resistance testing was used to estimate corrosion rates. These tests were performed on all the STT samples. Polarization resistance testing consisted of measuring the current vs. applied voltage across a specified potential range in relation to the open circuit potential to determine the polarization resistance. Cyclic polarization resistance testing was used to estimate Stern-Geary coefficients and gain insight on passivation and pitting tendencies. The polarization resistance and Stern-Geary coefficients were used to calculate the corrosion current, which was then converted to a corrosion rate. For information on the calculation procedure followed for determination of corrosion rates, refer to Appendix C. The STT mass loss data and calculated corrosion rates are provided in Appendix D. The incremental corrosion currents were summed and averaged over the 28 to 29 day testing period. The average corrosion current for each sample was then used to estimate the corrosion rate for each metallic sample.

Figure 4.13 shows a scatter plot of corrosion rate versus estimated corrosion rate for all the STT CL_1 samples. Estimated corrosion rates were generally underestimated or were in agreement with measured corrosion rates for all CL_1 samples. Underestimates of measured corrosion rate were highest for CC_G_CL_1 and RAP_G_CL_1 samples, with corrosion rates 65 to 95 percent underestimated.

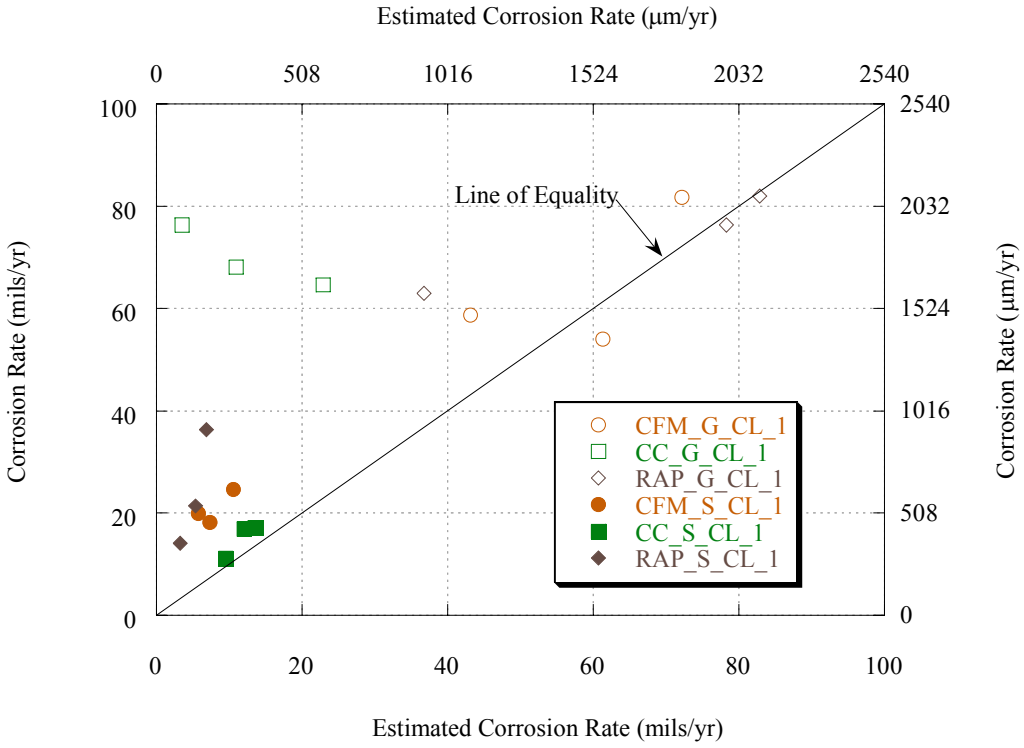

Figure 4.13. Corrosion Rate Calculated from Mass Loss Versus the Estimated Corrosion Rate Calculated from Polarization Resistance Measurements for the CL_1 STT Samples.

The estimated corrosion rate values are split evenly between overestimates and underestimates of measured corrosion rates for the STT CL_100 samples, as shown in Figure 4.14. All corrosion rate estimates for the S_CL_100 group were underestimates, while all the corrosion rate estimates for the G_CL_100 group, with the exception of one, were overestimates. The estimates for RAP_G_CL_100 were the most different from that measured, with the estimated corrosion rate being from 120 to 320 percent higher.

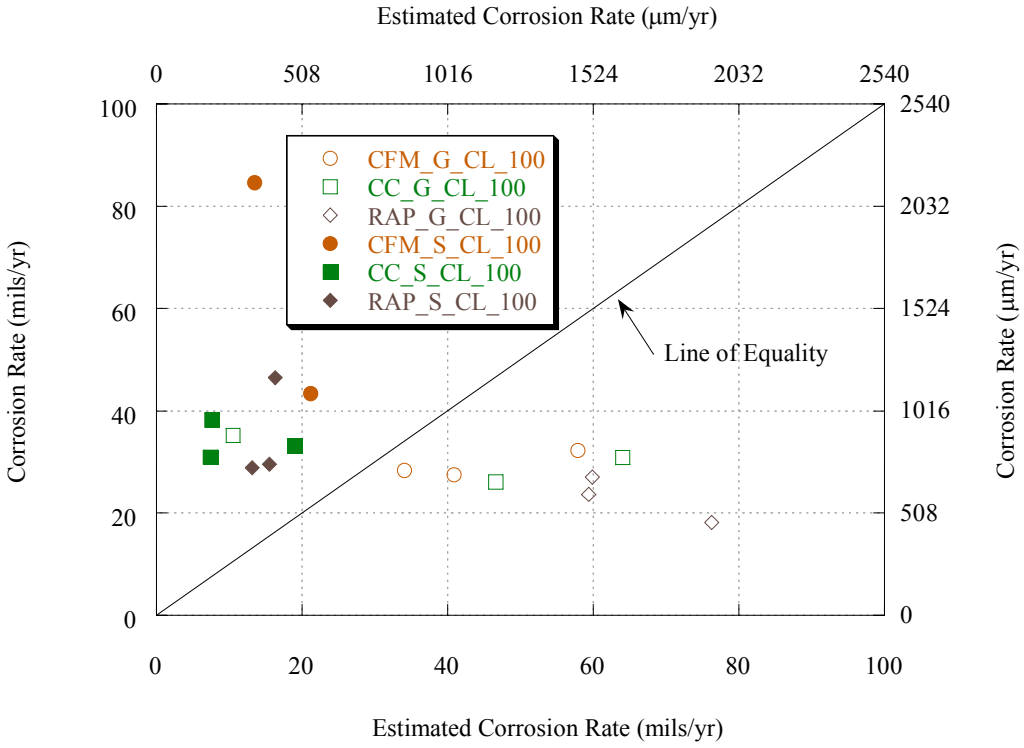

Figure 4.14. Corrosion Rate Calculated from Mass Loss Versus the Estimated Corrosion Rate Calculated from Polarization Resistance Measurements for the CL_100 STT Samples.

Figure 4.15 shows the measured corrosion rate versus estimated corrosion rate for all STT NCL_1 samples. For all the NCL_1 samples, the measured corrosion rates were underestimated from 70 to 100 percent. Figure 4.16 shows similar results for the corrosion rate comparison for all STT NCL_100 samples. They were also underestimated from 70 to 100 percent.

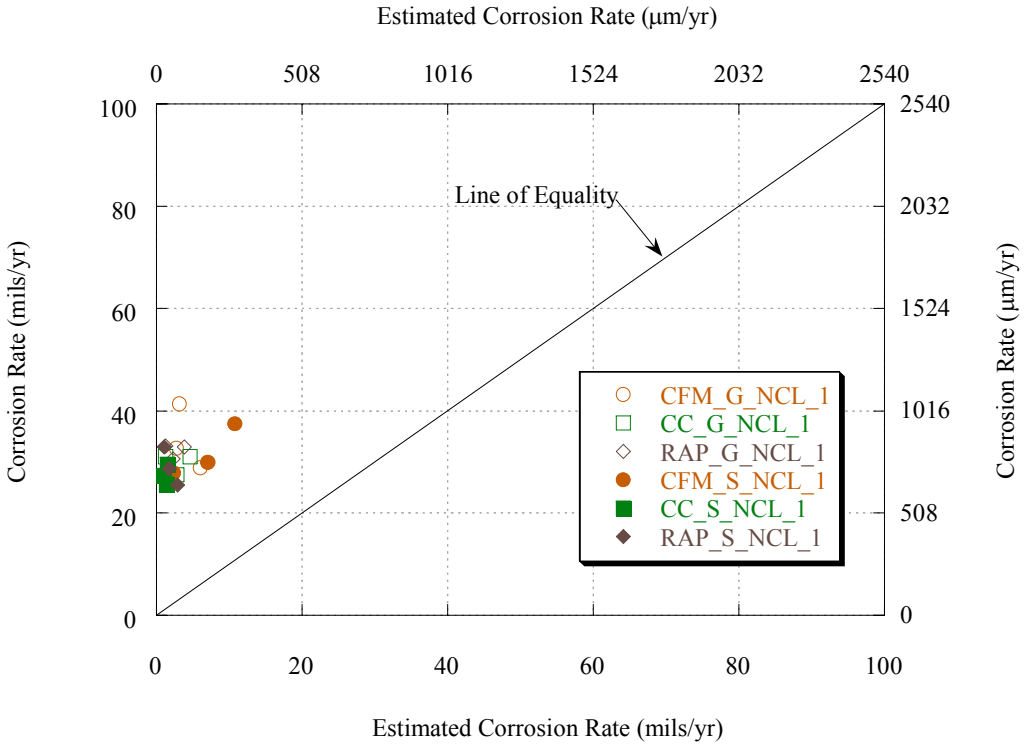

Figure 4.15. Corrosion Rate Calculated from Mass Loss Versus the Estimated Corrosion Rate Calculated from Polarization Resistance Measurements for the NCL_1 STT Samples.

It is suspected that the corrosion rate values are skewed toward overestimation for the STT NCL samples because of the possibility of epoxy flaking off of the samples, which would have been interpreted through the measurements as mass loss (of metal). The corrosion rate values for the NCL samples could be more sensitive to underestimation of corrosion rate due to the higher solution resistance of NCL compared to CL. The higher solution resistance can make polarization resistance testing less accurate. The solution resistance was not compensated for in the STT, but was compensated for in the LTT polarization resistance testing.

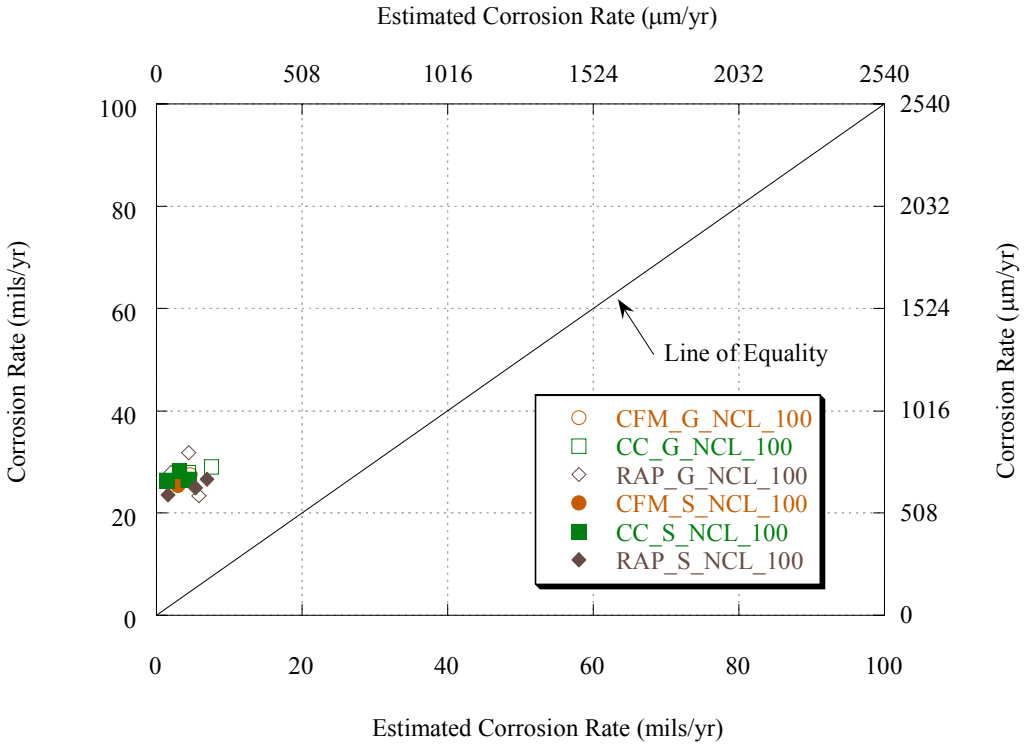

Figure 4.16. Corrosion Rate Calculated from Mass Loss Versus the Estimated Corrosion Rate Calculated from Polarization Resistance Measurements for the NCL_100 STT Samples.

4.2.3.2 Cyclic Polarization Resistance

The Stern-Geary coefficient for each sample was estimated by interpreting graphs of the cyclic polarization resistance testing. The cyclic polarization resistance graphs for the STT are shown in Appendix E. The estimation of Stern-Geary coefficients is an essential step to predict corrosion rate values using linear polarization resistance data. Appendix C described the procedure for estimating the Stern-Geary coefficients from the cyclic polarization plots.

Figure 4.17 and Figure 4.18 show the ranges of the Stern-Geary coefficients for the STT samples. In general, the lower the value of the Stern-Geary coefficient, the more active the corrosion. For steel corrosion in concrete, the Stearn-Geary coefficient is approximately 25 for active and 50 for passive. When used alone, the Stern-Geary coefficients were poor predictors of mass loss. The results of the cyclic polarization testing were not found to correlate well with the mass loss data. A more detailed interpretation of the cyclic polarization results is included in Appendix F.

The results in Appendix F includes speculation on whether or not pits initiate and grow; whether the sample is passive, psedo-passive, or active; and other information for both STT and LTT. These results for the STT will not be discussed in this thesis because no significant correlations were found between these results and the mass loss. No trends in pitting could be confirmed by visual inspection.

Figure 4.17 shows the Stearn-Geary coefficients determined from the cyclic polarization testing of the G_STT samples. There were significant differences between the first and 100th drainages for the RAP_G_NCL, CC_G_CL, and CFM_G_CL Stearn-Geary coefficients. Thus, for the G_STT samples in general, the cyclic polarization results were dissimilar between the first and 100th drainages. In general, for the G_STT 100th drainages, the Stearn-Geary coefficients were slightly more passive for NCL compared to CL, however the differences were not significant. The STT cyclic polarization resistance results with pore solution from the 100th drainage indicate that the CFM is least passive and the RAP is most passive. This order is also represented in the G_NCL_1 STT results. However, the differences between the backfill materials' Stearn-Geary coefficients are not significant, and this order is not always supported by the mean values.

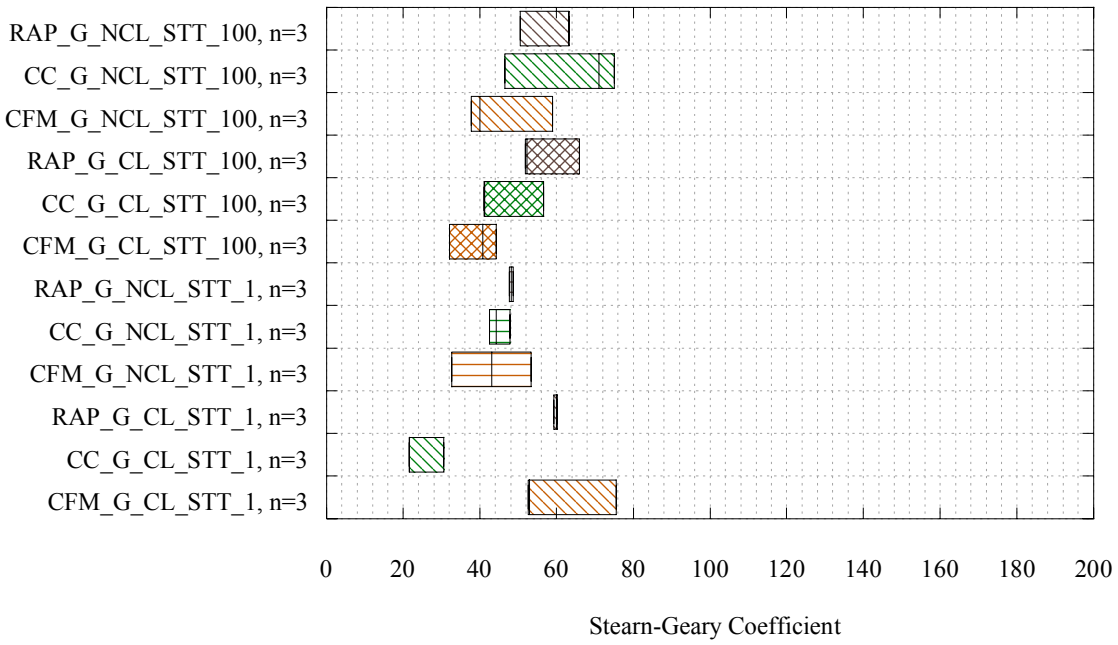

Figure 4.17. Boxplot of Stern-Geary Coefficients Derived from Cyclic Polarization Testing Plots for All the STT G Samples.

Figure 4.18 shows the Stearn-Geary coefficients determined from the cyclic polarization testing of the S_STT groups. There is no significant difference in the results between the first and 100th drainage for the S_STT groups. Several significant differences are present in the results within subgroups. All the S_NCL groups are more passive than the S_CL groups and are all significantly different, with the exception of CC_S. The CC_S_NCL group is slightly more passive than the CC_S_CL group when the average Stearn-Geary coefficients are compared, however the two groups are not significantly different.

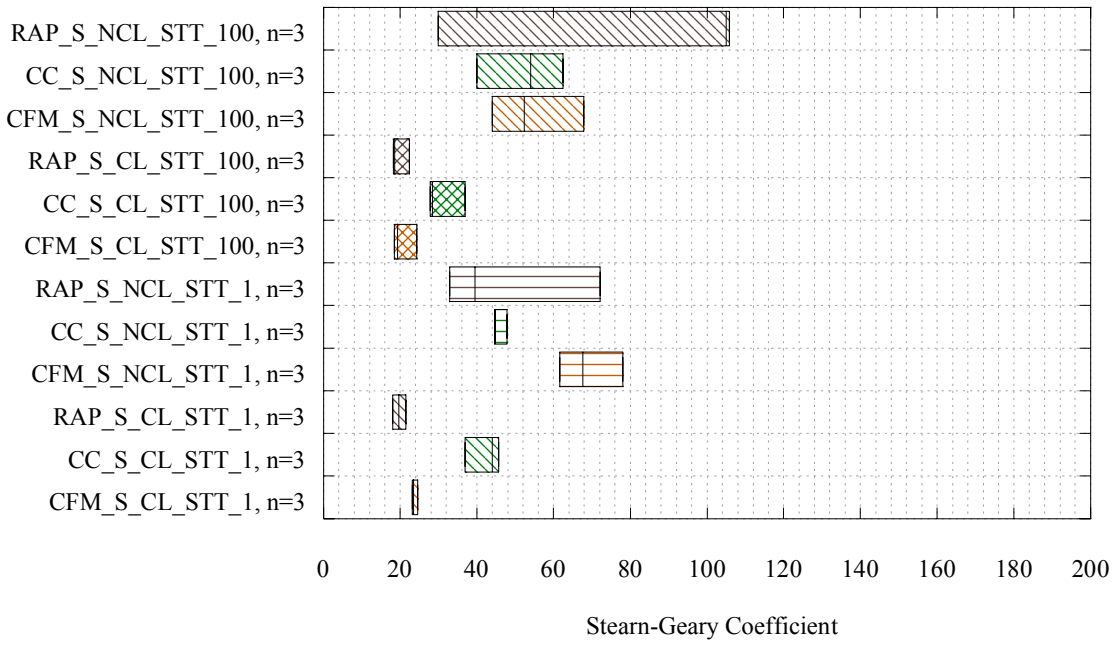

Figure 4.18. Boxplot of Stern-Geary Coefficients Derived from Cyclic Polarization Testing Plots for All the STT S Samples.

The S_CL_1 groups are all significantly different from each other. RAP_S_CL was most active with a Stearn-Geary coefficient of approximately 19, followed by CFM_S_CL at 24. CC_S_CL was more passive with a Stearn-Geary coefficient of approximately 44. The backfill materials had the same rank from most to least active for the 100th drainage, however the Stearn-Geary coefficient values are closer together. RAP_S_CL_100 has an average Stearn-Geary coefficient of approximately 18, followed by CFM_S_CL_100 at 19, and then CC_S_CL at 28. There is no significant difference between RAP_S_CL_100 and CFM_S_CL_100, but CC_S_CL_100 is significantly different from the other backfill materials in the S_CL_100 group. For the first and 100th drainages of the S_NCL groups, there are no significant differences between any of the

groups, except for the difference between CC_S_NCL and CFM_S_NCL. CFM_S_NCL_1 is more passive than CC_S_NCL_1 with an average Stearn-Geary coefficient of approximately 67 compared to 44. There was less variability in the S_CL groups compared to the S_NCL groups. The RAP_S_NCL groups had the most variability in the Stearn-Geary coefficient values.

According to the mean values, the order of least to most passive for the S_NCL_100 group was CFM, CC, and RAP. The order is opposite for the S_NCL_1 group (RAP, CC, and CFM). For the first and 100th S_CL drainages, the order of most active to least active or passive is RAP, CFM, and CC.

4.2.4 Summary

The number of drainages through the backfill materials has an effect on the solution properties, but whether or not the effect is significant often depends on whether the solution is CL or NCL. There is little difference in corrosion rates between NCL samples tested in the first and 100th drainages. The differences in corrosion rates between CL samples tested in the first and 100th drainages can be attributed to the larger chloride concentration of the 100th drainage. The STT period did not have a sufficiently long duration to adequately distinguish mass loss between CL and NCL groups, which is known to cause significant differences in mass loss. The cyclic polarization testing results were not a good indication of mass loss.

4.3 LONG-TERM TESTING RESULTS

The LTT results consist of measurements made on the backfill material, metal, or material-metal-environment. Backfill material characteristics were described in Subsection 3.2.1. The results shown here include measurements on the backfill materials after an exposure period to a particular environment, which may influence the characteristics of the backfill. For details on how measurements were performed, refer to Subsection 3.2.1.

4.3.1 Potential Readings

Potential readings were measured versus Cu-Cu_2SO_4 (Copper-Copper Sulfate). Two plot types were used to examine the potential readings: distribution of potential and potential versus time. The first plot type shows the distribution of the potential readings (percent of potential readings versus potential). These plots were made for each LTT sample and grouped by each material-metal-environment combination group as shown in Appendix G. The average distributions for each group were plotted for comparison. The average distributions for the LTT galvanized-steel samples in Figure 4.19 show that the ranking of average potential from more negative to least negative is RAP, CFM, and CC.

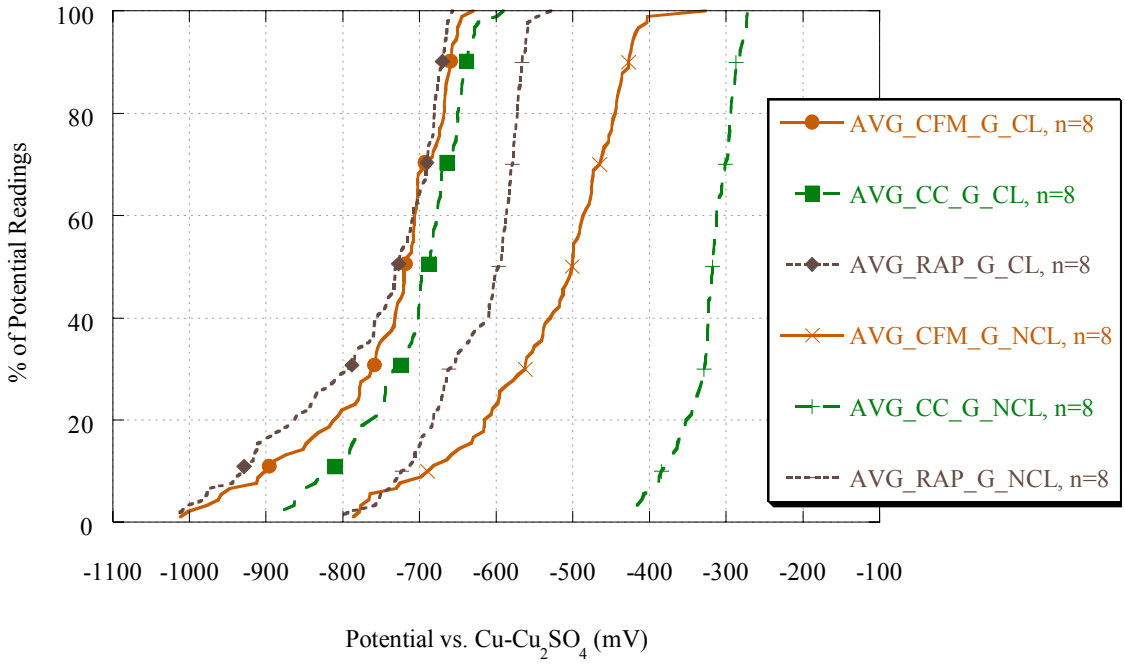

Figure 4.19. Distribution Plot of Average Cu-Cu_2SO_4 Potential Readings for LTT G Samples.

The plots in Figure 4.19 indicate less chemical activity for CC_G compared to RAP and CFM. There were larger differences in average potential between the galvanized-steel samples in the NCL environment compared to the CL environment. The CC_G_NCL average distribution is at least 140 mV more positive than the CFM_G_NCL average distribution, and is at least 270 mV more positive than the RAP_G_NCL average distribution, whereas the average G_CL distributions were typically within 100 mV of each other.

The average distributions for the LTT steel samples in Figure 4.20 show that the ranking of average potential from more negative to least negative is CFM, RAP, and CC for the CL environment and RAP, CFM, and CC for the NCL environment.

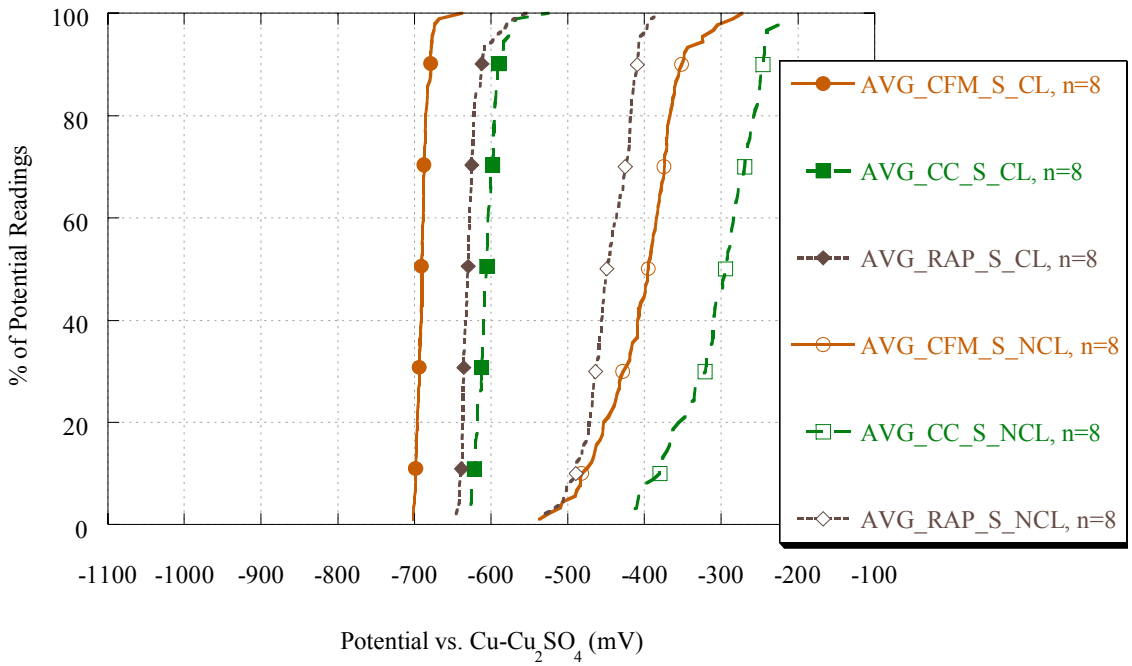

Figure 4.20. Distribution Plot of Average Cu-Cu_2SO_4 Potential Readings for LTT S Samples.

Using the ranges proposed by Applegate (1960) for probable corrosiveness of steel, CC_S_NCL is mild to very mild, RAP_S_NCL and CFM_S_NCL are moderate to mild, and all S_CL groups have severe probable corrosiveness based on their potential readings.

The potential versus time from first solution application plots display how the potential readings change with time. All the potential versus time plots start at 14 or 15 days (which was when the first potential reading measurements were made following the first solution application to the samples) and end at 336 or 337 days. Frequent variations are observed in the plots because before-solution-application and after-solution-application potential readings were measured. The average potential versus time plots for the LTT galvanized-steel samples are shown in Figure 4.21.

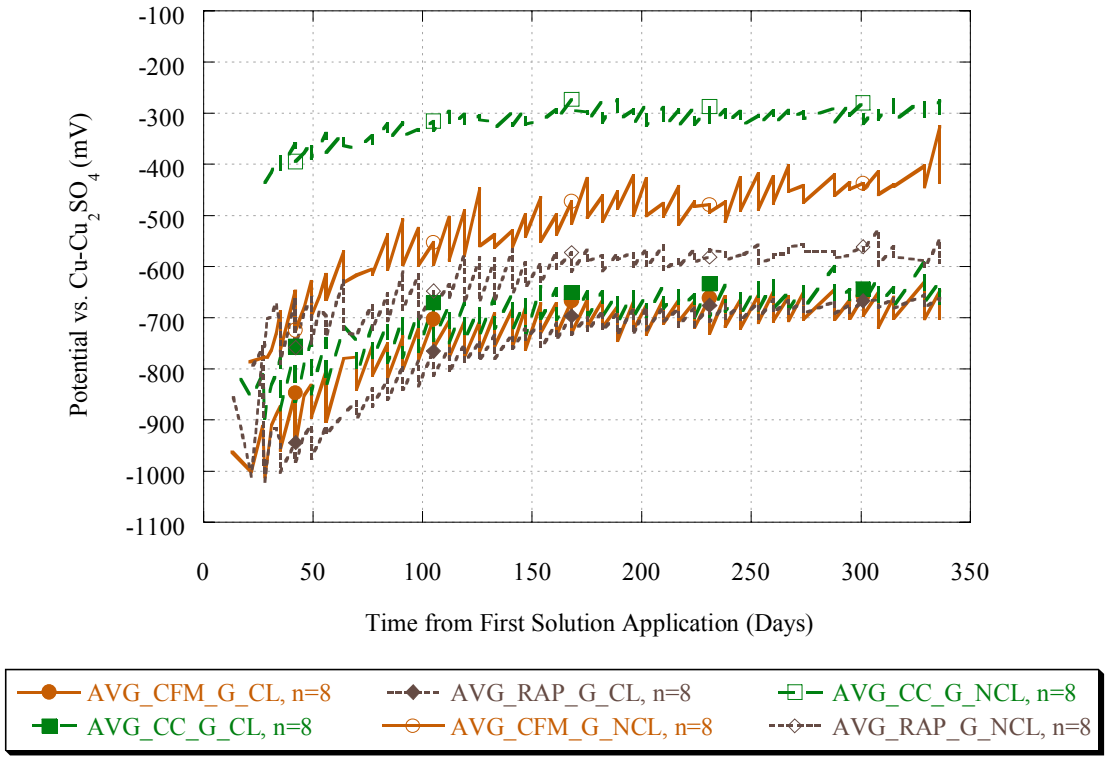

Figure 4.21. Average Cu-Cu_2SO_4 Potential Readings Versus Time Plot of LTT G Samples.

The potential versus time plots for all G material-environment combinations in Figure 4.21 exhibit similar behavior by initially increasing at a decreasing rate until approximately 150 days and then increase slightly at a constant rate. At 336 days, the G_CL samples had the same average potential reading of approximately -675 mV for each backfill. All G_CL samples tended to have the same degree of variation between the before and after solution application measurements.

The average potential versus time plots for the G_NCL samples exhibit differing behavior between the backfill materials. After 336 days, the potential readings for CC_G_NCL samples were more positive than CFM_G_NCL, which more positive than RAP. The degree of variation in the G_NCL samples between the before-solution-application readings and the after-solution-application readings differs between the G_NCL groups. CC has the least amount of variation followed by CFM, then RAP. The RAP_G_NCL potential readings were unstable initially.

In general, the RAP potential readings were more difficult to take than the readings for CFM and CC due to the higher resistance of the RAP backfill. The potential readings for the RAP_G_CL samples became more stable after 40 days due to the decrease in resistance of the backfill with the addition of chlorides.

It is reasonable to assume that the CC and RAP G_NCL samples reached or were close to reaching a point of constant surface chemical activity on the galvanization from the almost constant linear portions of the G_NCL plots after 150 days. It appeared that the CFM_G_NCL samples did not reach equilibrium of surface chemical activity because the potential readings versus time plots continue to increase steadily to the end of the testing. Thus, it could be expected that CC would continue to have less chemical activity, on the order of 320 mV compared to RAP. The difference in potential readings between CC_G_NCL and CFM_G_NCL at the end of the test period should not be expected to be constant past 336 days. The equilibrium potential for CFM_G_NCL is unknown and would require a test period longer than 336 days to determine. However, the potential readings of CC_G_NCL indicate less chemical activity, on the order of at least 120 mV, compared to CFM_G_NCL.

The average potential versus time S_CL plots in Figure 4.22 show an initial decrease in potential over the first 20 days of readings. The S_CL potential readings were fairly constant for the entire test period for CFM and RAP. The CC_S_CL readings showed a linear slightly decreasing trend. At the end of the test period, the S_CL readings for CC and RAP were about the same, while the CFM_S_CL readings were about 60 mV more negative. The potential versus time plots for the S_CL samples displayed less variation due to differences between the before-solution-application and the after-solution-application potential readings when compared to the S_NCL samples.

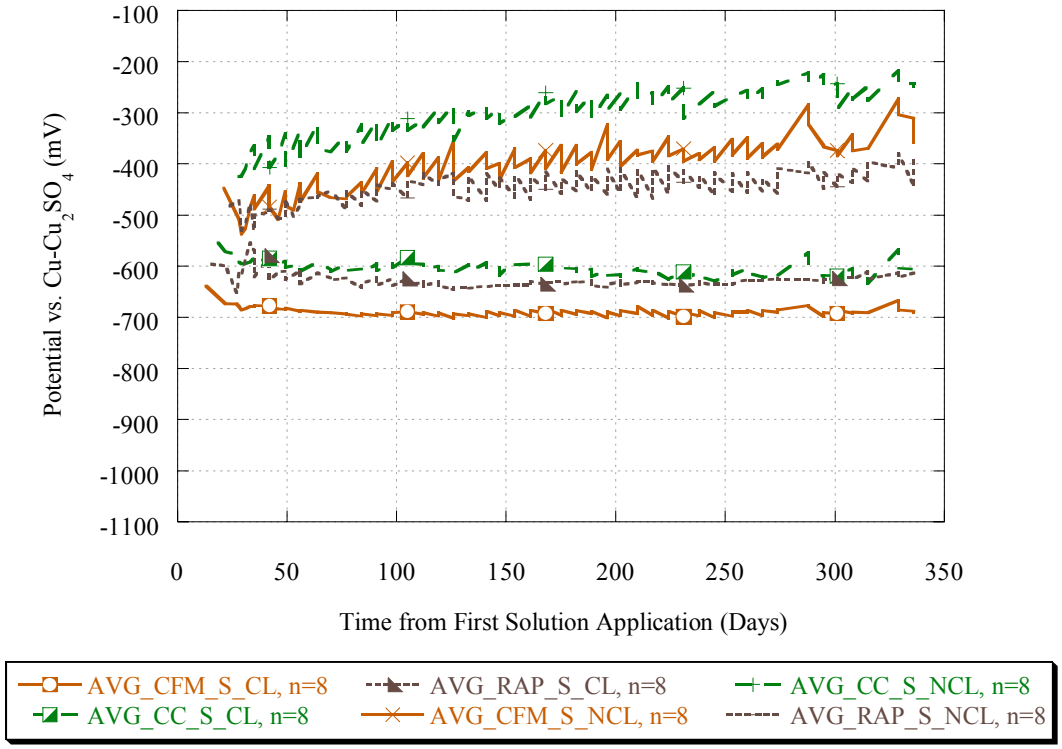

Figure 4.22. Average Cu-Cu_2SO_4 Potential Readings Versus Time Plot of LTT S Samples.

Similar to all other metal-environment combinations, for the S_NCL combination, there is less chemical activity with CC, compared to CFM and RAP. Similar to the galvanized-steel potential reading comparisons, the difference in the average distributions of potential readings between CC and the other backfills is greater in the NCL environment, compared to the CL environment. Thus, if lower potential readings for CC represent less chemical activity, which represents less corrosion, then CC could be expected to outperform CFM and RAP. CC would outperform the other backfills to a larger degree for G_NCL over G_CL and for S_NCL over S_CL. Likewise, CC_G_NCL would outperform a G_NCL combination with CFM or RAP to a larger degree than CC_S_NCL would outperform a S_NCL combination with CFM or RAP. The degree of variation in the S_NCL samples between the before-solution-application readings and the after-solution-application readings differs between the three backfills, CC has the least amount of variation followed by CFM and RAP, which have similar amounts of variation. The RAP_S_NCl did not show as large a degree of initial instability compared to the readings with RAP in the other metal-environment combinations.

There were several samples with potential readings that deviated significantly from the other samples. CFM_G6.1_P_CL exhibited a different distribution of potential readings from the other samples but the cause of this is unclear. It is unclear why the CFM G5.6_P_CL sample consistently had potential reading values that were significantly higher than all the other samples in the CFM_G_CL group. Both CFM_G_NCL samples for polarization resistance testing, CFM_G3.6_R_NCL and CFM_G4.3_R_NCL, were contaminated with 3 percent chloride solution by accident after 200 days. Two CC_G_NCL samples, CC_G1.3_R_NCL and CC_G4.5_P_NCL, were contaminated with chloride solution. CC_G1.3_R_NCL had a leaking probe and was accidentally filled with one percent chloride solution instead of 0.1 percent, which leaked out onto the sample. The cause of chloride contamination of sample CC_G4.5_P_NCL is unknown. The averages of the potential readings do average in the values from the defected samples.

Several general observations were made regarding the potential readings. The galvanized-steel samples showed more variation in the potential readings compared to steel samples. For the steel samples, the NCL potential readings showed more variation compared to the CL readings. S_CL potential readings had a narrow distribution of potential reading values compared to the other metal-environment combinations. NCL potential reading distributions are more positive than CL potential reading distributions for all backfill-metal combinations. CC backfill had more positive potential readings than the other backfills for each metal-environment combination indicating less corrosion activity.

4.3.2 Backfill Material Characteristics

The following backfill material characteristics were measured for each material-metal-environment combination: density, pH, resistivity, oxidation-reduction potential, and soluble salts. The measurements were taken at the end of the one year LTT period. Over the entire LTT duration, solution was applied approximately 45 times, with applications typically occurring weekly.

4.3.2.1 Density

The densities of the LTT samples are shown in Figure 4.23. The results show no significant difference in sample densities between any of the groups, except for CFM_G_CL. It is suspected that the CFM_G_CL samples exhibited higher density because they were the first samples prepared. The target dry densities in lb/ft^3 (kg/m^3) for the samples are 125 (2002), 119 (1906), and 117 (1874) for CFM, CC, and RAP, respectively. Refer to Subsection 3.2.1.5, Relative-Density (Unit Weight), for a description of how the samples were prepared. All the samples have dry densities that are below the target, except for CFM_G_CL, in spite of following the compaction procedure outlined in Subsection 3.2.1.5. The average dry density for each group of samples, except CFM_G_CL is between 113 and 118 lb/ft^3 (1810 and 1890 kg/m^3). The

average dry density for CFM_G_CL is 125 lb/ft^3 (2002 kg/m^3). The CFM samples have the largest amount of density variation within groups.

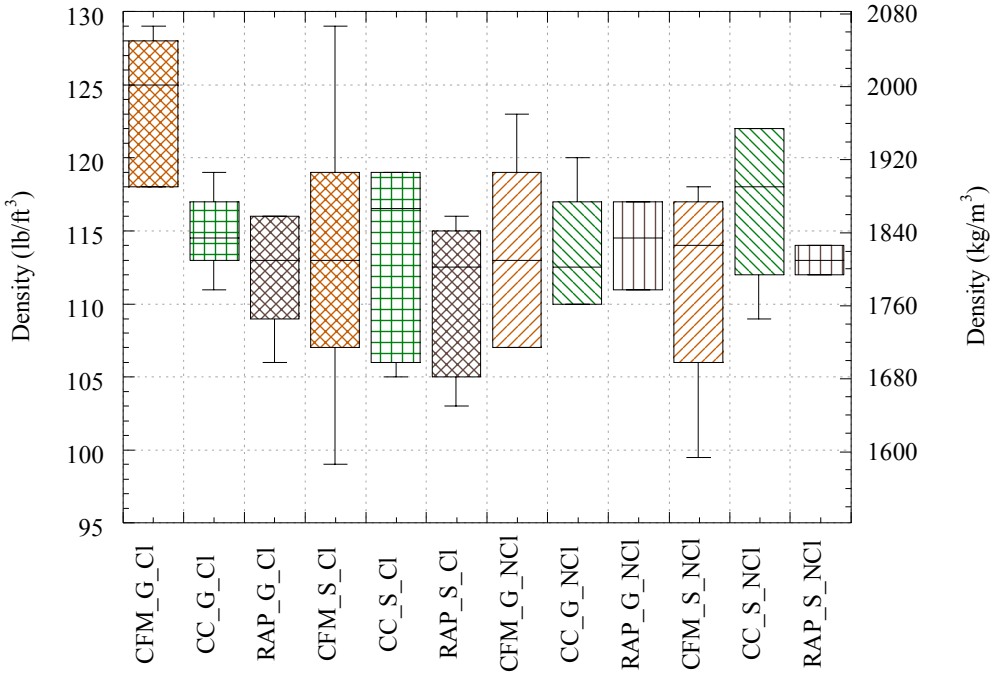

Figure 4.23. Boxplots of LTT Sample Densities.

4.3.2.2 pH

Figure 4.24 displays boxplots of the pH readings of the LTT samples. CC has the highest pH, followed by CFM, then RAP. The CC samples have no significant difference in pH. The mean pH of CC is between 11.5 and 12. For CFM and RAP, there is a significant difference in pH between G_CL and the other material environment combinations, except for RAP_G_CL and RAP_S_CL. These two groups are

significantly different, but have little overlap of boxplots. The mean pH of CFM is about 10.2 for the G_CL material-environment combination and between 9.4 and 9.6 for all other combinations. The mean pH of RAP is about 9.7 for the G_CL material environment combination and between 8.7 and 8.9 for all other combinations. No trends are observed in the variability of the pH readings between the groups. RAP_S_CL has the largest degree of variability.

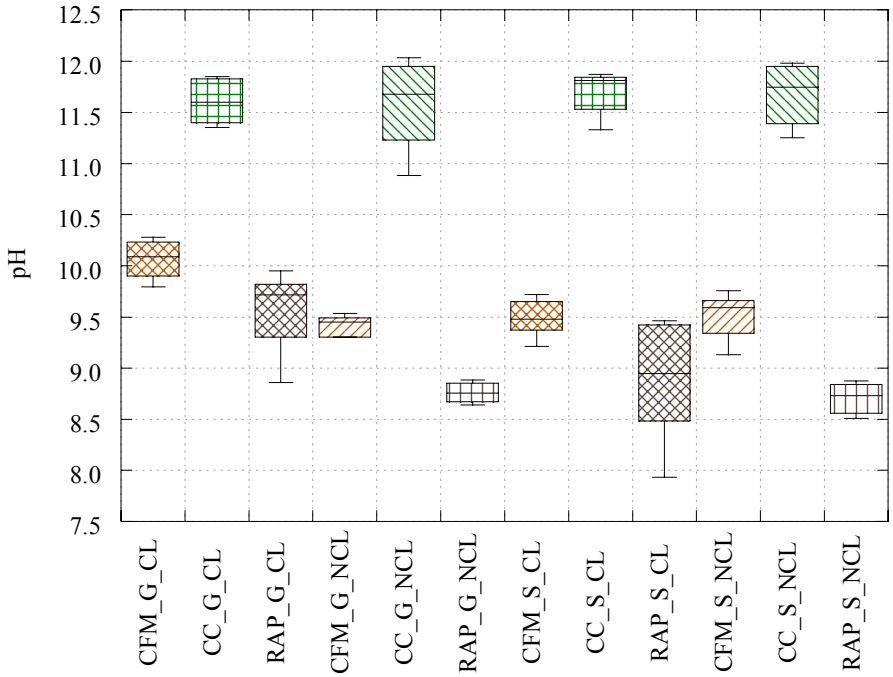

Figure 4.24. Boxplots of LTT pH readings.

As described in Subsection 3.3.1.2.3.2, samples were prepared to evaluate the changes in the backfill materials with the number of CL drainages. Figure 4.25 shows that the pH changes little as a function of the number of CL drainages. The results shown in Figure 4.25 are similar to the results shown in Figure 4.1 for the pH testing of

drainages during the STT. RAP shows a trend of increasing pH as the number of drainages increases. This trend also occurred in the STT.

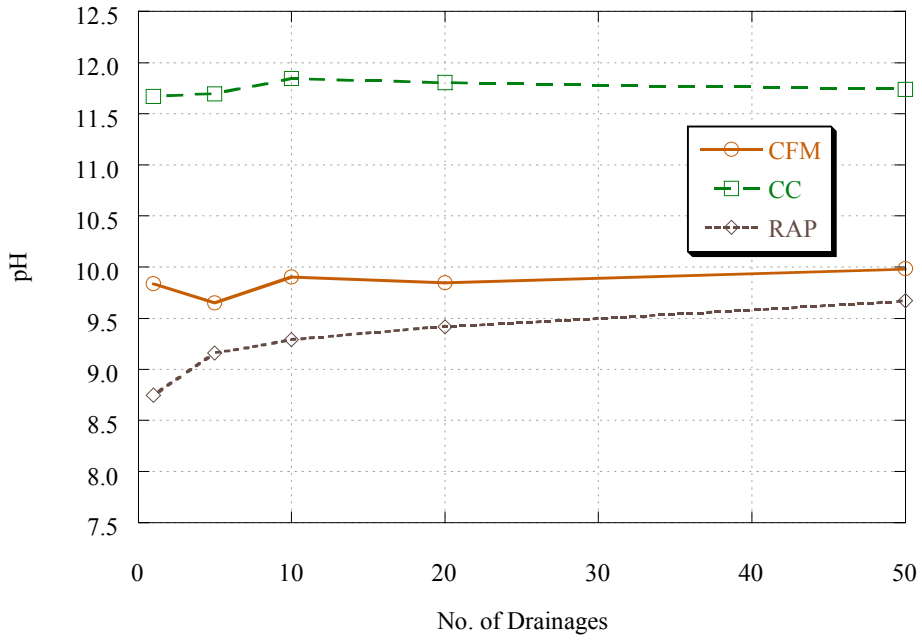

Figure 4.25. Plot of pH Versus Number of Drainages for Samples Exposed to CL Environment.

4.3.2.3 Resistivity

The conductivity of a solution obtained from the last drainage of the STT samples was measured. The conductivity readings were then converted into resistivity values.

Figure 4.26 shows that resistivity readings of the NCL samples are significantly higher than the CL readings. All three backfill materials in the NCL environment had significantly different resistivity readings. CFM had the highest readings followed by RAP, and then CC. There is a significant difference between CC compared to CFM and

RAP CL sample resistivities. There is also a trend in the variability of the readings, CFM has the most variability, followed by RAP and then CC.

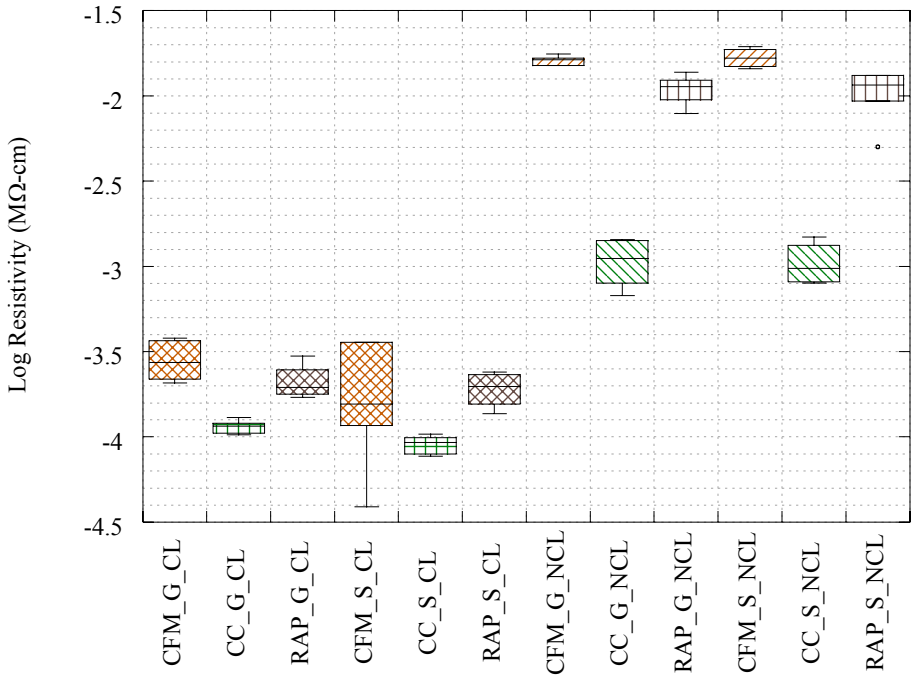

Figure 4.26. Boxplots of Log Resistivity Readings for LTT Samples.

Figure 4.27 shows the change in resistivity with the number of CL drainages through the backfill materials. All the backfill materials experienced a decrease in resistivity from the first to the fifth CL drainage, and a slight decrease form the fifth to the 20th CL drainage. The resistivity increased slightly from the 20th to 50th CL drainage for CFM and RAP, whereas the resistivity of CC stayed the same.

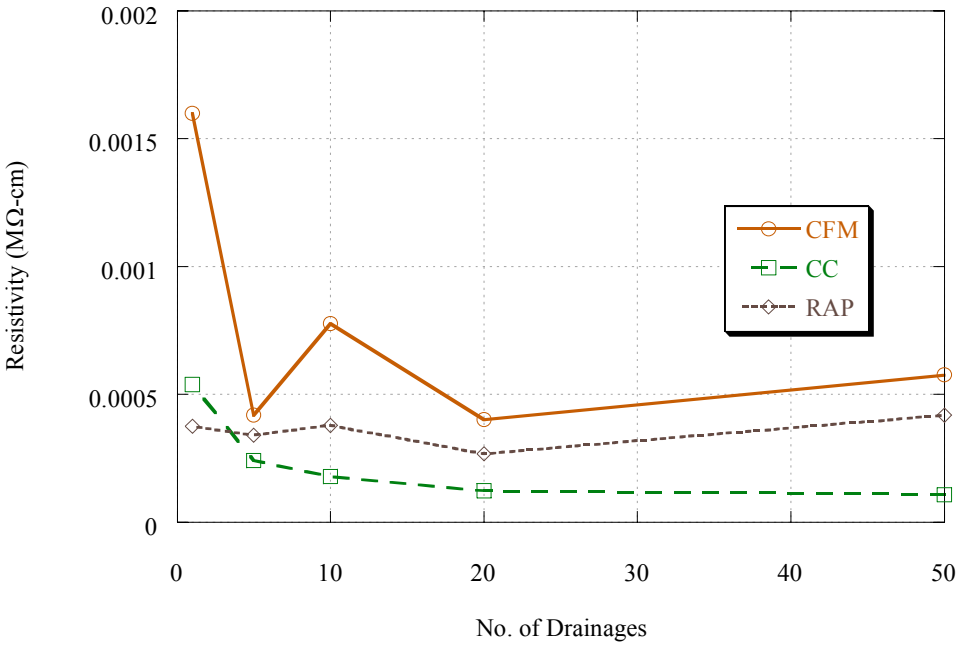

Figure 4.27. Plot of Resistivity Versus Number of Drainages for Samples Exposed to CL Environment.

4.3.2.4 Oxidation-Reduction Potential

The redox potential readings were significantly different between backfills. Redox potential has been used to indicate the presence of anaerobic bacteria. The redox potentials were slightly higher for an NCL environment versus CL, particularly for RAP, as shown in Figure 4.28. NCL redox readings are approximately 30 mV higher than CL readings for CFM and CC, whereas NCL redox potential readings are approximately 120 mV higher than CL readings for RAP. Backfills with a redox potential below 100 mV are thought to be severely aggressive towards corrosion (Elias 1990). Thus, CC would be considered severely aggressive. RAP and CFM would be considered moderately aggressive. However, the low redox readings do not necessarily indicate the presence of

anaerobic bacteria. One indication of the presence of anaerobic bacteria is sulfide. Anaerobic bacteria change sulfate to sulfide in the absence of oxygen. Sulfide testing was performed on all samples as described in Subsection 3.2.1.9 and no sulfides were discovered. This would be expected because the backfills are well-drained. It is possible that the CC has a lower redox potential because the hydraulic conductivity is lower than CFM and RAP and thus there is less aeration of the CC backfill. However, it is more likely that the difference in redox potential is due to the differences in the composition of the backfills.

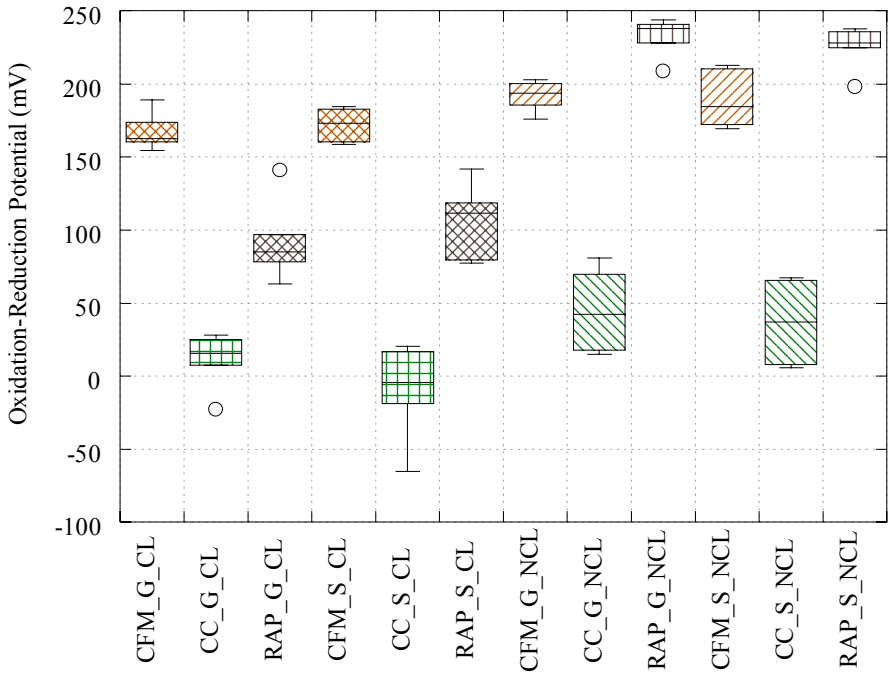

Figure 4.28. Boxplots of Oxidation-Reduction Potential Readings of LTT Samples.

The change in redox potential with the number of CL drainages is shown in Figure 4.29. The redox potential of CC is much lower than that of CFM and RAP. The CC and RAP exhibit a small negative drop in redox potential over the first ten days and

then the readings are more constant. The redox potential of CFM increased slightly over the last 30 drainages. Similar to the STT, it appears that the number of drainages has little affect on the redox potential.

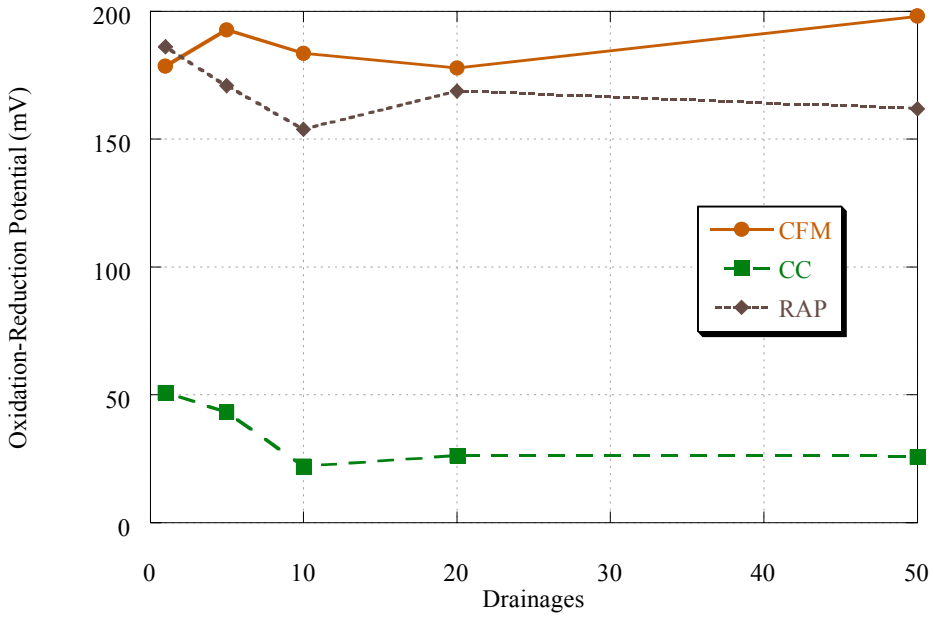

Figure 4.29. Oxidation-Reduction Potential Versus Number of CL Drainages.

4.3.2.5 Soluble Salts

The LTT samples were evaluated for the presence of chloride and sulfate ions. The concentration of chloride for the NCL samples was mostly below 30 mg/L. The chloride concentration for the NCL samples ranged between 750 to 4000 mg/L. A plot of log chloride concentration is shown for each LTT group in Figure 4.30. The CC samples have a significantly higher chloride concentration over CFM and RAP for most groups, and for all groups the average chloride concentration is higher for CC. There is no

significant difference between CFM and RAP chloride concentrations. This indicates that the CC samples may absorb chlorides more readily than the CFM and RAP samples.

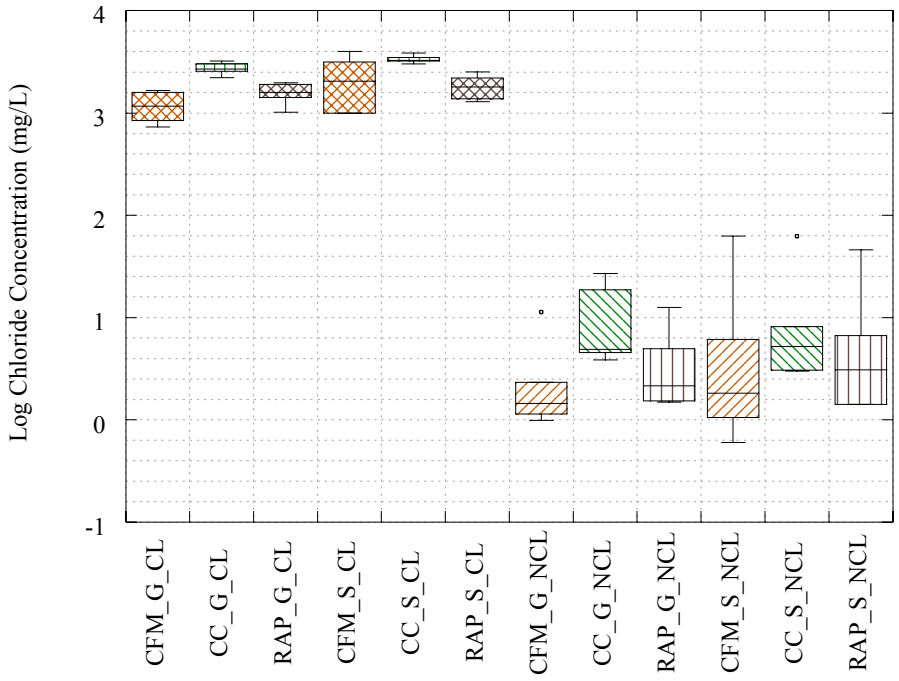

Figure 4.30. Boxplots of Log Chloride Concentration for Each LTT Group.

The sulfate concentration of the LTT samples is shown in Figure 4.31. CC exhibits a significantly higher sulfate concentration than CFM and RAP in both a CL and NCL environment. The sulfate concentrations of CFM and RAP were lower than 50 mg/L, whereas the sulfate concentration of CC samples ranged between 50 to 500 mg/L. There is more variability in the sulfate concentrations of CC over CFM and RAP. CC probably has a higher sulfate concentration due to the gypsum in cement. RAP has significantly higher concentrations of sulfate over CFM. This is probably due to the organic nature of the asphaltic coating.

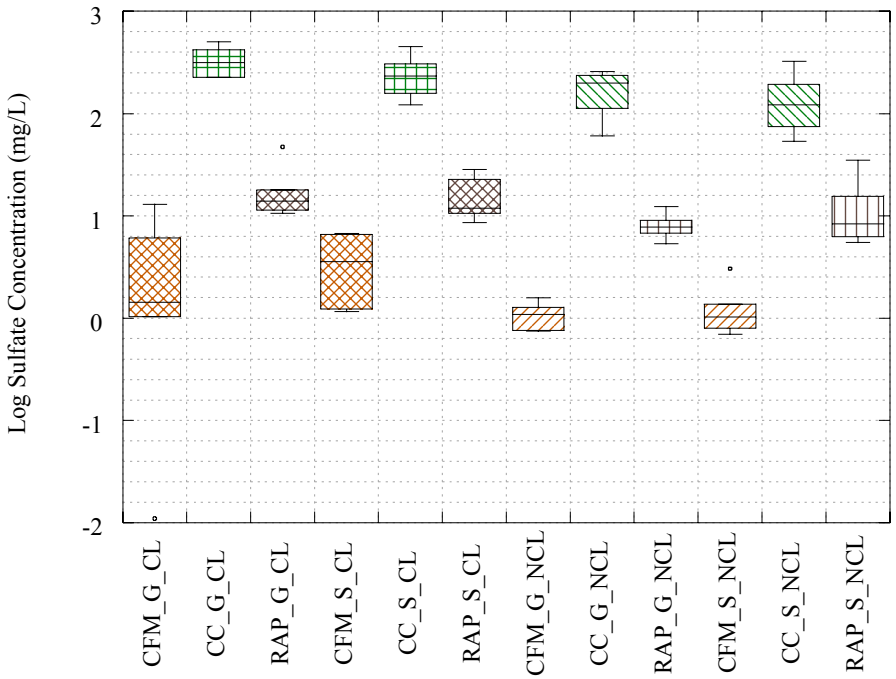

Figure 4.31. Boxplots of Log Sulfate Concentrations for Each LTT Group.

4.3.3 Mass Loss and Corrosion Rates

The mass loss of the samples was the most significant measurement made toward assessing the corrosivity of the backfill materials. The mass loss measurements were used to calculate the corrosion rate for each sample. The LTT samples were exposed to weekly applications of solution with or without added chloride for a period of approximately one year. Figure 4.32 shows that there is a significant difference in corrosion rate between a CL and NCL environment. There was no significant difference in corrosion rate between galvanized-steel and steel except for RAP in an NCL environment. The average corrosion rate for CFM_G and RAP_G was lower than

CFM_S and RAP_S. The average corrosion rate for CFM_G was approximately 3 mils/yr (76 μm/yr) higher than CFM_S for a CL environment. The average corrosion rate for all NCL sample groups was below 1.5 mils/yr (38 μm/yr). In general, the average corrosion rate was lowest for CC. There was more variability in the galvanized-steel mass loss measurements compared to steel. During the mass loss testing, it was observed that the epoxy coating was more likely to fall off of the galvanized-steel samples due to the erosion of the galvanized layer under the epoxy. This was probably the largest factor in increasing the variability. Another factor that could have caused the increase in variability is that the galvanized samples were only cleaned with an ammonium hydroxide based acid, while the steel samples were cleaned with a much stronger hydrochloric based acid according to specification ASTM G1. Some of the galvanization on the galvanized-steel samples had eroded to the steel and the steel had begun to corrode. Only the appropriate acid for galvanized-steel cleaning was used, regardless of whether or not the galvanization had eroded to the steel. This was done because the hydrochloric acid used to clean the steel samples would have quickly corroded through the remaining galvanization on the galvanized-steel samples. The corrosion rates for LTT samples with probes were compared to samples without probes to investigate another possible source of variability, but no significant differences in corrosion rate were found.

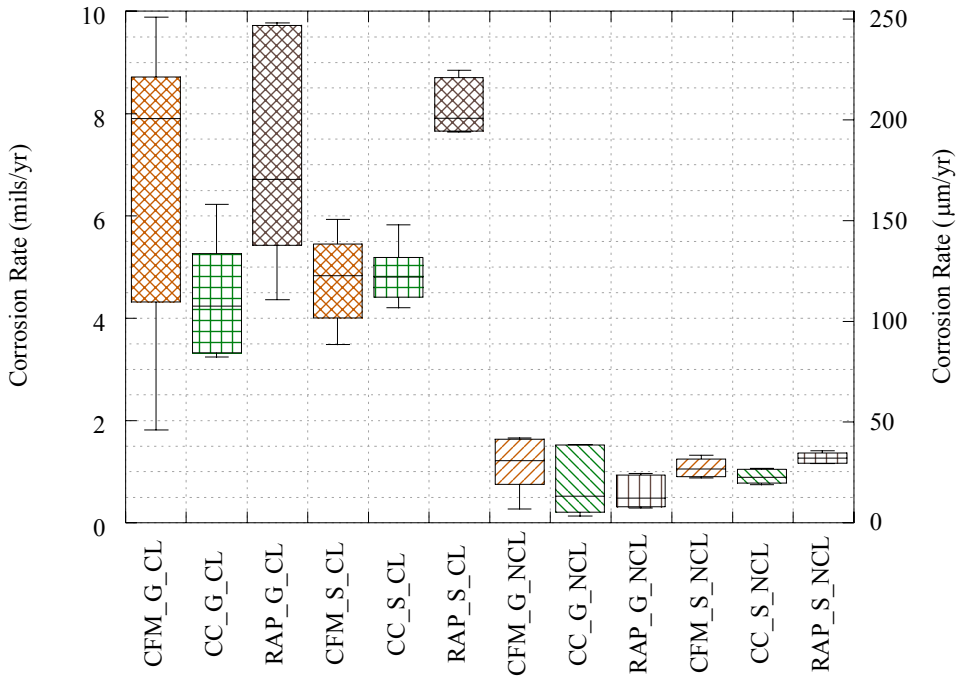

Figure 4.32. Boxplot of Corrosion Rates Calculated from Mass Loss Data for All LTT Samples.

4.3.4 Electrochemical Test Results

Electrochemical testing was performed on 24 of the 96 LTT samples. Non-destructive, linear polarization resistance testing was performed on these samples on a weekly basis. Destructive, cyclic polarization resistance testing was performed on these samples at the end of the LTT.

4.3.4.1 Linear Polarization Resistance

Similar to the STT samples, linear polarization resistance testing was performed for the LTT samples. However, linear polarization testing was only performed on 24

LTT samples, whereas it was performed on all the STT samples. The incremental corrosion currents for the LTT were summed and averaged over the 337-day testing period.

Figure 4.33 shows a scatter plot of actual mean measured corrosion rate versus estimated mean corrosion rate for all LTT CL test samples that were equipped with polarization resistance apparatus. The figure reveals that corrosion rate was overestimated for all samples except one CFM_G_CL and one CC_S_CL sample. The cause of the large discrepancy between the actual corrosion rate and estimated corrosion rates for the LTT CL samples is unknown.

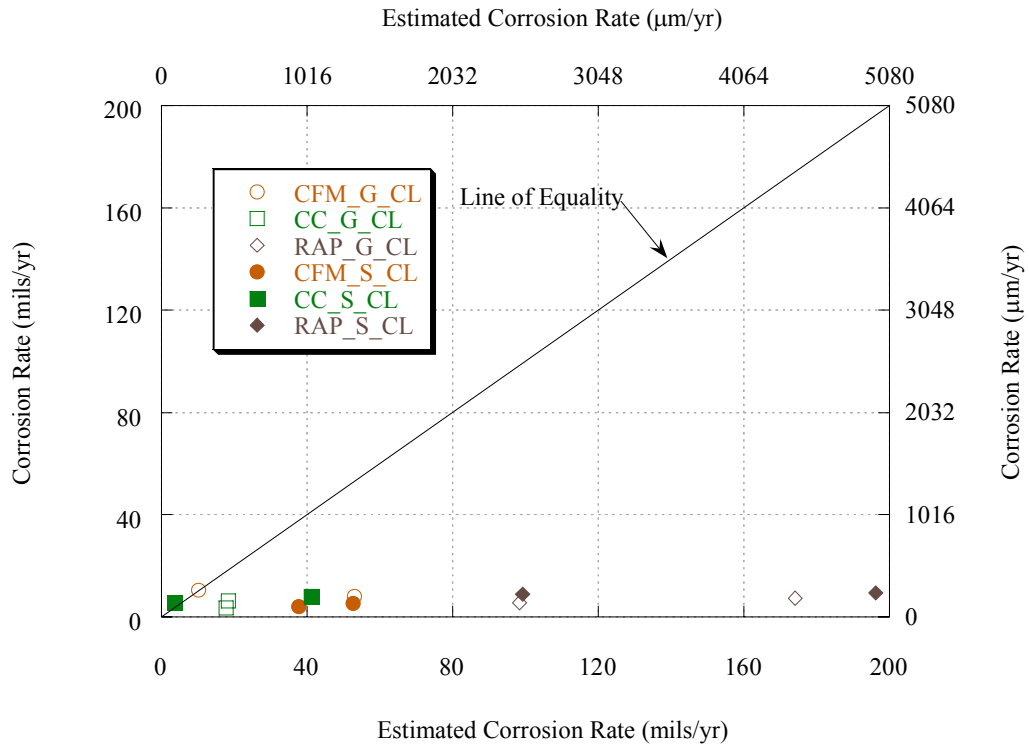

Figure 4.33. Corrosion Rate Calculated from Mass Loss Versus the Estimated Corrosion Rate Calculated from Polarization Resistance Measurements for the CL LTT Samples.

The actual measured corrosion rate versus estimated corrosion rate for all LTT NCL test samples equipped with polarization resistance apparatus is plotted in Figure 4.34. This plot shows that half of the estimated corrosion rates approximated the measured corrosion rates well while half were overestimates. The largest overestimates were for CFM_S_NCL.

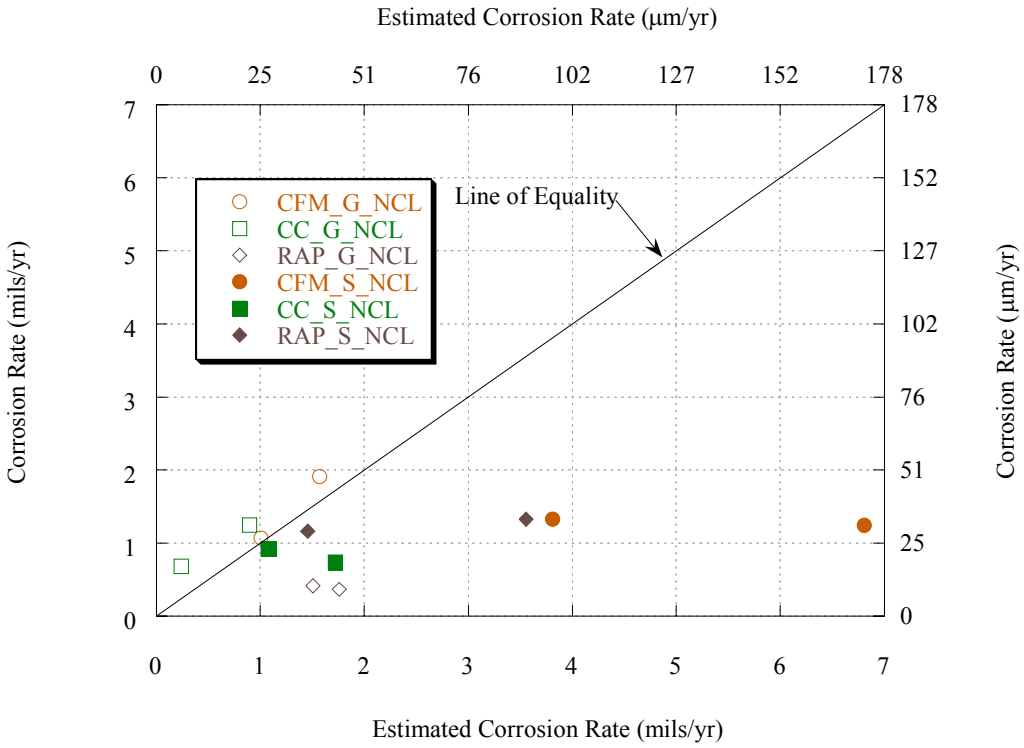

Figure 4.34. Corrosion Rate Calculated from Mass Loss Versus the Estimated Corrosion Rate Calculated from Polarization Resistance Measurements for the NCL LTT Samples.

Other researchers have found an approximately 20 percent difference between measured mass loss and mass loss calculated by the polarization resistance method when corrosion testing in soils was performed in identical conditions (Serra and Mannheimer 1981). The LTT measured corrosion rate and estimated corrosion rate calculated from

polarization resistance measurements exhibited order of magnitude differences, particularly for the chloride environment.

4.3.4.2 Cyclic Polarization Resistance

The Stearn-Geary coefficients do not remain constant over the length of the testing period. The electrochemical testing that is required to determine the Stearn-Geary coefficients has the potential to alter the corrosion process, which would jeopardize the reliability of the experiment. Therefore, the Stearn-Geary coefficients were only determined at the end of the experiment. The Stearn-Geary coefficients that were estimated were then assumed for the entire time of the LTT in order to estimate mass loss. Although the applied assumption likely introduces some error, the mass loss values could not have been estimated to any reasonable degree of accuracy without the application of a fair approximation for the Stearn-Geary coefficients. The cyclic polarization resistance graphs are shown in Appendix E.

Figure 4.35 shows the Stearn-Geary coefficients determined from the cyclic polarization testing of the G_LTT samples. Several significant differences in the Stearn-Geary coefficients between groups are noticed. For each backfill material, the G_CL group is less passive and significantly different from the G_NCL group with the exception of CC. The CC_G_NCL group has an average Stearn-Geary coefficient of approximately 52, whereas the CC_G_CL group has an average coefficient of approximately 56.

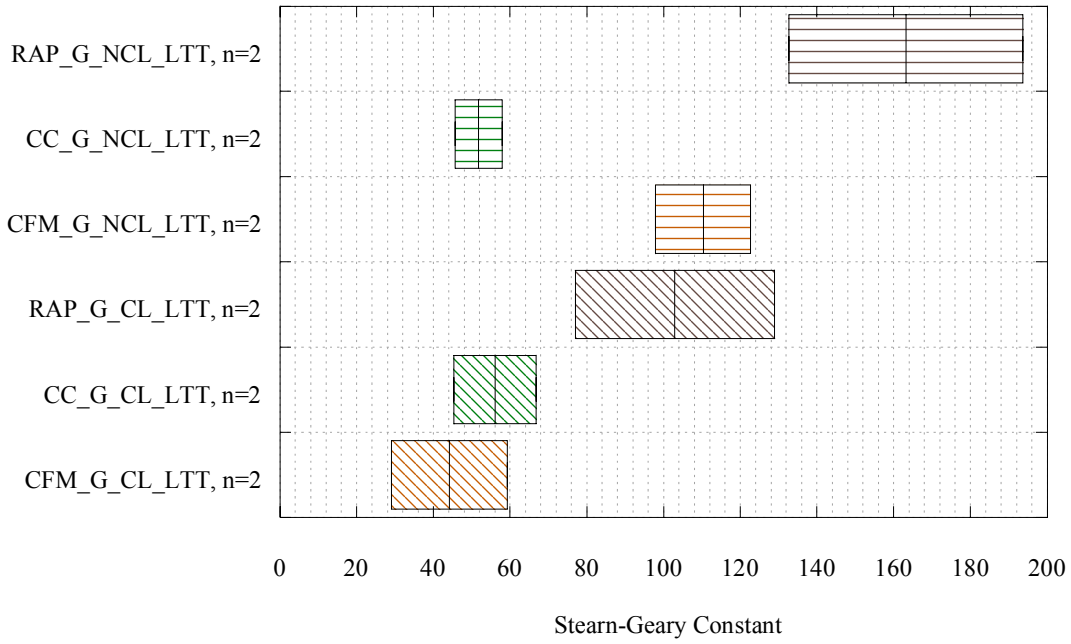

Figure 4.35. Boxplot of Stern-Geary Constants Derived from Cyclic Polarization Testing Plots for All the LTT G Samples.

For the G_CL group, the order of average Stearn-Geary values for the backfill materials from least passive to most passive is CFM at approximately 44, followed by CC at 56, and then RAP at 103. For the G_NCL group, the order of average Stearn-Geary values for the backfill materials from least passive to most passive is CC at approximately 52, followed by CFM at 110, and then RAP at 163. The RAP_G groups had the largest amount of variability.

The Stearn-Geary coefficients determined from the cyclic polarization testing of the S_LTT samples are shown in Figure 4.36. There are no significant differences within the S_CL or the S_NCL groups, except for the CFM_S group. In this instance,

CFM_S_CL is less passive with a Stearn-Geary coefficient of approximately 55, compared with CFM_S_NCL at approximately 95. For each backfill material, the average Stearn-Geary coefficient is more passive for S_NCL compared to S_CL. There is a larger amount of variation in the RAP_S groups.

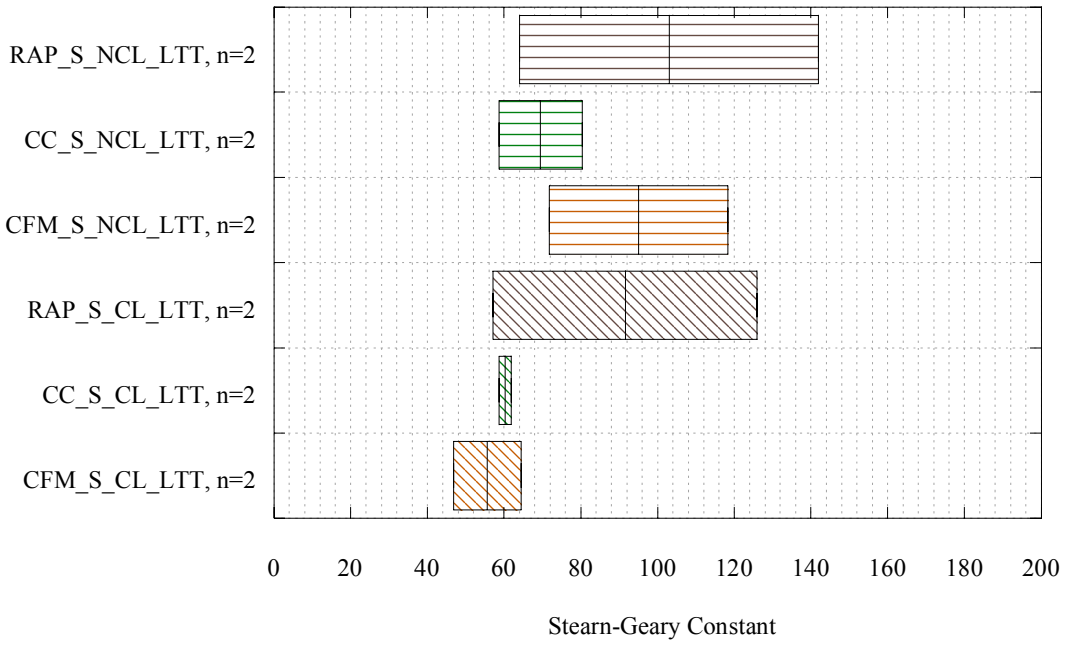

Figure 4.36. Boxplot of Stern-Geary Constants Derived from Cyclic Polarization Testing Plots for All the LTT S Samples.

4.3.5 Summary

There were several differences in measurements between the backfill materials for the LTT. NCL potential readings were more positive than CL readings for each LTT

material-metal group. Potential readings for CC were more positive than those for other backfills for each metal-environment combination, which indicates less corrosion activity. The pH of the backfill materials ranged from approximately 11 to 12 for CC, 9.3 to 10.3 for CFM, and 8 to 10 for RAP. Whether the environment is CL or NCL can affect the pH. The pH of RAP appears to be the most affected by the addition of chloride, while the pH of CC is the least affected by the type of solution application. CC had the lowest resistivity after approximately five drainages of all backfills for each environment, the lowest redox potential at all times, and the highest mean chloride and sulfate concentrations compared to the other backfill materials. There were no significant differences in corrosion rates between the backfill materials exposed to similar environments. There was also no significant difference in corrosion rate between metals except for the RAP with NCL. In general, the average corrosion rate was the lowest for CC for the samples tested in this research. The cyclic polarization resistance data does not correspond with the mass loss data, but was used to determine the Stearn-Geary coefficients for the estimation of mass loss.

4.4 COMPARISON OF SHORT AND LONG-TERM TEST RESULTS

As previously mentioned, the purpose of the STT was to determine if a shorter testing period could provide adequate insight and information on the corrosivity of the backfill materials. The STT also eliminates several variables that could be factors in the LTT such as backfill material density, frequency of solution application, and backfill material gradation. In general, measurements of the pore solution properties were similar between the STT and the LTT. With regard to the prediction of mass loss, the STT was not a good predictor of the LTT results. The physical size of the STT samples compared to the LTT samples may have been a factor. If epoxy flaked off of a STT sample, it had a much greater impact to the results than if this happened to a LTT sample. The LTT samples had much greater mass loss due to corrosion because the exposed area was larger and the samples were exposed for much longer periods. Thus, there was a larger percentage of the total sample weight that corroded compared to the STT samples. The

size of the STT samples was seemingly limited due to the size of the opening to the corrosion cells. The STT duration was insufficient to detect significant differences between the corrosivity of the backfill materials. The linear polarization and cyclic polarization results from the STT did not correspond well with the results from the LTT.

Experimentation by Serra and Mannheimer (1981) indicated corrosion rates two to four times higher for steel determined from using the mean current density obtained in the laboratory using water saturated soil versus corrosion rates determined from long-term field weight loss measurements. Compton (1981) reported that salt solutions do not realistically simulate soil conditions. Difference in results between the two could be attributed to factors such as ion mobility differences and the ion concentration at the soil-structure interface (Compton 1981).

4.5 GENERAL ASSESSMENT OF BACKFILL CORROSIVITY

Based on the LTT mass loss results, no one backfill material significantly outperformed another backfill material. However, the CC had the lowest average mass loss and the most positive potential readings, which indicates less mean corrosion activity at the surface. These results were in spite of CC having the highest chloride and sulfate concentration for the LTT and lower resistivity readings, in addition to the lowest redox potential, which typically indicates higher corrosion.

Due to the many factors known to influence corrosiveness in soil and the high degree of variability that often occurs in the data, the use of statistics was employed and is presented in the next section to compare the backfill materials. Current service-life models developed by others were also used to evaluate the backfill materials and compare currently available service-life prediction methods to the results presented in this thesis.

5. BACKFILL CORROSIVITY AND SERVICE-LIFE ESTIMATION

5.1 OVERVIEW

Backfill corrosivity should be examined to determine the effect on the service-life of MSE walls. To estimate the service-life of MSE walls backfilled with CFM, CC, or RAP, the existing methods for assessing backfill corrosivity were used, which includes the following assessment method types: point systems, empirical equations, categorical systems, and specifications. Models of service-life based on a statistical interpretation of the experimental results are compared to the existing methods.

5.2 BACKFILL CORROSIVITY ASSESSMENT METHODS

5.2.1 Point Systems

The three main point system assessment techniques are: AWWA, German Gas Engineering, and Eyre and Lewis. The backfill materials were assessed using these point systems and the results are shown in Table 5.1. According to the AWWA method, CC is considered corrosive to cast iron; whereas, CFM and RAP are not considered corrosive to cast iron. The assessment techniques by German Gas Engineering and Eyre and Lewis yielded the same assessment: CFM is considered unlikely to be aggressive and CC and RAP are considered to be mildly aggressive.

Some of the parameters were not straightforward determinations - for instance, the nature of soils was an issue. The German Gas Engineering Technique assessment criteria for nature of soils are more applicable to soil than for aggregate classified as gravel.

Table 5.1. Backfill Material Corrosivity Assessment Based on Point Systems.

PARAMETER	BACKFILL MATERIAL	POINT SYSTEM		
		AWWA	GERMAN GAS ENGINEERING	EYRE AND LEWIS
NATURE OF SOILS	CFM	N/A	+2	+2
	CC	N/A	0	+2
	RAP	N/A	0	+2
RESISTIVITY	CFM	0	-1	-1
	CC	+10	-3	-3
	RAP	+1	-2	-2
REDOX POTENTIAL	CFM	0	N/A	-2
	CC	+5	N/A	-4
	RAP	0	N/A	-2
CHLORIDE ION CONCENTRATION	CFM	N/A	0	0
	CC	N/A	0	0
	RAP	N/A	-1	-1
SULFATE ION CONCENTRATION	CFM	N/A	0	0
	CC	N/A	0	0
	RAP	N/A	0	0
PH	CFM	+3	0	0
	CC	+3	0	0
	RAP	0	0	0
ORGANIC MATERIAL	CFM	N/A	N/A	0
	CC	N/A	N/A	0
	RAP	N/A	N/A	0
SULFATE REDUCING BACTERIA	CFM	N/A	0	N/A
	CC	N/A	0	N/A
	RAP	N/A	0	N/A
SULPHIDE	CFM	0	0	0
	CC	0	0	0
	RAP	0	0	0
DRAINAGE	CFM	0	N/A	+1
	CC	0	N/A	+1
	RAP	0	N/A	+1
MOISTURE CONTENT	CFM	N/A	0	0
	CC	N/A	0	0
	RAP	N/A	0	0
CARBONATE	CFM	N/A	0	0
	CC	N/A	0	0
	RAP	N/A	0	0
SOIL CONDITION	CFM	N/A	0	0
	CC	N/A	0	0
	RAP	N/A	0	0
SCORING	CFM	+3	+1	0
	CC	+18	-3	-4
	RAP	+1	-3	-2
ASSESSMENT SUMMARY	CFM	-	Unlikely to be aggressive	Unlikely to be aggressive
	CC	Corrosive to cast iron	Mildly aggressive	Mildly aggressive
	RAP	-	Mildly aggressive	Mildly aggressive

5.2.2 Empirical Equations

Two corrosivity assessment methods that utilize empirical equations are the Caltrans (1993) Test Method 643 and Elias (1997) from data by Romanoff (1957). The method by Caltrans uses pH and resistivity values to determine the years to perforation of galvanized-steel culverts. The years to perforation is not the total useful service-life of culverts, but is defined as, "a common point at which it is likely that maintenance funds could be spent to repair corrosion damage," otherwise known as maintenance free service-life (Caltrans 1993). The resistivity and pH values used to perform the Caltrans assessment were taken from the first NCL pore solution drainage of the backfill materials. The calculated years to perforation are shown in Table 5.2. According to the Caltrans assessment, galvanized-steel culverts backfilled with CFM are estimated to have a longer maintenance free service-life followed by those backfilled with RAP and CC.

Table 5.2. Backfill Material Service-life Assessment Based on CalTrans (1993) Empirical Equation.

Backfill Material	Resistivity (Ω-cm)	pH	Years to Perforation*
CFM	4400	8.6	45.8
CC	410	11.8	17.3
RAP	1700	7.4	31.0

* for an 18 gage (52 mil [1321 μm]) galvanized-steel culvert having 2 oz/ft^2 (0.61 kg/m^2) of zinc coating

Figure 5.1 shows the maximum and average expected loss of thickness over time for galvanized-steel and carbon-steel using the empirical equations presented by Elias (1997) developed from interpretation of data by Romanoff (1957).

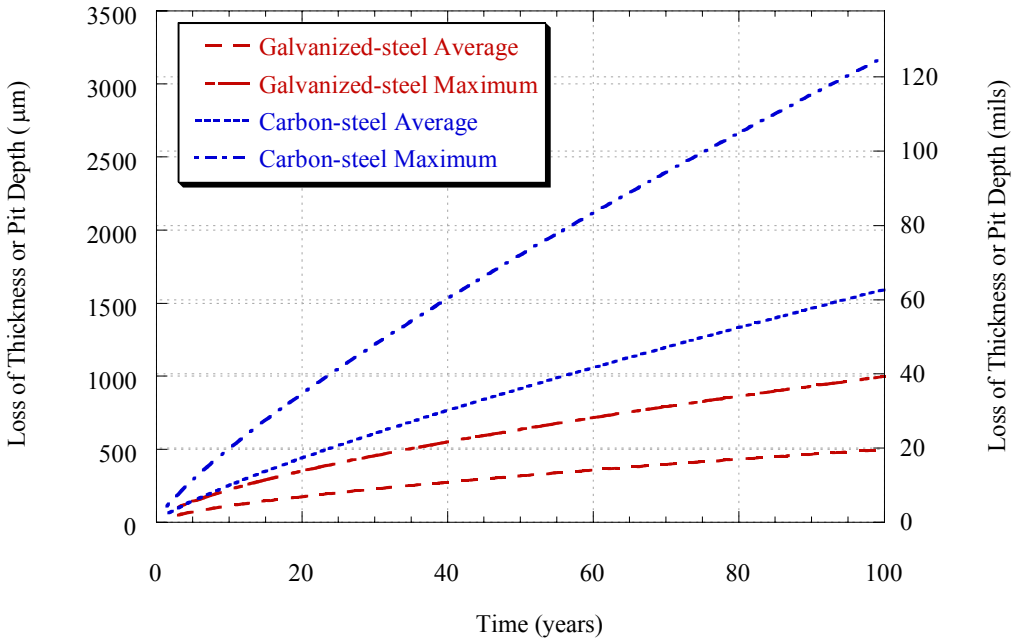

Figure 5.1. Plots of Estimated Corrosion of Galvanized-steel and Carbon-steel Using Generalized Soil Corrosion Predictive Empirical Equations by Elias (1997) from data by Romanoff (1957).

The average and maximum predicted corrosion rates from the LTT are shown in Table 5.3 are can be compared to corrosion rates estimated from the empirical equations by Elias (1997), although such a comparison may be unreasonable because these equations estimate long-term loss of thickness, whereas the LTT corrosion rates were determined from only one year of study. According to the empirical equations by Elias (1997), the loss of thickness for the first year would be a maximum of 2.0 mil (50 µm) for galvanized-steel and 3.1 mil (80 µm) for plain-steel. The LTT corrosion rate maximum for a NCL environment are 1.65 mil (42 µm) for galvanized-steel and 1.42 mil (36 µm) for plain-steel, which are below the maximum estimated by empirical equations by Elias (1997). These empirical equations estimate the corrosion rate of carbon-steel to

be higher than galvanized-steel, whereas the LTT results indicate slightly higher or the same corrosion rates for galvanized-steel compared to carbon-steel. The LTT maximum corrosion rates for CL environment are 9.8 mil (251 μm) for galvanized-steel and 8.9 mil (225 μm) for plain-steel, which are underestimated by the empirical equations by Elias (1997).

Table 5.3. Average and Maximum Corrosion Rates from the LTT.

	LTT Corrosion Rates			
	Average (mils/yr)	**Maximum (mils/yr)**	**Average (μm/yr)**	**Maximum (μm/yr)**
CFM_G_CL	7.1	9.9	179	251
CC_G_CL	4.4	6.2	112	158
RAP_G_CL	7.1	9.8	180	248
CFM_G_NCL	1.1	1.7	29	42
CC_G_NCL	0.7	1.5	19	39
RAP_G_NCL	0.6	1.0	15	24
CFM_S_CL	4.8	5.9	122	151
CC_S_CL	4.9	5.8	123	148
RAP_S_CL	8.1	8.8	205	225
CFM_S_NCL	1.1	1.3	27	34
CC_S_NCL	0.9	1.1	23	27
RAP_S_NCL	1.3	1.4	32	36

5.2.3 Categorical Systems

The corrosivity assessment based on King (1977) relies on measurements of the resistivity and redox potential. Table 5.4 shows that CC is considered very corrosive, RAP - corrosive, and CFM - moderately corrosive based on this assessment method. The

results of this assessment do not correspond with the results from the LTT, which found that the average corrosion rate of CC was generally comparable to or less than that of CFM and RAP.

Table 5.4. Backfill Material Corrosivity Assessment Based on King (1977).

Backfill Material	Resistivity (Ω-cm)	Redox Potential (mV)	Corrosivity Assessment
CFM	4400	187	Moderately Corrosive
CC	410	-31	Very Corrosive
RAP	1700	120	Corrosive

The corrosivity assessment results for the backfill materials based on Applegate (1960) are shown in Table 5.5 and Table 5.6. The corrosivity assessment using potential readings correctly estimates that the reinforcement samples evaluated in a CL environment are likely to experience severe corrosion, whereas samples in the NCL environment should experience mild to moderate corrosiveness. The assessment can differ depending on whether the potential or the ratio of min to max potential is used.

Table 5.5. Backfill Material Corrosivity Assessment for Steel Based on Applegate (1960).

Backfill Material-Metal-Environment	Average Potential vs. Cu-Cu_2SO_4 (mV)	Average Ratio of Min to Max Potential	Probable Corrosiveness Based on Potential	Probable Corrosiveness Based on Ratio
CFM_S_CL	-683	1.12	Severe	Severe
CC_S_CL	-590	1.21	Severe	Severe
RAP_S_CL	-614	1.31	Severe	Moderate
CFM_S_NCL	-442	2.27	Mild	Very Mild
CC_S_NCL	-354	2.15	Mild	Very Mild
RAP_S_NCL	-468	1.58	Moderate	Mild

Applegate (1960) presented a corrosivity assessment method for steel only. However, the values of the ranges provided by Applegate were shifted by 323 mV, which is the difference in potential between Fe^{2+} and Zn^{2+} on the electromotive series to provide a similar assessment for zinc which is shown in Table 5.6. The ratio of min to max potential is shown in Table 5.6 for information only and was not used to assess probable corrosiveness.

Table 5.6. Backfill Material Corrosivity Assessment for Galvanized-steel (adapted from Applegate 1960).

Backfill Material-Metal-Environment	Average Potential vs. Cu-Cu_2SO_4 (mV)	Average Ratio of Min to Max Potential	Probable Corrosiveness Based on Potential
CFM_G_CL	-824	1.63	Severe
CC_G_CL	-758	1.52	Mild
RAP_G_CL	-862	1.64	Severe
CFM_G_NCL	-633	2.74	Mild
CC_G_NCL	-357	2.11	Practically None
RAP_G_NCL	-694	1.83	Mild

The corrosivity assessment by Chaker (1981) was not used to assess the backfill materials because the resistivity data was not obtained from field measurement using the Wenner Four Electrode method.

5.2.4 Specifications

The acceptability of the backfill materials differs among the various specifications. From these specifications, (which may not be applicable for recycled materials), CFM meets the requirements of all the specifications listed in Table 5.7 except those of the United Kingdom. CC and RAP do not meet any of the specifications and fail primarily on the basis of low resistivity values.

Table 5.7. Acceptability of MSE Wall Backfill Materials Using Various Specifications.

Specification	Backfill Material	Meets Specification?	Comments
U.S. FHWA	CFM	Y	
	CC	N	Res. low, pH high
	RAP	N	Res. low
France	CFM	Y	
	CC	N	Res. low, pH high
	RAP	N	Res. low, Cl high
United Kingdom	CFM	N	Res. low, Redox low
	CC	N	Res. low, pH high, Redox low
	RAP	N	Res. low, Redox low
Germany	CFM	Y	
	CC	N	Res. low, pH high, Redox low
	RAP	N	Res. low, Cl high
TxDOT	CFM	Y	
	CC	N	Res. low, pH high
	RAP	N	Res. low, Cl high

5.3 ESTIMATION OF SERVICE-LIFE FROM EXPERIMENTAL RESULTS

The factors thought to have an impact on backfill corrosivity were tested. These results were presented in Section 4. The results were used to perform statistical analysis with Statistical Analysis Software (SAS). Models were built based on the LTT data only, since there was poor correlation between the STT and LTT results as described in Subsection 4.4.

Several classification variables were used when analyzing the data, backfill material, metal type, and environment. The data that were analyzed to formulate the

models were corrosion rate, density, resistivity, chloride, sulfate, redox potential, and pH. The raw data collected for each of these variables are provided in Appendix H.

5.3.1 Backfill Corrosivity Modeling

Backfill corrosivity modeling was performed using the LTT data. All models presented in this subsection have a 0.05 significance level. First, all the LTT data were examined collectively. Examination of the data was performed with and without the use of classification variables. When all the LTT data were examined with classification variables only (backfill, environment, and metal type), only backfill and environment were found to significantly affect the expected value of the corrosion rate. Equation 5.1 has an adjusted R-square of 79 percent. The model for estimating corrosion rate of galvanized-steel or steel embedded in CFM, CC, or RAP using the backfill and environment type is:

$$k = 1.709 - 1.537(Bfill = 'CC') - 0.737(Bfill = 'CFM') + 5.102(Env = 'CL') \quad (5.1)$$

where,

- k is the estimated corrosion rate in mils/yr,
- the parenthesis Bfill term is one if the statement is true and zero if false, for example if the backfill type is CC then Bfill = 'CC' becomes one, and
- the parenthesis Env term is one if the statement is true and zero if false, for example if the environment is CL then Env = 'CL' becomes one.

Equation 5.1 shows that with the objective of reducing corrosion rate, using CC in a NCL environment is predicted to be the best combination. The CC backfill is estimated to have the lowest corrosivity, followed by CFM, and then RAP. The equation also shows that a CL or NCL environment is most influential on the corrosion rate. Interaction between terms exists in the above model that uses classification variables.

If the significance of the classification variables is ignored to create a model based on measured variables only, all variables were found to be significant. The order of significance is log chloride, log resistivity, pH, density, log sulfate, and redox potential. The logarithm was taken for resistivity, chloride, and sulfate because the measured values are often several magnitudes apart. Density is not a commonly measured variable in corrosion assessments. Furthermore the significance of density is probably attributed more to the significance of the backfill materials since each backfill material had a different target density for the testing. Therefore, the density term was eliminated. Also, it was questionable whether both log chloride and log resistivity were both necessary since they are highly correlated. The log resistivity variable was kept and log chloride was removed because resistivity is a typical measurement that is easier to perform. Other researchers have pointed to resistivity as being the predominant factor in assessing backfill corrosivity (Chaker 1981). Equation 5.2 shows the model based on measured variables only and has an adjusted R-square of 81 percent.

$$k = 15.77 - 2.755\rho - 1.691pH - 1.088[SO_4^{2-}] - 0.019\phi_X \tag{5.2}$$

where,

- ρ is log resistivity in MΩ
- pH is pH (negative logarithm of the hydronium ion concentration)
- $[SO_4^{2-}]$ is log sulfate concentration in mg/L
- ϕ_X is the oxidation-reduction potential in mV

The model shown in Equation 5.2 may be of use for other materials or environments that are not easily classified into CL or NCL. Further experimentation on other materials and environments with varying values of data should be tested. Equation 5.2 is only applicable for estimation of first year average corrosion rate for backfill with measured variables that lie within the ranges shown in Table 5.8. The ranges were developed using the 5 percent and 95 percent quantiles for the experimental data obtained

from the LTT. All backfill materials had undetectable sulfide concentrations. Therefore, use of the above equation for estimation of corrosion rate for materials with sulfides present, in spite of all measured variables being within the ranges shown in Table 5.8, would be invalid.

Table 5.8. Ranges of Applicability for Using Corrosion Rate Prediction Equations Developed from LTT.

Variable	Range
Chloride Concentration (mg/L)	1 to 3260
Density (lb/ft^3)	105 to 126
Redox Potential (mV)	-5 to 238
Resistivity (MΩ)	$9.02E^{-05}$ to $1.67E^{-02}$
Sulfate Concentration (mg/L)	1 to 323
pH	8 to 12

Since backfill material type was found to be a significant variable in corrosion rate prediction, each backfill material was examined independently and models were formulated. When backfill materials were examined independently, the redox potential and sulfate concentration variables lost significance. These two variables were predictors of backfill type. Therefore, redox potential and sulfate concentration were not used in each backfill corrosion rate prediction model. For each backfill material, log resistivity and pH were used to predict the corrosion rate. The model for CFM is shown in Equation 5.3 has an adjusted R-square of 86 percent.

$$k = -45.07 + 4.498\,pH - 2.017\,\rho \tag{5.3}$$

The model for CC has an adjusted R-square of 92 percent. The model is shown in Equation 5.4.

$$k = -1.701 - 0.704\,pH - 3.604\rho \quad (5.4)$$

The model for RAP has an adjusted R-square for the predicted model of 87 percent. The predicted model is shown in Equation 5.5.

$$k = -2.156 - 0.525\,pH - 3.928\rho \quad (5.5)$$

When the models for the backfill materials that do not use the classification variables were examined, resistivity was the dominant variable in all the models, with the next most influential variable being pH. This agrees with the CalTrans (1993) service-life prediction model where resistivity and pH are the only variables used to estimate service-life of galvanized-steel culverts.

5.3.2 Reinforcing Strip Service-life

The end of MSE wall reinforcing strip service-life is the point at which the original allowable cross-sectional loss of the metal reinforcing strip is reduced by corrosion such that the minimum structural steel required to sustain the load is all that remains. This allowable cross-sectional loss is often referred to as the sacrificial thickness. This thickness includes steel and zinc in the case of a galvanized-steel metal reinforcing strip. The term sacrificial coating refers to the sacrificial anode coating such as zinc. The minimum structural steel required to sustain the load at the end of the service-life is determined using calculated values from the allowable reinforcement stress equations, AASHTO 10.32 for reinforcing strips and AASHTO 5.8.7 for bar mats and welded wire meshes (Reinforced Earth Company 1995).

Two types of service-life calculations are made using the experimental results: sacrificial thickness estimated for 75 year service-life and an estimated service-life assuming AASHTO (Elias 1997) specified sacrificial thickness of 62.6 mil (1590 μm), 3.4 mil (86 μm) of which is galvanization, currently specified by AASHTO (Elias 1997) for MSE walls. Table 5.9 shows the estimated sacrificial thicknesses required for 75 year service-life specified by AASHTO (Elias 1997) using the corrosion rate prediction

models based on the findings of the LTT for each backfill material - environment combination. The estimated years of service-life assuming the AASHTO (Elias 1997) 75 year service-life sacrificial thickness and using the corrosion rate prediction models for the backfill materials is shown in Table 5.10.

Several assumptions are made to estimate the service-life of reinforcing strips embedded in the backfill materials. The first assumption is that the service-life for reinforcing strips is the depletion point of the total sacrificial thickness. This assumption is consistent with that made by Elias (1997) to recommend the sacrificial thickness required by AASHTO for MSE walls. The second assumption is that the use of the average corrosion rates determined from the backfill materials' experimental results to calculate is conservative, as opposed to using the maximum rate which may be overly conservative. The average corrosion rates obtained from the experimental results are considered conservative because they were obtained from samples in the laboratory with samples in an environment conducive to maximizing corrosion. For example, solution was applied on a weekly basis, so the samples were constantly undergoing a wet - dry process, and the samples were only embedded six inches deep, so depletion of oxygen from the backfill was unlikely. The third assumption is that the corrosion rate for the galvanized and steel layers remains constant over time. This assumption is also conservative because given consistent environmental conditions over time, the corrosion rate is highest during the first year of exposure.

The estimated total sacrificial thickness for each backfill material - environment combination shown in Table 5.9 is higher than the sacrificial thickness specified by AASHTO (1997). For a CL environment, it is estimated that a 477 to 866 percent increase in sacrificial thickness would be required to obtain a 75 year service-life using the backfill materials. For a NCL environment, between 7 to 45 percent more required sacrificial thickness was estimated. The values in Table 5.9 show that the sacrificial thickness required for a CL environment is 4.5 to 7 times higher than that required for an NCL environment.

Table 5.9. Estimated Sacrificial Thickness to Obtain 75 Year Service-life for Various Backfill Material - Environment Combinations Based on the Backfill Materials' Corrosion Rate Prediction Models.

Backfill Material - Environment Combination	Estimated Average Steel Sacrificial Thickness		Estimated Average Total Sacrificial Thickness*	
	(mil)	(μm)	(mil)	(μm)
CFM_CL	358	9090	361	9170
CC_CL	359	9130	365	9260
RAP_CL	601	15270	605	15360
CFM_NCL	77	1940	80	2030
CC_NCL	64	1620	67	1710
RAP_NCL	87	2220	91	2300

* a sacrificial galvanized coating of 3.4 mil (86 μm) was assumed corresponding to a coating weight of 2 oz/ft^2 (0.61 kg/m^2)

Table 5.10 shows the estimated service-life of reinforcing strips embedded in the backfill materials when the sacrificial thickness specified by AASHTO (1997) is assumed. CC with an NCL environment is the best combination, resulting in an estimated service-life of approximately 70 years, followed by CFM_NCL at 59 years, and RAP_NCL at 53 years. A chloride ion environment drastically reduces the estimated service-life to an estimated range of 13 to 8 years. It should be noted that chloride ion contents used in this study were very high.

Table 5.10. Estimated Service-life in Years For Reinforcing Strips of Sacrificial Thickness Currently Specified by AASHTO (Elias 1997) for MSE Walls.

Backfill Material - Environment Combination	Estimated Time to Deplete Sacrificial Galvanization (years)	Estimated Time to Deplete Sacrificial Steel (years)	Estimated Average Service-life* (years)	95 Percent Confidence Interval for Average Estimated Service-life (years)
CFM_CL	0.5	12.3	12.8	11.6 – 14.0
CC_CL	0.8	12.2	13.0	11.6 – 14.4
RAP_CL	0.5	7.3	7.8	7.3 – 8.3
CFM_NCL	3.0	55.7	58.7	53.3 – 64.1
CC_NCL	4.5	65.4	69.9	61.2 – 78.6
RAP_NCL	5.7	47.0	52.7	45.9 – 59.5

* a total sacrificial thickness of 62.6 mil (1590 μm) of which 3.4 mil (86 μm) is galvanization was assumed

5.4 COMPARISON OF PROPOSED MODEL WITH EXISTING MODELS

The backfill material corrosivity assessment based on the point systems does not correspond well with the corrosivity assessment based on the experimental results. The point systems by German Gas Engineering and Eyre and Lewis (1987) are somewhat in agreement with the corrosivity assessment based on the experimental results, unlike the AWWA method assessment. The application of the point systems requires much quantitative data gathering and only provides a limited qualitative assessment that is not associated with actual corrosion rate values. Thus, the point system approach seems to require much experimentation in order to apply a simplified approach that provides limited value. It seems that a point system method would be more applicable to simplifying the amount of testing and analysis required to formulate a reasonable approximation of soil corrosivity for specific geographic regions with common soil

characteristics and predictable corrosion behavior. An all inclusive point system for the assessment of corrosivity seems futile based on the findings of this research.

Empirical equations provide the power of performing calculations resulting in a quantitative assessment. The CalTrans (1993) method used to estimate service-life of galvanized-steel culvert pipe is a simple equation using only resistivity and pH values. The service-life assessment based on the CalTrans (1993) method does not agree with the corrosivity assessment based on the experimental results from this research. Using the CalTrans (1993) method, the service-life for the backfill materials in an NCL environment is estimated as: CFM - 46 years, RAP - 31 years, and CC - 17 years. The estimate of service-life based on the experimental results for an NCL environment is: CC - 70 years, CFM - 59 years, and RAP - 53 years. The estimated service-life from the two methods is not directly comparable because the sacrificial thicknesses differ between culverts and reinforcing strips. CalTrans (1993) does not provide the total sacrificial thickness or a procedure for calculating it for different pipe gauges. The method is based on the time to first full penetration. Therefore, estimated service-life from the experimental results cannot be accurately compared directly to the CalTrans (1993) method.

The empirical equations by Elias (1997) provide envelopes for soil corrosion and were formulated based on a wide range of corrosion data and are said to be conservative (Elias 1997, Reinforced Earth Company 1995). However, the loss of thickness of reinforcing strips embedded in the backfill materials for one year in a CL environment is far beyond the maximum envelope provided by Elias (1997). Therefore, these empirical equations may not be applicable for estimating loss of thickness for metals embedded in soils with high chloride exposure. These empirical equations by Elias (1997) do appear conservative when compared to the assessment based on the experimental results of reinforcing strips in the backfills in an NCL environment.

The categorical systems are fairly simple methods of assessing backfill corrosivity. The assessment method by King (1977) did not agree with the experimental results. CFM was considered moderately corrosive, RAP corrosive, and CC very

corrosive using the assessment based on King (1977). The order of corrosivity based on the experimental results from least to most was CC, CFM, and then RAP.

The corrosivity assessment based on Applegate (1960) was in general agreement with the assessment based on the experimental results. It is suspected that the Applegate (1960) method was successful because potential data was collected from the time of initial reinforcing strip embedment and collected periodically on consistent time intervals. Like point systems, categorical systems have the weakness of providing a limited qualitative assessment that is not associated with actual corrosion rate values.

Specifications are used to determine the acceptability of various materials as backfill. The CFM used in this research is considered an acceptable backfill material for MSE walls by all specifications listed in Table 5.7 with the exception of the United Kingdom. CC and RAP do not meet any of the specifications. All these specifications found CC to be unacceptable when the corrosivity assessment from the experimental results found CC to be less corrosive than CFM. One disadvantage of specifications is that for the sake of clarity, they often have a strict interpretation and do not allow conditional statements, thereby possibly excluding materials that might otherwise be acceptable.

Popova et al. (1998) found that the corrosivity of CC appears to be comparable to, or slightly better than conventional fill. The corrosivity assessment from the experimental results is in agreement with Popova et al. (1998). The corrosion rates associated with CC from the LTT are higher than corrosion rates reported by Popova et al. (1998). The maximum corrosion rate for CC_G_NCL from the LTT is 1.5 mils/yr (39 μm), whereas Popova et al. (1998) reported a maximum corrosion rate of 0.79 mils/yr (20 μm) for backfill with 4 percent cement content. The percent of unhydrated cement of the CC backfill material was not determined.

Several reasons are suspected for the general disagreement between the corrosivity assessments based on existing models and the assessment based on the experimental data. Almost all existing corrosivity assessment models consider high pH to be a negative influence on corrosivity. Many of the existing assessment models appear to apply methods that accept values outside the range of data that the data are based on.

Ranges of applicability for existing assessment models are not provided. The higher pH associated with CC is a factor that could be attributed to the better service-life estimated for reinforcing strips embedded in CC. For all existing corrosivity assessment models, cement content is not a factor. Cement has the potential in some instances to bind chlorides which would affect corrosion. Corrosion is often underestimated for high chloride environments because data used to formulate the existing assessment methods is predominately based on naturally occurring soil. High concentration of chlorides from de-icing salts exists as an unnatural occurrence nearby elevated roadways and bridge structures. MSE walls, which are commonly found at bridge abutments should be designed considering the likelihood of chloride exposure. Corrosion is influenced by many different factors causing high variability in corrosion data and complicates the estimation of corrosion rate. Models for assessing corrosivity must be simple to be practical. Given the complexity of corrosion, oversimplification is easy.

The models developed from the corrosivity assessment based on the experimental data for the backfill materials are as simple as they can be and their applicability is justified by the use of statistics. Ranges of applicability are provided for these models in Table 5.8. The major weakness of the models from this research is they are based on corrosion testing for only one year. Thus, placing confidence in the ability of the models developed from the experimental data to estimate the corrosion rate for extended periods of time is risky.

6. CONCLUSIONS

6.1 CONCLUSIONS

CC appears to provide similar or longer service-life than MSE walls backfilled with CFM based on the one-year LTT experiment. Few significant differences in corrosion rate based on mass loss from the LTT were found between backfill materials exposed to similar environments. The variability of corrosion rate based on mass loss from the LTT was greater for galvanized-steel compared to plain-steel. In general, the average corrosion rate was lowest for CC. The estimation of corrosion rates based on polarization resistance testing did not agree with the corrosion rates based on mass loss for the LTT.

The STT period was of insufficient duration to show a significant difference between CL and NCL groups, therefore the one-month duration of the STT is considered to be too short for estimating corrosion rate, particularly by mass loss. The agreement was poor between STT corrosion rates based on mass loss and corrosion rates based on polarization resistance testing. STT results did not consistently agree with LTT results.

The initial characterization of the backfill materials used in the experimental program found several similarities and differences. The backfill materials had similar shape and surface characteristics. CFM and CC have similar adsorption. RAP had 1 percent adsorption, 3 percent lower adsorption than CFM and CC. CC had the lowest resistivity, lowest redox potential, and highest pH of the backfill materials. RAP had the highest chloride and sulfate ion concentrations.

The average of potential reading measurements indicated less chemical surface activity for CC for each metal – environment combination. The average potential readings varied more for the NCL group compared to CL.

The outcomes of existing corrosivity assessment methods are generally inconsistent. Some of these methods are likely to underestimate corrosion of reinforcing strips embedded in backfill materials with high chloride concentrations. CC and RAP did not meet current MSE wall backfill specifications. CC did not meet specifications

typically based on low resistivity and high pH. RAP did not meet specifications typically based on low resistivity and high chloride concentration. Of the various methods for assessing backfill corrosivity, empirical equations are more helpful for service-life prediction than point or categorical systems.

The sacrificial thickness required for reinforcing strips in a CL environment is 4.5 to 7 times higher than that required for a NCL environment. The estimated service-life of MSE walls based on the corrosion of galvanized-steel earth reinforcing strips embedded in backfill material with a 75 year design sacrificial thickness specified by AASHTO (1997) and the average corrosion rates based on mass loss testing from the LTT was approximately 59 years for CFM, 70 years for CC, and 53 years for RAP exposed to a NCL environment. For a CL environment, a reduction of 80 to 90 percent of the typical 75 year design service-life was estimated: 13 years for CFM, 13 years for CC, and 8 years for RAP.

Resistivity, pH, redox potential, and sulfate concentration are significant factors in the estimation of corrosion rate for each backfill material. Chloride concentration is also a significant factor, but was excluded from the multiple regression prediction equation on the basis that chloride concentration is highly correlated with resistivity. Sulfate concentration and pH variables together were found to be capable of distinguishing the CFM, CC, and RAP. Resistivity and pH independent variables were found capable of predicting corrosion rate for each individual backfill material.

6.2 RECOMMENDATIONS

When CFM, CC, or RAP backfill is used with galvanized-steel or plain-steel reinforcing strips, sacrificial thickness greater than that specified by AASHTO (Elias 1997) for MSE walls should be considered, particularly when future high chloride contamination is a possibility.

Use of CC for MSE walls should be considered. RAP should not be used for MSE walls due to the possibility of increased corrosion activity. The authors of MSE wall specifications may want to consider allowing CC if additional testing by other

researchers also indicates similar or better corrosivity performance than backfill materials that meet the current specifications, such as CFM.

6.3 FUTURE RESEARCH

The influences of low pH, high pH, cement content, and high chloride concentration on the corrosion rate of reinforcing strips should be investigated.

Longer term corrosion testing should be performed on recycled backfill materials to increase confidence in service-life estimation for recycled backfill materials.

The accuracy of mass loss testing appears to be influenced by the type of epoxy used on the samples. Research to discover an epoxy that minimizes variability in mass loss testing is recommended.

REFERENCES

AASHTO (2000). "Determining Water Soluble Chloride Ion Content in Soil (T291-94)." Vol. TS-1a. T291-1 – T291-10.

AASHTO (1999). "Determining Water Soluble Sulfate Ion Content in Soil (T290-95)." Vol. TS-1a. T290-1 – T290-9.

Al-Rousan, T., Masad, E., Myers, L., and Speigelman, C. (2005). "New Methodology for Shape Classification of Aggregates." *Transportation Research Record: Journal of the Transportation Research Board, Issue 1913*, 11-23.

American Water Works Association (1988). *American National Standard for Polyethylene Encasement for Ductile- Iron Piping for Water and Other Liquids* (ANSI/AWWA C105/A21.5-88). American Water Works Association, Denver, CO.

Applegate, L.M. (1960). *Cathodic Protection*, McGraw-Hill Book Co, Inc., New York, NY.

ASTM (1997 a). "Standard Guide for Direct Current Plasma Emission Spectrometry Analysis (E1097-97)." Annual Book of ASTM Standards, American Society for Testing and Materials, West Conshohocken, PA.

ASTM (1999 a). "Standard Practice for Conducting and Evaluating Laboratory Corrosion Tests in Soils (G162-99)." Annual Book of ASTM Standards, American Society for Testing and Materials, West Conshohocken, PA.

ASTM (1994 a). "Standard Practice for Preparing, Cleaning, and Evaluating Corrosion Test Specimens (G1-90)." Annual Book of ASTM Standards, American Society for Testing and Materials, West Conshohocken, PA.

ASTM (1998 a). "Standard Practice for Reducing Samples of Aggregate Testing Size (C702-98)." Annual Book of ASTM Standards, American Society for Testing and Materials, West Conshohocken, PA.

ASTM (1997 b). "Standard Practice for Sampling Aggregates (D75-97)." Annual Book of ASTM Standards, American Society for Testing and Materials, West Conshohocken, PA.

ASTM (1999 b). "Standard Reference Test Method for Making Potentiostatic and Potentiodynamic Anodic Polarization Measurements (G5-94[1999]e1)." Annual Book of ASTM Standards, American Society for Testing and Materials, West Conshohocken, PA.

ASTM (1999 c). "Standard Specification for Epoxy-Resin-Base Bonding Systems for Concrete (C881-99)." Annual Book of ASTM Standards, American Society for Testing and Materials, West Conshohocken, PA.

ASTM (1999 d). "Standard Specification for Reagent Water (D1193-99)." Annual Book of ASTM Standards, American Society for Testing and Materials, West Conshohocken, PA.

ASTM (1997 c). "Standard Test Method for Anions in Water by Chemically Suppressed Ion Chromatography (D4327-97)." Annual Book of ASTM Standards, American Society for Testing and Materials, West Conshohocken, PA.

ASTM (2001 a). "Standard Test Method for Density, Relative Density (Specific Gravity), and Absorption of Coarse Aggregate (C127-01)." Annual Book of ASTM Standards, American Society for Testing and Materials, West Conshohocken, PA.

ASTM (2001 b). "Standard Test Method for Density, Relative Density (Specific Gravity), and Absorption of Fine Aggregate (C128-01)." Annual Book of ASTM Standards, American Society for Testing and Materials, West Conshohocken, PA.

ASTM (1994 b). "Standard Test Method for Determination of Water (Moisture) Content of Soil by Direct Heating Method (D4959-89)." Annual Book of ASTM Standards, American Society for Testing and Materials, West Conshohocken, PA.

ASTM (1995 a). "Standard Test Method for Field Measurement of Soil Resistivity Using the Wenner Four-Electrode Method (G57-95a)." Annual Book of ASTM Standards, American Society for Testing and Materials, West Conshohocken, PA.

ASTM (1998 b). "Standard Test Method for Laboratory Determination of Water (Moisture) Content of Soil and Rock by Mass (D2216-98). Annual Book of ASTM Standards, American Society for Testing and Materials, West Conshohocken, PA.

ASTM (1995 b). "Standard Test Method for Measuring pH of Soil for Use in Corrosion Testing (G51-95)." Annual Book of ASTM Standards, American Society for Testing and Materials, West Conshohocken, PA.

ASTM (1999 e). "Standard Test Method for Optical Emission Vacuum Spectrometric Analysis of Carbon and Low-Alloy Steel (E415-99a)." Annual Book of ASTM Standards, American Society for Testing and Materials, West Conshohocken, PA.

ASTM (1995 c). "Standard Test Method for pH of Soils (D4972-95a)." Annual Book of ASTM Standards, American Society for Testing and Materials, West Conshohocken, PA.

ASTM (1998 c). "Standard Test Method for Particle-Size Analysis of Soils (D422-63)." Annual Book of ASTM Standards, American Society for Testing and Materials, West Conshohocken, PA.

ASTM (2000 a). "Standard Test Method for Permeability of Granular Soils (Constant Head) (D2434-68)." Annual Book of ASTM Standards, American Society for Testing and Materials, West Conshohocken, PA.

ASTM (2001 c). "Standard Test Method for Sieve Analysis of Fine and Coarse Aggregates (C136-01)." Annual Book of ASTM Standards, American Society for Testing and Materials, West Conshohocken, PA.

ASTM (2000 b). "Standard Test Method for Specific Gravity of Soils (D854-00)." Annual Book of ASTM Standards, American Society for Testing and Materials, West Conshohocken, PA.

ASTM (1996). "Standard Test Method for Sulfide Ion in Water (D4658-92)." Annual Book of ASTM Standards, American Society for Testing and Materials, West Conshohocken, PA.

ASTM (2001 d). "Standard Test Method for Weight [Mass] of Coating on Iron and Steel Articles with Zinc or Zinc-Alloy Coatings (A90/A90M-01)." Annual Book of ASTM Standards, American Society for Testing and Materials, West Conshohocken, PA.

Booth, G.H., Cooper, A.W., Cooper, P.M., and Wakerley, D.S. (1967). "Criteria of Soil Aggressiveness towards Buried Metals." *British Corrosion Journal*, Vol. 2.

Briaud, J., Griffin, R.B., Yeung, A.T., Soto, A., Suroor, A., and Park, H. (1998). "Long-term Behavior of Ground Anchors and Tieback Walls." *Texas Transportation Institute Research Report 1391-1*, College Station, TX.

Bushman, J.B. and Mehalick, T.E. (1989). "Statistical Analysis of Soil Characteristics to Predict Mean Time to Corrosion Failure of Underground Structures." *Effects of Soil Characteristics on Corrosion*, ASTM STP 1013, V. Chaker and J.D. Palmer, eds., American Society of Testing Materials, Philadelphia, 107-118.

California Department of Transportation (1993). *Method for Estimating the Service Life of Steel Culverts*. Division of New Technology and Materials Research, Sacramento, CA.

Camitz, G. and Vinka, T.G. (1989). "Corrosion of Steel and Metal-Coated Steel in Swedish Soils- Effects of Soil Parameters." *Effects of Soil Characteristics on Corrosion, ASTM STP 1013*, V. Chaker and J.D. Palmer, eds., American Society for Testing and Materials, Philadelphia, 37-53.

Chaker, V. (1981). "Simplified Methods for the Electrical Soil Resistivity Measurement." *Underground Corrosion, ASTM STP 741*, Edward Escalante, ed., American Society for Testing and Materials, Philadelphia, 61-91.

Chandan, C., Sivakumar, K., Masad, E., and Fletcher, T. (2004). "Application of Imaging Techniques to Geometry Analysis of Aggregate Particles." Journal of Computing in Civil Engineering, 18(1), 75-82.

Davis, J.R. (1996). *Carbon and Alloy Steels: ASM Specialty Handbook.* ASM International, Materials Park, OH.

Elias, V. (1990). "Durability/Corrosion of Soil Reinforced Structures", *Federal Highway Administration Report No. FHWA-RD-89-186*, 173 pages.

Elias, V. (1997). "Corrosion/Degradation of Soil Reinforcements for Mechanically Stabilized Earth Walls and Reinforced Soil Slopes", *Federal Highway Administration Report No. FHWA-SA-96-072*, 105 pages.

Elias, V., and Christopher, B. (1996). "Mechanically Stabilized Earth Walls and Reinforced Soil Slopes Design and Construction Guidelines." *FHWA Demonstration Project 82, FHWA SA-96-071*, 371 pages.

Escalante, E. (1989). "Concepts of Underground Corrosion." *Effects of Soil Characteristics on Corrosion, ASTM STP 1013*, V. Chaker and J. D. Palmer, eds., American Society for Testing and Materials, Philadelphia, 81-94.

Eyre, D. and Lewis, D.A. (1987). *Soil Corrosivity Assessment, Transport and Road Research Laboratory*. Crowthorne, Berkshire, England.

Fetter, C.W. (2001). *Applied Hydrogeology*, 4th Edition, Prentice Hall, Upper Saddle River, NJ.

Fischer, K.P. and Bue, B. (1981). "Corrosion and Corrosivity of Steel in Norwegian Marine Sediments," *Underground Corrosion, ASTM STP 741*, E. Escalante, ed., American Society for Testing and Materials, Philadelphia, 24-32.

Frondistou-Yannas, S. (1985). "Corrosion Susceptibility of Internally Reinforced Soil Retaining Structures", *Federal Highway Administration Report No. FHWA-RD-83-105*, 77 pages.

King, R.A. (1977). *A Review of Soil Corrosiveness with Particular Reference to Reinforced Earth*. Crowthorne, Berkshire, England, Report 316, 1-20.

Miller, F.P., Foss, J.E. and Wolf, D.C. (1981). "Soil Surveys: Their Synthesis, Confidence Limits, and Utilization." *Underground Corrosion, ASTM STP 741*, E. Escalante, ed., American Society for Testing and Materials, Philadelphia, 3-23.

Moore, T.J. and Hallmark, C.T. (1987). "Soil Properties Influencing Corrosion of Steel in Texas Soils," *Soil Science Society of America Journal*, 51(5), Madison, WI.

Morris, D.V., and Delphia, J.G. (1999). "Specifications for Backfill of Reinforced-Earth Retaining Walls." *Texas Transportation Institute, FHWA/TX-99/1431-S*, 204 pages.

Ogolla, M. (2002). "Durability of Recycled Crushed Concrete and Recycled Asphalt Pavements in Mechanically Stabilized Earth Retaining Walls." Master's Thesis, University of Texas at Austin, Austin, TX.

Parker, M.E. (1977). "Corrosion by Soils." *NACE Basic Corrosion Course*, Eighth Edition, National Association of Corrosion Engineers, Houston, TX, 6:1- 6:26.

Popova, S.N., Popova, B.N., White, R.E., Petrou, M.F., and Morris, D. (1998). "Corrosion Effects of Stabilized Backfill on Steel Reinforcement." *ACI Structural Journal, Title No. 95-S51, 95(5)*.

Pourbaix, M. (1966). *Atlas of Electrochemical Equilibria in Aqueous Solutions*. Pergamon Press, New York.

Princeton Applied Research (2000). "Electrochemistry and Corrosion Overview and Techniques." Application Note CORR-4. http://www.princetonappliedresearch.com/products/appnotes.cfm

Rabeler, R.C. (1989). "Soil Corrosion Evaluation of Screw Anchors." *Effects of Soil Characteristics on Corrosion, ASTM STP 1013*, V. Chaker and J.D. Palmer, eds., American Society of Testing Materials, Philadelphia, 54-80.

Rathje, E.M., Rauch, A.F., Folliard, K.J., Trejo, D., Little, D., Viyanant, C., Ogolla, M., and Esfeller, M. (2001). "Recycled asphalt pavement and crushed concrete backfill: State-of-the-art review and material characterization." *Texas Department of Transportation Research Report 0-4177-1*, Austin, TX.

Reinforced Earth Company (1995). "Service Life, Allowable Reinforcement Stress and Metal Loss Rates to be Used in the Design of Permanent MSE Structures," *Revised Technical Bulletin MSE-1*. Vienna, VA. http://www.reinforcedearth.com/technicalbulletins.asp

Romanoff, M. (1957). "Underground Corrosion", *NBS Circular 579*, National Bureau of Standards, U.S. Government Printing Office, Washington, DC.

Serra, E.T. and Mannheimer, W.A. (1981) "On the Estimation of the Corrosion Rates of Metals in Soils by Electrochemical Measurements." *Underground Corrosion, ASTM STP 741*, Edward Escalante, ed., American Society for Testing and Materials, Philadelphia, 111-122.

Tait, W.S. (1994). *An Introduction to Electrochemical Corrosion Testing for Practicing Engineers and Scientists*. Pair O Docs Publications, Racine, WI.

Texas Department of Transportation, TEX-113-E, (2001). "Laboratory Compaction Characteristics and Moisture-Density Relationship of Base Materials." Soils & Aggregates Test Procedures, 100-E, 14-1 – 14-16.

Tomashov, N.D. (1966). *Theory of Corrosion and Protection of Metals*, The Macmillan Company, New York.

Whitecavage, J.B. (1990). "Fundamentals of pH Field Test Methods and Instrumentation." *Appalachian Underground Corrosion Short Course. Proc., 35th Annual*, Durham, A. and Noah, M., eds, West Virginia University, 135-144.

APPENDIX A

SHAPE AND SURFACE GRAPHS

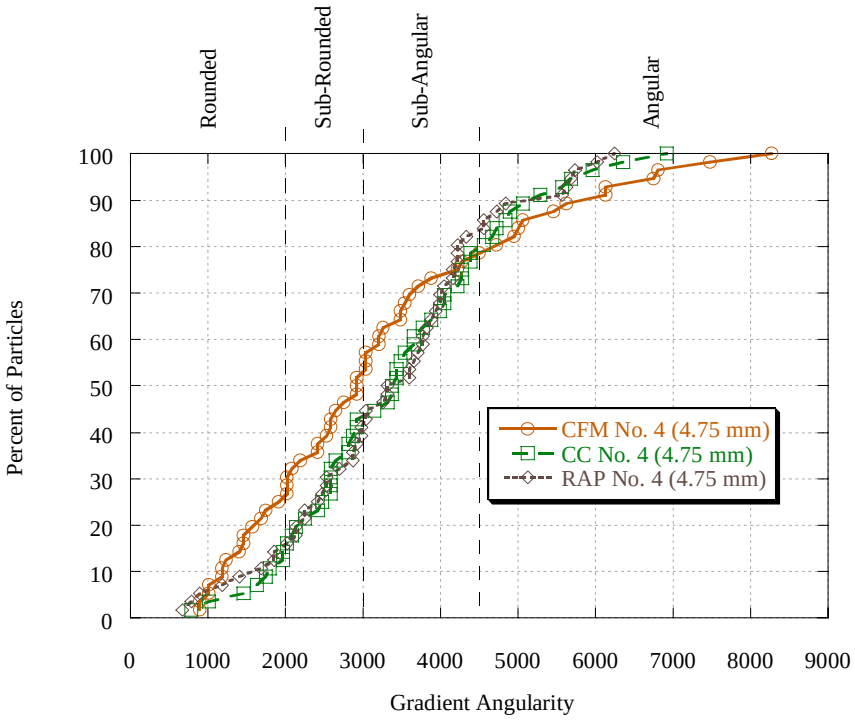

Figure A.1. Backfill Material Particles Retained on the No. 4 (4.75 mm) - Gradient Angularity.

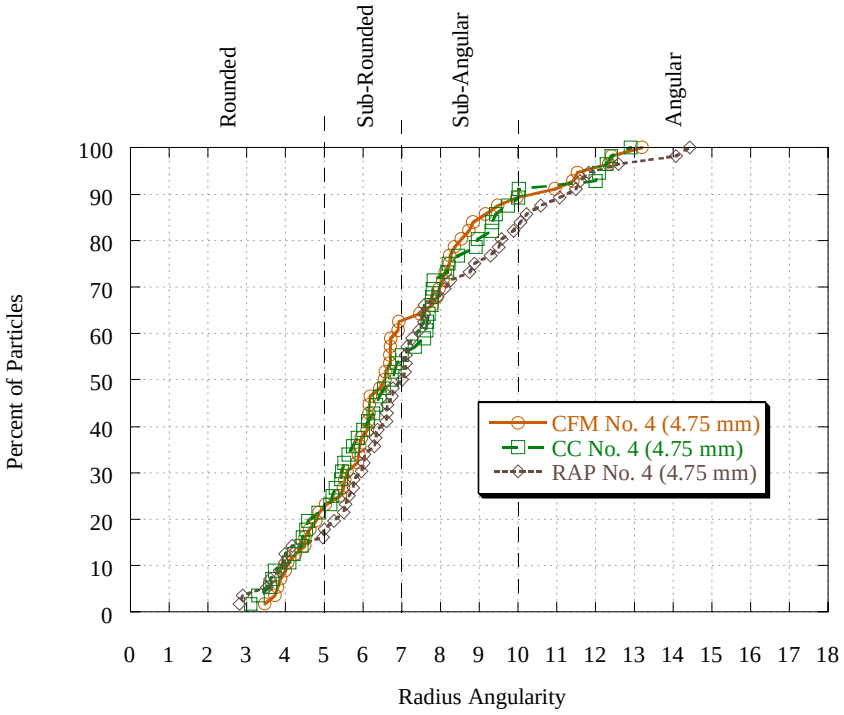

Figure A.2. Backfill Material Particles Retained on the No. 4 (4.75 mm) - Radius Angularity.

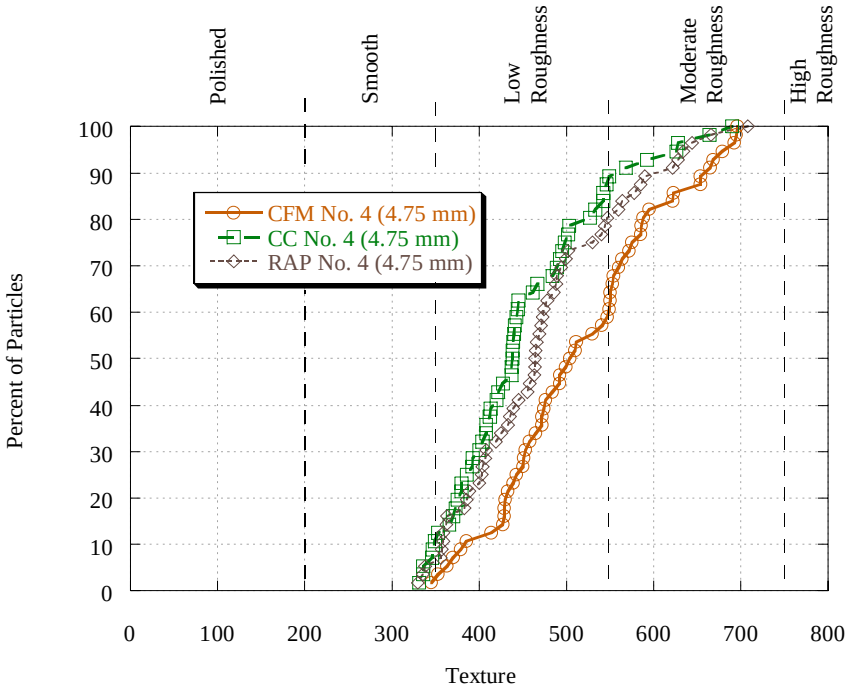

Figure A.3. Backfill Material Particles Retained on the No. 4 (4.75 mm) - Texture.

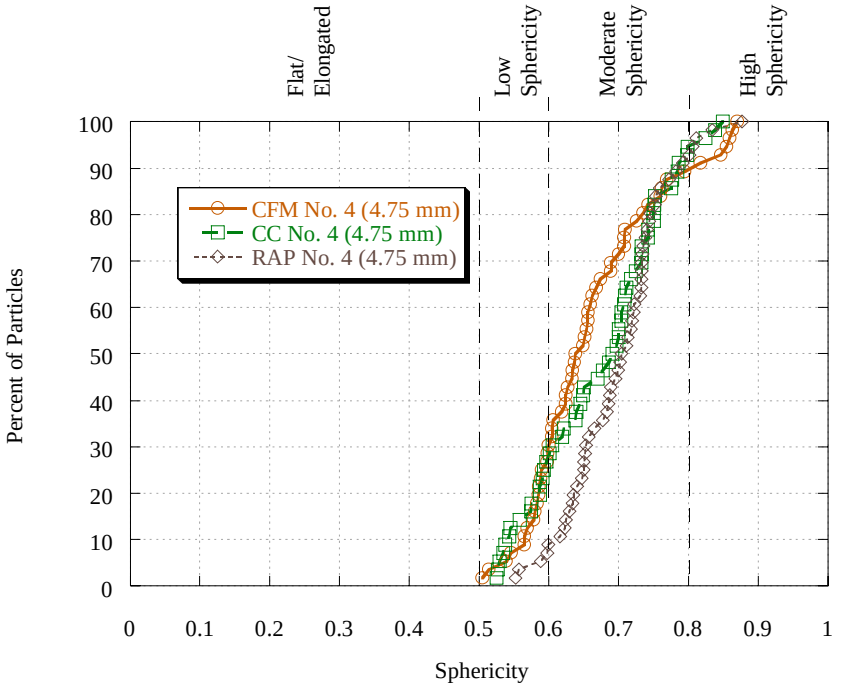

Figure A.4. Backfill Material Particles Retained on the No. 4 (4.75 mm) - Sphericity.

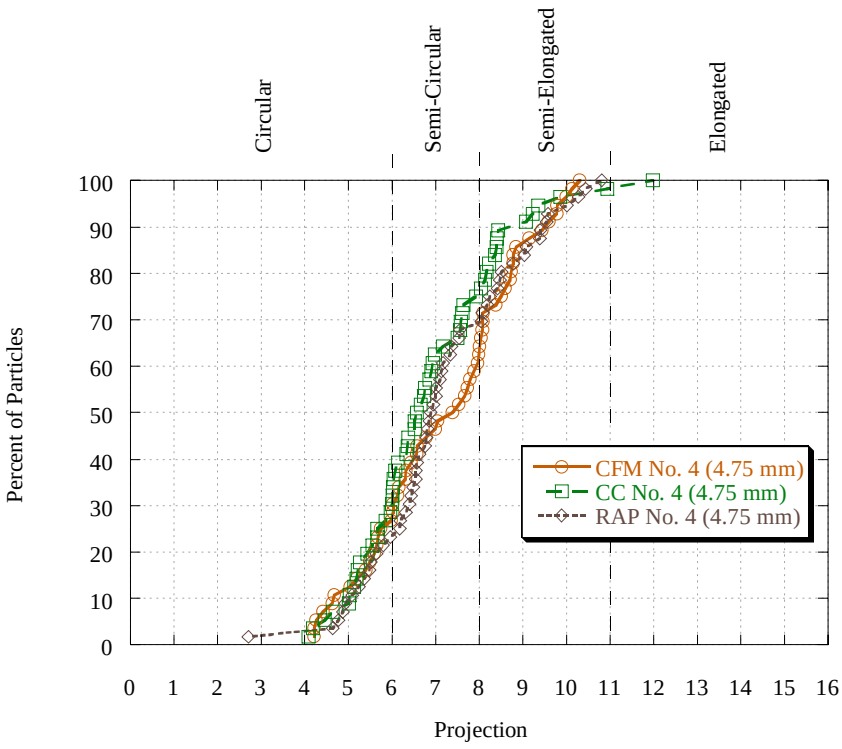

Figure A.5. Backfill Material Particles Retained on the No. 4 (4.75 mm) - Projection.

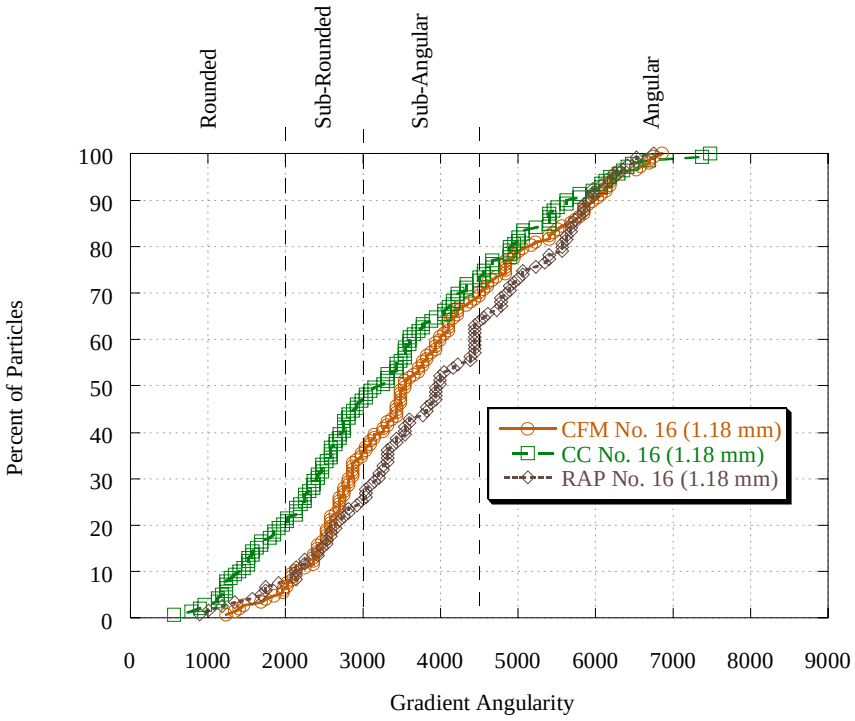

Figure A.6. Backfill Material Particles Retained on the No. 16 (1.18 mm) - Gradient Angularity.

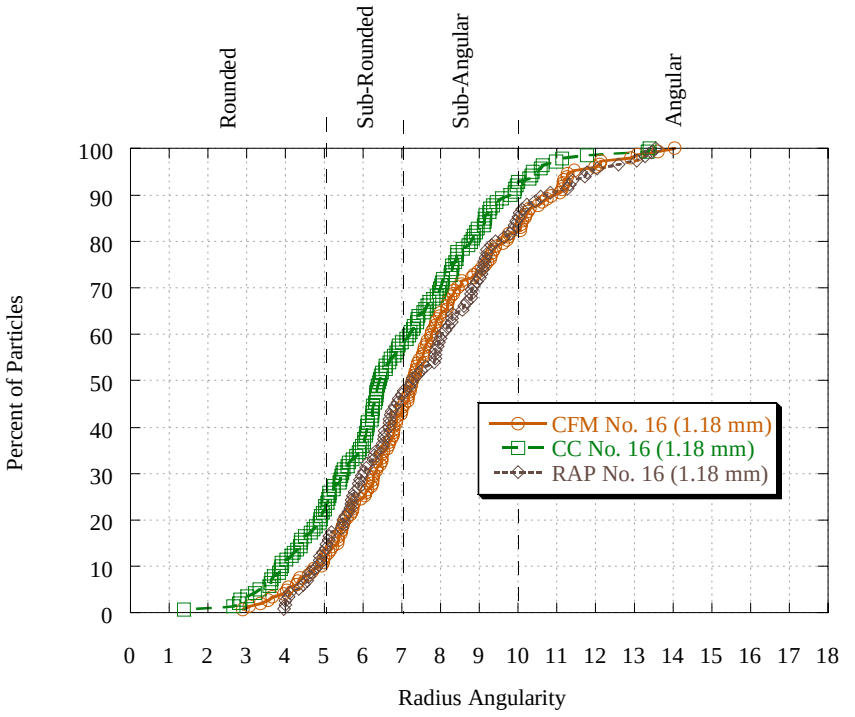

Figure A.7. Backfill Material Particles Retained on the No. 16 (1.18 mm) - Radius Angularity.

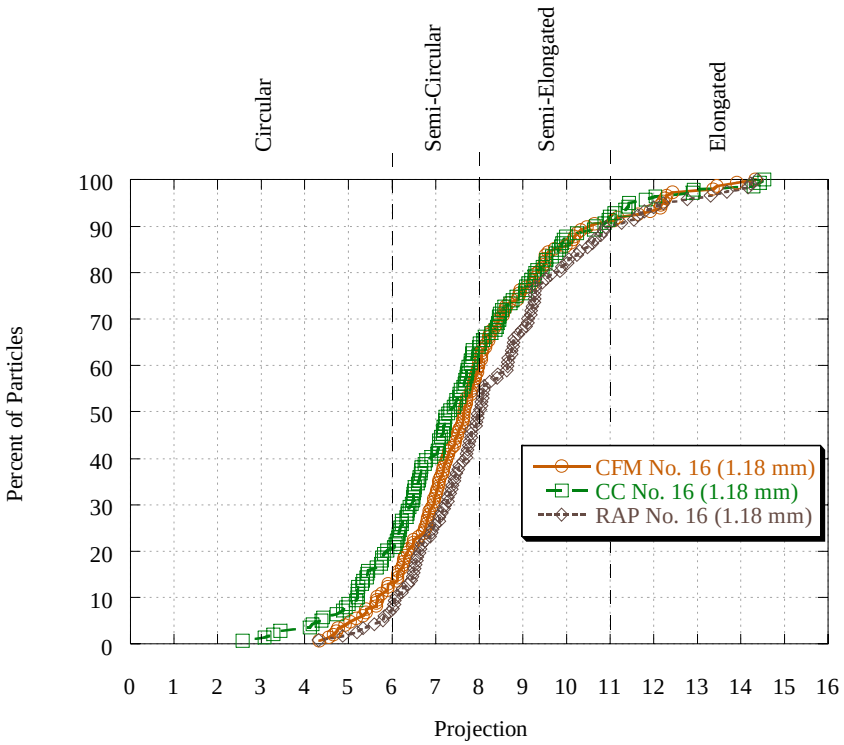

Figure A.8. Backfill Material Particles Retained on the No. 16 (1.18 mm) - Projection.

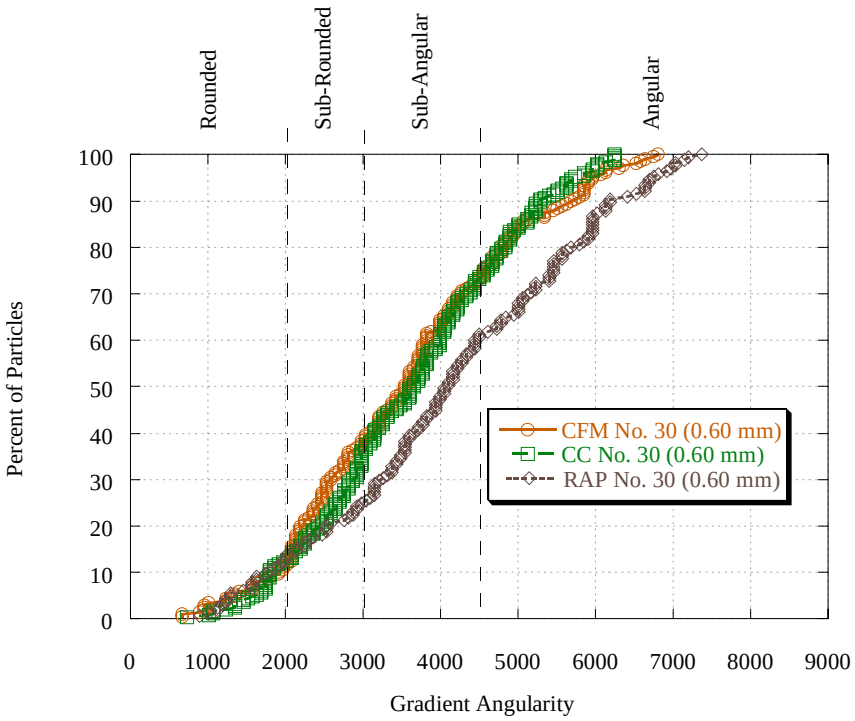

Figure A.9. Backfill Material Particles Retained on the No. 30 (0.60 mm) - Gradient Angularity.

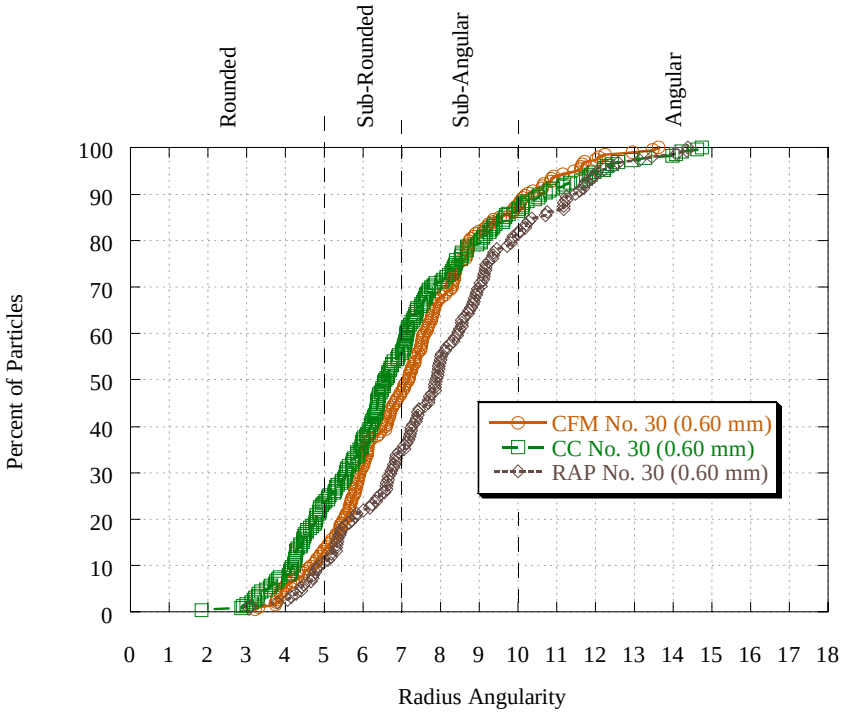

Figure A.10. Backfill Material Particles Retained on the No. 30 (0.60 mm) - Radius Angularity.

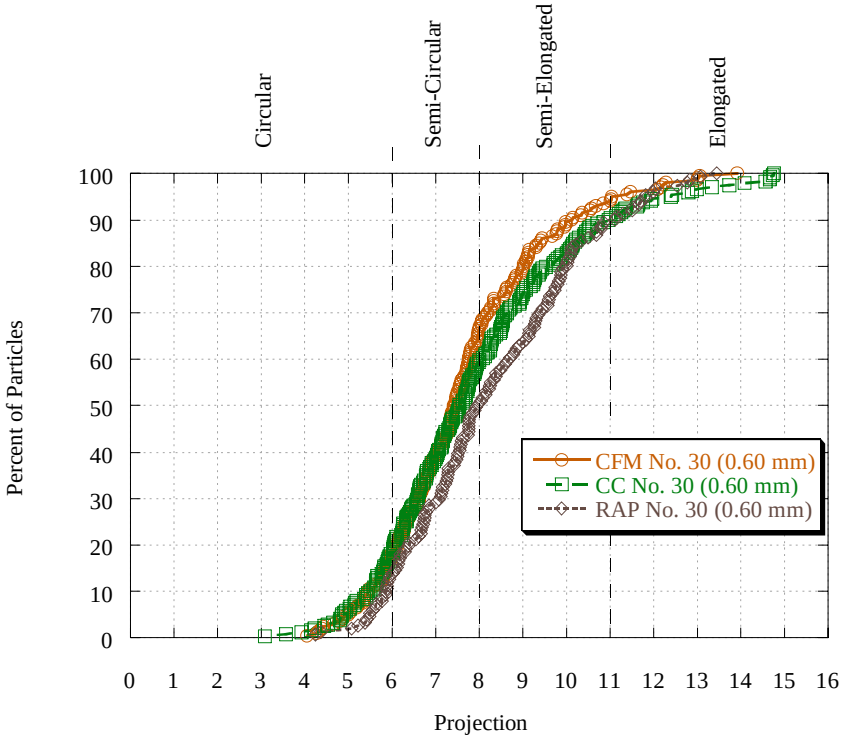

Figure A.11. Backfill Material Particles Retained on the No. 30 (0.60 mm) - Projection.

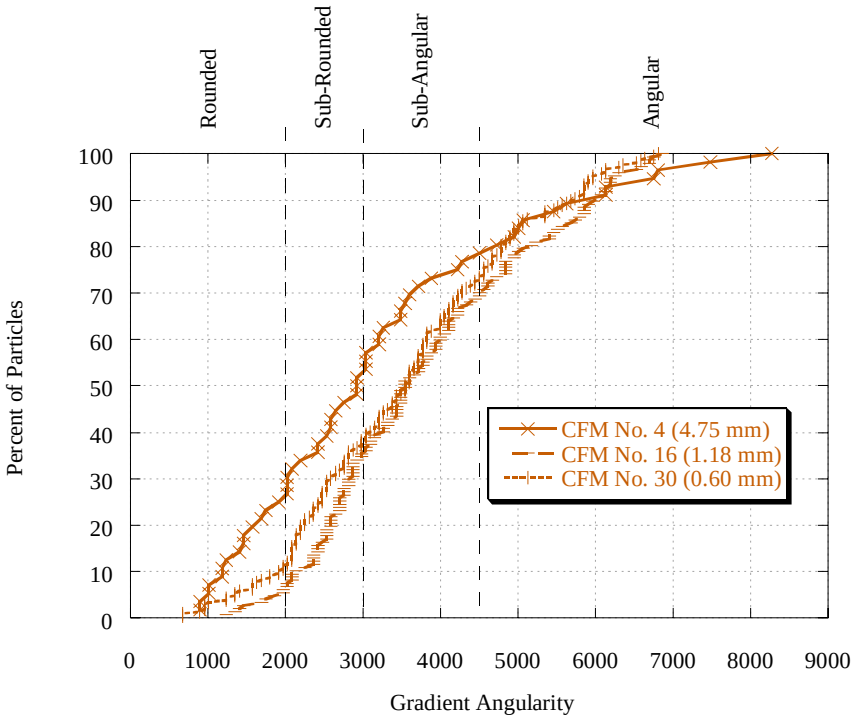

Figure A.12. CFM Coarse and Fine Aggregate Particles - Gradient Angularity.

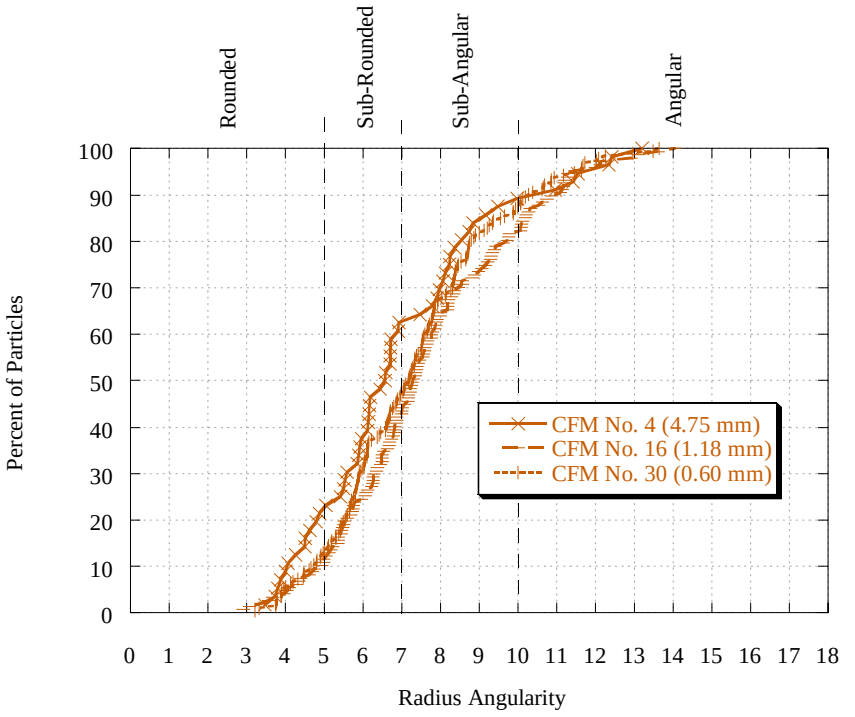

Figure A.13. CFM Coarse and Fine Aggregate Particles - Radius Angularity.

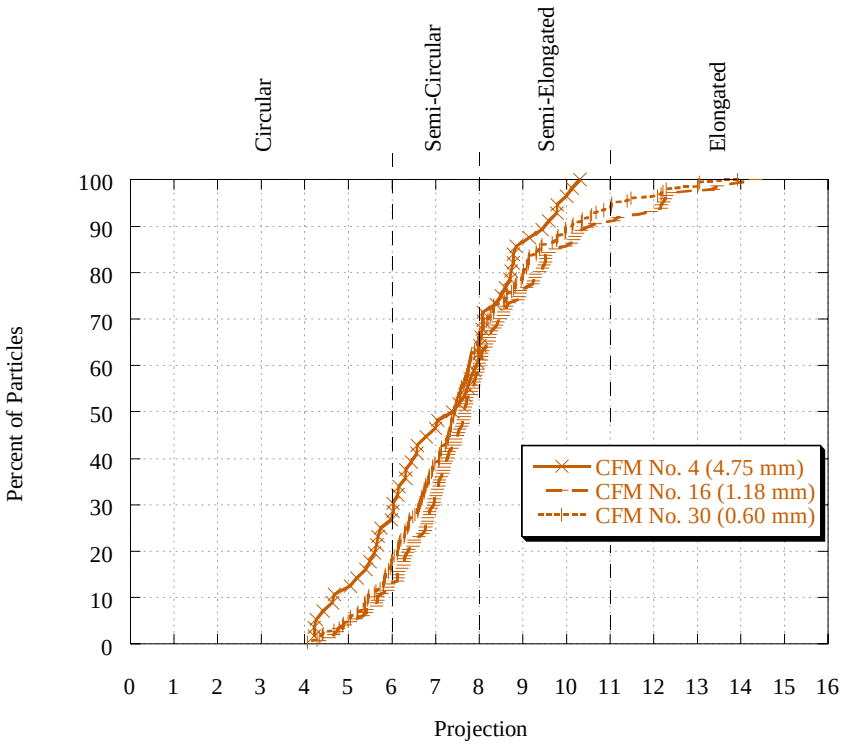

Figure A.14. CFM Coarse and Fine Aggregate Particles - Projection.

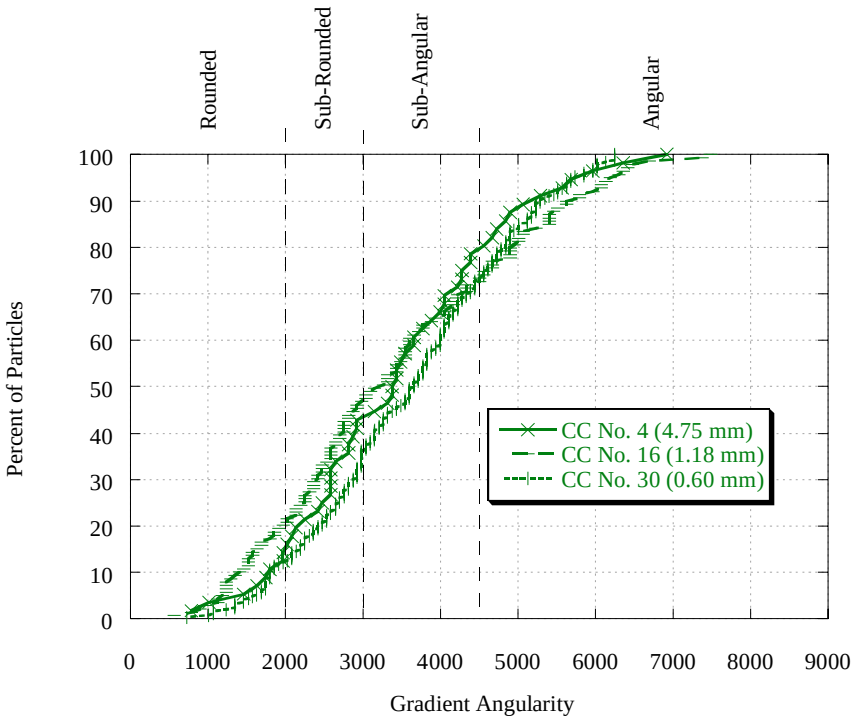

Figure A.15. CC Coarse and Fine Aggregate Particles - Gradient Angularity.

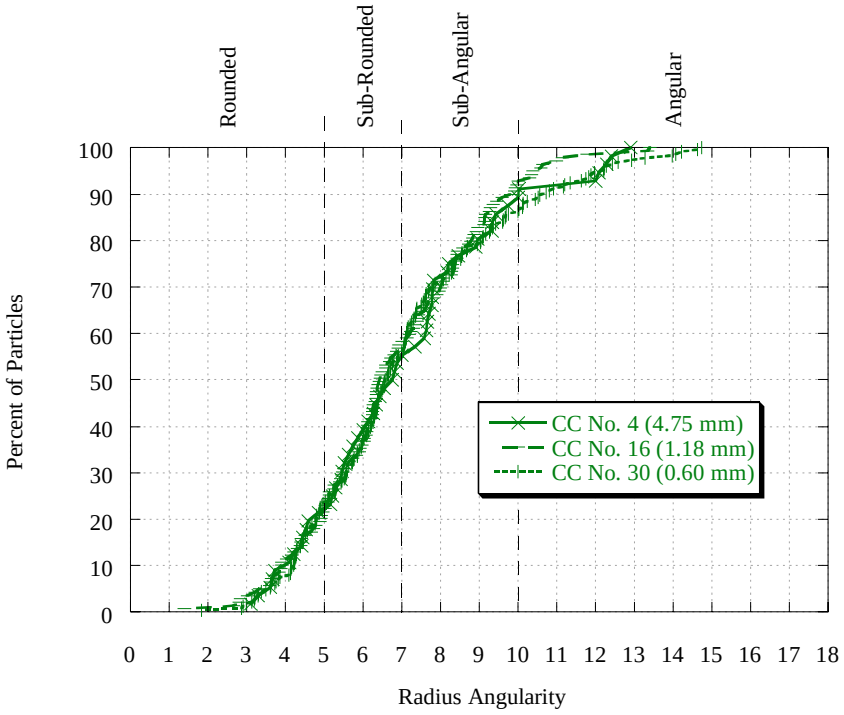

Figure A.16. CC Coarse and Fine Aggregate Particles - Radius Angularity.

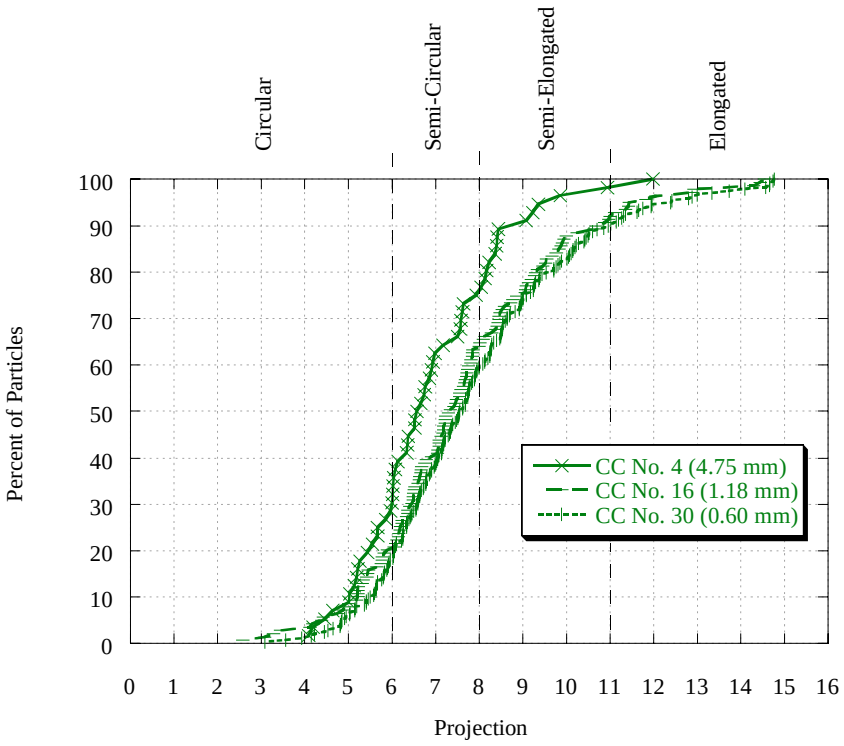

Figure A.17. CC Coarse and Fine Aggregate Particles - Projection.

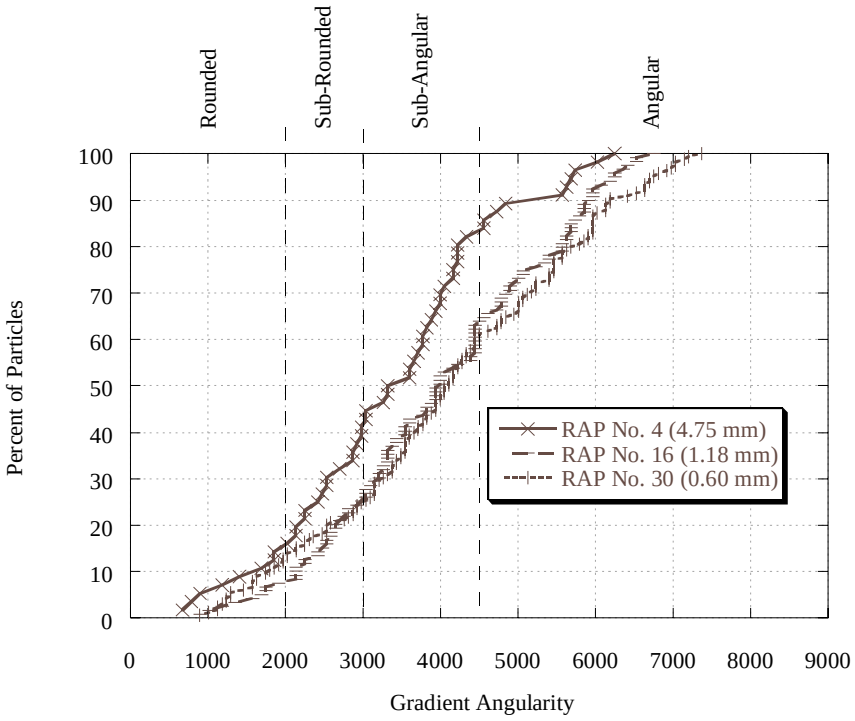

Figure A.18. RAP Coarse and Fine Aggregate Particles - Gradient Angularity.

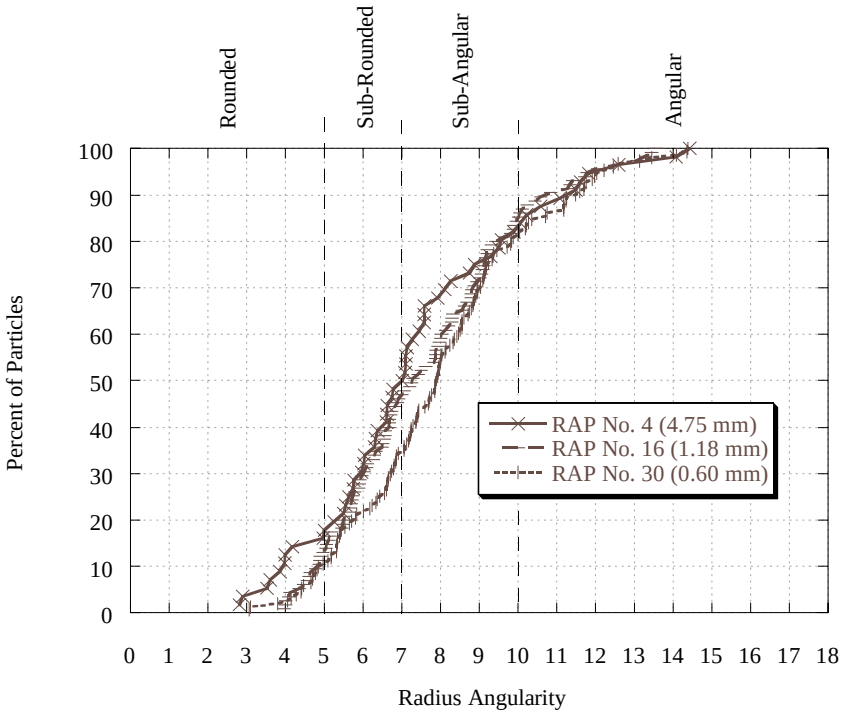

Figure A.19. RAP Coarse and Fine Aggregate Particles - Radius Angularity.

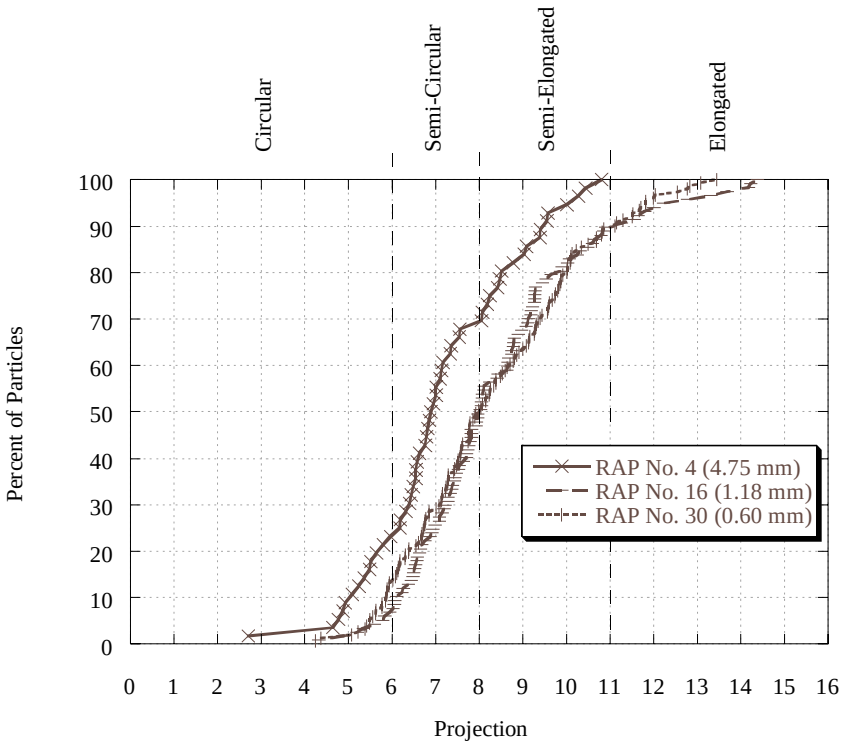

Figure A.20. RAP Coarse and Fine Aggregate Particles - Projection.

APPENDIX B

POLARIZATION TEST SETTINGS

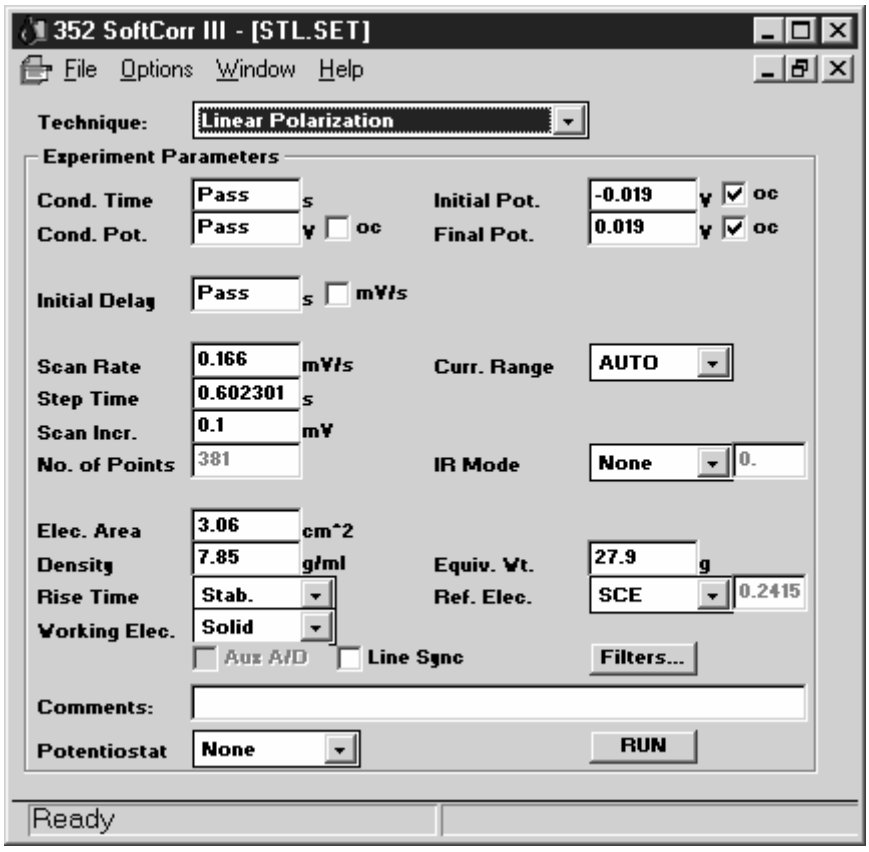

Figure B.1. Verstat II™ Plain-Steel Sample Short-term Testing - Linear Polarization Test Setup.

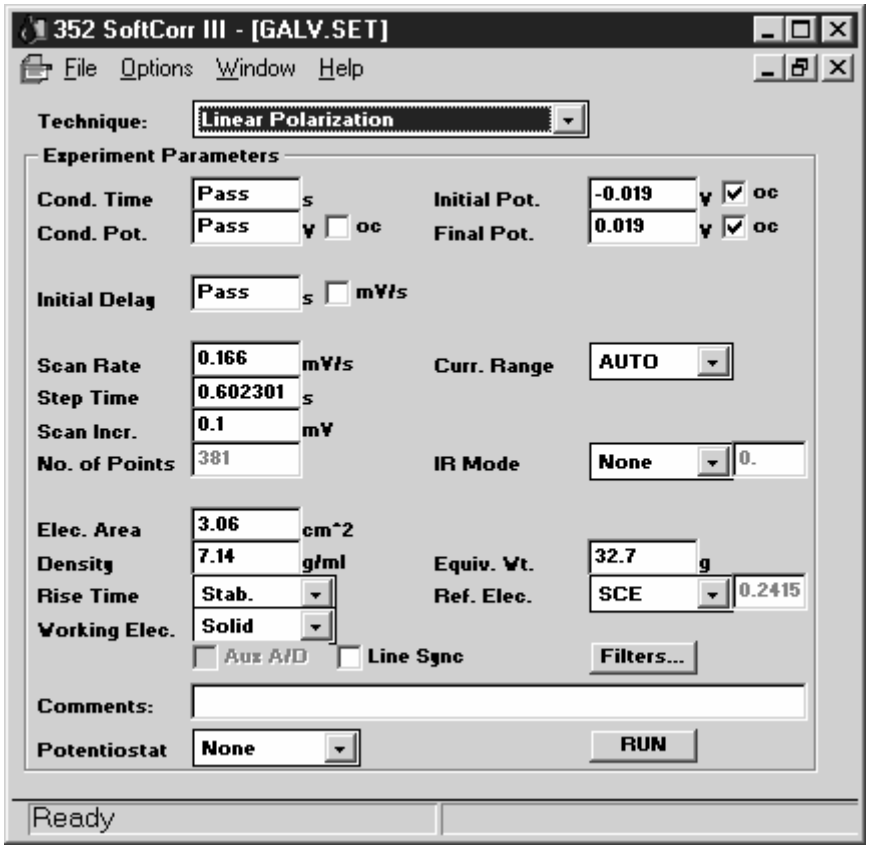

Figure B.2. Verstat II™ Galvanized-Steel Sample Short-term Testing - Linear Polarization Test Setup.

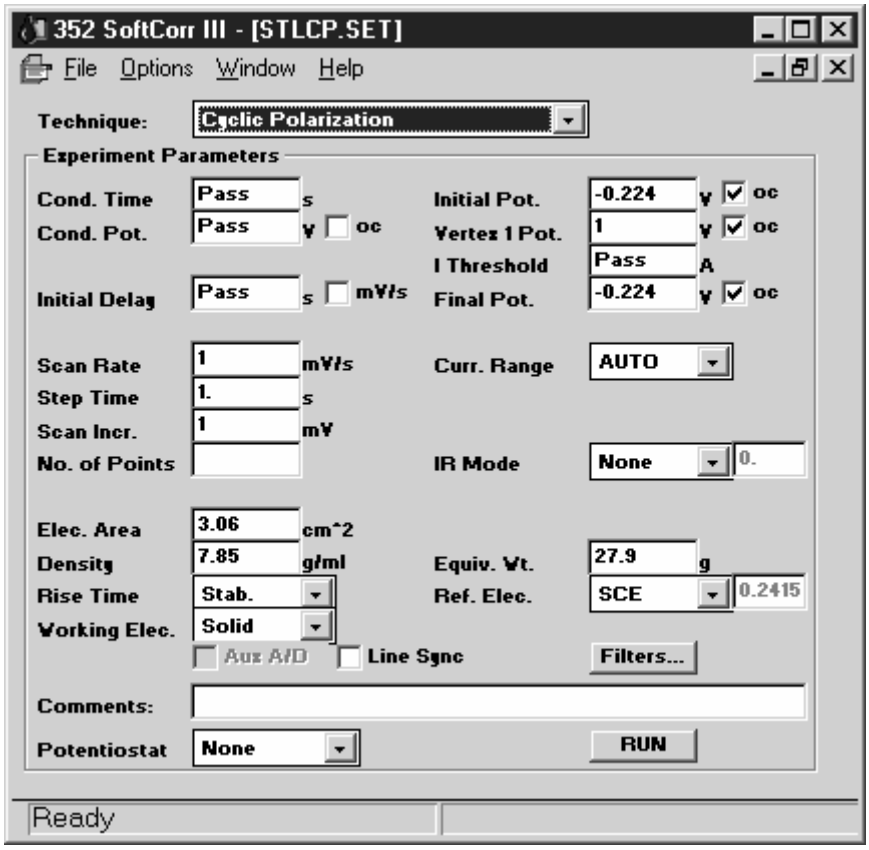

Figure B.3. Verstat II™ Plain-Steel Sample Short-term Testing - Cyclic Polarization Test Setup.

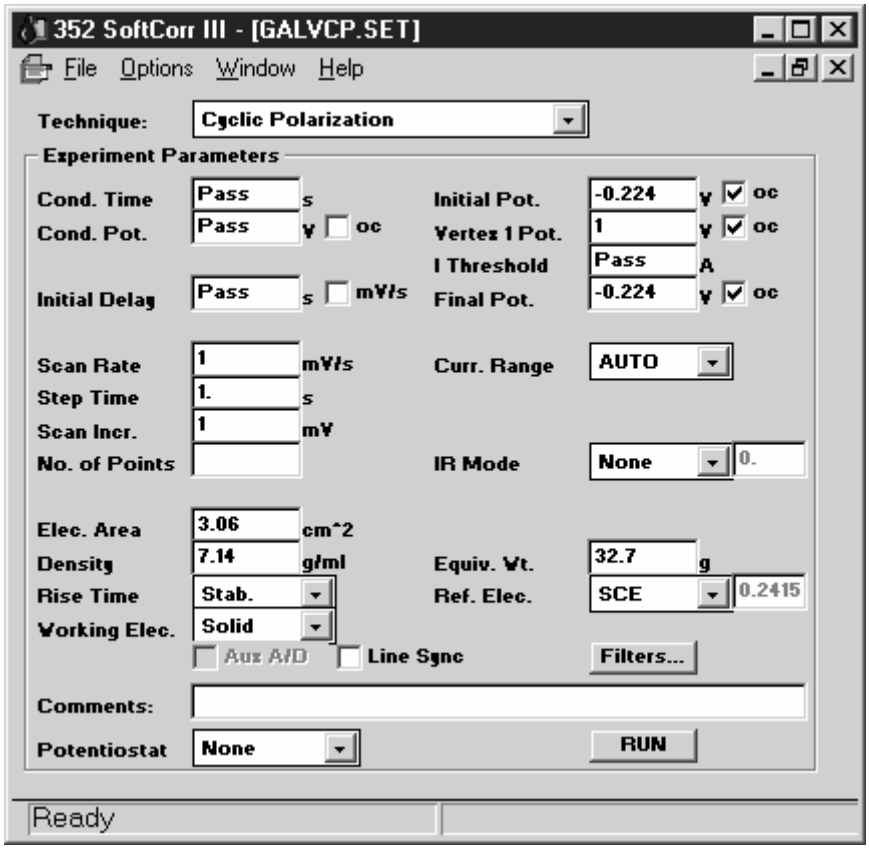

Figure B.4. Verstat II™ Galvanized-Steel Sample Short-term Testing - Cyclic Polarization Test Setup.

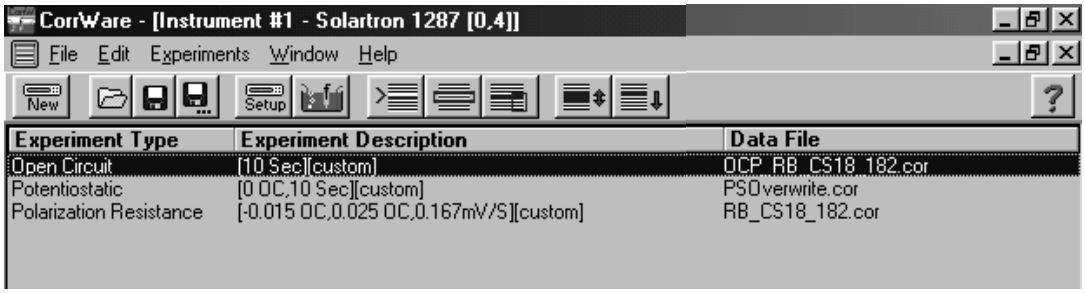

Figure B.5. Solartron™ 1287 Experiment Long-term Testing Setup for Linear Polarization Resistance Tests.

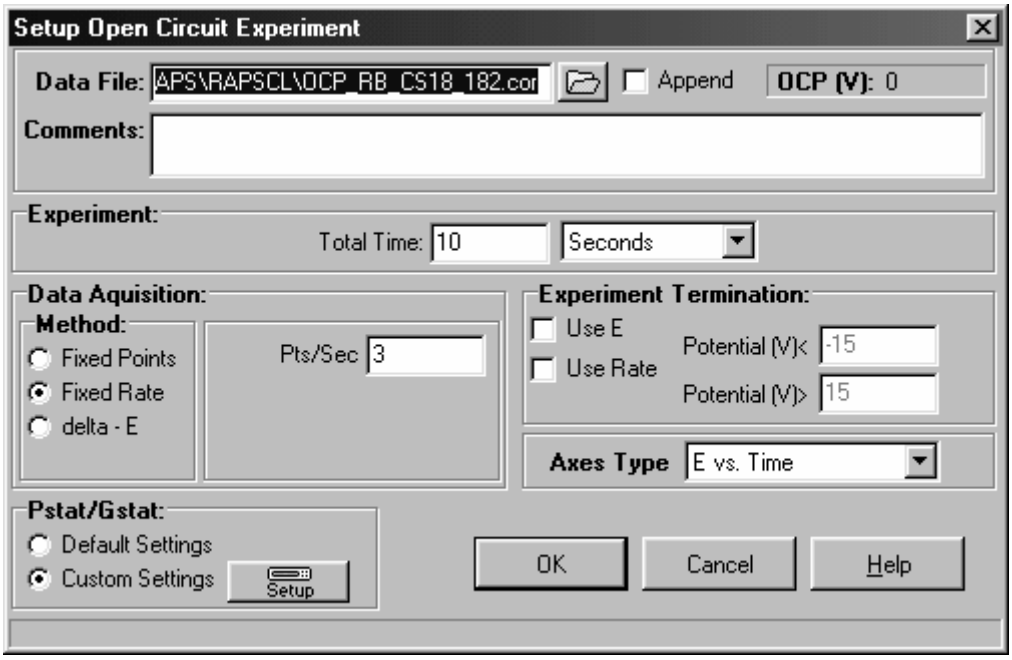

Figure B.6. Solartron™ 1287 Long-term Testing Open Circuit Experiment Setup for Linear Polarization Resistance Tests.

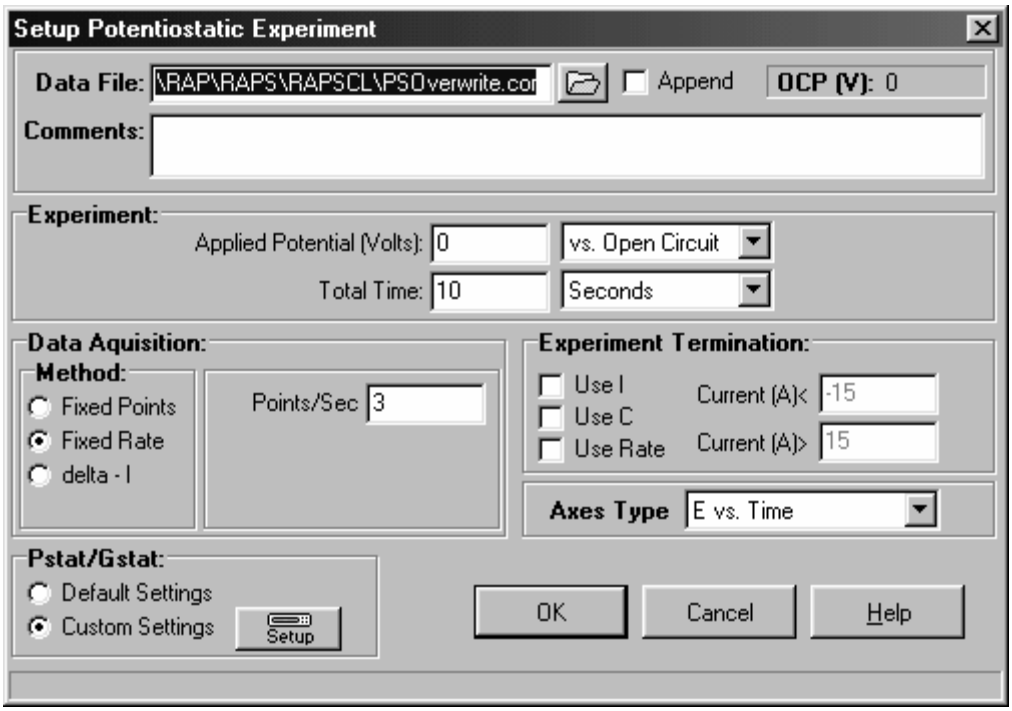

Figure B.7. Solartron™ 1287 Long-term Testing Potentiostatic Experiment Setup for Linear Polarization Resistance Tests.

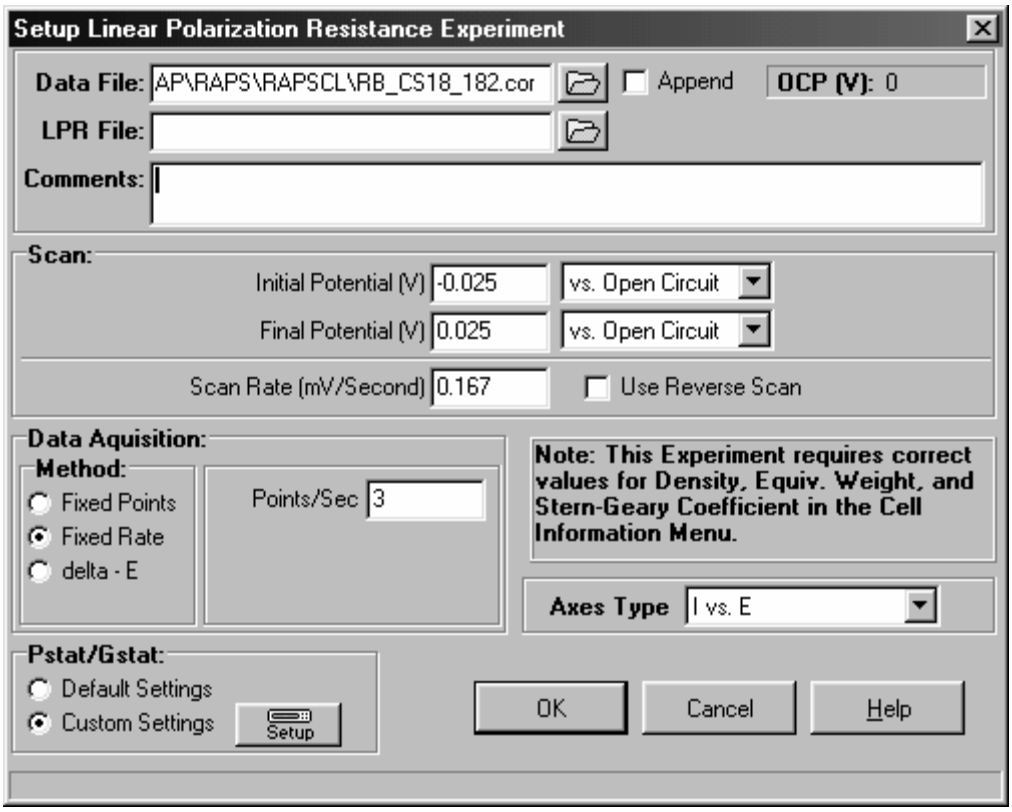

Figure B.8. Typical Solartron™ 1287 Long-term Testing Potentiostatic Experiment Setup for Linear Polarization Resistance Tests.

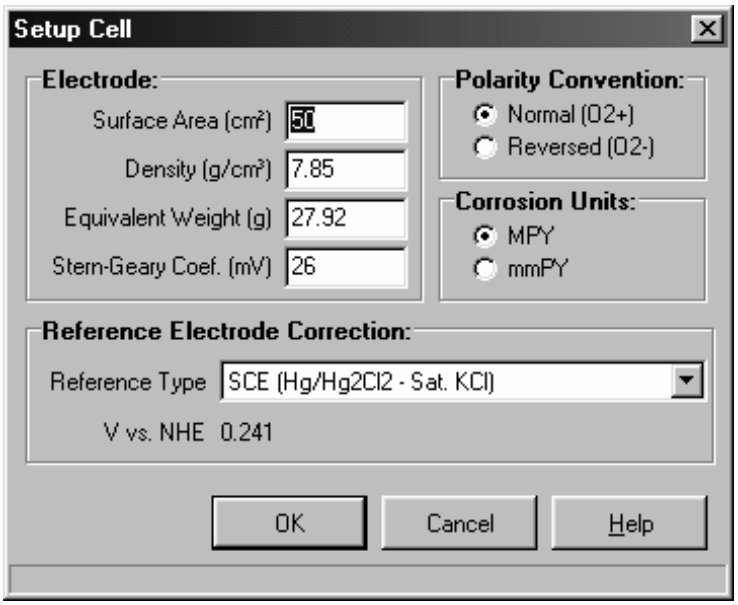

Figure B.9. Solartron™ 1287 Plain-Steel Sample Long-term Testing - Cell Setup.

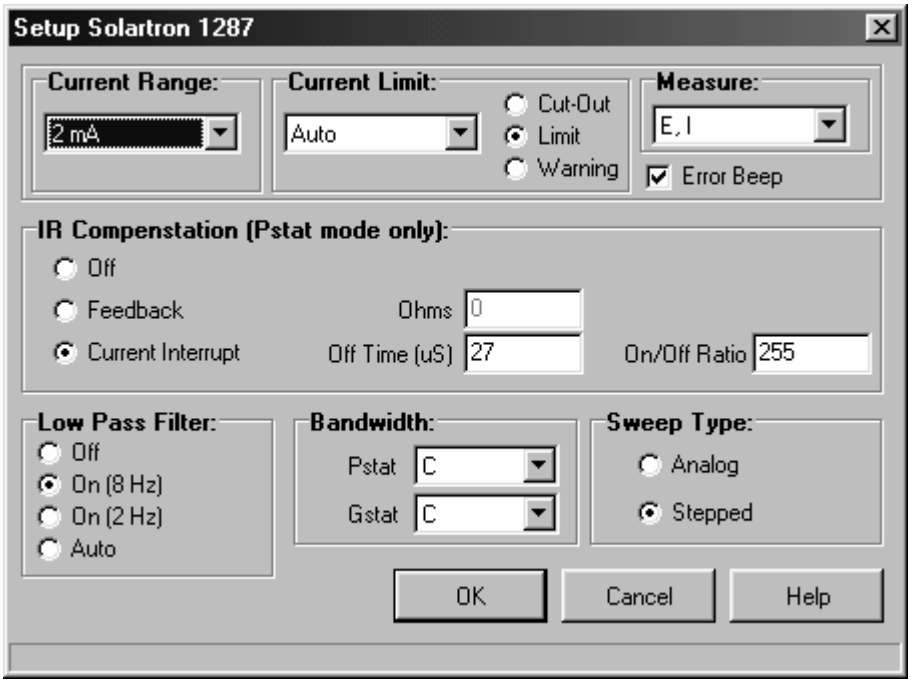

Figure B.10. Solartron™ 1287 Plain-Steel Sample Long-term Testing - Linear Polarization Resistance Settings.

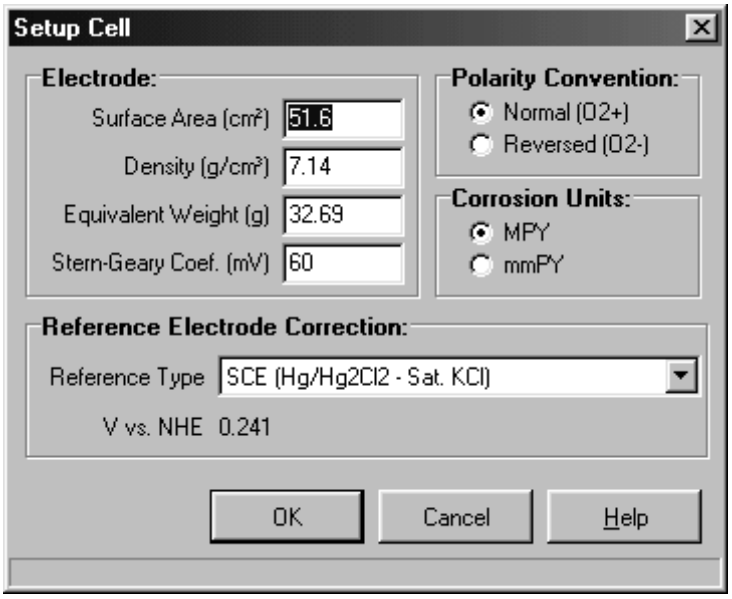

Figure B.11. Solartron™ 1287 Galvanized-Steel Sample Long-term Testing - Cell Setup.

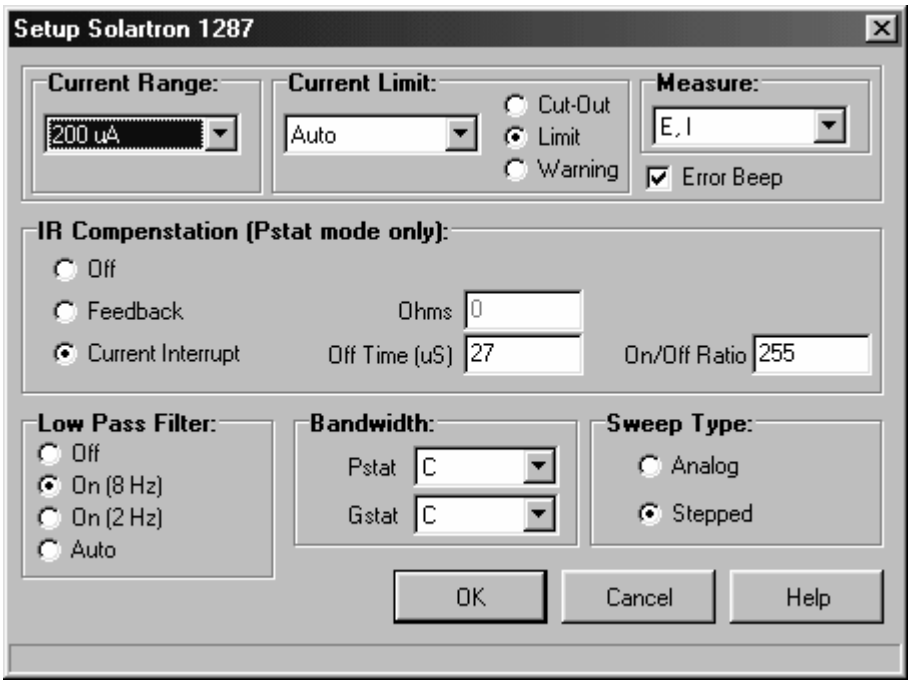

Figure B.12. Solartron™ 1287 Galvanized-Steel Sample Long-term Testing - Linear Polarization Resistance Settings.

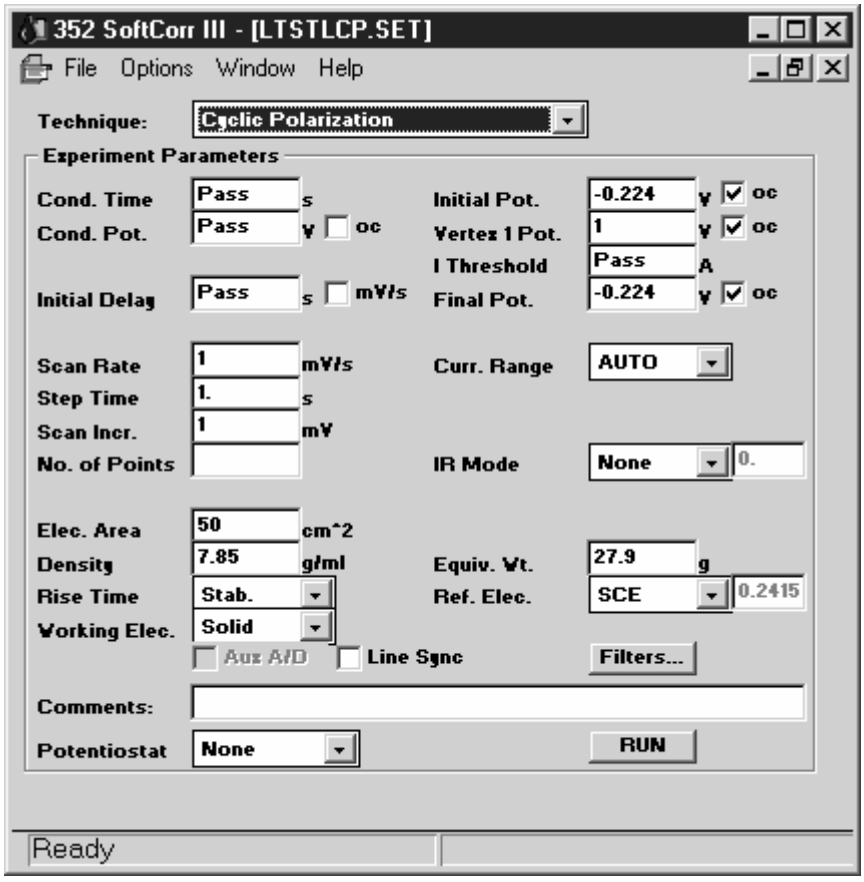

Figure B.13. Verstat II™ Plain-Steel Sample Long-term Testing - Cyclic Polarization Test Setup.

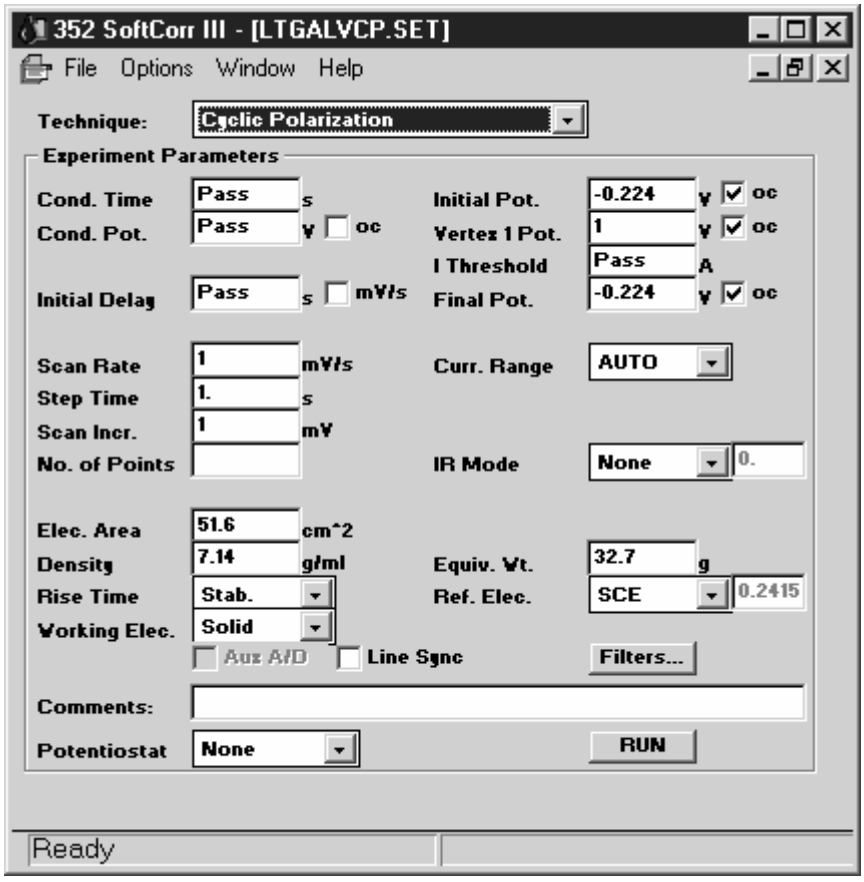

Figure B.14. Verstat II™ Plain-Steel Sample Long-term Testing - Cyclic Polarization Test Setup.

APPENDIX C

CALCULATION PROCEDURES

C.1 DETERMINATION OF POLARIZATION RESISTANCE

The polarization resistance experiment involved a scan of the working electrode potential and a measurement of the resulting current, which is referred to as a potentiodynamic scan. The polarization resistance experiment typically scanned a range of approximately + 20 mV about the open circuit potential. The applied potential vs. the measured current was plotted. This plot is typically referred to as the polarization resistance plot. The polarization resistance is determined from the plot using Equation 1:

$$R_P = \frac{\Delta E}{\Delta i} \tag{C.1}$$

where R_P is polarization resistance (Ω-cm^2), ΔE is change in potential (Volts), and Δi is change in current (Amps/cm^2).

Graphically speaking, the polarization resistance is the slope of change in potential versus change in current, often represented by a linear fit, at the point where the current equals zero, as shown in Figure 1. From the equation below, polarization resistance is inversely proportional to corrosion current, and thus assesses the relative ability of a material to resist corrosion (PAR). The strict definition of polarization resistance is “the resistance of a specimen to oxidation during the application of an external potential” (PAR).

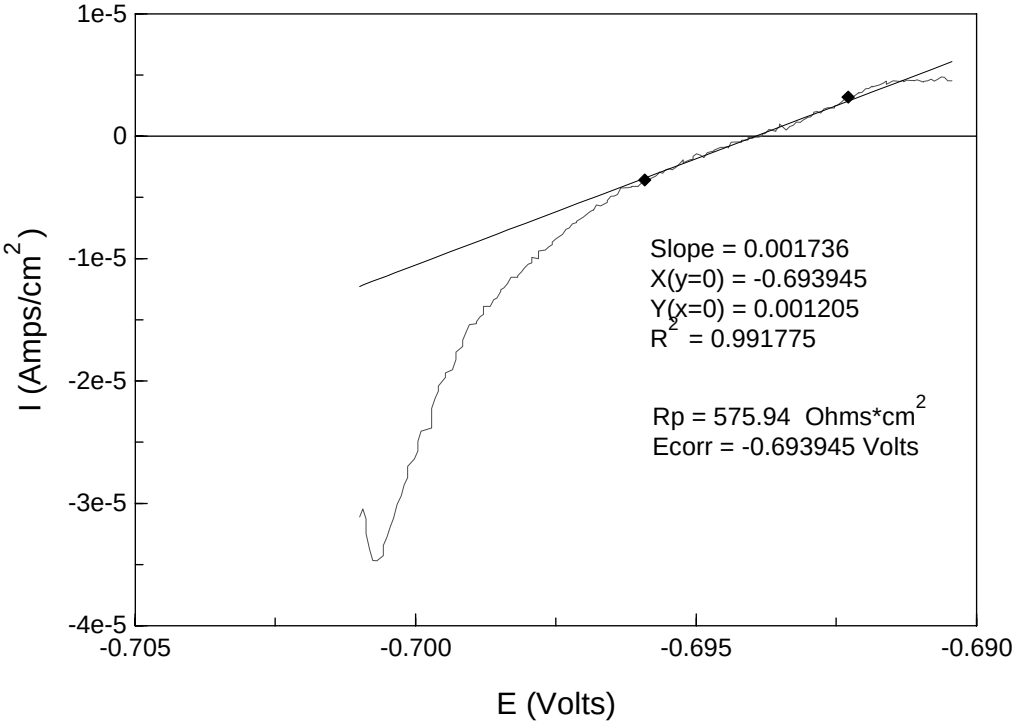

Figure C.1. Sample Polarization Resistance Plot of Current Density Versus Potential Used to Calculate Polarization Resistance.

C.2 DETERMINATION OF CORROSION CURRENT

The corrosion current can be determined using Equation 2 by Stearn-Geary:

$$i_{CORR} = \frac{\beta_A \beta_C}{2.3 \cdot R_P \left(\beta_A + \beta_C\right)} \tag{C.2}$$

where β_A is the anodic Tafel slope (Volts/decade of current), β_C is the cathodic Tafel slope (Volts/decade of current), 2.3 is the natural log of ten, and i_{CORR} is the corrosion current (Amps/cm^2).

Often Equation 2 is simplified by combining all beta (β) terms as shown in Equation 3.

$$B = \frac{\beta_A \beta_C}{(\beta_A + \beta_C)} \tag{C.3}$$

B is referred to as the Tafel constant. The Stearn-Geary coefficient is (1/2.3)*B*. Thus the corrosion current is determined by multiplying the Stearn-Geary coefficient by the inverse of polarization resistance. A Stern-Geary coefficient was estimated for each sample by interpreting graphs of the cyclic polarization resistance testing to determine the Tafel slope constants.

C.3 DETERMINATION OF TAFEL SLOPES

The anodic and cathodic Tafel slopes are typically determined by scanning from open circuit potential to typically -250 mV (for cathodic Tafel plot) and then performing a separate scan from open circuit potential to +250 mV (for anodic Tafel plot). It is possible to obtain both Tafel plots in a single scan by continuous scanning from -250 mV to +250 mV, however this practice is discouraged because the cathodic scan may alter the surface of the working electrode, which affects the outcome of the anodic scan. For the LTT and STT, the Tafel slopes were obtained from continuous scans during cyclic polarization testing. Due to its destructive nature, the cyclic polarization testing was only performed at the end of the experiments.

C.4 DETERMINATION OF CORROSION RATE

After performing the linear and cyclic polarization resistance testing and calculating the corrosion current, the corrosion rate was determined. Corrosion rate can be determined from the corrosion current using Equation 4:

$$MPY = i_{CORR}(\Lambda)(\frac{1}{\rho})(\varepsilon) \tag{C.4}$$

where MPY is corrosion rate (mils/year), i_{CORR} is the corrosion current (Amps/cm^2), Λ is 1.2866X10^5 (equivalents·sec·mils)/(Coulombs·cm·years), ρ is metal density (grams/cm^3), and ε is equivalent weight (grams/equivalent).

The *MPY* corrosion rate can be converted to weight loss in grams for a specified time period by the Equation 5 conversion:

$$WL(g) = \frac{MPY\left(\frac{mils}{yr}\right)\cdot 2.54\left(\frac{cm}{in}\right)\cdot \rho\left(\frac{g}{cm^3}\right)\cdot A(cm^2)\cdot \frac{t(d)}{365\left(\frac{d}{yr}\right)}}{1000\left(\frac{mils}{in}\right)} \tag{C.5}$$

where *WL* is weight loss, *A* is area, and *t* is time. Equation 5 units are shown in parenthesis. A density of 7.14 g/cm^3 was assumed for galvanized-steel and 7.85 g/cm^3 for plain-steel.

APPENDIX D

POLARIZATION RESISTANCE VALUES

Table D.1. Polarization Resistance ($\Omega \cdot cm^2$) Values for STT Samples.

Time (Hours)	CFM_G8.2_CL_1	CFM_G9.7_CL_1	CFM_G10.9_CL_1	CC_G9.1_CL_1	CC_G9.2_CL_1	CC_G10.2_CL_1	RAP_G9.8_CL_1	RAP_G9.9_CL_1	RAP_G10.1_CL_1
24	348	487	288	758	478	672	994	351	359
48	455	556	382	455	582	3498	1148	393	330
96	544	767	493	5780	616	4045	1600	242	292
168	627	633	509	3124	9397	6074	1226	263	335
384	262	662	720	2135	562	5979	774	571	488
528	1656	941	879	2629	647	4538	840	1059	528
672	2216	1146	1281	306	1288	2109	972	1417	637

Table D.2. Polarization Resistance ($\Omega \cdot cm^2$) Values for STT Samples.

Time (Hours)	CFM_S9.4_CL_1	CFM_S10.1_CL_1	CFM_S10.9_CL_1	CC_S9.2_CL_1	CC_S9.8_CL_1	CC_S10.7_CL_1	RAP_S9.1_CL_1	RAP_S10.2_CL_1	RAP_S10.4_CL_1
24	644	925	920	865	1071	1632	2309	2788	1642
48	655	999	1164	1158	1208	1863	2797	3042	1803
96	1054	1478	1970	1652	1885	2219	4058	1977	1486
168	1183	1565	2156	1681	1994	2432	3672	1543	1501
384	1206	1623	1738	1773	1493	2152	2945	1525	1327
528	1087	1725	2156	1210	1499	2564	2592	1625	1200
672	1308	1388	1993	1057	1369	1346	2192	848	962

Table D.3. Polarization Resistance ($\Omega \cdot cm^2$) Values for STT Samples.

Time (Hours)	CFM_G9.6_CL_100	CFM_G10.4_CL_100	CFM_G10.7_CL_100	CC_G9.3_CL_100	CC_G9.4_CL_100	CC_G9.5_CL_100	RAP_G9.10_CL_100	RAP_G10.3_CL_100	RAP_G10.8_CL_100
24	235	260	195	1545	1205	1093	101	132	216
48	264	284	219	1564	364	748	168	153	231
96	490	422	354	318	435	816	315	328	349
168	633	634	554	4813	550	844	559	619	436
384	647	708	569	8638	1006	266	1009	842	715
528	691	788	513	11940	957	241	1123	1015	729
696	700	873	516	12629	1143	441	1162	1159	1062

Table D.4. Polarization Resistance ($\Omega \cdot cm^2$) Values for STT Samples.

Time (Hours)	CFM_S9.3_CL_100	CFM_S9.9_CL_100	CFM_S9.10_CL_100	CC_S9.5_CL_100	CC_S9.6_CL_100	CC_S9.7_CL_100	RAP_S10.5_CL_100	RAP_S10.8_CL_100	RAP_S10.10_CL_100
24	200	224	194	594	595	373	269	168	302
48	266	403	325	694	752	456	294	318	343
96	454	659	459	1358	1410	811	524	621	475
168	544	854	746	1957	2081	1305	663	713	570
384	699	622	613	2531	2480	1185	899	952	632
528	594	799	747	2263	2081	987	660	783	685
696	649	737	622	1777	2082	711	743	625	614

Table D.5. Polarization Resistance (Ω·cm^2) Values for STT Samples.

Time (Hours)	CFM_G7.8_NCL_1	CFM_G8.6_NCL_1	CFM_G8.10_NCL_1	CC_G7.5_NCL_1	CC_G7.10_NCL_1	CC_G8.8_NCL_1	RAP_G7.6_NCL_1	RAP_G7.7_NCL_1	RAP_G8.9_NCL_1
24	3828	6986	3623	7228	11175	15028	12552	12066	14559
48	6368	9945	6561	9410	11760	17864	18681	20074	20560
72	16845	23632	20233	11790	13733	19422	29046	30169	30095
192	4134	4012	4327	5591	15477	14850	21466	28844	12892
336	8675	4850	14397	10067	20499	7739	17234	27855	16080
504	9801	4434	8210	3473	24039	9939	24575	3146	19954
672	7277	4865	13684	3409	28883	4385	26463	4171	3981

Table D.6. Polarization Resistance (Ω·cm^2) Values for STT Samples.

Time (Hours)	CFM_S7.2_NCL_1	CFM_S8.3_NCL_1	CFM_S8.4_NCL_1	CC_S7.3_NCL_1	CC_S7.4_NCL_1	CC_S8.2_NCL_1	RAP_S7.6_NCL_1	RAP_S7.10_NCL_1	RAP_S8.9_NCL_1
24	15040	2732	3329	16741	16083	4162	3231	4878	29419
48	2583	2039	3400	13944	20309	24547	5471	6261	4002
72	15961	2916	3742	15872	20006	18134	10615	8580	6616
192	16747	3816	4122	16169	28219	28323	15759	11637	11579
336	18167	2894	4780	12393	24734	25615	17886	14734	12632
504	12898	3730	4985	19024	23984	24410	21044	14321	11867
672	12922	4507	4976	18287	3390	24446	18060	12014	11845

Table D.7. Polarization Resistance (Ω·cm^2) Values for STT Samples.

Time (Hours)	CFM_G7.2_NCL_100	CFM_G7.3_NCL_100	CFM_G7.4_NCL_100	CC_G7.9_NCL_100	CC_G8.1_NCL_100	CC_G8.4_NCL_100	RAP_G7.1_NCL_100	RAP_G8.3_NCL_100	RAP_G8.7_NCL_100
24	-	-	-	-	-	-	-	-	-
48	8375	9633	15419	12206	18825	26240	3794	4786	20686
96	3158	21362	11509	18397	27962	3651	20686	14104	10924
192	3369	17017	13580	27818	4440	5312	8057	8614	15343
384	4868	20052	6603	15829	4566	4498	3963	7580	22858
528	6062	4755	3103	21053	4321	12883	11429	22050	11184
696	19036	4605	3461	4636	5563	15823	4299	4002	17427

Table D.8. Polarization Resistance (Ω·cm^2) Values for STT Samples.

Time (Hours)	CFM_S7.1_NCL_100	CFM_S7.5_NCL_100	CFM_S8.10_NCL_100	CC_S7.7_NCL_100	CC_S8.1_NCL_100	CC_S8.6_NCL_100	RAP_S7.8_NCL_100	RAP_S7.9_NCL_100	RAP_S8.5_NCL_100
24	-	-	-	-	-	-	-	-	-
48	19257	26708	6484	6906	11940	8170	5465	5153	8850
96	19688	5373	8124	7023	17944	14817	6080	6579	9997
192	25239	3914	15936	4737	30040	18320	13170	7225	22519
384	7546	6937	12965	8415	3883	18697	9630	6096	6753
528	5738	25227	11441	5058	4826	19128	13690	11163	7451
696	5294	4755	11288	4394	4685	23776	4994	5343	8014

Table D.9. Polarization Resistance ($\Omega \cdot cm^2$) Values for LTT G_CL Samples.

B or A	Time (days)	CFM_G2.7_CL	CFM_G3.4_CL	CC_G5.1_CL	CC_G3.5_CL	RAP_G4.8_CL	RAP_G4.2_CL
B	22	*4333*	*4333*	12599	5017	5241	6314
A	22	16	*17*	64	44	111	44
A	28	570	1198	2208	1460	1135	494
A	29	572	1191	2786	1700	1247	521
A	31	653	1920	3727	2276	1776	569
A	33	737	2066	3968	2812	1717	674
B	35	*747*	2249	4324	3088	*1717*	*674*
A	35	623	*1128*	1559	1331	1004	247
A	42	521	773	1556	1422	751	214
B	49	747	2065	4869	2916	1051	458
A	49	538	1065	1638	1228	635	114
B	64	886	2139	5366	2985	907	468
A	64	604	1046	1574	1280	715	155
B	70	676	2027	5962	3205	683	404
A	70	664	1345	1571	1175	415	*181*
B	77	695	2128	4944	2726	686	488
A	77	529	1212	1219	1069	393	218
B	84	782	2280	5031	2981	563	688
A	84	458	1553	1386	2144	354	291
B	91	904	2169	4716	2985	473	673
A	91	523	1687	1005	1788	303	315
B	98	1068	2306	5353	3219	362	818
A	98	622	1414	1181	1400	299	314
B	105	1103	2543	5742	1521	473	878
A	105	661	1399	1502	873	266	353
B	112	1112	2081	5541	1651	622	956
A	112	691	1502	1550	914	197	361
B	119	1084	2255	5594	1941	938	888
A	119	669	1561	1507	2338	167	477
B	126	1064	2395	5694	1789	1010	905
A	126	609	1617	1348	1278	181	473
B	133	1016	2588	6009	1902	641	717
A	133	611	1674	1371	1461	447	672
B	141	1158	2573	5833	2016	650	698
A	141	495	1516	1389	859	560	772
B	147	1000	2483	6101	1922	559	691
A	147	494	1042	1392	888	553	748
B	154	1236	2592	6664	2495	685	595
A	154	403	1246	1321	1079	296	166
B	161	977	2178	4794	1747	468	335
A	161	548	1103	1075	1084	368	398
B	168	968	1789	4070	1681	579	681

Note: Values in italics are averages of adjacent readings due to the inability to obtain a valid reading.

Table D.9. CONTINUED.

B or A	Time (days)	CFM_G2.7_CL	CFM_G3.4_CL	CC_G5.1_CL	CC_G3.5_CL	RAP_G4.8_CL	RAP_G4.2_CL
A	168	492	1493	1280	1136	683	491
B	175	490	2061	4478	1443	999	452
A	175	445	1149	1163	1062	331	350
B	182	610	1705	3593	1377	492	443
A	182	469	1089	1043	1031	53	525
B	189	844	1832	3993	1344	468	533
A	189	304	978	1114	1015	380	496
B	196	752	1994	4166	1528	459	504
A	196	366	1065	1234	1050	329	424
B	202	790	1856	4987	1666	468	554
A	202	378	933	1352	1079	149	807
B	217	999	2645	5918	2030	531	964
A	217	465	1599	1287	1069	279	694
B	224	1210	3239	6203	2052	748	927
A	224	345	1093	1257	1047	533	653
B	231	839	2253	5382	1870	608	586
A	231	403	1151	1293	1070	327	573
B	238	939	2352	5230	1847	519	646
A	238	377	1396	1217	1042	491	582
B	245	1086	1911	3489	1440	554	470
A	245	335	1146	1325	1067	412	782
B	253	908	2179	4951	1683	436	317
A	253	329	1134	1194	1045	368	541
B	260	891	2060	3990	1650	473	*377*
A	260	333	1207	1039	1027	437	550
B	267	867	2008	3494	1460	532	465
A	267	335	1169	1123	1373	436	612
B	274	791	1783	3817	1529	597	373
A	274	374	1164	820	959	473	827
B	288	1012	2520	5572	1709	418	122
A	288	340	1034	1014	827	328	529
B	295	740	1894	3373	1272	646	589
A	295	363	1196	969	969	455	824
B	301	816	1762	3059	1237	500	649
A	301	396	1230	984	930	426	650
B	308	820	1970	3592	1313	462	705
A	308	320	1137	962	896	601	631
B	315	826	1935	3172	1157	609	697
A	315	351	1264	1444	978	568	662
B	329	1219	2674	4992	1390	658	377
A	329	336	1833	997	987	362	656

Note: Values in italics are averages of adjacent readings due to the inability to obtain a valid reading.

Table D.10. Polarization Resistance (Ω·cm2) Values for LTT S_CL Samples.

B or A	Time (days)	CFM_S3.6_CL	CFM_S6.9_CL	CC_S2.9_CL	CC_S6.7_CL	RAP_S1.8_CL	RAP_S4.3_CL
B	22	2158	4106	34641	16498	7999	8644
A	22	69	87	304	65	104	129
A	28	2005	2787	7839	1906	1474	2168
A	29	2046	2909	8152	2087	1376	2502
A	31	1700	2712	8717	2743	1065	2504
A	33	1600	2739	9429	3303	*1065*	2642
B	35	1644	2567	10136	3647	*1065*	*2642*
A	35	1815	2387	7729	1192	934	1943
A	42	1482	2280	7101	1023	1030	1317
B	49	2235	2235	8839	3068	747	1864
A	49	1374	2106	7199	854	633	1218
B	64	1303	1831	9098	3401	736	1555
A	64	1155	1609	7262	818	584	1084
B	70	1383	1862	8746	2643	666	1547
A	70	1201	1635	7126	750	*492*	1181
B	77	1139	1609	8208	2775	604	1258
A	77	1007	1414	6832	799	424	858
B	84	1132	1511	8247	3166	531	1101
A	84	1115	1365	7187	743	440	936
B	91	980	1382	8118	2798	503	1042
A	91	953	1266	6984	681	350	733
B	98	1012	1302	8448	2805	451	931
A	98	964	1209	7086	696	377	637
B	105	907	1169	8664	2742	600	928
A	105	878	1047	7465	687	332	587
B	112	862	1042	8822	2610	624	819
A	112	820	926	7391	654	360	542
B	119	823	1054	7999	2375	498	771
A	119	717	928	7106	631	286	517
B	126	731	982	7779	2315	509	665
A	126	684	896	6993	635	276	466
B	133	650	930	7576	2482	522	648
A	133	705	791	6781	622	190	643
B	141	637	863	8000	2351	451	628
A	141	587	784	7036	610	247	545
B	147	618	809	7291	2172	302	612
A	147	537	743	5996	530	163	402
B	154	560	866	7461	2352	446	593
A	154	541	743	6276	488	190	341
B	161	495	747	6906	1946	615	467
A	161	548	681	6437	462	198	358
B	168	489	682	7211	1787	229	378

Note: Values in italics are averages of adjacent readings due to the inability to obtain a valid reading.

Table D.10. CONTINUED.

B or A	Time (days)	CFM_S3.6_CL	CFM_S6.9_CL	CC_S2.9_CL	CC_S6.7_CL	RAP_S1.8_CL	RAP_S4.3_CL
A	168	580	683	6318	581	207	362
B	175	493	795	6671	1730	189	352
A	175	489	610	5973	443	166	281
B	182	540	651	6613	1541	276	293
A	182	548	582	6406	393	147	313
B	189	496	628	6777	1454	217	320
A	189	547	609	6367	397	170	370
B	196	490	607	6487	1378	263	272
A	196	548	554	8135	*389*	*167*	265
B	202	527	660	6439	1339	207	252
A	202	589	552	6030	381	164	245
B	217	480	637	6707	1503	272	191
A	217	425	523	6169	336	230	337
B	224	514	504	6319	1409	295	191
A	224	424	384	5991	323	180	225
B	231	529	506	7365	1275	309	*191*
A	231	434	411	6116	257	161	218
B	238	434	473	6329	1170	258	*191*
A	238	427	471	6122	250	161	195
B	245	424	446	*6115*	*1108*	613	*191*
A	245	417	330	5572	223	129	184
B	253	428	360	5915	1053	356	*191*
A	253	431	428	5748	227	135	193
B	260	433	422	5792	1041	1097	*191*
A	260	386	421	5519	230	102	176
B	267	*418*	*438*	5692	938	231	*191*
A	267	*386*	*419*	5694	226	212	196
B	274	405	454	5613	1001	318	*191*
A	274	386	418	5781	240	194	*185*
B	288	414	375	7041	1190	310	*191*
A	288	385	173	6520	268	96	*185*
B	295	398	402	5722	975	149	*191*
A	295	370	116	5590	227	147	*185*
B	301	377	328	5759	882	186	133
A	301	410	149	5606	222	184	129
B	308	376	326	5915	996	151	179
A	308	372	189	6037	242	117	160
B	315	336	336	5922	756	108	185
A	315	403	181	5686	229	154	270
B	329	365	372	6731	1065	188	179
A	329	371	142	6262	237	131	223

Note: Values in italics are averages of adjacent readings due to the inability to obtain a valid reading.

Table D.11. Polarization Resistance (Ω·cm2) Values for LTT G_NCL Samples.

B or A	Time (days)	CFM_G3.6_NCL	CFM_G4.3_NCL	CC_G1.3_NCL	CC_G1.7_NCL	RAP_G2.2_NCL	RAP_G4.7_NCL
A	22	38014	32813	36215	97207	70077	*73922*
A	28	38449	12131	74360	79078	82060	73922
A	29	41574	13111	73411	83755	39066	79833
A	31	40917	40148	84915	111722	86419	49709
A	33	53847	47108	74657	112108	45399	88094
B	35	41756	43491	80765	90031	43645	29783
A	35	48317	42729	97892	148351	51853	33278
A	42	32786	6991	89984	98047	51323	39928
B	49	38942	56523	126422	139560	97367	25550
A	49	49911	17387	109474	107058	62047	69418
A	64	86459	11336	66621	124694	68896	85616
A	70	87050	58644	101841	88073	106505	109811
A	77	95994	39144	123580	97499	45287	138467
B	84	145414	14449	138733	160802	21640	213395
A	84	98530	52844	107768	102637	28581	127021
A	91	113102	27833	101487	95413	46098	58141
A	98	125483	87580	122961	122020	75764	175593
A	105	123013	72218	138195	167785	77492	155400
B	112	118112	58443	204018	192721	14040	88755
A	112	199862	24048	150987	184175	105850	170996
A	119	174919	17020	145887	105378	155076	153004
A	126	127164	24088	40050	90059	131926	171436
A	133	52987	90583	38747	178388	139605	139552
B	141	91909	20414	75084	189353	33846	164682
A	141	191868	18996	55885	120622	209373	102415
A	147	160187	43039	59255	165174	162044	186300
A	154	189050	88043	97969	128224	162764	153311
A	161	120784	37893	81546	172049	75421	48407
B	168	41893	42543	101262	118295	14014	12523
A	168	134429	15259	75915	77522	195327	35024
A	175	116592	52813	27214	169558	188378	43223
A	182	172174	32704	25081	77865	176104	112074
A	189	150298	72541	20450	130391	197388	237032
B	196	38531	50395	35999	87407	308020	216703
A	196	155354	88049	25399	112006	187834	262972
A	202	240964	114882	21793	152654	107518	151392
A	217	*48430*	*59472*	22934	58675	206284	219724
B	224	26920	40121	39271	179014	22881	86612
A	224	103207	53080	26553	99705	196005	64548
A	231	93893	113132	30519	145479	163071	119518
A	238	124491	43907	18806	118646	276861	78368

Note: Values in italics are averages of adjacent readings due to the inability to obtain a valid reading.

Table D.11. CONTINUED.

B or A	Time (days)	CFM_G3.6_NCL	CFM_G4.3_NCL	CC_G1.3_NCL	CC_G1.7_NCL	RAP_G2.2_NCL	RAP_G4.7_NCL
A	245	80480	121235	21568	90221	263211	79047
B	253	89674	56928	38859	151807	*254503*	*100058*
A	253	79290	105319	27029	133265	246352	136283
A	260	80153	163491	24554	157309	235060	123833
A	267	23007	20707	38033	126349	127871	27429
A	274	77096	101801	26944	152002	222774	79525
B	283	*44363*	27132	*32968*	*140552*	*15707*	*52551*
A	283	31141	*44344*	*32968*	*140552*	*15707*	*52551*
A	288	91759	121291	*32968*	130706	8140	39241
B	295	102889	15111	42462	122100	*15167*	*32728*
A	295	101380	97477	25772	115535	110898	28069
A	301	105773	92336	24973	140094	99006	25285
A	308	101841	124844	32226	138210	231440	310522
A	315	89127	132363	31852	101325	208200	42450
A	329	86646	87012	28878	*101325*	22662	*42450*

Note: Values in italics are averages of adjacent readings due to the inability to obtain a valid reading.

Table D.12. Polarization Resistance (Ω·cm2) Values for LTT S_NCL Samples.

B or A	Time (days)	CFM_S3.9_NCL	CFM_S4.9_NCL	CC_S2.7_NCL	CC_S6.3_NCL	RAP_S3.2_NCL	RAP_S3.7_NCL
A	22	19279	7188	32884	23162	8922	*19101*
A	28	17359	6659	23094	16026	11339	19101
A	29	20229	4063	23829	22876	8683	21628
A	31	19322	4454	29148	26380	7055	25150
A	33	13290	3837	34093	23623	6527	22727
B	35	17554	5677	23325	17444	10049	18803
A	35	16275	3071	38841	25069	8261	20874
A	42	19480	5382	21456	19389	10161	18051
B	49	19952	3125	35653	21608	6847	12599
A	49	20145	5127	22024	17268	8991	30768
A	64	21346	3393	20731	17775	11430	32520
A	70	18716	21632	20515	16381	9179	30587
A	77	19388	3885	21035	25179	9410	40325
B	84	21421	5260	37342	15428	8925	31982
A	84	16671	4593	19965	17173	9090	29561
A	91	15800	2316	20416	16805	11254	30138
A	98	15655	4100	23638	17079	9163	38287
A	105	17099	4026	26371	17504	9931	35152
B	112	21250	6864	42257	24909	12749	45164
A	112	19599	5767	24298	16921	11922	35472
A	119	24048	3453	23972	18300	10621	30193
A	126	21183	4082	22010	18570	14585	57642
A	133	24882	7194	23320	17970	8519	53305
B	141	23817	4378	39960	23149	13894	59298
A	141	23567	6714	18354	18698	10841	59771
A	147	24337	7448	16863	19711	11208	56091
A	154	19013	3894	23632	21891	8906	62872
A	161	16705	16576	25166	22482	8233	66116
B	168	*17555*	*7947*	37497	29620	11896	97914
A	168	18497	5226	21338	22362	8693	67248
A	175	12409	3147	15290	23325	10181	70814
A	182	14682	3448	9528	21900	8075	72466
A	189	20762	3519	19481	21753	8155	74710
B	196	21249	3532	*17678*	*20313*	10396	101313
A	196	17437	3184	16180	*20313*	8274	71596
A	202	18662	4834	15640	19052	8409	81408
A	217	*7949*	*4830*	22166	26319	7862	81030
B	224	5050	4825	37385	35089	8655	43588
A	224	4853	4188	20882	22036	7701	69088
A	231	12953	4162	21384	21272	9126	68493
A	238	10527	5237	25295	22132	7669	59288

Note: Values in italics are averages of adjacent readings due to the inability to obtain a valid reading.

Table D.12. CONTINUED.

B or A	Time (days)	CFM_G2.7_CL	CFM_G3.4_CL	CC_G5.1_CL	CC_G3.5_CL	RAP_G4.8_CL	RAP_G4.2_CL
A	245	9130	5490	25027	20047	8287	75397
B	253	17884	6106	53720	34806	7040	74913
A	253	15259	7010	22792	19843	8705	66886
A	260	8603	5353	27983	21509	8357	74034
A	267	3515	3819	45757	20286	8857	73143
A	274	21637	6839	45839	22250	6798	71108
B	283	6904	4288	51037	37209	5996	93304
A	283	10364	*5186*	*41161*	*27612*	*6915*	*71810*
A	288	20777	6561	34488	21951	8167	*71810*
B	295	4440	4290	52553	23155	5229	58365
A	295	10848	6416	29707	21696	6024	81656
A	301	22883	7075	24609	21433	6148	85436
A	308	9683	5349	24748	21039	4347	*83271*
A	315	9843	6031	26698	21468	4932	81212
A	329	23176	4964	40117	24882	7370	80585

Note: Values in italics are averages of adjacent readings due to the inability to obtain a valid reading.

APPENDIX E

CYCLIC POLARIZATION PLOTS

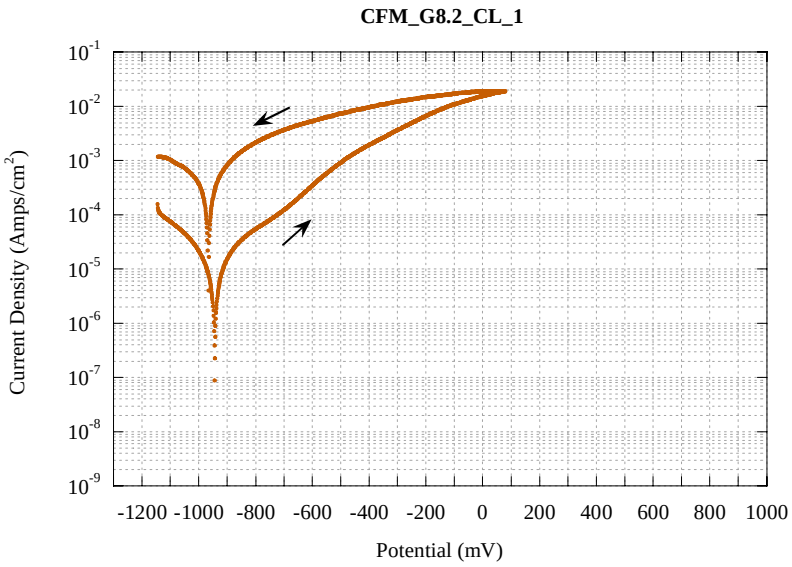

Figure E.1. Cyclic Polarization Test for CFM_G8.2_CL_1.

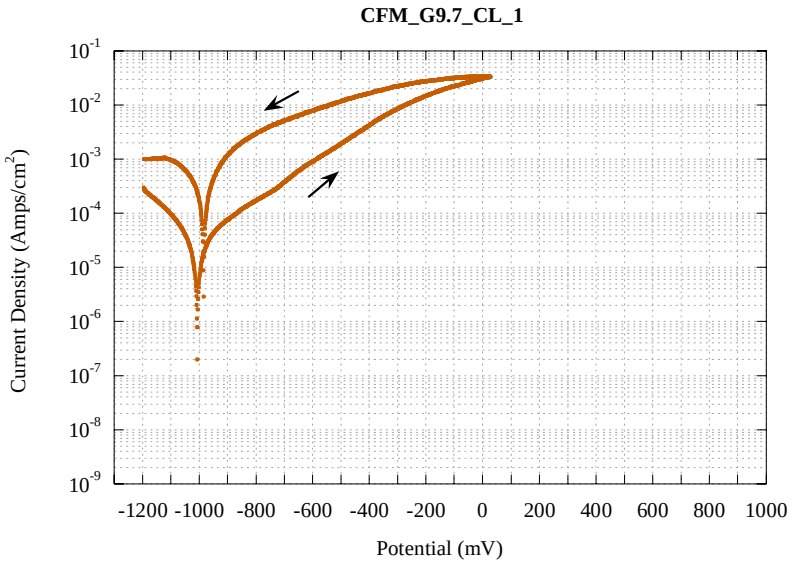

Figure E.2. Cyclic Polarization Test for CFM_G9.7_CL_1.

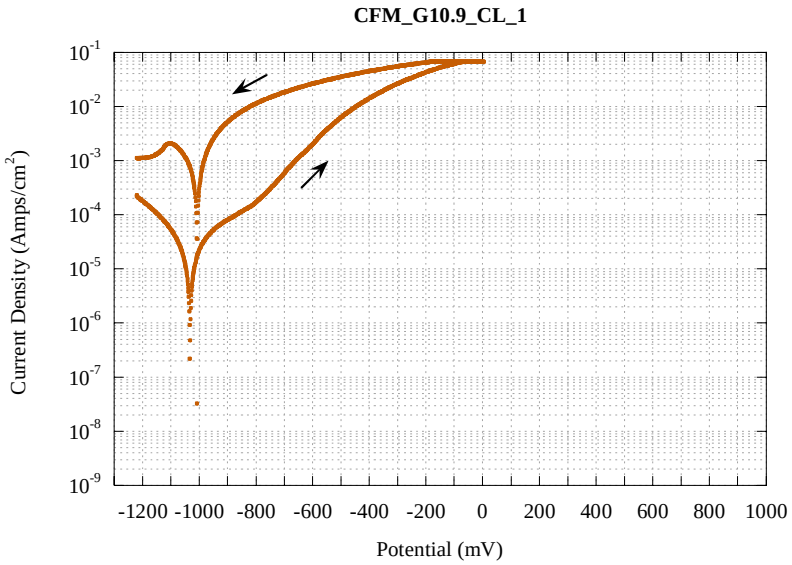

Figure E.3. Cyclic Polarization Test for CFM_G10.9_CL_1.

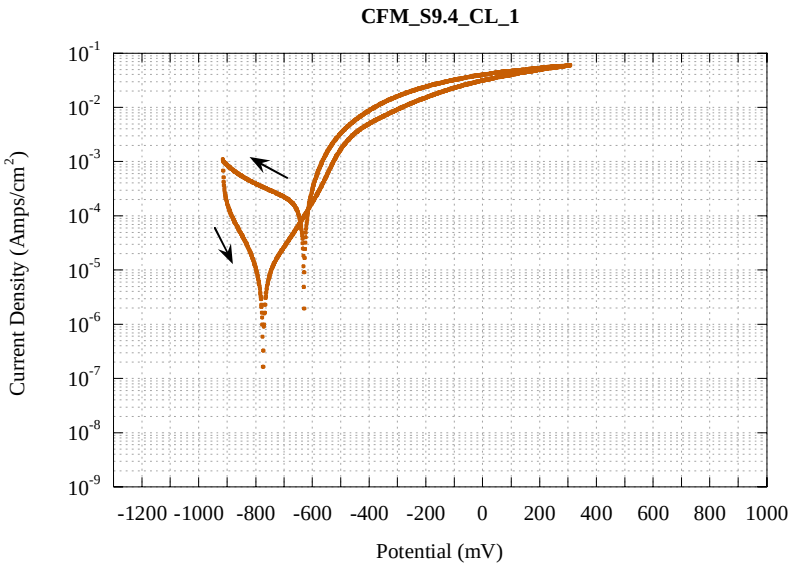

Figure E.4. Cyclic Polarization Test for CFM_S9.4_CL_1.

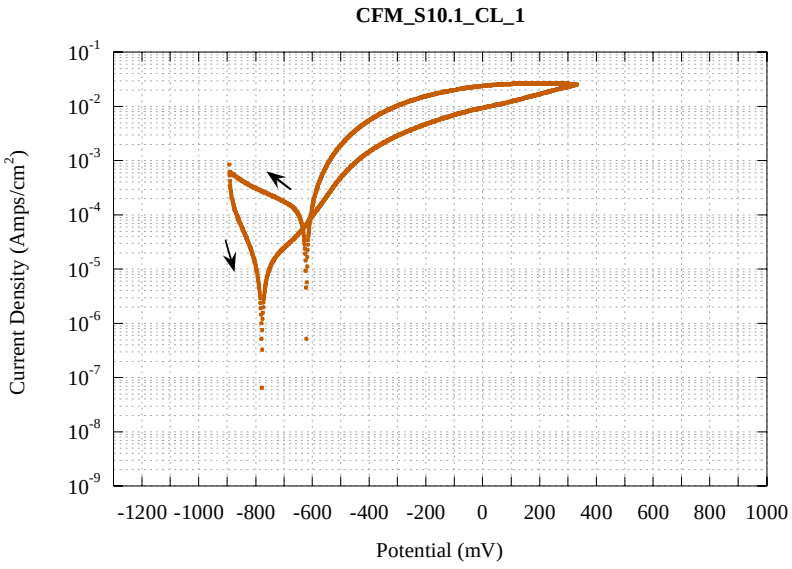

Figure E.5. Cyclic Polarization Test for CFM_S10.1_CL_1.

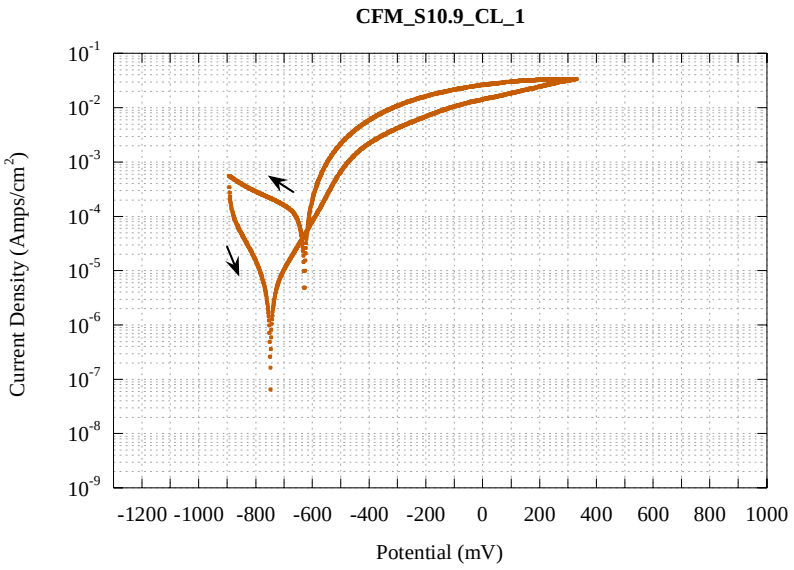

Figure E.6. Cyclic Polarization Test for CFM_S10.9_CL_1.

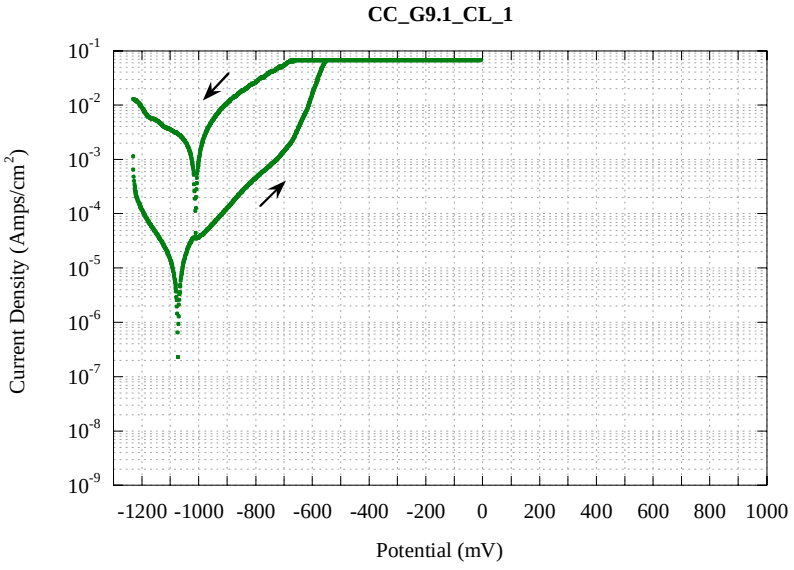

Figure E.7. Cyclic Polarization Test for CC_G9.1_CL_1.

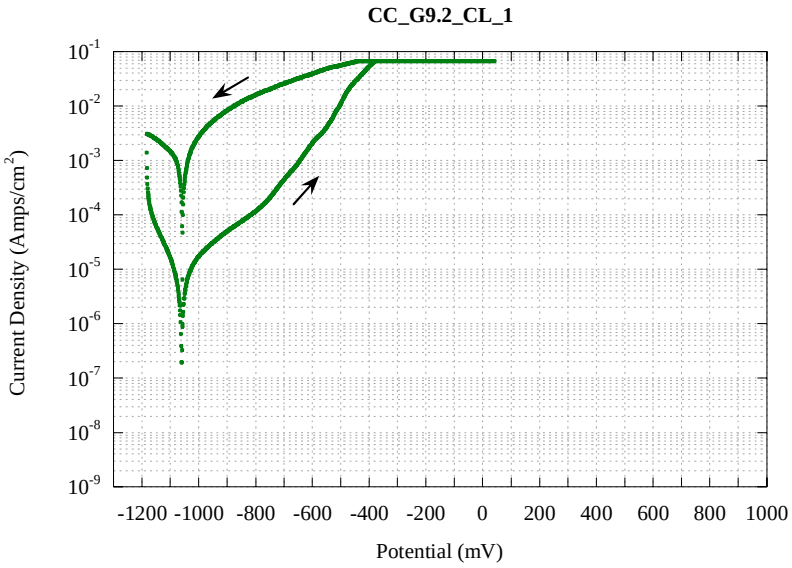

Figure E.8. Cyclic Polarization Test for CC_G9.2_CL_1.

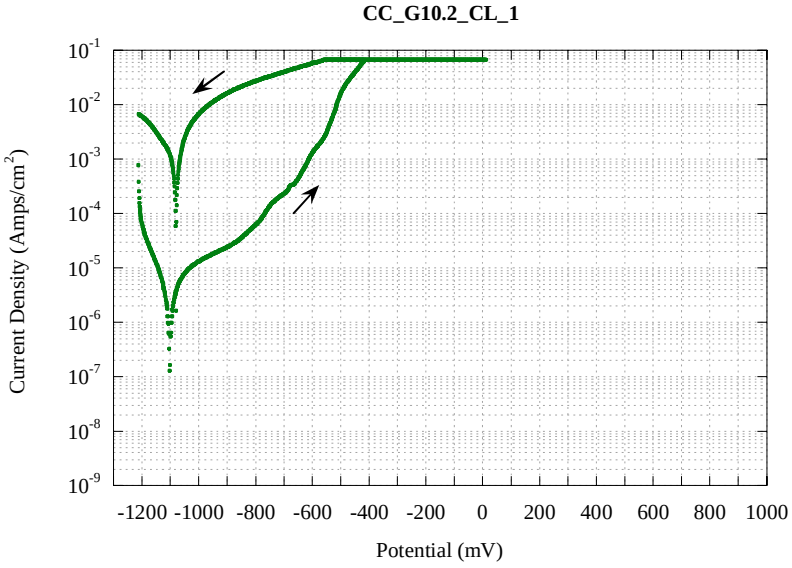

Figure E.9. Cyclic Polarization Test for CC_G10.2_CL_1.

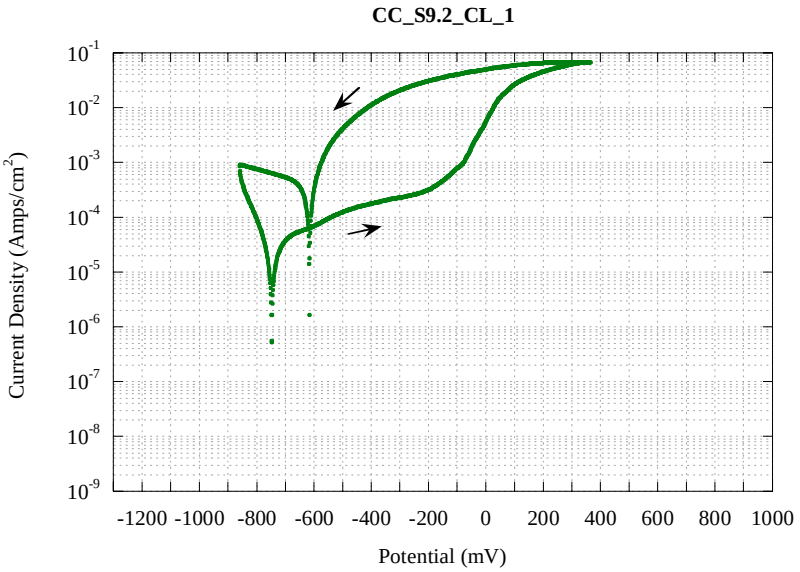

Figure E.10. Cyclic Polarization Test for CC_S9.2_CL_1.

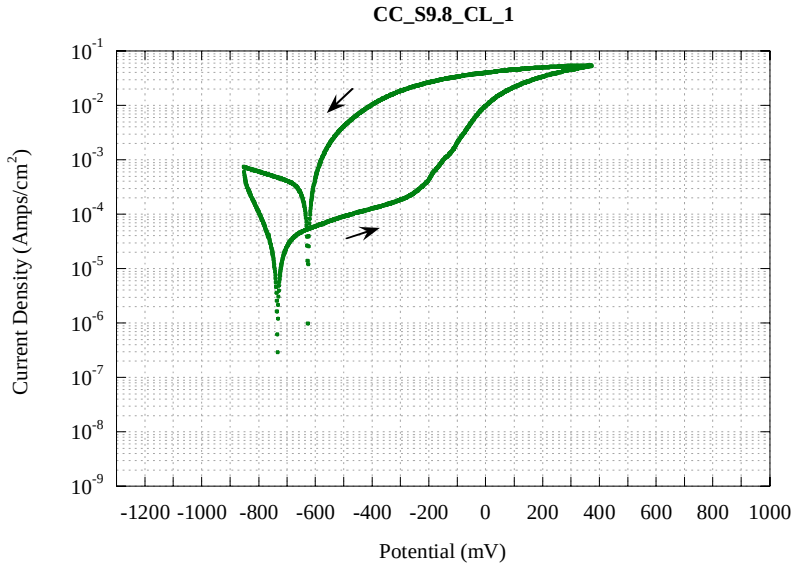

Figure E.11. Cyclic Polarization Test for CC_S9.8_CL_1.

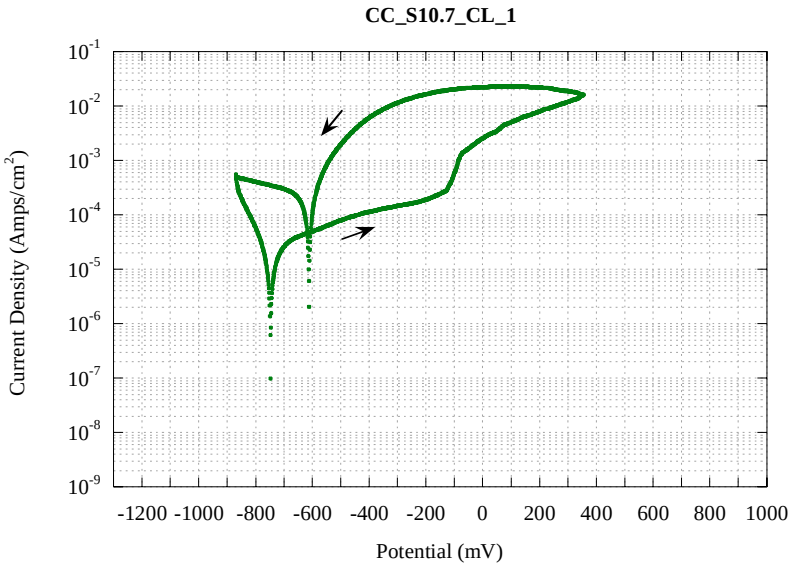

Figure E.12. Cyclic Polarization Test for CC_S10.7_CL_1.

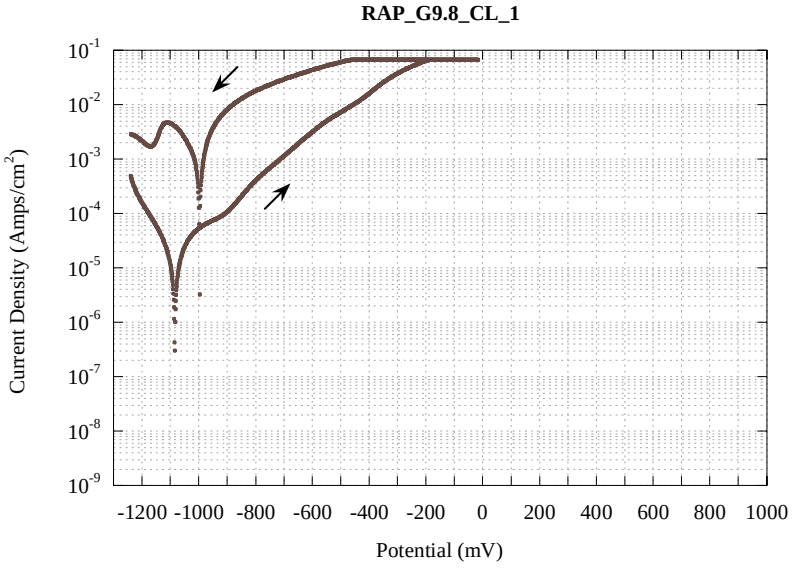

Figure E.13. Cyclic Polarization Test for RAP_G9.8_CL_1.

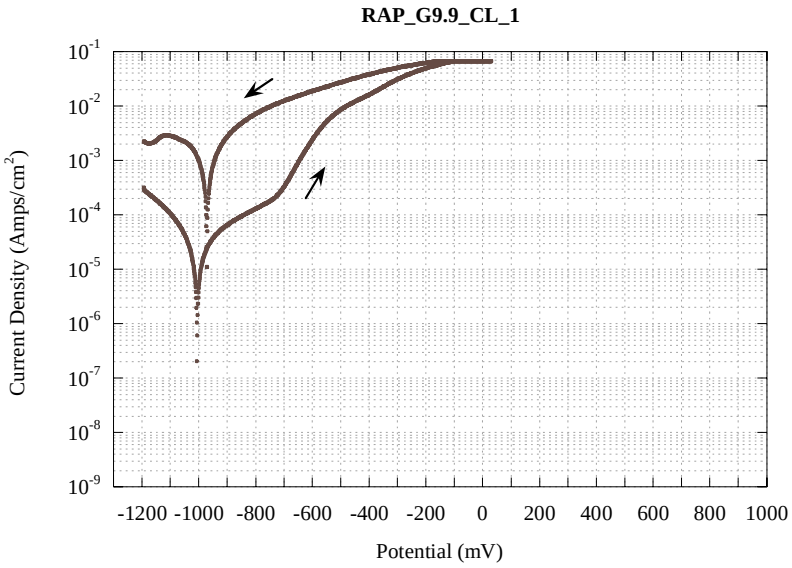

Figue E.14. Cyclic Polarization Test for RAP_G9.9_CL_1.

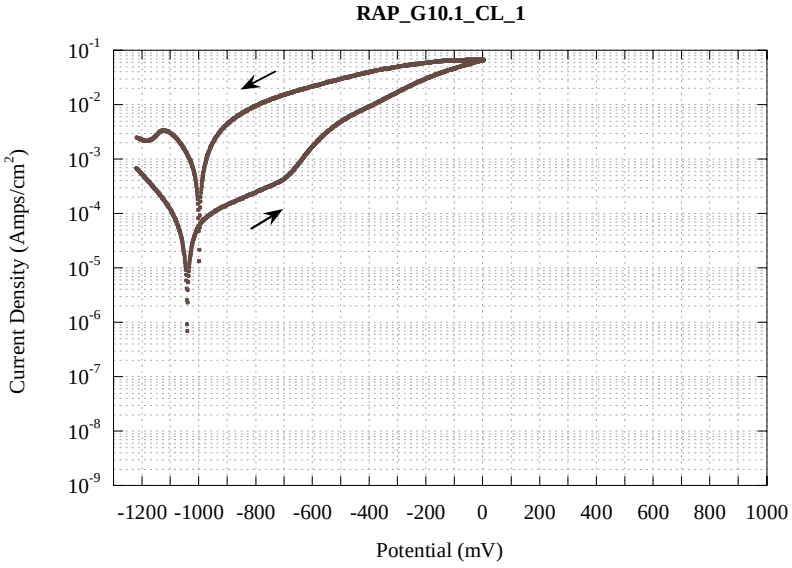

Figure E.15. Cyclic Polarization Test for RAP_G10.1_CL_1.

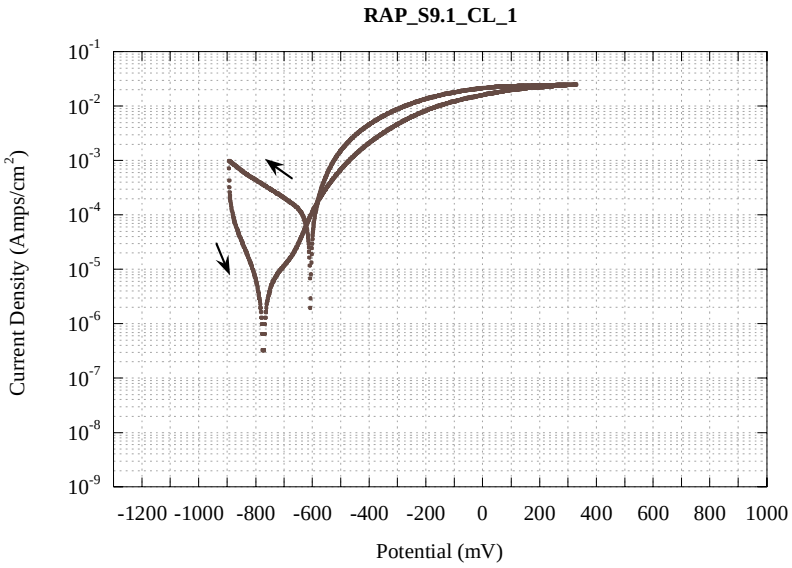

Figure E.16. Cyclic Polarization Test for RAP_S9.1_CL_1.

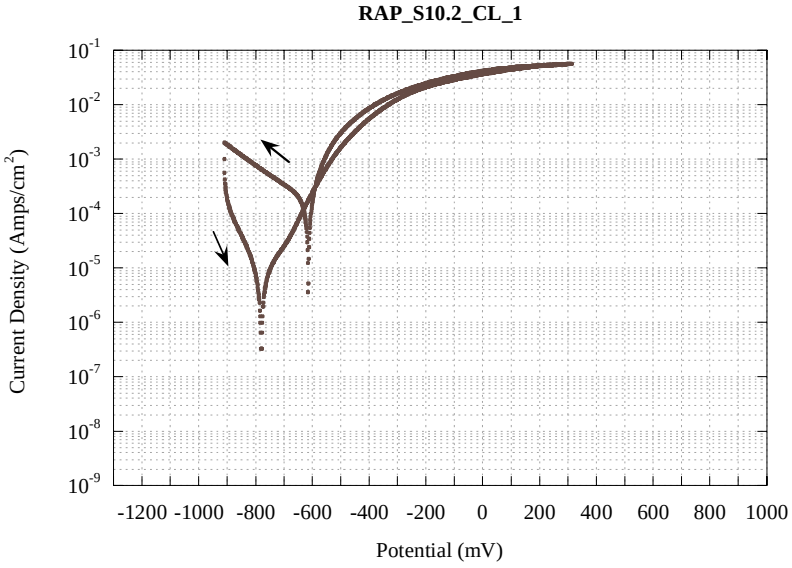

Figure E.17. Cyclic Polarization Test for RAP_S10.2_CL_1.

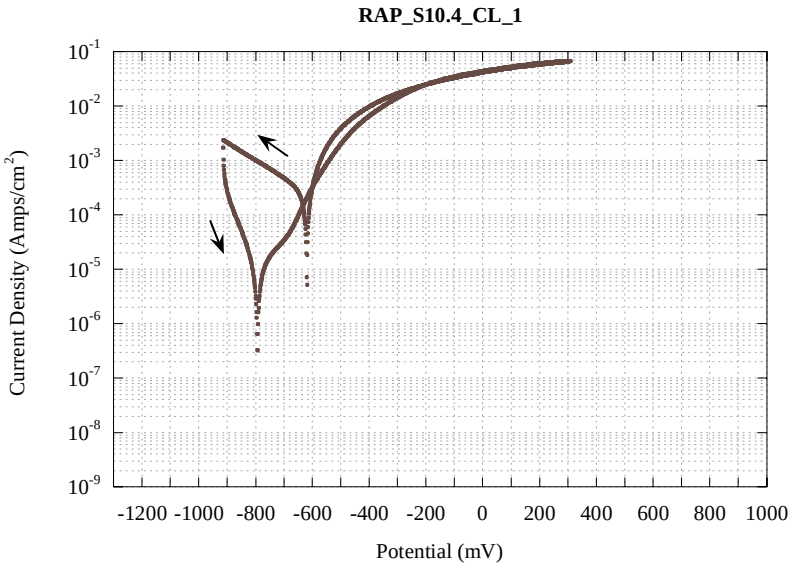

Figure E.18. Cyclic Polarization Test for RAP_S10.4_CL_1.

THIS PLOT POSITION INTENTIONALLY LEFT BLANK

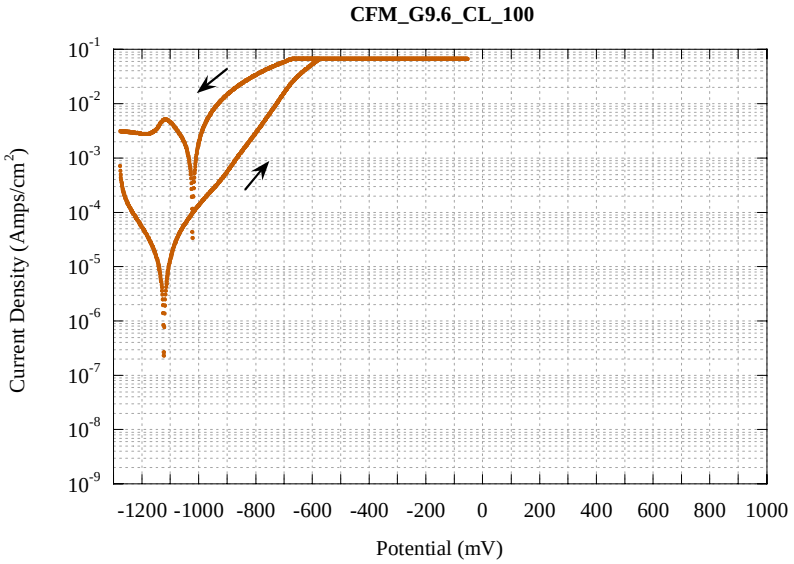

Figure E.19. Cyclic Polarization Test for CFM_G9.6_CL_100.

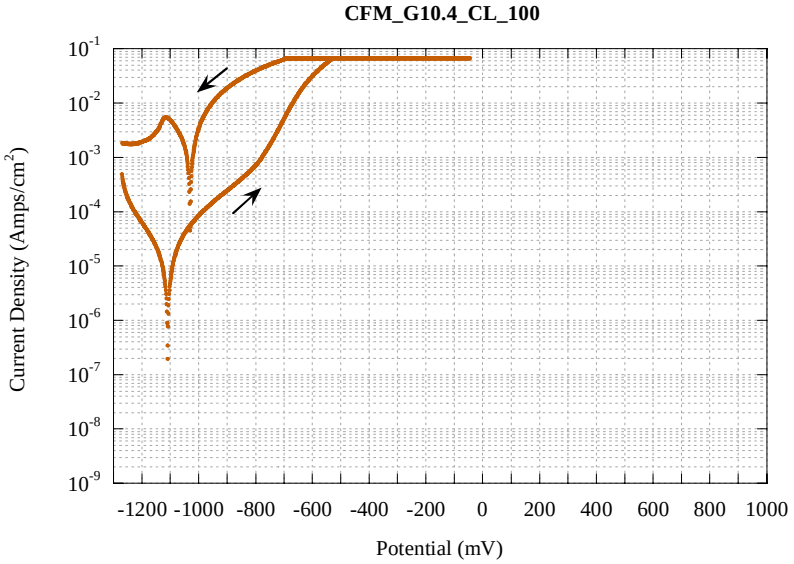

Figure E.20. Cyclic Polarization Test for CFM_G10.4_CL_100.

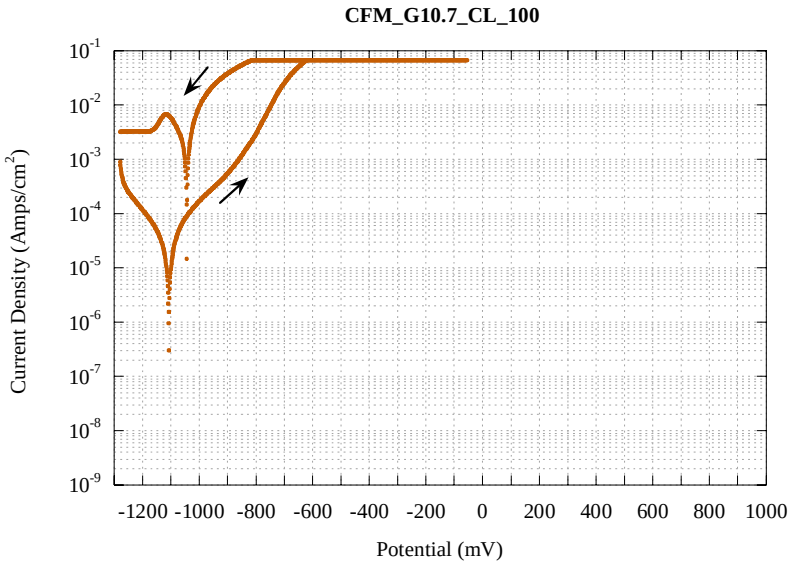

Figure E.21. Cyclic Polarization Test for CFM_G10.7_CL_100.

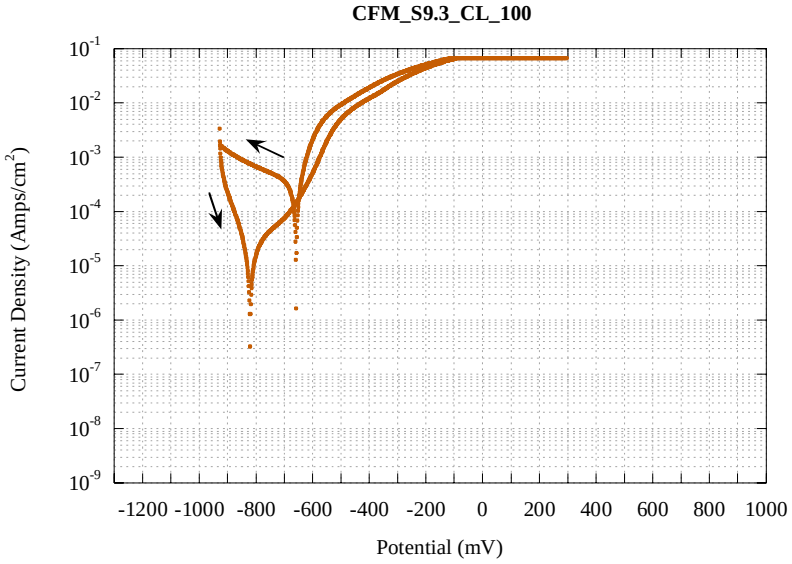

Figure E.22. Cyclic Polarization Test for CFM_S9.3_CL_100.

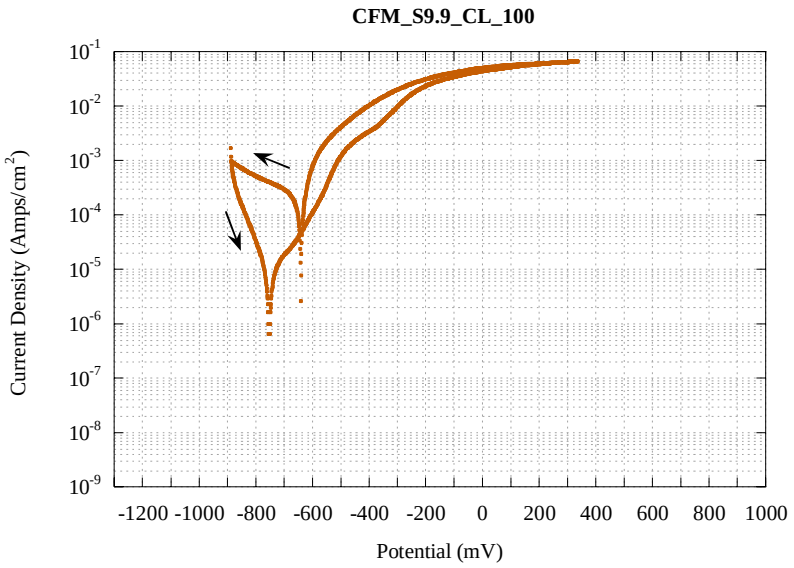

Figure E.23. Cyclic Polarization Test for CFM_S9.9_CL_100.

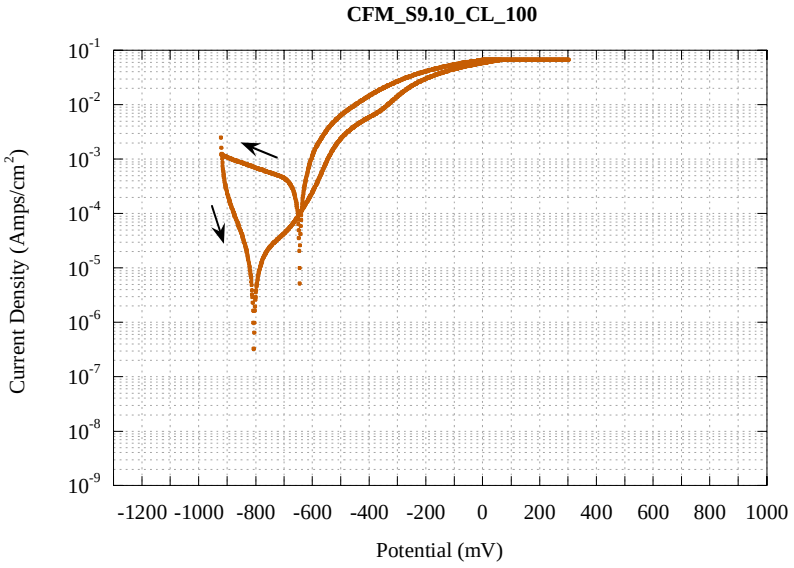

Figure E.24. Cyclic Polarization Test for CFM_S9.10_CL_100.

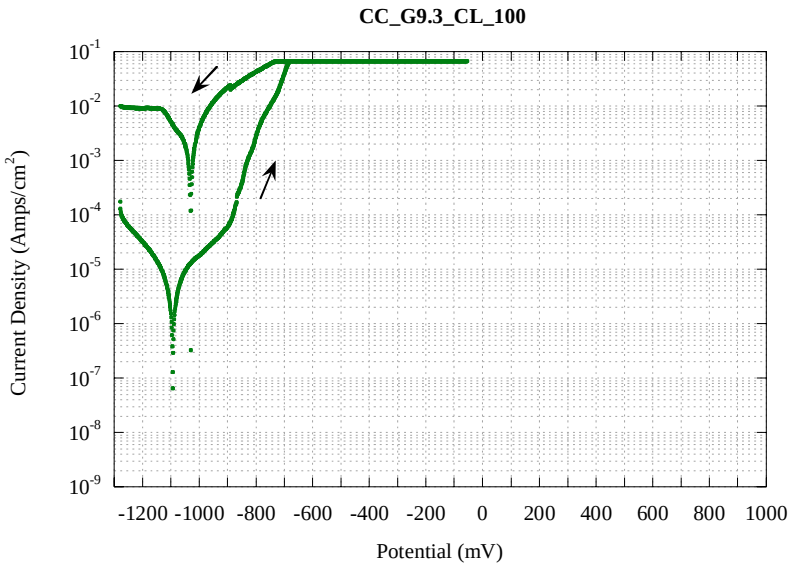

Figure E.25. Cyclic Polarization Test for CC_G9.3_CL_100.

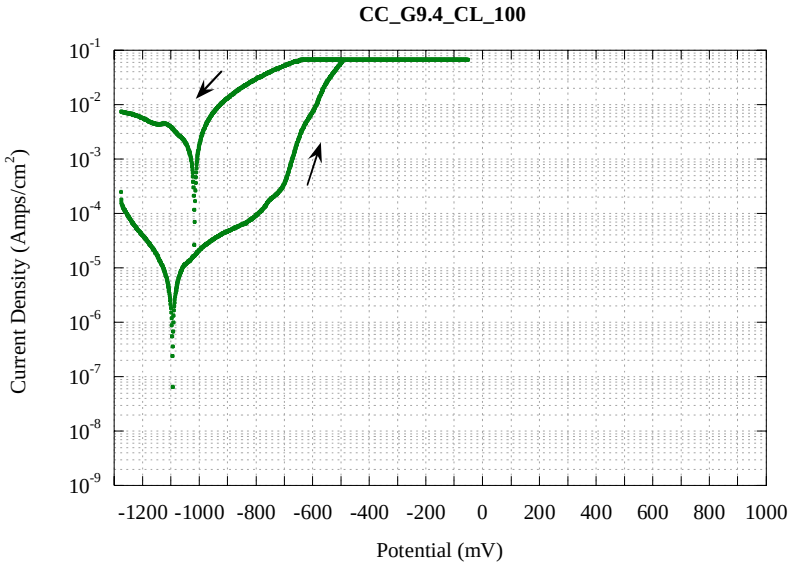

Figure E.26. Cyclic Polarization Test for CC_G9.4_CL_100.

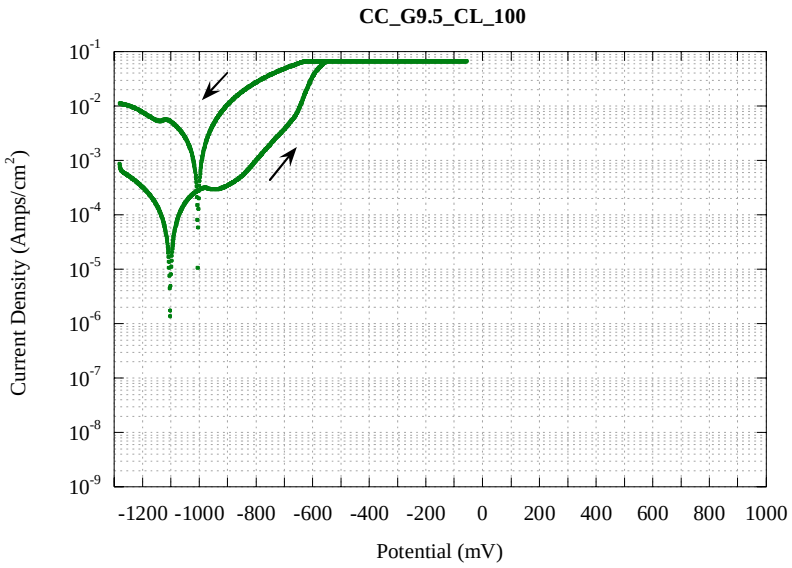

Figure E.27. Cyclic Polarization Test for CC_G9.5_CL_100.

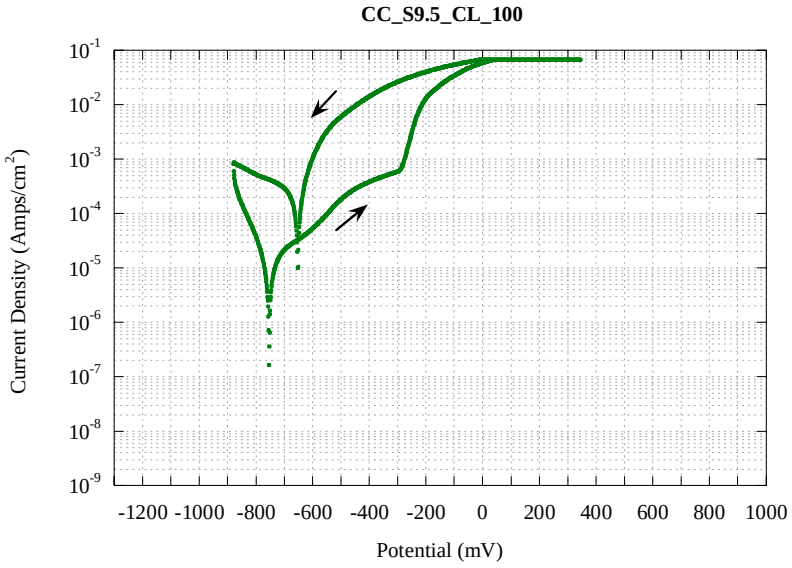

Figure E.28. Cyclic Polarization Test for CC_S9.5_CL_100.

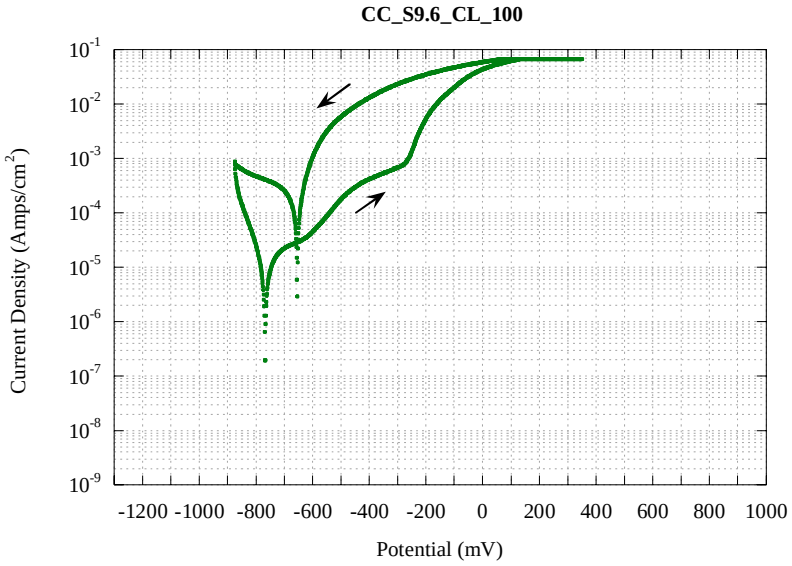

Figure E.29. Cyclic Polarization Test for CC_S9.6_CL_100.

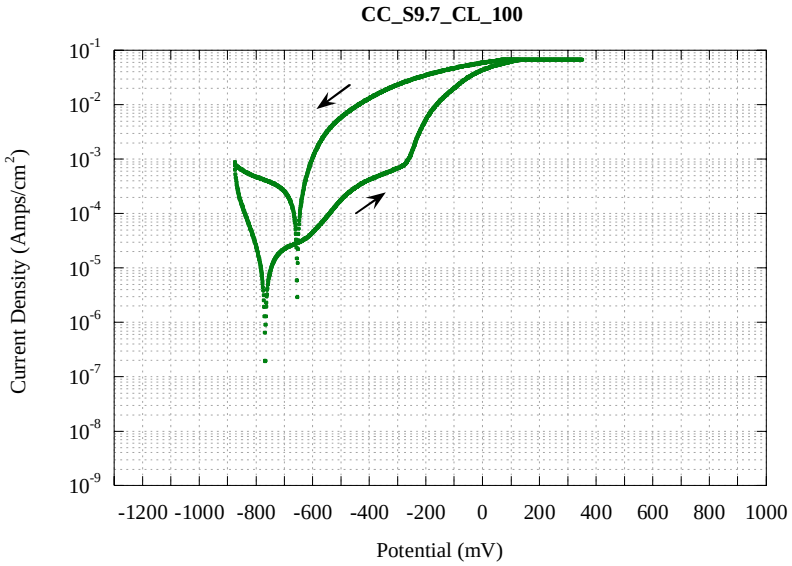

Figure E.30. Cyclic Polarization Test for CC_S9.7_CL_100.

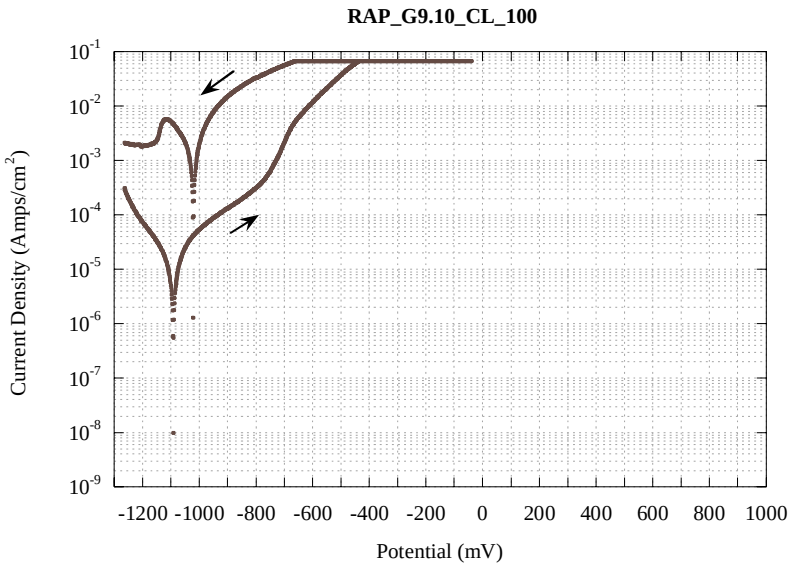

Figure E.31. Cyclic Polarization Test for RAP_G9.10_CL_100.

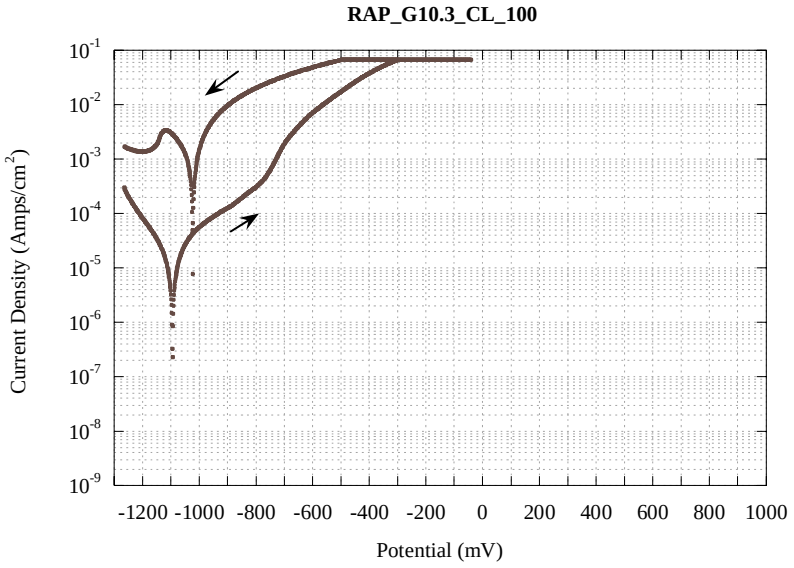

Figue E.32. Cyclic Polarization Test for RAP_G10.3_CL_100.

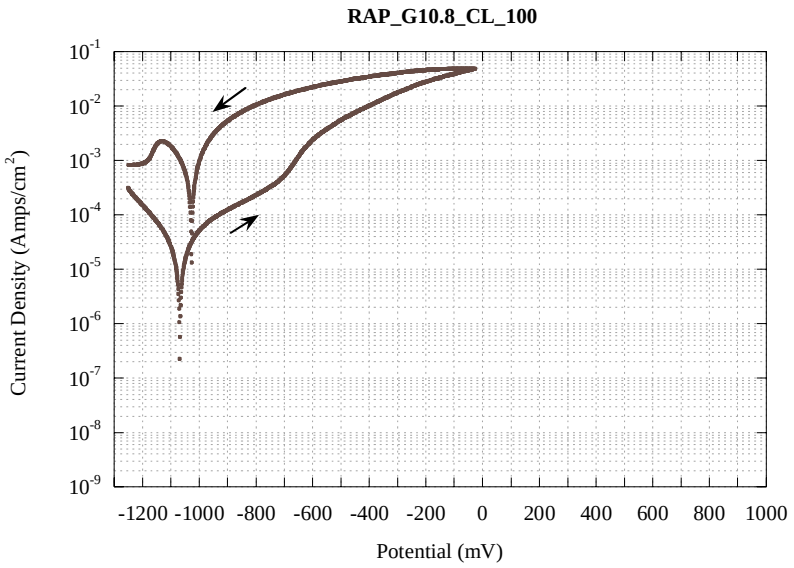

Figure E.33. Cyclic Polarization Test for RAP_G10.8_CL_100.

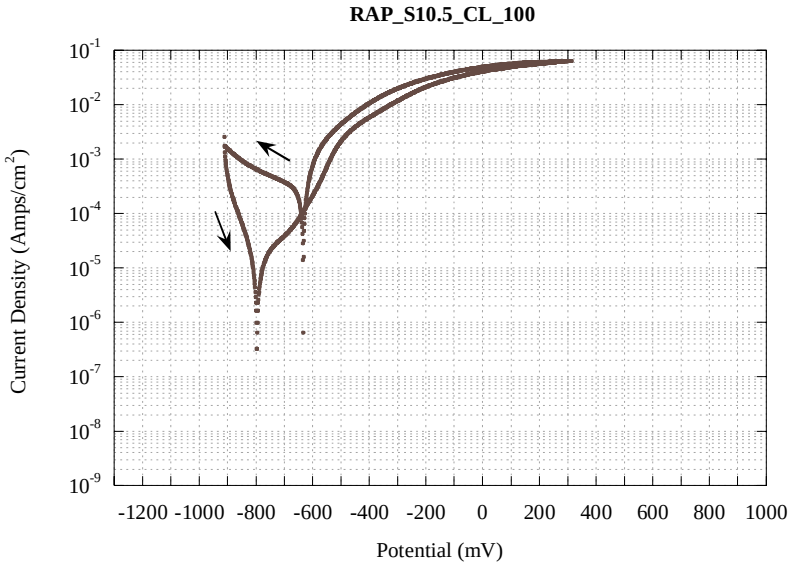

Figure E.34. Cyclic Polarization Test for RAP_S10.5_CL_100.

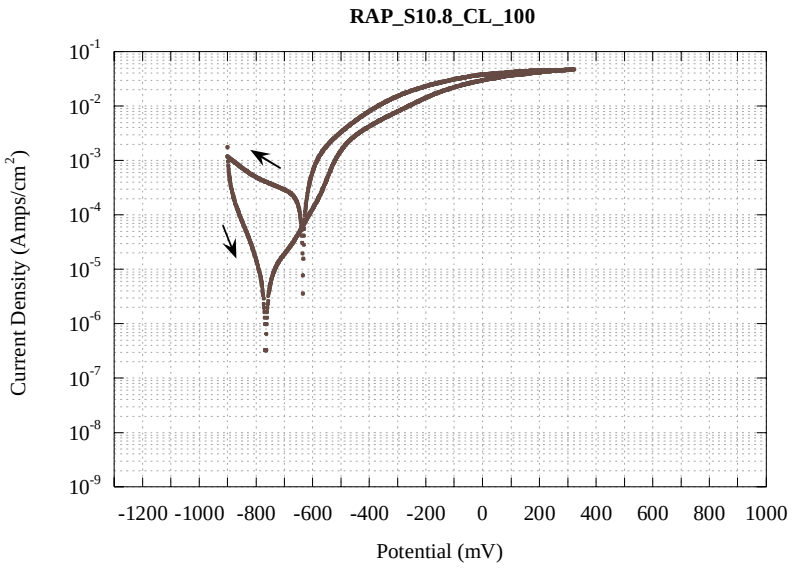

Figure E.35. Cyclic Polarization Test for RAP_S10.8_CL_100.

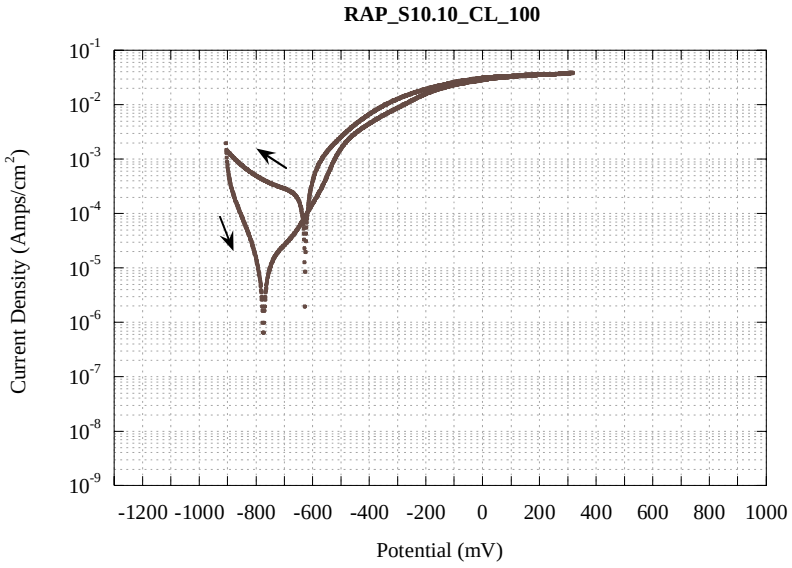

Figure E.36. Cyclic Polarization Test for RAP_S10-10_CL_100.

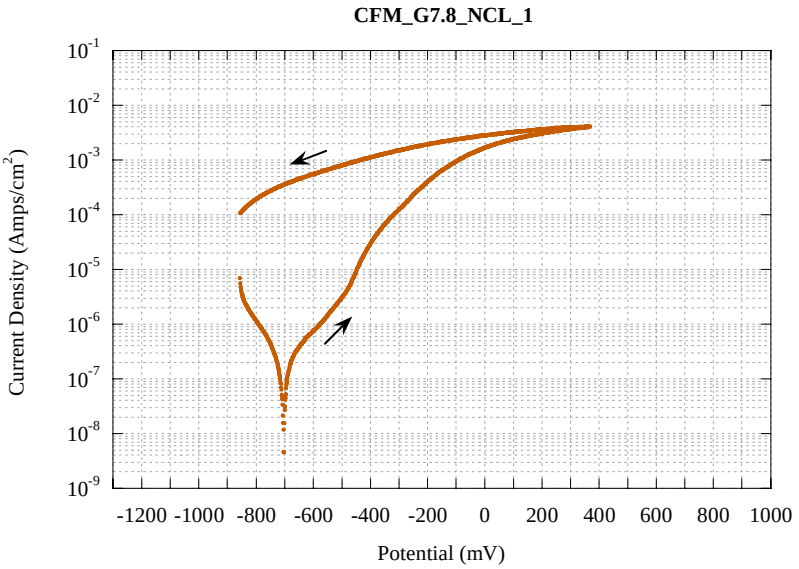

Figure E.37. Cyclic Polarization Test for CFM_G7.8_NCL_1.

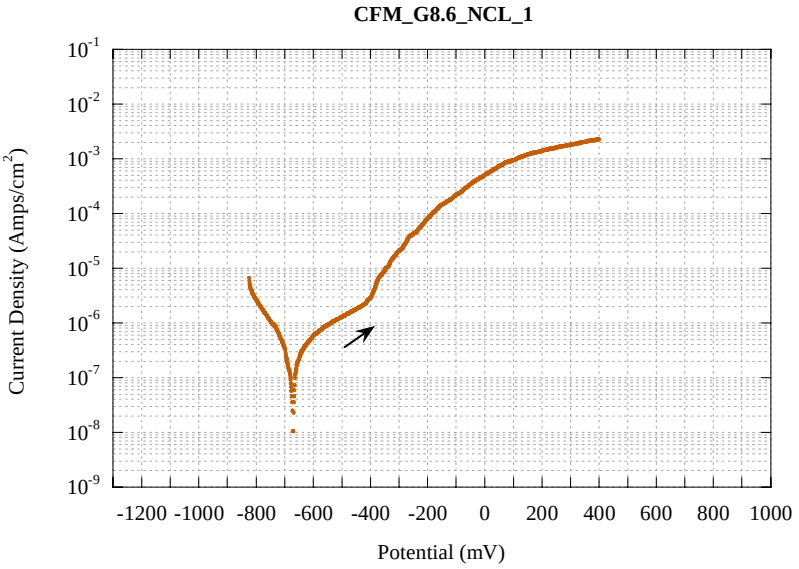

Figure E.38. Cyclic Polarization Test for CFM_G8.6_NCL_1.

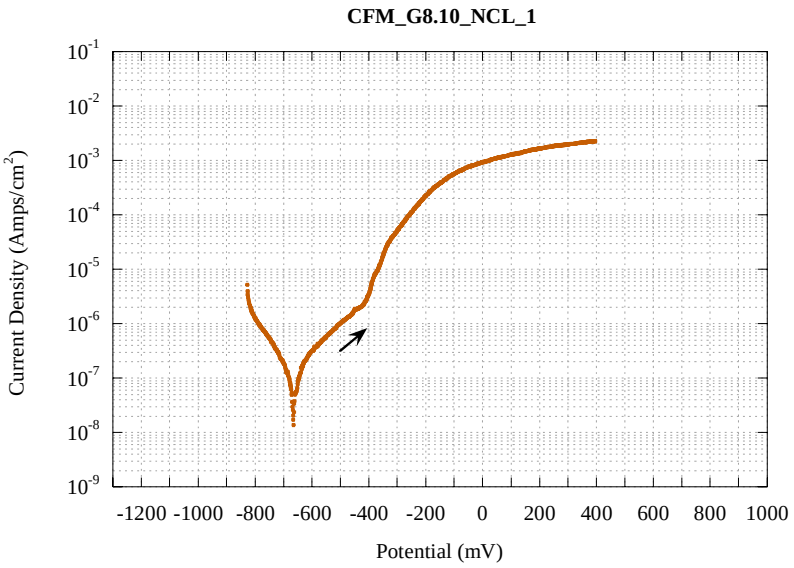

Figure E.39. Cyclic Polarization Test for CFM_G8.10_NCL_1.

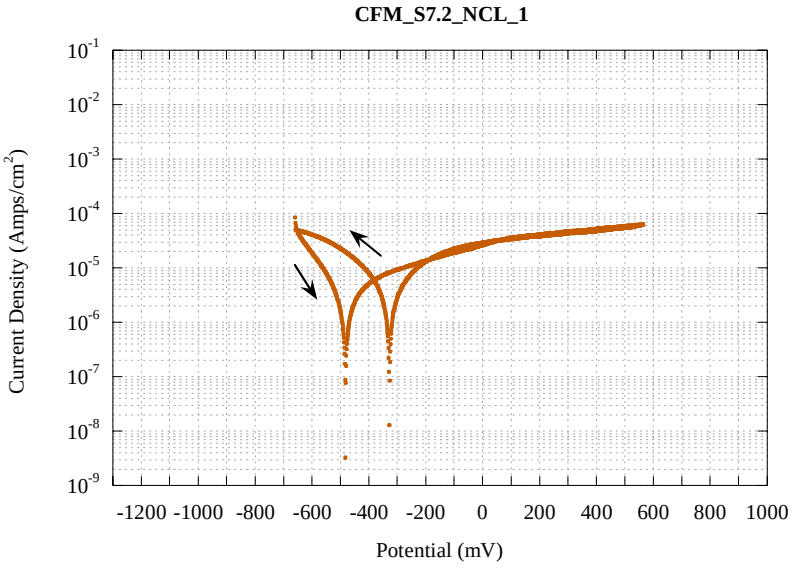

Figure E.40. Cyclic Polarization Test for CFM_S7.2_NCL_1.

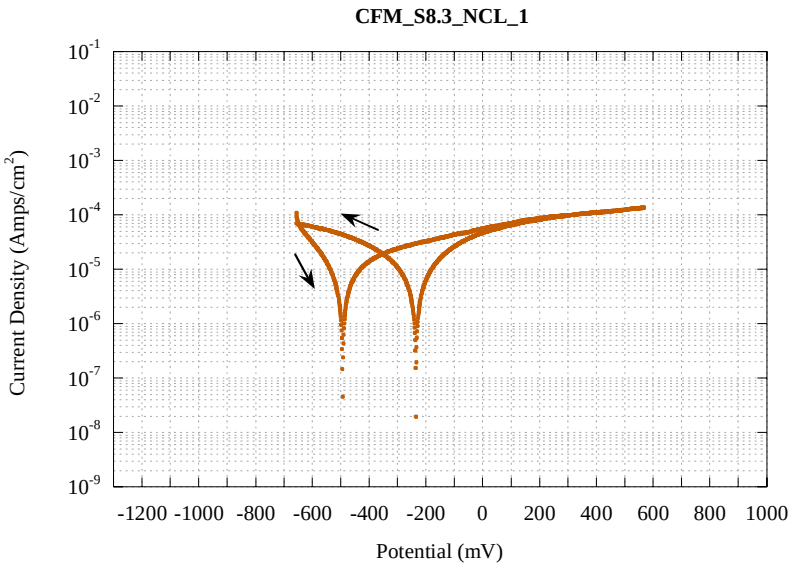

Figure E.41. Cyclic Polarization Test for CFM_S8.3_NCL_1.

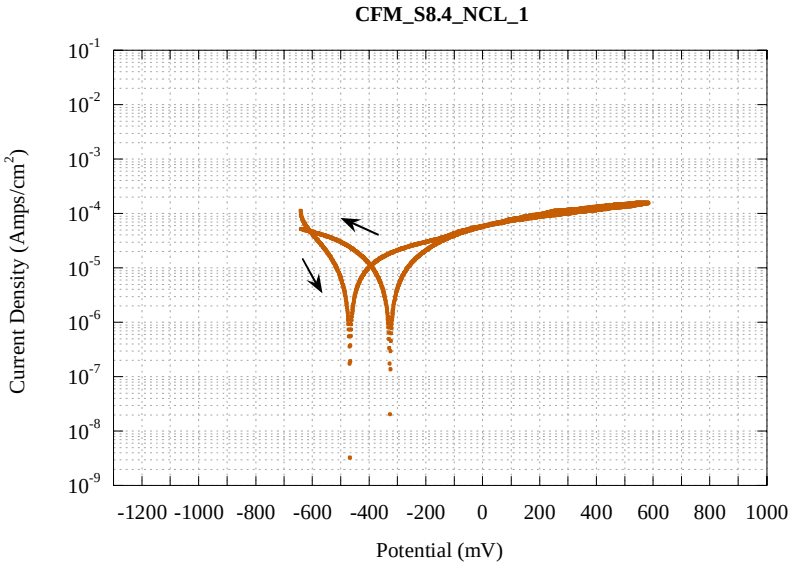

Figure E.42. Cyclic Polarization Test for CFM_S8.4_NCL_1.

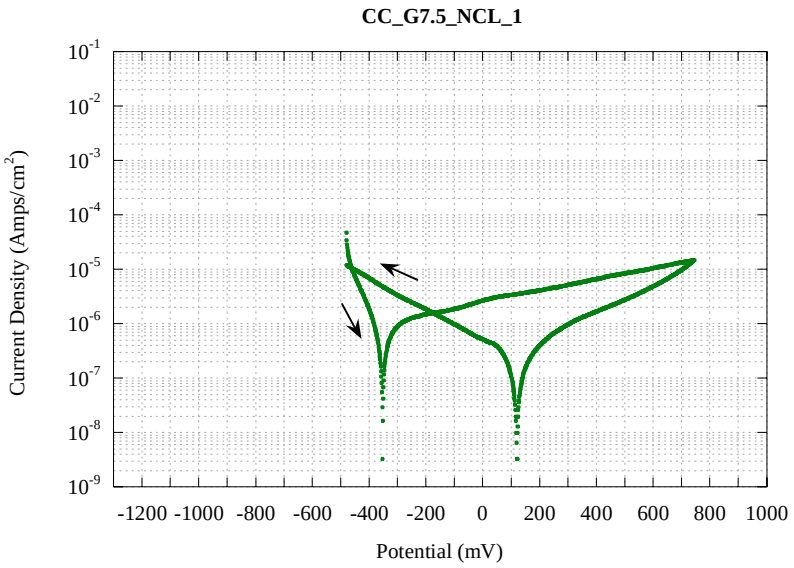

Figure E.43. Cyclic Polarization Test for CC_G7.5_NCL_1.

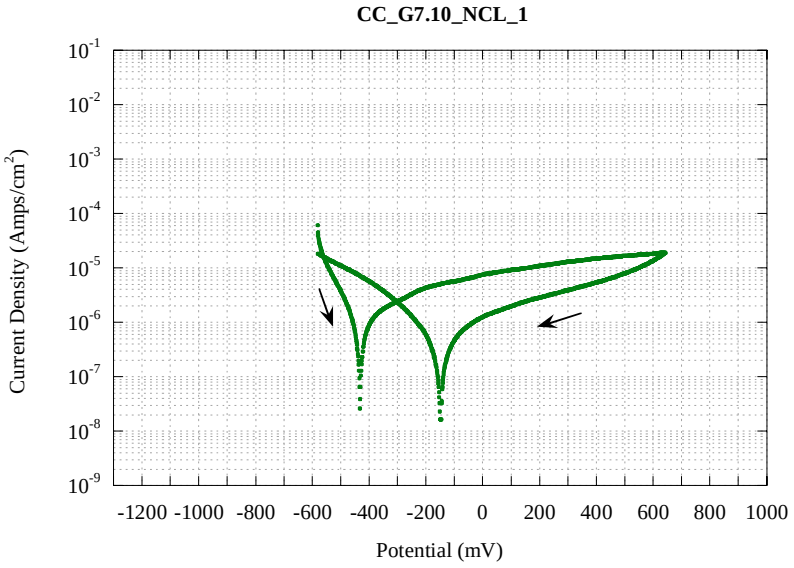

Figure E.44. Cyclic Polarization Test for CC_G7.10_NCL_1.

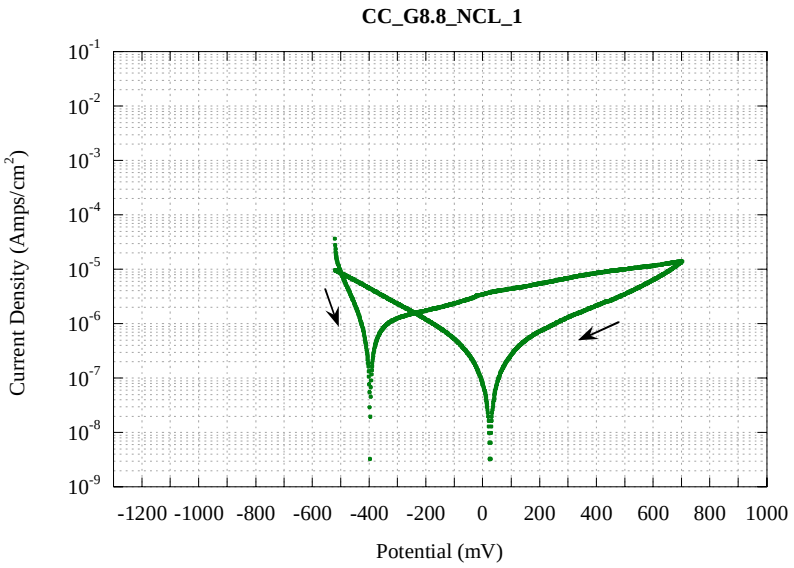

Figure E.45. Cyclic Polarization Test for CC_G8.8_NCL_1.

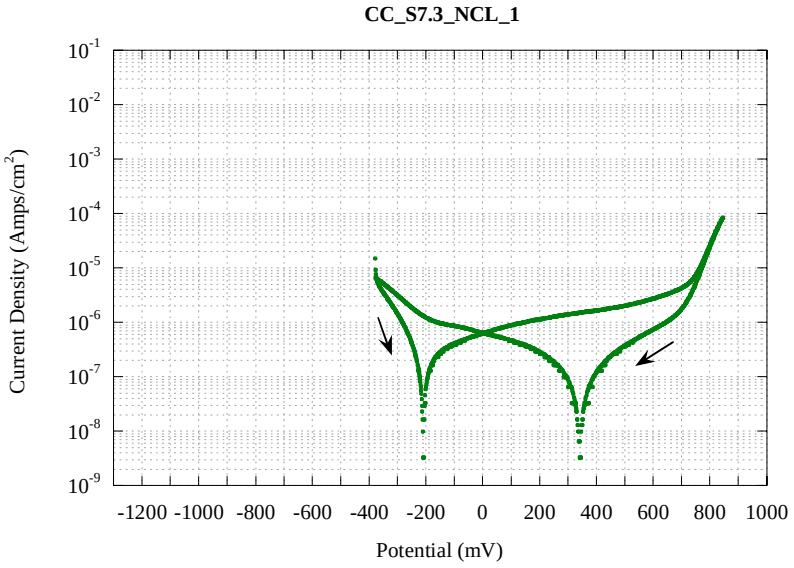

Figure E.46. Cyclic Polarization Test for CC_S7.3_NCL_1.

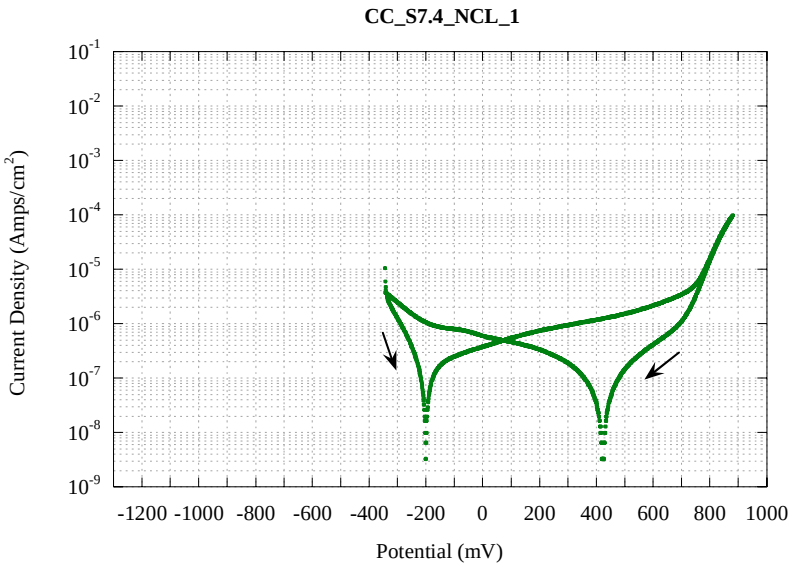

Figure E.47. Cyclic Polarization Test for CC_S7.4_NCL_1.

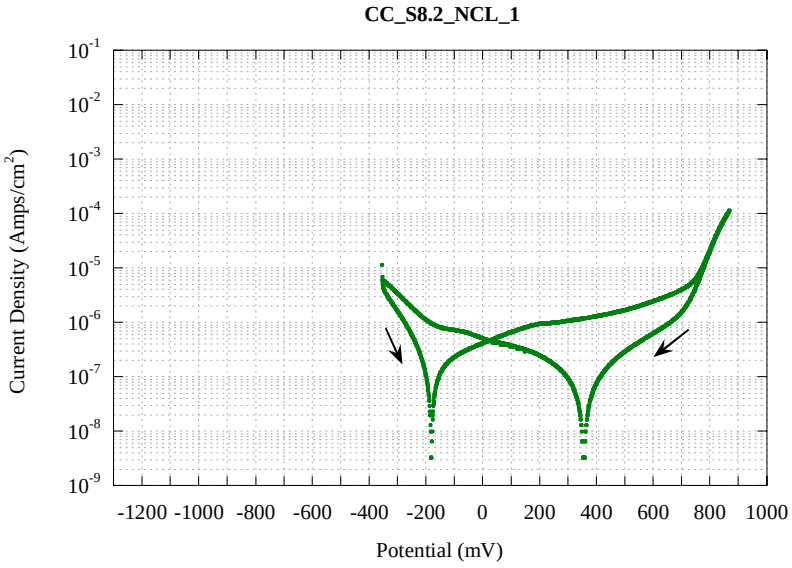

Figure E.48. Cyclic Polarization Test for CC_S8.2_NCL_1.

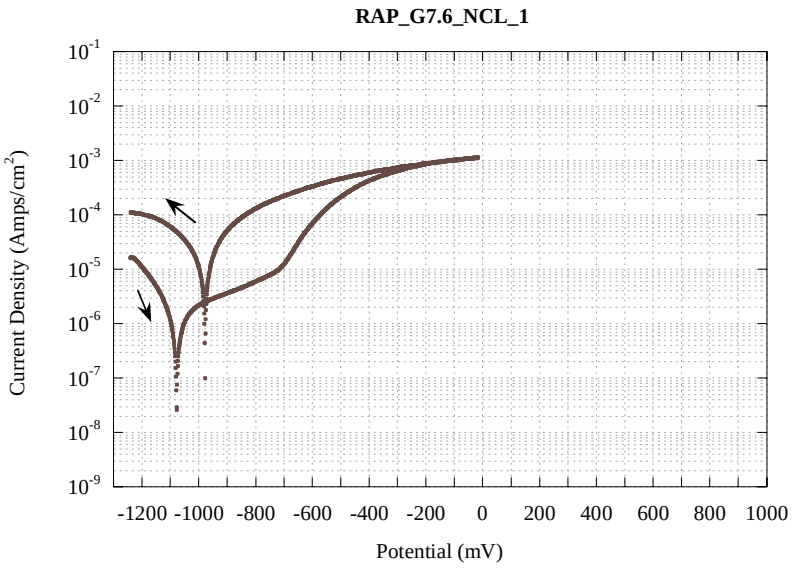

Figure E.49. Cyclic Polarization Test for RAP_G7.6_NCL_1.

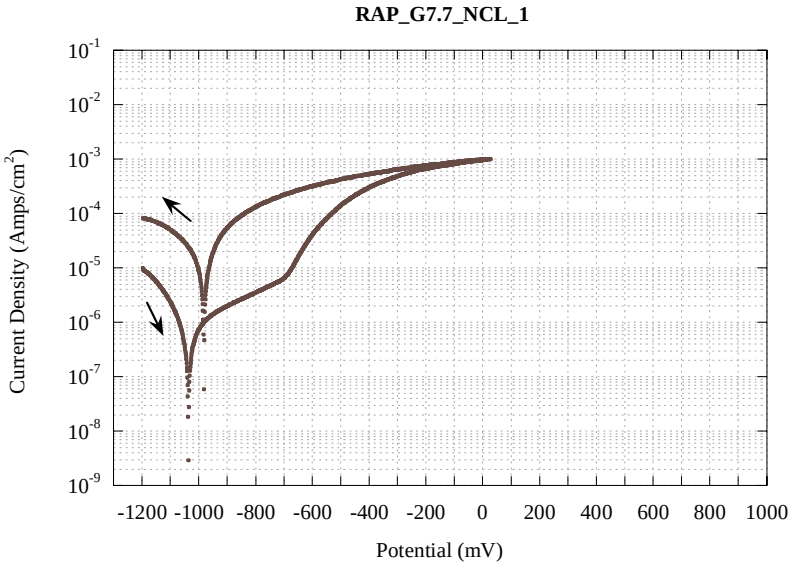

Figue E.50. Cyclic Polarization Test for RAP_G7.7_NCL_1.

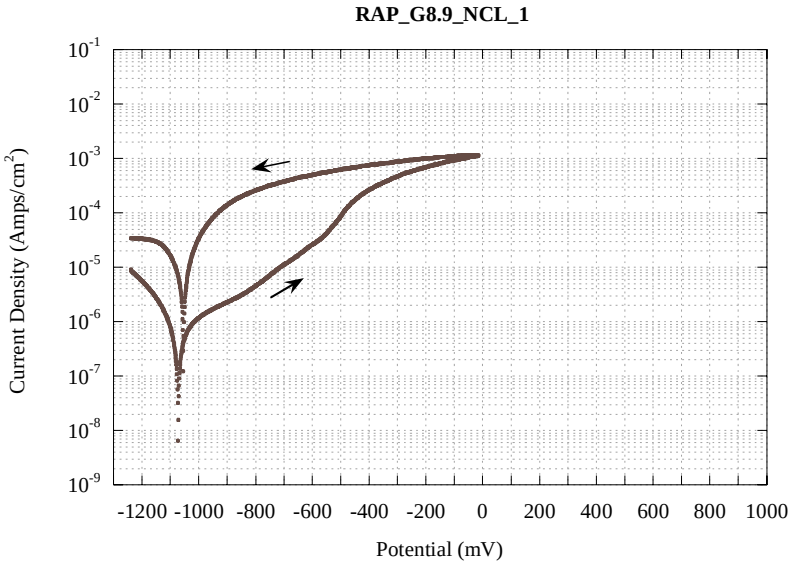

Figure E.51. Cyclic Polarization Test for RAP_G8.9_NCL_1.

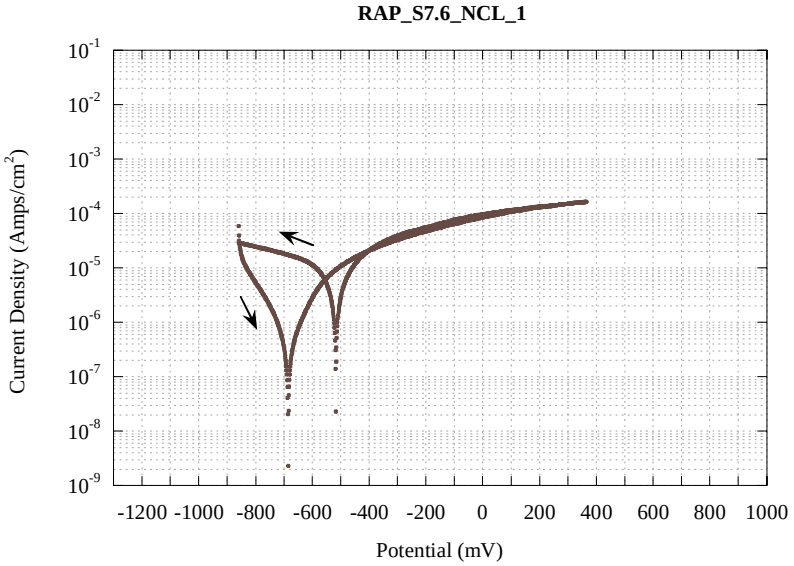

Figure E.52. Cyclic Polarization Test for RAP_S7.6_NCL_1.

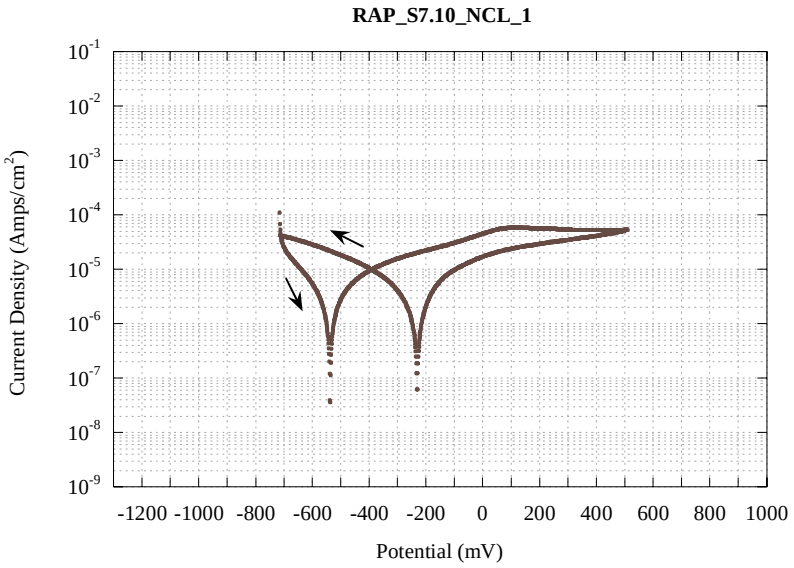

Figure E.53. Cyclic Polarization Test for RAP_S7.10_NCL_1.

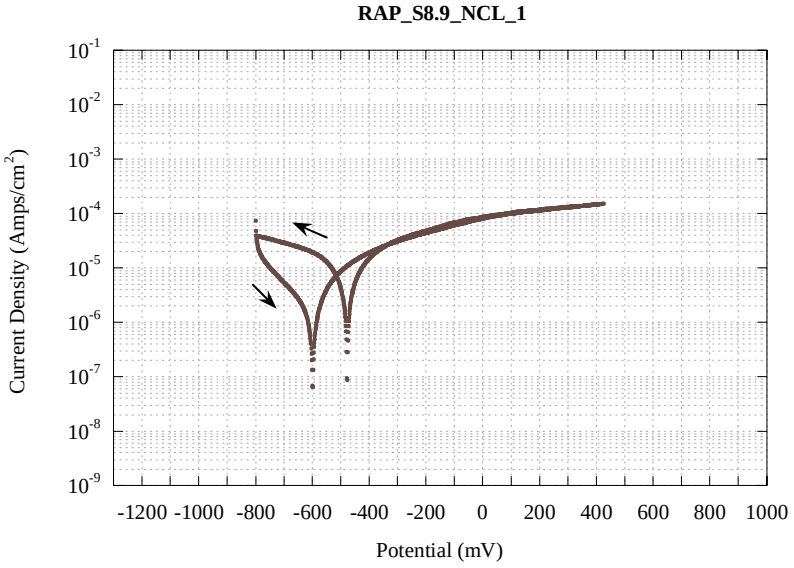

Figure E.54. Cyclic Polarization Test for RAP_S8.9_NCL_1.

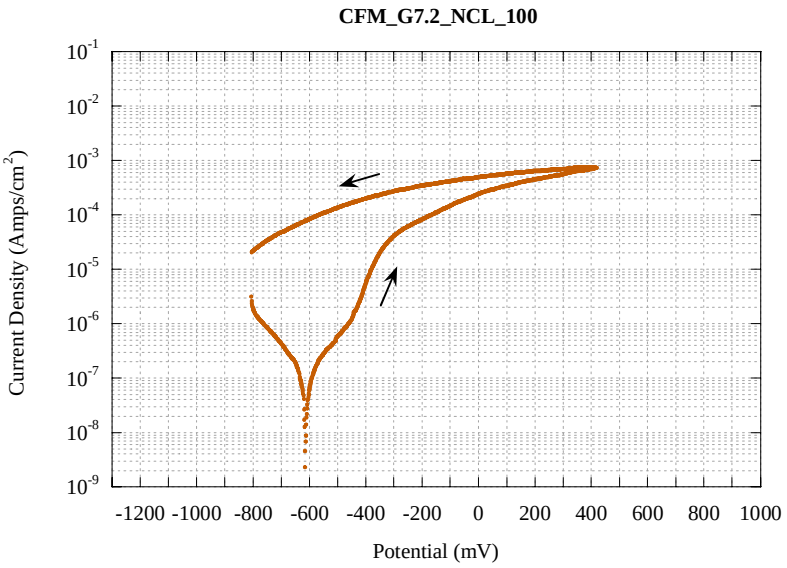

Figure E.55. Cyclic Polarization Test for CFM_G7.2_NCL_100.

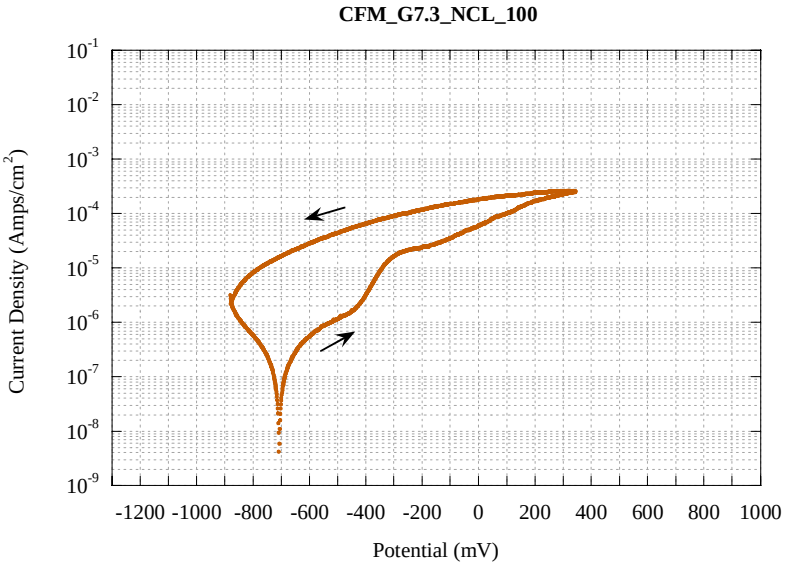

Figure E.56. Cyclic Polarization Test for CFM_G7.3_NCL_100.

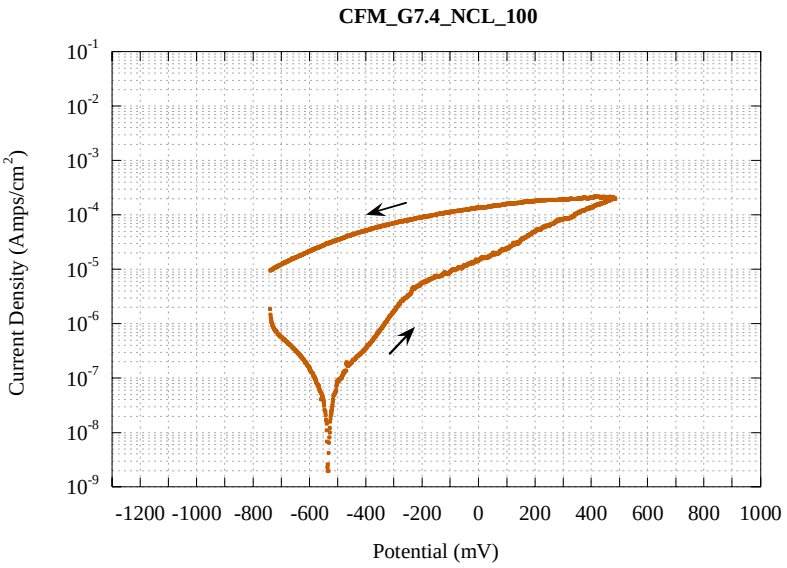

Figure E.57. Cyclic Polarization Test for CFM_G7.4_NCL_100.

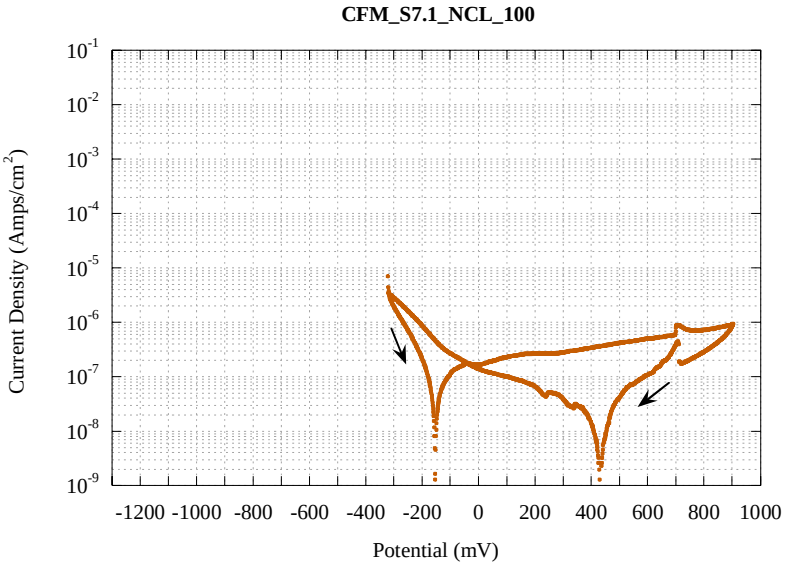

Figure E.58. Cyclic Polarization Test for CFM_S7.1_NCL_100.

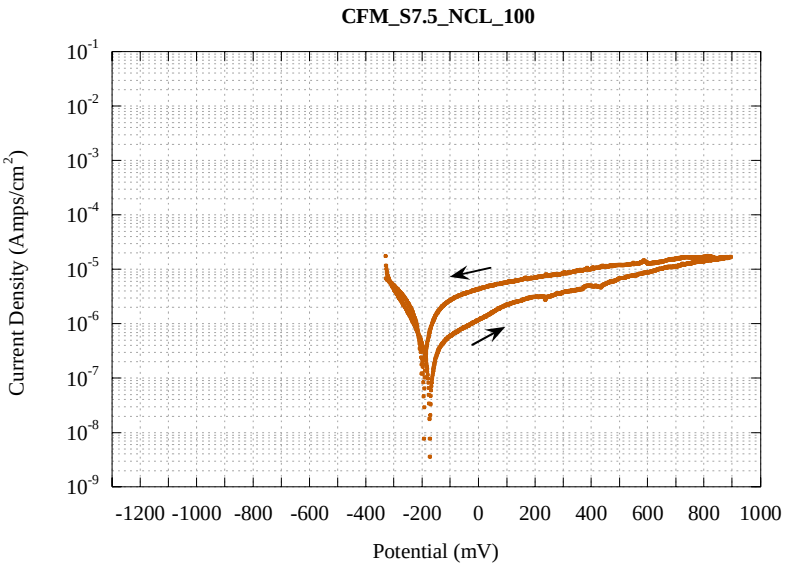

Figure E.59. Cyclic Polarization Test for CFM_S7.5_NCL_100.

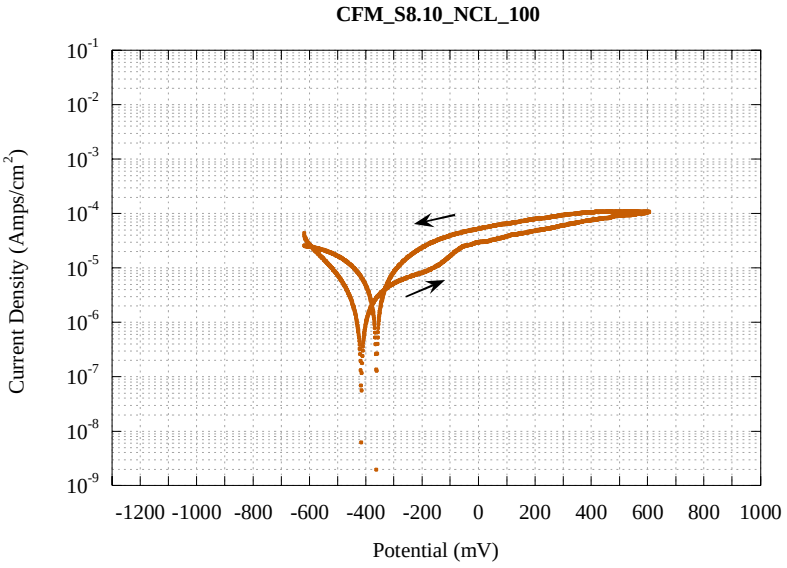

Figure E.60. Cyclic Polarization Test for CFM_S8.10_NCL_100.

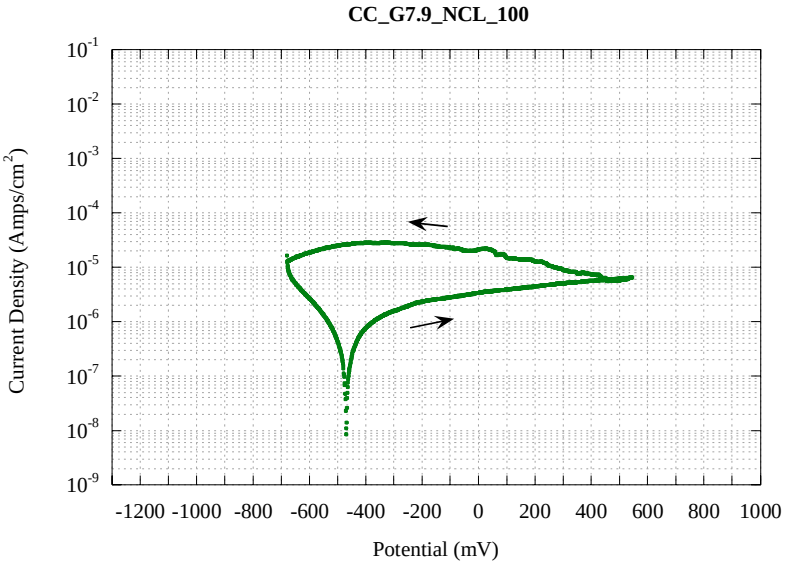

Figure E.61. Cyclic Polarization Test for CC_G7.9_NCL_100.

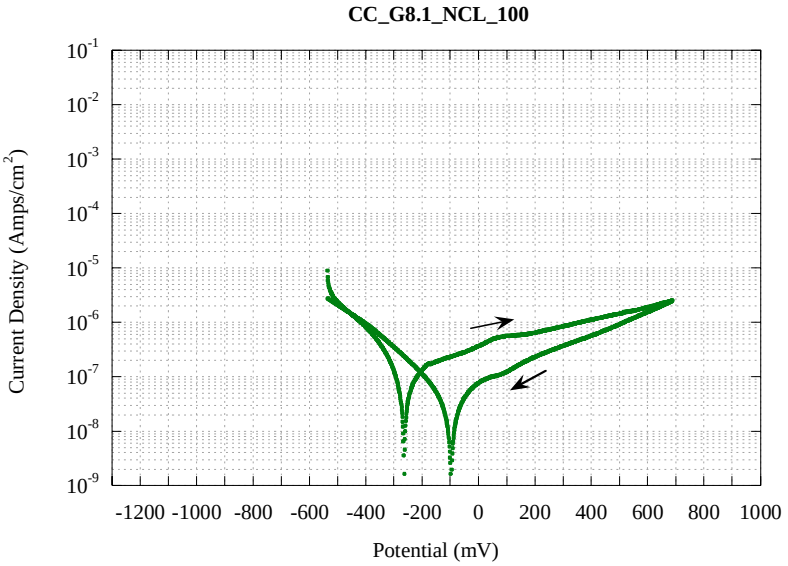

Figure E.62. Cyclic Polarization Test for CC_G8.1_NCL_100.

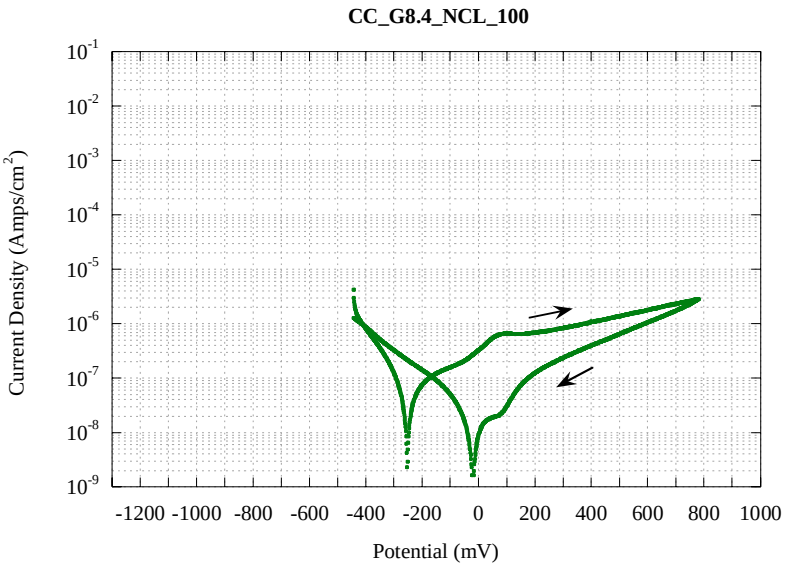

Figure E.63. Cyclic Polarization Test for CC_G8.4_NCL_100.

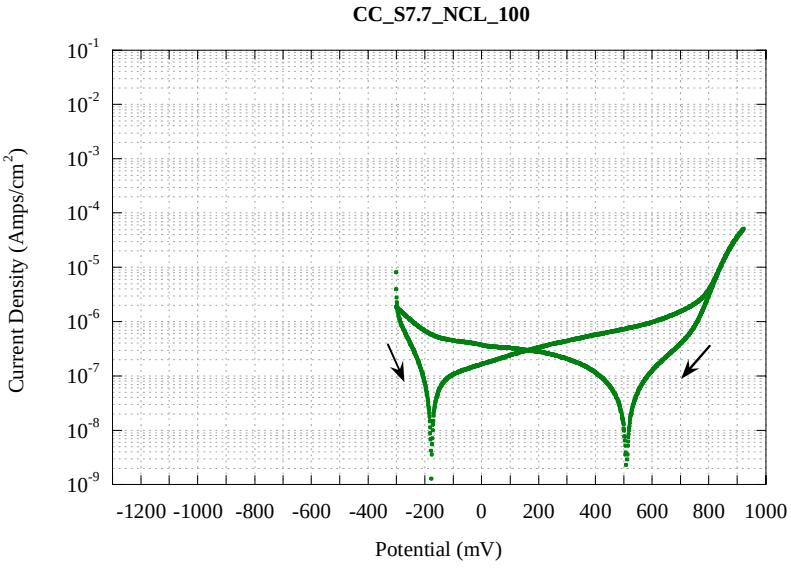

Figure E.64. Cyclic Polarization Test for CC_S7.7_NCL_100.

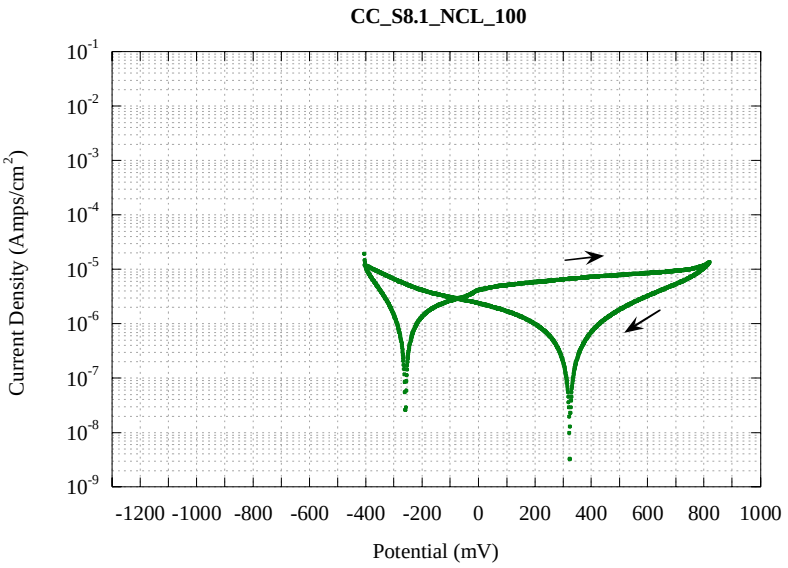

Figure E.65. Cyclic Polarization Test for CC_S8.1_NCL_100.

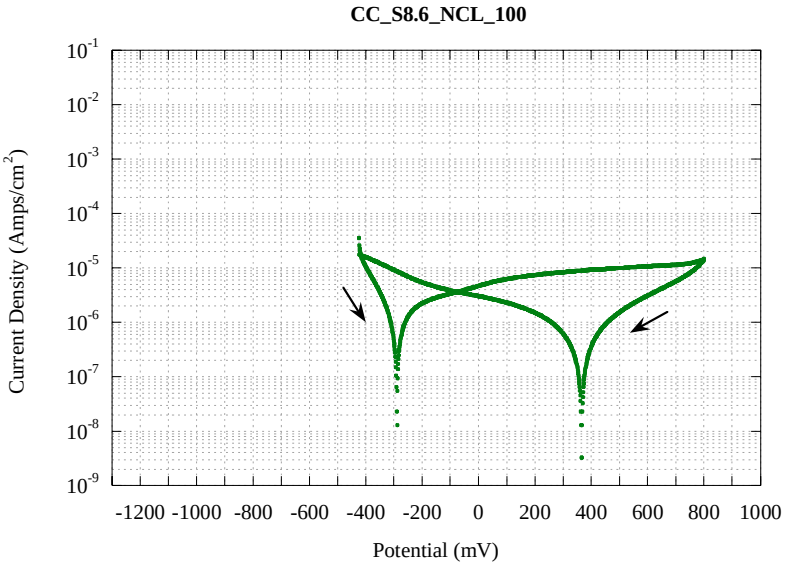

Figure E.66. Cyclic Polarization Test for CC_S8.6_NCL_100.

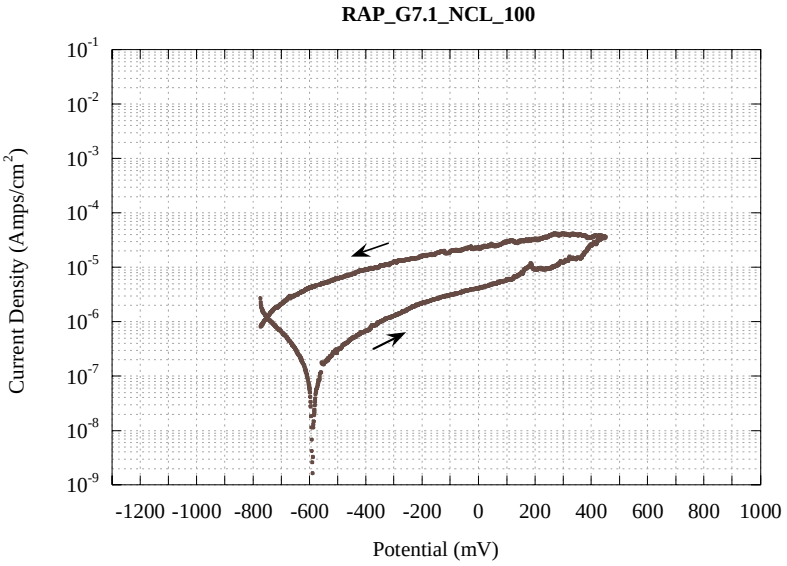

Figure E.67. Cyclic Polarization Test for RAP_G7.1_NCL_100.

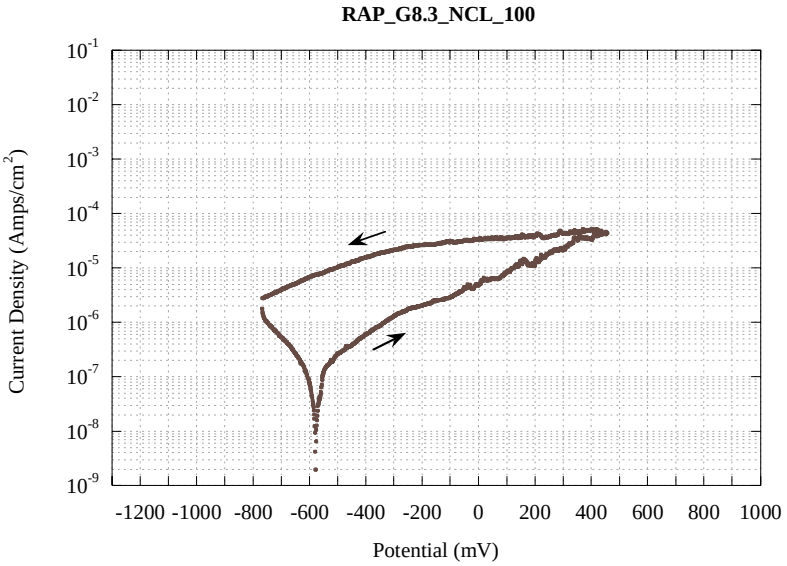

Figue E.68. Cyclic Polarization Test for RAP_G8.3_NCL_100.

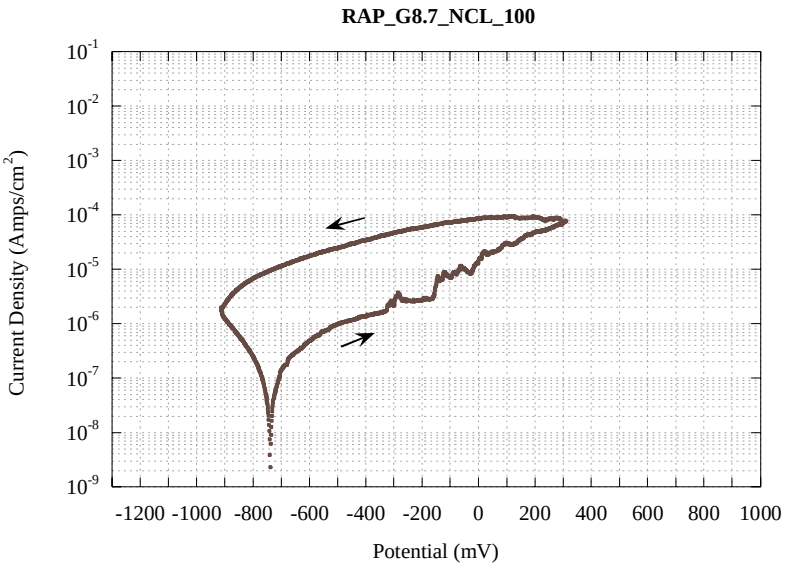

Figure E.69. Cyclic Polarization Test for RAP_G8.7_NCL_100.

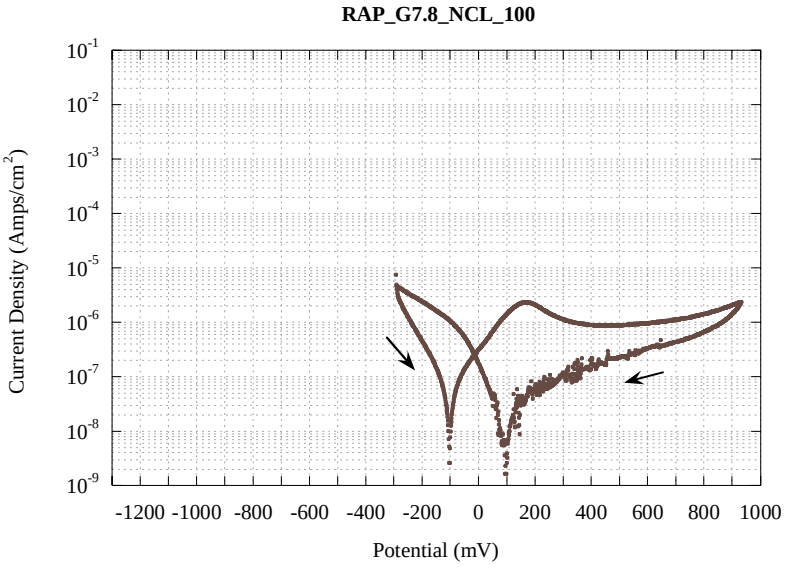

Figure E.70. Cyclic Polarization Test for RAP_G7.8_NCL_100.

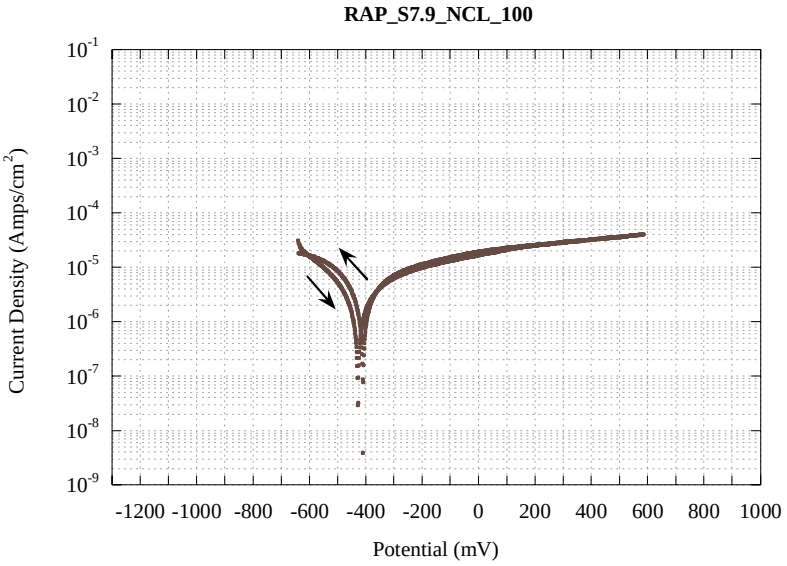

Figure E.71. Cyclic Polarization Test for RAP_S7.9_NCL_100.

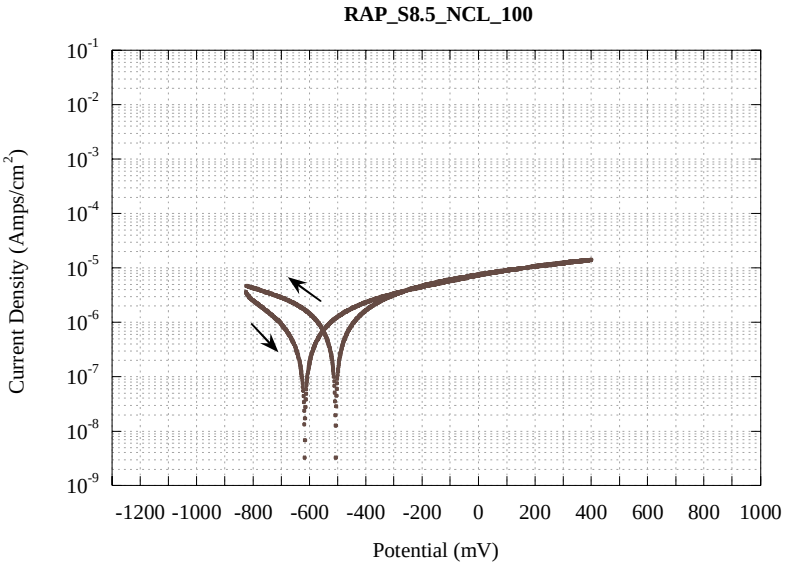

Figure E.72. Cyclic Polarization Test for RAP_S8.5_NCL_100.

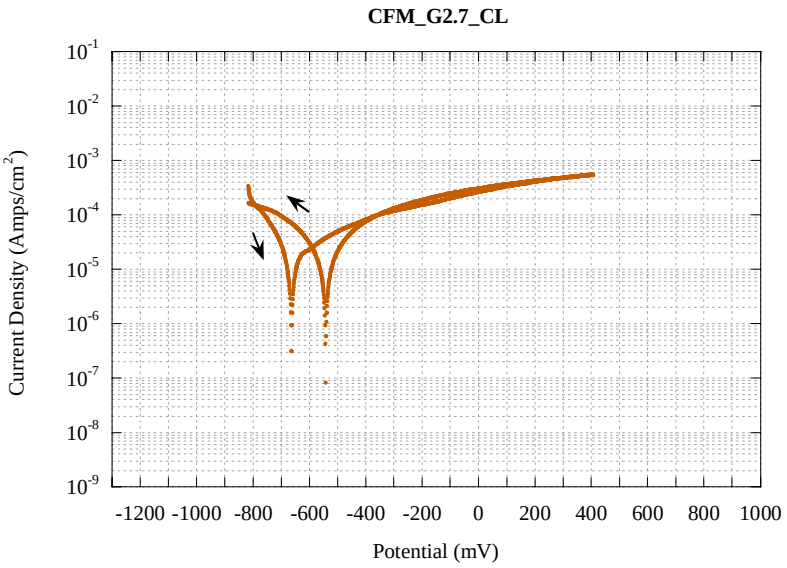

Figure E.73. Cyclic Polarization Test for CFM_G2.7_CL.

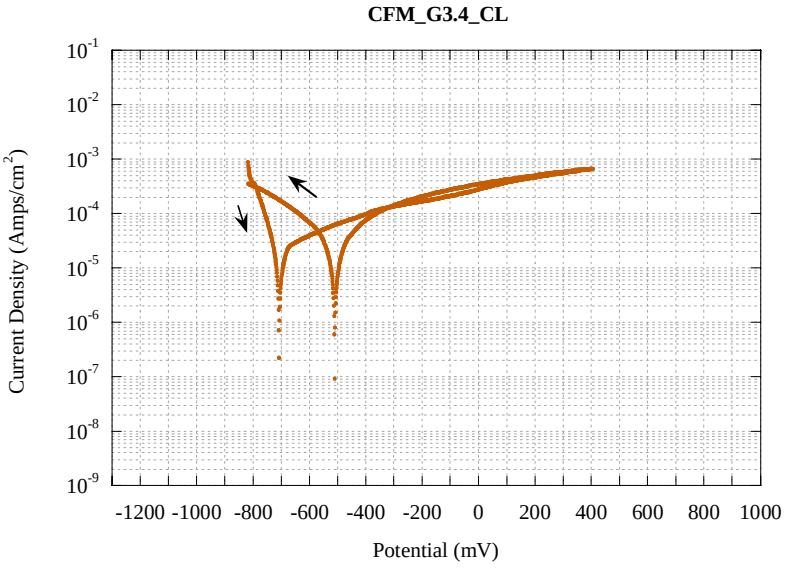

Figure E.74. Cyclic Polarization Test for CFM_G3.4_CL.

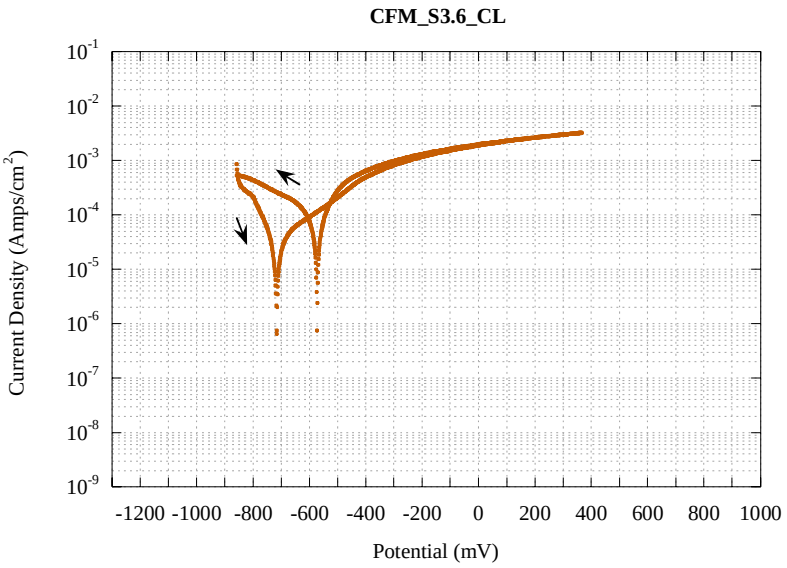

Figure E.75. Cyclic Polarization Test for CFM_S3.6_CL.

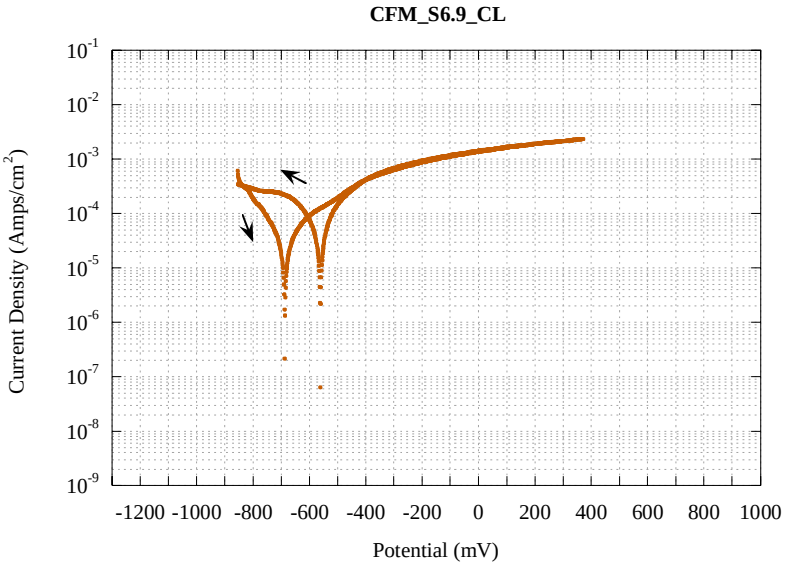

Figure E.76. Cyclic Polarization Test for CFM_S6.9_CL.

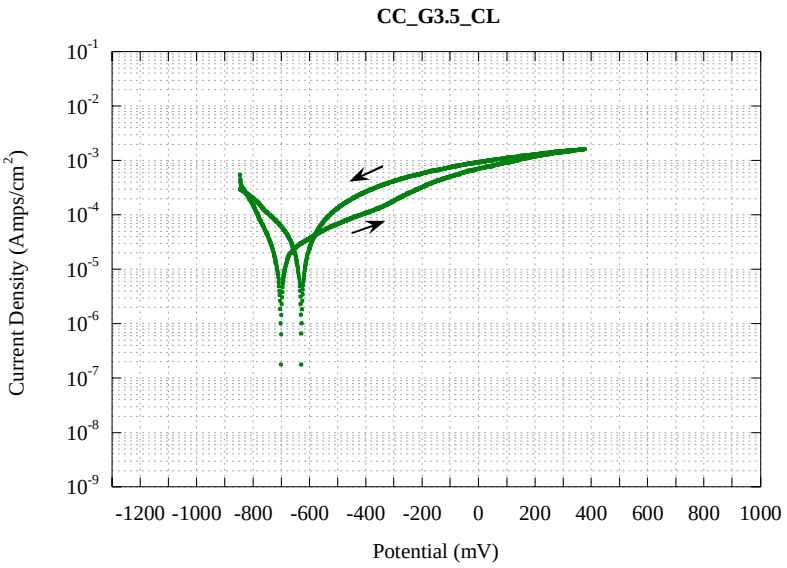

Figure E.77. Cyclic Polarization Test for CC_G3.5_CL.

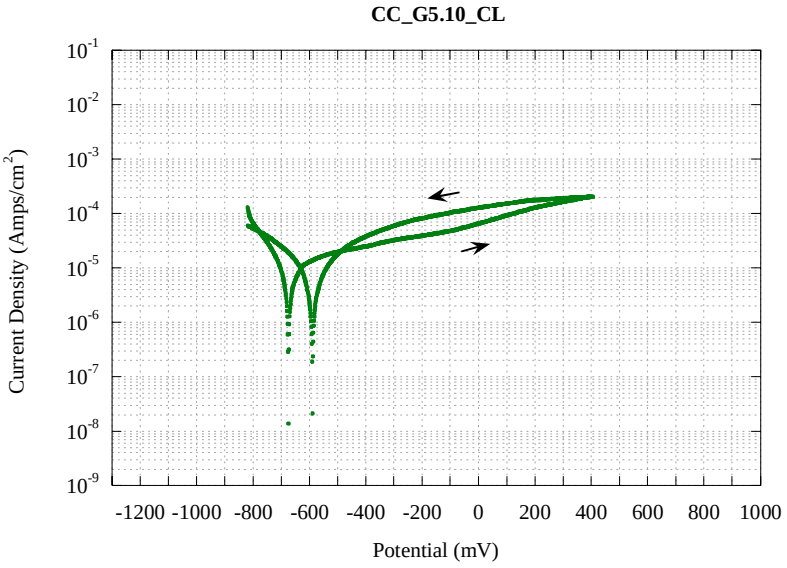

Figure E.78. Cyclic Polarization Test for CC_G5.10_CL.

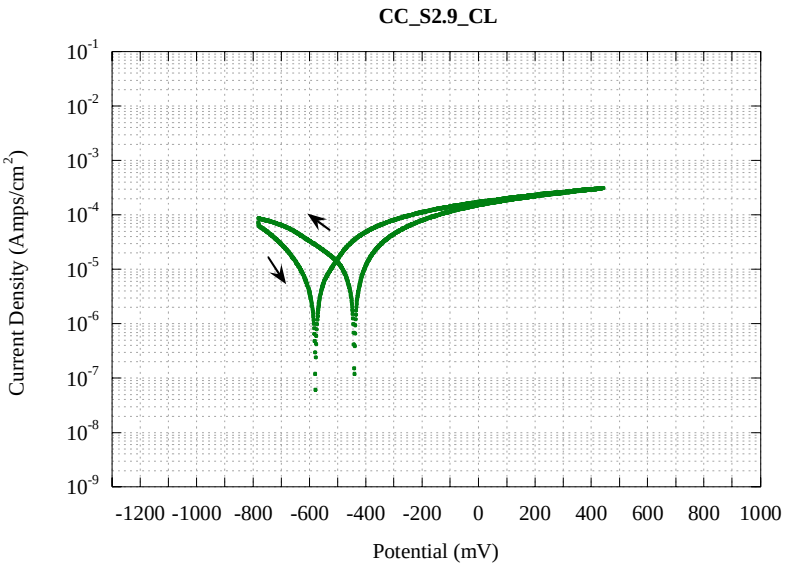

Figure E.79. Cyclic Polarization Test for CC_S2.9_CL.

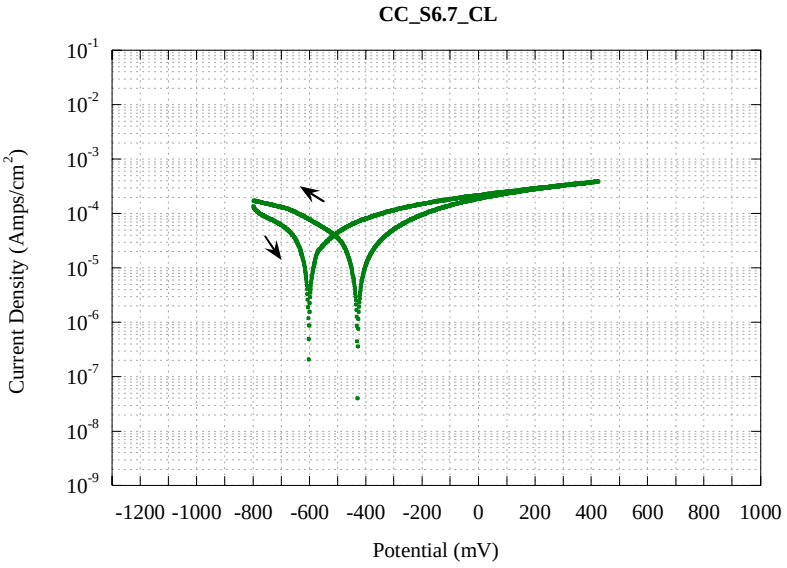

Figure E.80. Cyclic Polarization Test for CC_S6.7_CL.

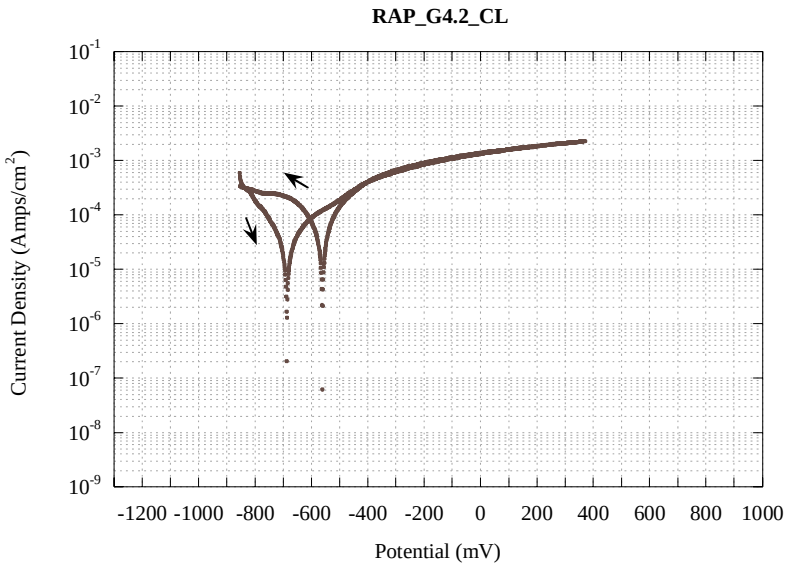

Figure E.81. Cyclic Polarization Test for RAP_G4.2_CL.

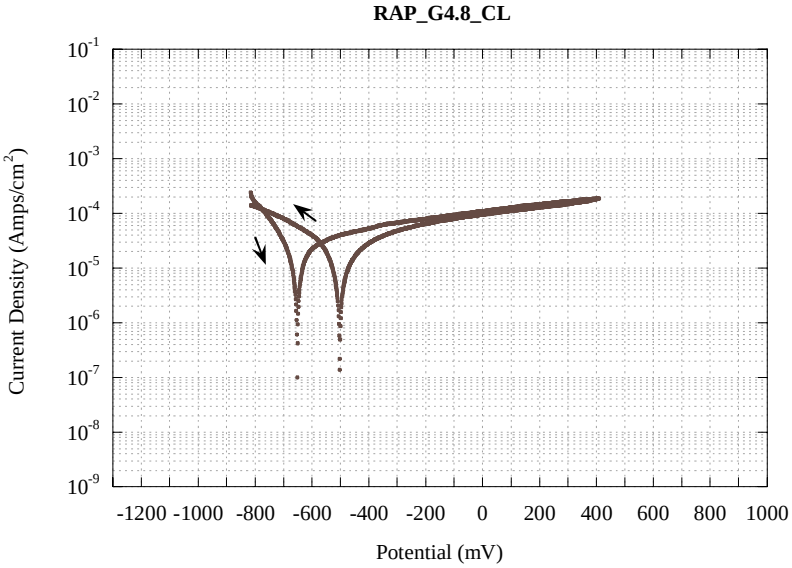

Figure E.82. Cyclic Polarization Test for RAP_G4.8_CL.

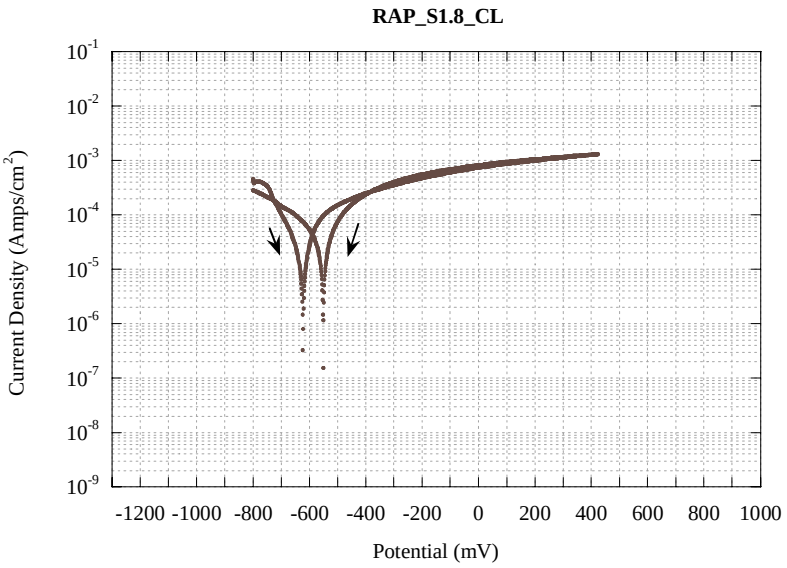

Figure E.83. Cyclic Polarization Test for RAP_S1.8_CL.

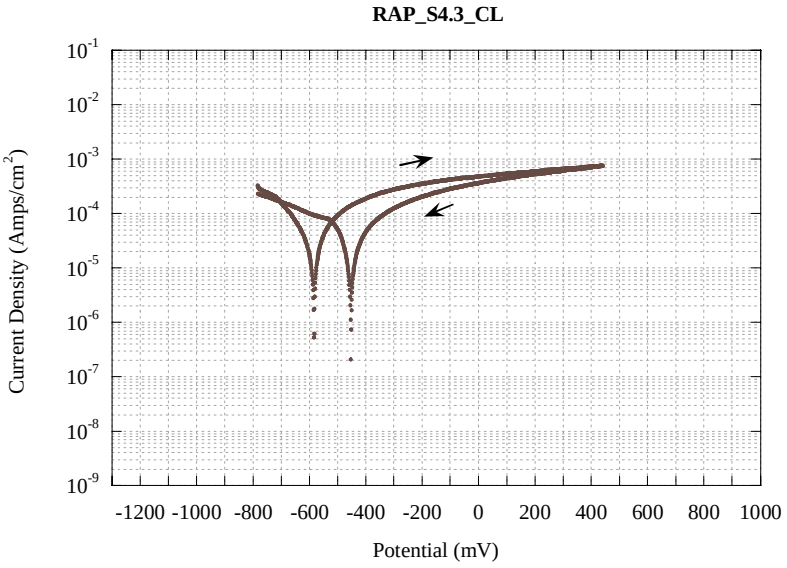

Figure E.84. Cyclic Polarization Test for RAP_S4.3_CL.

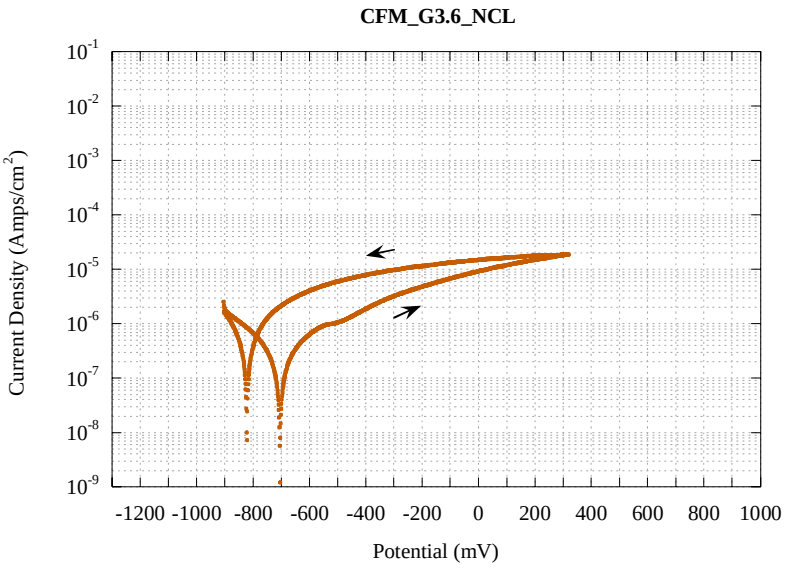

Figure E.85. Cyclic Polarization Test for CFM_G3.6_NCL.

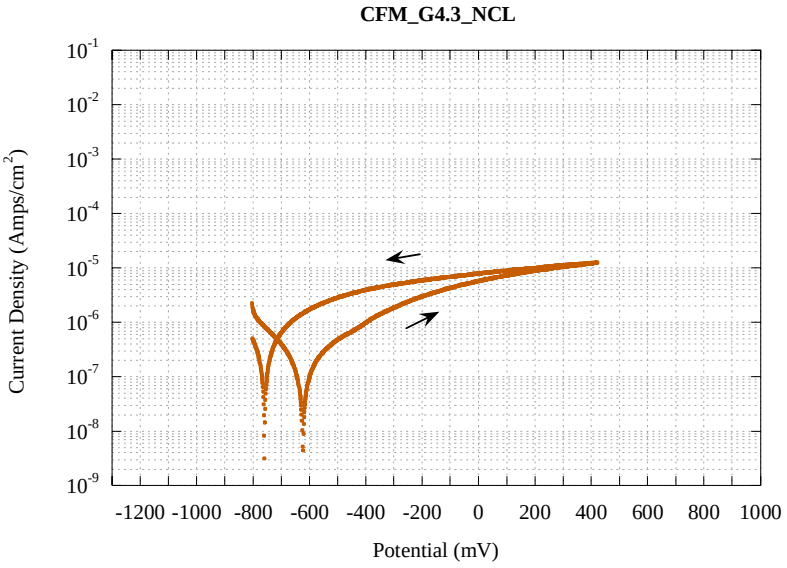

Figue E.86. Cyclic Polarization Test for CFM_G4.3_NCL.

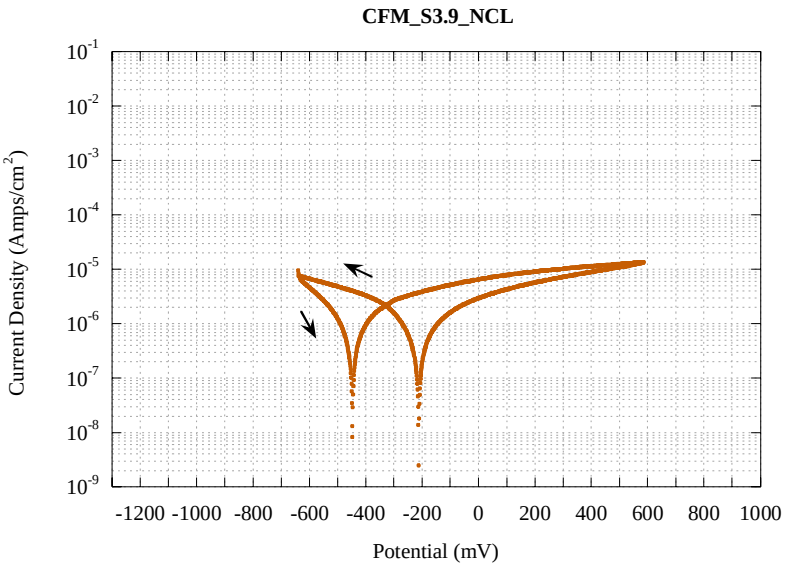

Figure E.87. Cyclic Polarization Test for CFM_S3.9_NCL.

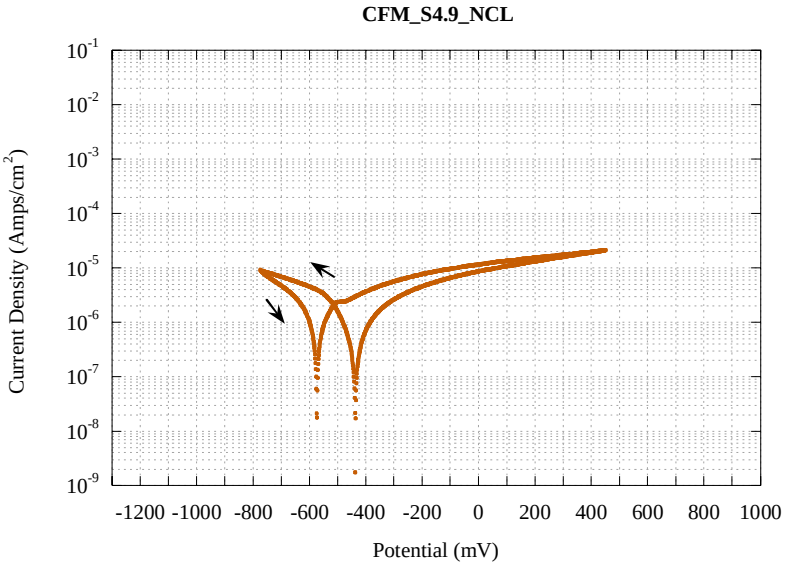

Figure E.88. Cyclic Polarization Test for CFM_S4.9_NCL.

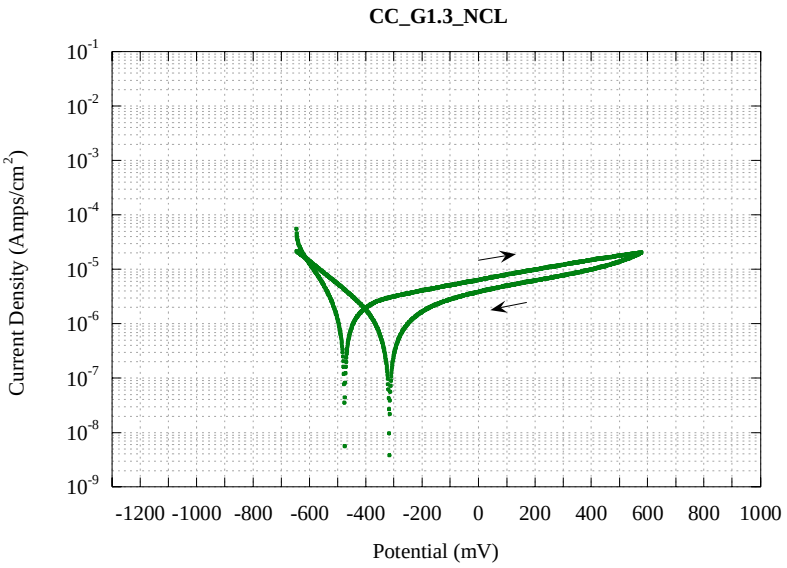

Figure E.89. Cyclic Polarization Test for CC_G1.3_NCL.

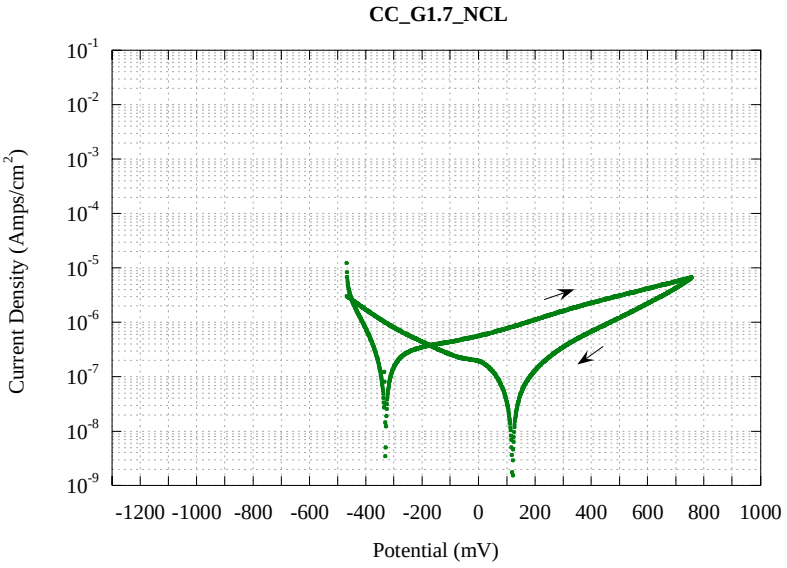

Figure E.90. Cyclic Polarization Test for CC_G1.7_NCL.

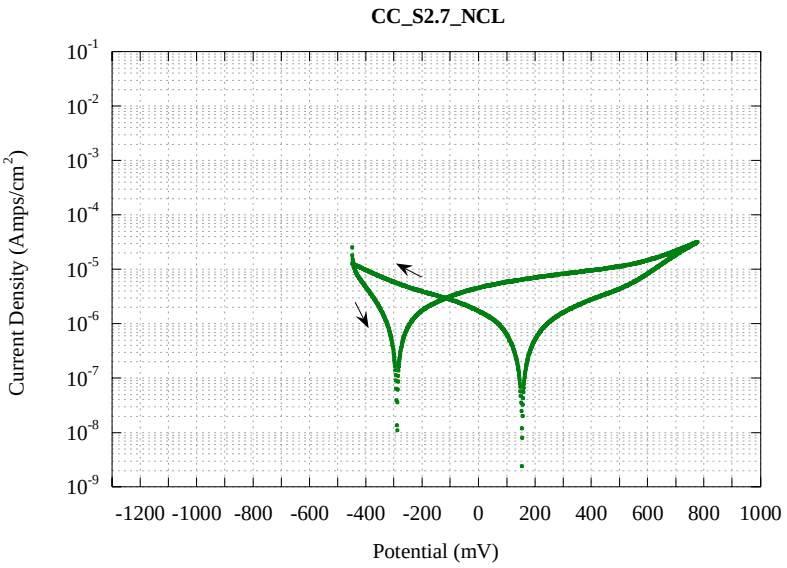

Figure E.91. Cyclic Polarization Test for CC_S2.7_NCL.

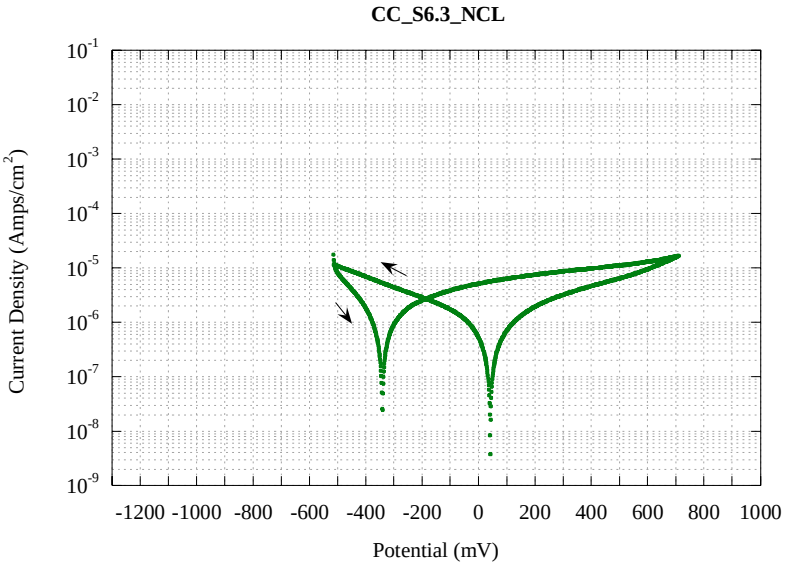

Figure E.92. Cyclic Polarization Test for CC_S6.3_NCL.

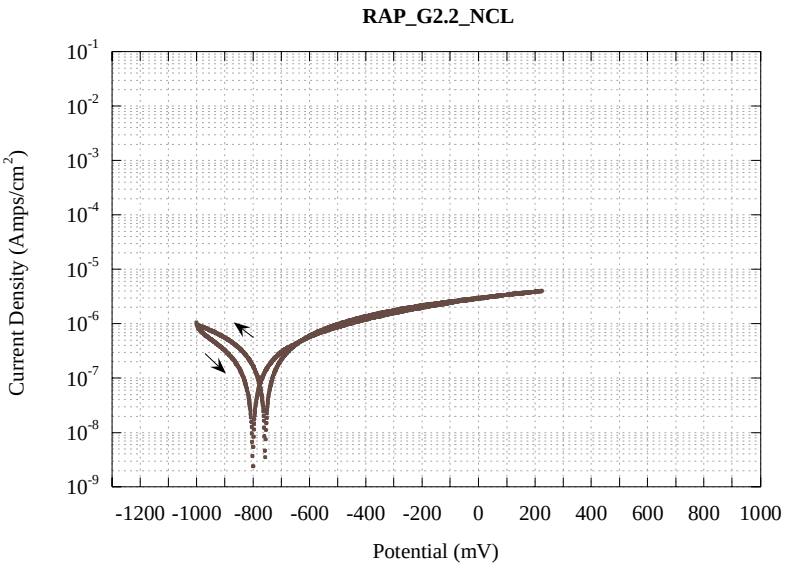

Figure E.93. Cyclic Polarization Test for RAP_G2.2_NCL.

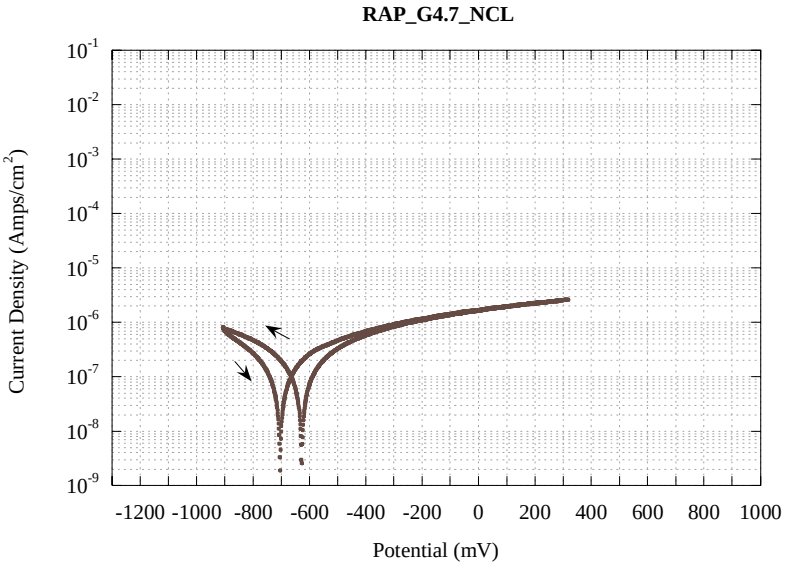

Figure E.94. Cyclic Polarization Test for RAP_G4.7_NCL.

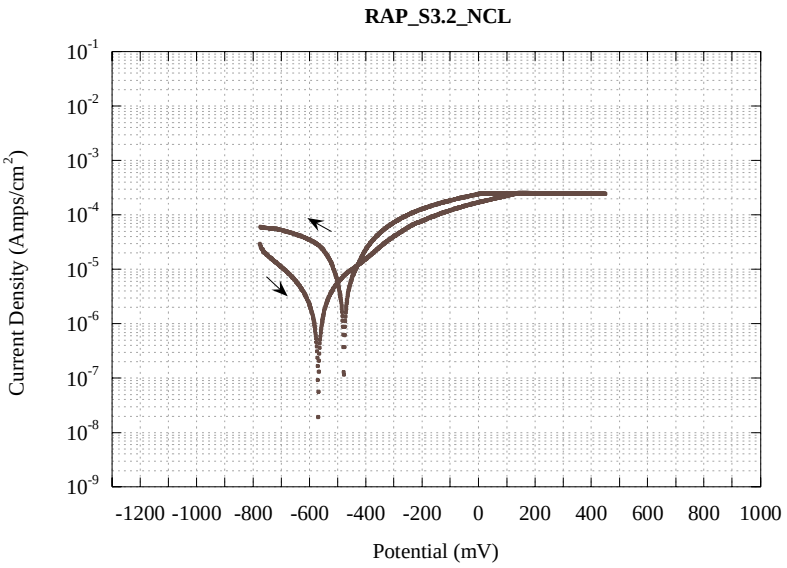

Figure E.95. Cyclic Polarization Test for RAP_S3.2_NCL.

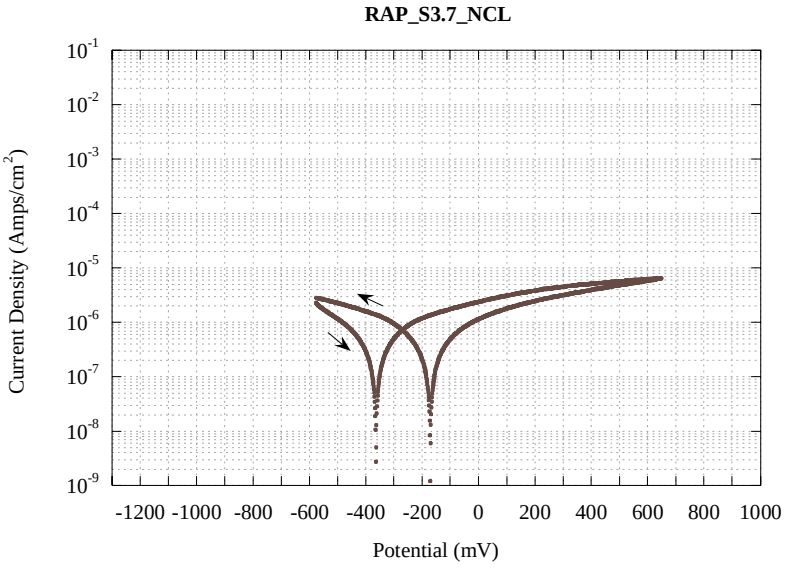

Figure E.96. Cyclic Polarization Test for RAP_S3.7_NCL.

APPENDIX F

CYCLIC POLARIZATION DATA INTERPRETATION

Table F.1. Measured and Interpreted Values from Cyclic Polarization Resistance Testing for STT Samples.

Description of Measurement or Interpreted Value	CFM_G8.2_CL_1	CFM_G9.7_CL_1	CFM_G10.9_CL_1	CC_G9.1_CL_1	CC_G9.2_CL_1	CC_G10.2_CL_1
Corr Rate (mpy)	10.0	23.2	30.7	6.4	5.6	1.06
E (I=0) (mV)	-943.7	-1007	-1033	-1073	-1061	-1101
Ba (mV/decade)	264	303	457	84	226	188
Bc (mV/decade)	224	204	281	121	102	68
B, Tafel Const.	121	122	174	50	70	50
Stern-Geary	52.6	52.9	75.6	21.5	30.5	21.7
Hysteresis (decade)	1.5	1.2	1.8	1.8	2	2.6
OCP, SCE (mV)	-921	-972	-996	-1007	-960	-989
Epp (mV)	-858	-900	-969	-1030	-1000	-1013
Eb (mV)	-685	-704	-760	-672	-777	-813
Erp (mV)	-966	-981	-1004	-1015	-1062	-1071
Graph OCP (mV)	-942	-1004	-1031	-1073	-1062	-1098
Type (1,2,or 3)*	2	2	2	2	2	2
PasRegWidth (mV)	173	196	209	358	223	200
OCP-Erp (mV)	45	9	8	8	102	82
Pits Initiate?	Y	Y	Y	Y	Y	Y
Pits Grow?	Y	Y	Y	Y	Y	Y
GrphOCP-OCP (mV)	-21	-32	-35	-66	-102	-109
GrphOCP-Erp (mV)	24	-23	-27	-58	0	-27
Calc Pit Rate?	Y	N	N	N	N	N
Epp-OCP (mV)	63	72	27	-23	-40	-24
Eb-OCP (mV)	236	268	236	335	183	176
Active?	N	N	N	Y	Y	Y
Transpassive?	N	N	N	N	N	N
Epp-GrphOCP (mV)	84	104	62	43	62	85
Eb-GrphOCP (mV)	257	300	271	401	285	285
Gen&PitCorr?	N	N	N	N	N	N
Ipit (Amps/cm2)	2.5E-5					
MPYpit Galv. (mpy)	295					
MPYpit Steel (mpy)	229					

* Types: 1 - passive, 2 - psedo-passive, 3 - active

Table F.1. CONTINUED.

Description of Measurement or Interpreted Value	RAP_G9.8_CL_1	RAP_G9.9_CL_1	RAP_G10.1_CL_1	CFM_G9.6_CL_100	CFM_G10.4_CL_100	CFM_G10.7_CL_100
Corr Rate (mpy)	26.1	26.6	51.1	11.3	14.0	31.2
E (I=0) (mV)	-1084	-1006	-1040	-1122	-1109	-1107
Ba (mV/decade)	466	402	487	149	202	200
Bc (mV/decade)	195	212	190	147	175	208
B, Tafel Const.	137	139	137	74	94	102
Stern-Geary	59.7	60.3	59.3	32.1	40.7	44.3
Hysteresis (decade)	1.6	1.6	1.6	1.4	1.8	1.8
OCP, SCE (mV)	-1016	-970	-995	-1053	-1046	-1055
Epp (mV)	-1014	-917	-951	-1061	-1019	-1043
Eb (mV)	-891	-717	-693	-910	-787	-848
Erp (mV)	-995	-972	-1000	-1024	-1028	-1043
Graph OCP (mV)	-1085	-1003	-1040	-1123	-1109	-1109
Type (1,2,or 3)*	2	2	2	2	2	2
PasRegWidth (mV)	123	200	258	151	232	195
OCP-Erp (mV)	-21	2	5	-29	-18	-12
Pits Initiate?	Y	Y	Y	Y	Y	Y
Pits Grow?	N	Y	Y	N	N	N
GrphOCP-OCP (mV)	-69	-33	-45	-70	-63	-54
GrphOCP-Erp (mV)	-90	-31	-40	-99	-81	-66
Calc Pit Rate?	N	N	N	N	N	N
Epp-OCP (mV)	2	53	44	-8	27	12
Eb-OCP (mV)	125	253	302	143	259	207
Active?	N	N	N	Y	N	N
Transpassive?	N	N	N	N	N	N
Epp-GrphOCP (mV)	71	86	89	62	90	66
Eb-GrphOCP (mV)	194	286	347	213	322	261
Gen&PitCorr?	N	N	N	N	N	N
Ipit (Amps/cm2)						
MPYpit Galv. (mpy)						
MPYpit Steel (mpy)						

* Types: 1 - passive, 2 - psedo-passive, 3 - active

Table F.1. CONTINUED.

Description of Measurement or Interpreted Value	CC_G9.3_CL_100	CC_G9.4_CL_100	CC_G9.5_CL_100	RAP_G9.10_CL_100	RAP_G10.3_CL_100	RAP_G10.8_CL_100
Corr Rate (mpy)	4.86	8.97	41.7	17.0	17.8	30.7
E (I=0) (mV)	-1093	-1094	-1102	-1091	-1094	-1069
Ba (mV/decade)	215	378	244	278	299	402
Bc (mV/decade)	169	199	155	212	199	244
B, Tafel Const.	95	130	95	120	119	152
Stern-Geary	41.1	56.6	41.2	52.2	51.9	65.9
Hysteresis (decade)	2.6	2.6	1.5	2.1	1.8	1.7
OCP, SCE (mV)	-1055	-1052	-1057	-1039	-1040	-1026
Epp (mV)	-1023	-995	-986	-1014	-1019	-971
Eb (mV)	-891	-725	-886	-753	-772	-711
Erp (mV)	-1023	-1014	-1000	-1014	-1019	-1033
Graph OCP (mV)	-1089	-1094	-1099	-1090	-1095	-1066
Type (1,2,or 3)*	2	2	1	2	2	2
PasRegWidth (mV)	132	270	100	261	247	260
OCP-Erp (mV)	-32	-38	-57	-25	-21	7
Pits Initiate?	Y	Y	Y	Y	Y	Y
Pits Grow?	N	N	N	N	N	Y
GrphOCP-OCP (mV)	-34	-42	-42	-51	-55	-40
GrphOCP-Erp (mV)	-66	-80	-99	-76	-76	-33
Calc Pit Rate?	N	N	N	N	N	N
Epp-OCP (mV)	32	57	71	25	21	55
Eb-OCP (mV)	164	327	171	286	268	315
Active?	N	N	N	N	N	N
Transpassive?	N	N	N	N	N	N
Epp-GrphOCP (mV)	66	99	113	76	76	95
Eb-GrphOCP (mV)	198	369	213	337	323	355
Gen&PitCorr?	N	N	N	N	N	N
Ipit (Amps/cm2)						
MPYpit Galv. (mpy)						
MPYpit Steel (mpy)						

* Types: 1 - passive, 2 - psedo-passive, 3 - active

Table F.1. CONTINUED.

Description of Measurement or Interpreted Value	CFM_G7.8_NCL_1	CFM_G8.6_NCL_1	CFM_G8.10_NCL_1	CC_G7.5_NCL_1	CC_G7.10_NCL_1	CC_G8.8_NCL_1
Corr Rate (mpy)	0.136	0.316	0.126	0.624	0.769	0.660
E (I=0) (mV)	-702.9	-671.2	-665.1	-352.9	-432.1	-396.9
Ba (mV/decade)	181	420	240	946	443	949
Bc (mV/decade)	129	174	169	109	117	114
B, Tafel Const.	75	123	99	98	93	102
Stern-Geary	32.7	53.4	43.1	42.4	40.2	44.2
Hysteresis (decade)	2.7			-0.8	-0.8	-0.8
OCP, SCE (mV)	-632	-600	-603	-256	-357	-297
Epp (mV)	-671	-607	-586	-350	-432	-396
Eb (mV)	-471	-389	-403	-350	-432	-396
Erp (mV)				118	-146	23
Graph OCP (mV)	-702	-670	-668	-350	-432	-396
Type (1,2,or 3)*	2	2	2	3	3	3
PasRegWidth (mV)	200	218	183	0	0	0
OCP-Erp (mV)	N/A	N/A	-603	-374	-211	-320
Pits Initiate?	Y	Y	Y	N	N	N
Pits Grow?	Y	Y	N	N	N	N
GrphOCP-OCP (mV)	-70	-70	-65	-94	-75	-99
GrphOCP-Erp (mV)	N/A	N/A	-668	-468	-286	-419
Calc Pit Rate?	Y	Y	Y	N	N	N
Epp-OCP (mV)	-39	-7	17	-94	-75	-99
Eb-OCP (mV)	161	211	200	-94	-75	-99
Active?	Y	Y	N	Y	Y	Y
Transpassive?	N	N	N	Y	Y	Y
Epp-GrphOCP (mV)	31	63	82	0	0	0
Eb-GrphOCP (mV)	231	281	265	0	0	0
Gen&PitCorr?	N	N	N	Y	Y	Y
Ipit (Amps/cm2)						
MPYpit Galv. (mpy)						
MPYpit Steel (mpy)						

* Types: 1 - passive, 2 - psedo-passive, 3 - active

Table F.1. CONTINUED.

Description of Measurement or Interpreted Value	RAP_G7.6_NCL_1	RAP_G7.7_NCL_1	RAP_G8.9_NCL_1	CFM_G7.2_NCL_100	CFM_G7.3_NCL_100	CFM_G7.4_NCL_100
Corr Rate (mpy)	1.072	0.651	0.559	0.0898	0.1799	0.0463
E (I=0) (mV)	-1078	-1036	-1073	-613.5	-707.2	-533.2
Ba (mV/decade)	497	443	383	172	340	183
Bc (mV/decade)	143	150	154	176	226	185
B, Tafel Const.	111	112	110	87	136	92
Stern-Geary	48.2	48.7	47.7	37.8	58.9	39.9
Hysteresis (decade)	1.3	1.6	1.7	2.2	1.3	2.2
OCP, SCE (mV)	-1017	-973	-1015	-582	-656	-515
Epp (mV)	-1001	-962	-1020	-570	-600	-480
Eb (mV)	-703	-685	-547	-439	-427	-384
Erp (mV)	-977	-977	-1053			
Graph OCP (mV)	-1076	-1035	-1067	-616	-710	-533
Type (1,2,or 3)*	2	2	2	2	2	2
PasRegWidth (mV)	298	277	473	131	173	96
OCP-Erp (mV)	-40	4	38	N/A	N/A	N/A
Pits Initiate?	Y	Y	Y	Y	Y	Y
Pits Grow?	N	Y	Y	Y	Y	Y
GrphOCP-OCP (mV)	-59	-62	-52	-34	-54	-18
GrphOCP-Erp (mV)	-99	-58	-14	N/A	N/A	N/A
Calc Pit Rate?	N	N	N	Y	Y	Y
Epp-OCP (mV)	16	11	-5	12	56	35
Eb-OCP (mV)	314	288	468	143	229	131
Active?	N	N	Y	N	N	N
Transpassive?	N	N	N	N	N	N
Epp-GrphOCP (mV)	75	73	47	46	110	53
Eb-GrphOCP (mV)	373	350	520	177	283	149
Gen&PitCorr?	N	N	N	N	N	N
Ipit (Amps/cm2)					7.60E-05	
MPYpit Galv. (mpy)					896	
MPYpit Steel (mpy)					695	

* Types: 1 - passive, 2 - psedo-passive, 3 - active

Table F.1. CONTINUED.

Description of Measurement or Interpreted Value	CC_G7.9_NCL_100	CC_G8.1_NCL_100	CC_G8.4_NCL_100	RAP_G7.1_NCL_100	RAP_G8.3_NCL_100	RAP_G8.7_NCL_100
Corr Rate (mpy)	0.564	0.1103	0.0482	0.1540	0.1228	0.1035
E (I=0) (mV)	-469	-262.9	-252	-588.8	-577.9	-739.2
Ba (mV/decade)	643	843	448	416	355	308
Bc (mV/decade)	236	203	141	224	246	187
B, Tafel Const.	173	164	107	146	145	116
Stern-Geary	75.0	71.0	46.6	63.2	63.1	50.5
Hysteresis (decade)	1.1	-0.7	-1	1	1.5	1.5
OCP, SCE (mV)	-455	-312	-219	-550	-543	-689
Epp (mV)	-471	-229	-186	-464	-510	-620
Eb (mV)	-471	-179	-32	136	82	-168
Erp (mV)		-100	-21			
Graph OCP (mV)	-471	-264	-254	-589	-579	-741
Type (1,2,or 3)*	3	2	2	2	2	2
PasRegWidth (mV)	0	50	154	600	592	452
OCP-Erp (mV)	N/A	-212	-198	N/A	N/A	N/A
Pits Initiate?	Y	N	N	Y	Y	Y
Pits Grow?	Y	N	N	Y	Y	Y
GrphOCP-OCP (mV)	-16	48	-35	-39	-36	-52
GrphOCP-Erp (mV)	N/A	-164	-233	N/A	N/A	N/A
Calc Pit Rate?	Y	N	N	Y	Y	Y
Epp-OCP (mV)	-16	83	33	86	33	69
Eb-OCP (mV)	-16	133	187	686	625	521
Active?	Y	N	N	N	N	N
Transpassive?	Y	N	N	N	N	N
Epp-GrphOCP (mV)	0	35	68	125	69	121
Eb-GrphOCP (mV)	0	85	222	725	661	573
Gen&PitCorr?	Y	Y	N	N	N	N
Ipit (Amps/cm2)	9.5E-4			9.8E-5	8.5E-5	9.2E-5
MPYpit Galv. (mpy)	11196			1155	1002	1084
MPYpit Steel (mpy)	8688			896	777	841

* Types: 1 - passive, 2 - psedo-passive, 3 - active

Table F.1. CONTINUED.

Description of Measurement or Interpreted Value	CFM_S9.4_CL_1	CFM_S10.1_CL_1	CFM_S10.9_CL_1	CC_S9.2_CL_1	CC_S9.8_CL_1	CC_S10.7_CL_1
Corr Rate (mpy)	3.72	4.09	2.18	17.77	19.67	14.39
E (I=0) (mV)	-774	-777.8	-747.7	-747.5	-733.3	-747.1
Ba (mV/decade)	135	168	118	509	723	620
Bc (mV/decade)	97	80	98	102	123	121
B, Tafel Const.	56	54	54	85	105	101
Stern-Geary	24.5	23.5	23.2	36.9	45.6	44.0
Hysteresis (decade)	0.4	0.5	0.5	1.9	1.6	1.8
OCP, SCE (mV)	-691	-668	-669	-635	-628	-645
Epp (mV)	-738	-739	-709	-681	-647	-685
Eb (mV)	-577	-623	-580	-115	-239	-127
Erp (mV)	-631	-623	-631	-619	-623	-612
Graph OCP (mV)	-773	-777	-748	-746	-737	-746
Type (1,2,or 3)*	2	2	2	2	2	2
PasRegWidth (mV)	161	116	129	566	408	558
OCP-Erp (mV)	-60	-45	-38	-16	-5	-33
Pits Initiate?	Y	Y	Y	Y	Y	Y
Pits Grow?	N	N	N	N	N	N
GrphOCP-OCP (mV)	-82	-109	-79	-111	-109	-101
GrphOCP-Erp (mV)	-142	-154	-117	-127	-114	-134
Calc Pit Rate?	N	N	N	N	N	N
Epp-OCP (mV)	-47	-71	-40	-46	-19	-40
Eb-OCP (mV)	114	45	89	520	389	518
Active?	Y	Y	Y	Y	Y	Y
Transpassive?	N	N	N	N	N	N
Epp-GrphOCP (mV)	35	38	39	65	90	61
Eb-GrphOCP (mV)	196	154	168	631	498	619
Gen&PitCorr?	N	N	N	N	N	N
Ipit (Amps/cm2)						
MPYpit Galv. (mpy)						
MPYpit Steel (mpy)						

* Types: 1 - passive, 2 - psedo-passive, 3 - active

Table F.1. CONTINUED.

Description of Measurement or Interpreted Value	RAP_S9.1_CL_1	RAP_S10.2_CL_1	RAP_S10.4_CL_1	CFM_S9.3_CL_100	CFM_S9.9_CL_100	CFM_S9.10_CL_100
Corr Rate (mpy)	1.056	1.422	3.69	9.78	1.938	3.65
E (I=0) (mV)	-773	-780	-793	-820.5	-752.5	-806
Ba (mV/decade)	144	104	130	213	142	134
Bc (mV/decade)	75	69	69	76	65	62
B, Tafel Const.	49	41	45	56	45	42
Stern-Geary	21.4	18.0	19.6	24.3	19.4	18.4
Hysteresis (decade)	0.3	0.2	0.2	0.2	0.7	0.4
OCP, SCE (mV)	-670	-686	-690	-704	-664	-697
Epp (mV)	-741	-749	-765	-780	-722	-757
Eb (mV)	-655	-655	-675	-639	-620	-627
Erp (mV)	-604	-616	-620	-659	-635	-639
Graph OCP (mV)	-776	-780	-796	-820	-757	-800
Type (1,2,or 3)*	2	2	2	2	2	2
PasRegWidth (mV)	86	94	90	141	102	130
OCP-Erp (mV)	-66	-70	-70	-45	-29	-58
Pits Initiate?	Y	Y	Y	Y	Y	Y
Pits Grow?	N	N	N	N	N	N
GrphOCP-OCP (mV)	-106	-94	-106	-116	-93	-103
GrphOCP-Erp (mV)	-172	-164	-176	-161	-122	-161
Calc Pit Rate?	N	N	N	N	N	N
Epp-OCP (mV)	-71	-63	-75	-76	-58	-60
Eb-OCP (mV)	15	31	15	65	44	70
Active?	Y	Y	Y	Y	Y	Y
Transpassive?	N	N	N	N	N	N
Epp-GrphOCP (mV)	35	31	31	40	35	43
Eb-GrphOCP (mV)	121	125	121	181	137	173
Gen&PitCorr?	N	N	N	N	N	N
Ipit (Amps/cm2)						
MPYpit Galv. (mpy)						
MPYpit Steel (mpy)						

* Types: 1 - passive, 2 - psedo-passive, 3 - active

Table F.1. CONTINUED.

Description of Measurement or Interpreted Value	CC_S9.5_CL_100	CC_S9.6_CL_100	CC_S9.7_CL_100	RAP_S10.5_CL_100	RAP_S10.8_CL_100	RAP_S10.10_CL_100
Corr Rate (mpy)	6.49	6.46	19.08	5.86	1.598	1.823
E (I=0) (mV)	-753.7	-767	-714	-796	-765.5	-773.5
Ba (mV/decade)	247	319	282	188	119	144
Bc (mV/decade)	89	80	122	71	65	61
B, Tafel Const.	65	64	85	52	42	43
Stern-Geary	28.4	27.8	37.0	22.4	18.3	18.6
Hysteresis (decade)	1.5	1.5	1.5	0.4	0.6	0.5
OCP, SCE (mV)	-655	-650	-626	-687	-677	-681
Epp (mV)	-718	-722	-663	-753	-725	-737
Eb (mV)	-286	-271	-306	-639	-576	-659
Erp (mV)	-655	-659	-655	-639	-635	-627
Graph OCP (mV)	-761	-773	-717	-797	-765	-776
Type (1,2,or 3)*	2	2	2	2	2	2
PasRegWidth (mV)	432	451	357	114	149	78
OCP-Erp (mV)	0	9	29	-48	-42	-54
Pits Initiate?	Y	Y	Y	Y	Y	Y
Pits Grow?	Y	Y	Y	N	N	N
GrphOCP-OCP (mV)	-106	-123	-91	-110	-88	-95
GrphOCP-Erp (mV)	-106	-114	-62	-158	-130	-149
Calc Pit Rate?	N	N	N	N	N	N
Epp-OCP (mV)	-63	-72	-37	-66	-48	-56
Eb-OCP (mV)	369	379	320	48	101	22
Active?	Y	Y	Y	Y	Y	Y
Transpassive?	N	N	N	N	N	N
Epp-GrphOCP (mV)	43	51	54	44	40	39
Eb-GrphOCP (mV)	475	502	411	158	189	117
Gen&PitCorr?	N	N	N	N	N	N
Ipit (Amps/cm2)						
MPYpit Galv. (mpy)						
MPYpit Steel (mpy)						

* Types: 1 - passive, 2 - psedo-passive, 3 - active

Table F.1. CONTINUED.

Description of Measurement or Interpreted Value	CFM_S7.2_NCL_1	CFM_S8.3_NCL_1	CFM_S8.4_NCL_1	CC_S7.3_NCL_1	CC_S7.4_NCL_1	CC_S8.2_NCL_1
Corr Rate (mpy)	2.51	6.98	5.63	0.1488	0.0975	0.0920
E (I=0) (mV)	-482	-493.2	-468	-208.7	-200.7	-180.6
Ba (mV/decade)	656	811	581	721	792	549
Bc (mV/decade)	181	231	213	130	118	127
B, Tafel Const.	142	180	156	110	103	103
Stern-Geary	61.6	78.1	67.7	47.8	44.6	44.8
Hysteresis (decade)	0	-0.2	0	-0.8	-0.8	-0.8
OCP, SCE (mV)	-435	-432	-417	-154	-120	-131
Epp (mV)	-482	-492	-468	-129	-123	-85
Eb (mV)	-482	-492	-468	-729	735	738
Erp (mV)	-329	-236	-329	343	423	354
Graph OCP (mV)	-482	-492	-468	-207	-200	-177
Type (1,2,or 3)*	3	3	3	2	2	2
PasRegWidth (mV)	0	0	0	-600	858	823
OCP-Erp (mV)	-106	-196	-88	-497	-543	-485
Pits Initiate?	Y	N	Y	N	N	N
Pits Grow?	N	N	N	N	N	N
GrphOCP-OCP (mV)	-47	-60	-51	-53	-80	-46
GrphOCP-Erp (mV)	-153	-256	-139	-550	-623	-531
Calc Pit Rate?	N	N	N	N	N	N
Epp-OCP (mV)	-47	-60	-51	25	-3	46
Eb-OCP (mV)	-47	-60	-51	-575	855	869
Active?	Y	Y	Y	N	Y	N
Transpassive?	Y	Y	Y	Y	N	N
Epp-GrphOCP (mV)	0	0	0	78	77	92
Eb-GrphOCP (mV)	0	0	0	-522	935	915
Gen&PitCorr?	Y	Y	Y	N	N	N
Ipit (Amps/cm2)						
MPYpit Galv. (mpy)						
MPYpit Steel (mpy)						

* Types: 1 - passive, 2 - psedo-passive, 3 - active

Table F.1. CONTINUED.

Description of Measurement or Interpreted Value	RAP_S7.6_NCL_1	RAP_S7.10_NCL_1	RAP_S8.9_NCL_1	CFM_S7.1_NCL_100	CFM_S7.5_NCL_100	CFM_S8.10_NCL_100
Corr Rate (mpy)	0.373	2.56	1.079	0.0728	0.238	1.859
E (I=0) (mV)	-685.1	-537.5	-599	-153.5	-172.5	-415.9
Ba (mV/decade)	172	490	152	1673	451	594
Bc (mV/decade)	135	251	227	130	131	212
B, Tafel Const.	76	166	91	121	102	156
Stern-Geary	32.8	72.1	39.5	52.4	44.1	67.8
Hysteresis (decade)	0.1	-0.5	0	-0.7	0.6	0.5
OCP, SCE (mV)	-635	-491	-575	-97	-105	-395
Epp (mV)	-685	-531	-599	-89	-69	-323
Eb (mV)	-685	-531	-599	687	46	-138
Erp (mV)	-519	-231	-476	427	-192	-362
Graph OCP (mV)	-685	-531	-599	-151	-173	-415
Type (1,2,or 3)*	3	3	3	2	2	2
PasRegWidth (mV)	0	0	0	776	115	185
OCP-Erp (mV)	-116	-260	-99	-524	87	-33
Pits Initiate?	Y	N	Y	N	Y	Y
Pits Grow?	N	N	N	N	Y	N
GrphOCP-OCP (mV)	-50	-40	-24	-54	-68	-20
GrphOCP-Erp (mV)	-166	-300	-123	-578	19	-53
Calc Pit Rate?	N	N	N	N	Y	N
Epp-OCP (mV)	-50	-40	-24	8	36	72
Eb-OCP (mV)	-50	-40	-24	784	151	257
Active?	Y	Y	Y	N	N	N
Transpassive?	Y	Y	Y	N	N	N
Epp-GrphOCP (mV)	0	0	0	62	104	92
Eb-GrphOCP (mV)	0	0	0	838	219	277
Gen&PitCorr?	Y	Y	Y	N	N	N
Ipit (Amps/cm2)					7.5E-6	
MPYpit Galv. (mpy)					88	
MPYpit Steel (mpy)					69	

* Types: 1 - passive, 2 - psedo-passive, 3 - active

Table F.1. CONTINUED.

Description of Measurement or Interpreted Value	CC_S7.7_NCL_100	CC_S8.1_NCL_100	CC_S8.6_NCL_100	RAP_S7.8_NCL_100	RAP_S7.9_NCL_100	RAP_S8.5_NCL_100
Corr Rate (mpy)	0.0441	0.814	0.972	0.0347	2.98	0.515
E (I=0) (mV)	-177.4	-259	-289.4	-103.2	-427.5	-616.8
Ba (mV/decade)	701	726	837	163	919	562
Bc (mV/decade)	106	179	146	119	328	430
B, Tafel Const.	92	144	124	69	242	244
Stern-Geary	40.0	62.4	54.0	29.9	105.0	105.8
Hysteresis (decade)	-0.7	-1	-0.8	-1	0.1	0
OCP, SCE (mV)	-78	-181	-200	-68	-415	-600
Epp (mV)	-176	-171	-210	-102	-429	-614
Eb (mV)	765			-102	-429	-614
Erp (mV)	507	320	364	98	-414	-507
Graph OCP (mV)	148	-263	-289	-102	-429	-614
Type (1,2,or 3)*	2	2	2	3	3	3
PasRegWidth (mV)	941	171	210	0	0	0
OCP-Erp (mV)	-585	-501	-564	-166	-1	-93
Pits Initiate?	N	N	N	N	Y	Y
Pits Grow?	N	N	N	N	N	N
GrphOCP-OCP (mV)	226	-82	-89	-34	-14	-14
GrphOCP-Erp (mV)	-359	-583	-653	-200	-15	-107
Calc Pit Rate?	N	N	N	N	N	N
Epp-OCP (mV)	-98	10	-10	-34	-14	-14
Eb-OCP (mV)	843	181	200	-34	-14	-14
Active?	Y	N	Y	Y	Y	Y
Transpassive?	N	N	N	Y	Y	Y
Epp-GrphOCP (mV)	-324	92	79	0	0	0
Eb-GrphOCP (mV)	617	263	289	0	0	0
Gen&PitCorr?	N	N	N	Y	Y	Y
Ipit (Amps/cm2)						
MPYpit Galv. (mpy)						
MPYpit Steel (mpy)						

* Types: 1 - passive, 2 - psedo-passive, 3 - active

Table F.2. Measured and Interpreted Values from Cyclic Polarization Resistance Testing for LTT Samples.

Description of Measurement or Interpreted Value	CFM_G2.7_CL	CFM_G3.4_CL	CC_G5.10_CL	CC_G3.5_CL	RAP_G4.8_CL	RAP_G4.2_CL
Corr Rate (mpy)	19.41	15.84	9.96	17.24	24.1	32.5
E (I=0) (mV)	-663.5	-707.2	-674.1	-700.8	-651.8	-667.1
Ba (mV/decade)	767	560	1391	546	835	892
Bc (mV/decade)	166	76	173	129	225	445
B, Tafel Const.	136	67	154	104	177	297
Stern-Geary	59.3	29.1	66.8	45.3	77.0	128.9
Hysteresis (decade)	0.05	0.1	0.3	0.4	-0.1	-0.05
OCP, SCE (mV)	-593	-594	-595	-622	-591	-617
Epp (mV)	-631	-669	-621	-671	-650	-669
Eb (mV)	-595	-669	-603	-657	-650	-669
Erp (mV)	-542	-508	-577	-621	-500	-543
Graph OCP (mV)	-662	-703	-673	-700	-650	-669
Type (1,2,or 3)*	2	3	1	1	3	3
PasRegWidth (mV)	36	0	18	14	0	0
OCP-Erp (mV)	-51	-86	-18	-1	-91	-74
Pits Initiate?	Y	Y	Y	Y	N	N
Pits Grow?	N	N	N	N	N	N
GrphOCP-OCP (mV)	-69	-109	-78	-78	-59	-52
GrphOCP-Erp (mV)	-120	-195	-96	-79	-150	-126
Calc Pit Rate?	N	N	N	N	N	N
Epp-OCP (mV)	-38	-75	-26	-49	-59	-52
Eb-OCP (mV)	-2	-75	-8	-35	-59	-52
Active?	Y	Y	Y	Y	Y	Y
Transpassive?	Y	Y	Y	Y	Y	Y
Epp-GrphOCP (mV)	31	34	52	29	0	0
Eb-GrphOCP (mV)	67	34	70	43	0	0
Gen&PitCorr?	Y	Y	Y	Y	Y	Y
Ipit (Amps/cm2)						
MPYpit Galv. (mpy)						
MPYpit Steel (mpy)						

* Types: 1 - passive, 2 - psedo-passive, 3 - active

Table F.2. CONTINUED.

Description of Measurement or Interpreted Value	CFM_G3.6_NCL	CFM_G4.3_NCL	CC_G1.3_NCL	CC_G1.7_NCL	RAP_G2.2_NCL	RAP_G4.7_NCL
Corr Rate (mpy)	0.477	0.261	1.365	0.1575	0.238	0.301
E (I=0) (mV)	-704.2	-623	-475.1	-329.7	-800.8	-703.7
Ba (mV/decade)	758	723	1092	950	767	1347
Bc (mV/decade)	450	328	152	118	508	667
B, Tafel Const.	282	226	133	105	306	446
Stern-Geary	122.6	98.0	57.9	45.6	132.7	193.7
Hysteresis (decade)	0.7	0.7	-0.3	-1	0.05	-0.05
OCP, SCE (mV)	-680	-579	-422	-244	-776	-682
Epp (mV)	-562	-539	-475	-332	-800	-705
Eb (mV)	-477	-423	-475	-332	-800	-705
Erp (mV)	-823	-762	-311	121	-757	-627
Graph OCP (mV)	-700	-623	-475	-332	-800	-705
Type (1,2,or 3)*	2	2	3	3	3	3
PasRegWidth (mV)	85	116	0	0	0	0
OCP-Erp (mV)	143	183	-111	-365	-19	-55
Pits Initiate?	Y	Y	N	N	Y	N
Pits Grow?	Y	Y	N	N	N	N
GrphOCP-OCP (mV)	-20	-44	-53	-88	-24	-23
GrphOCP-Erp (mV)	123	139	-164	-453	-43	-78
Calc Pit Rate?	Y	Y	N	N	N	N
Epp-OCP (mV)	118	40	-53	-88	-24	-23
Eb-OCP (mV)	203	156	-53	-88	-24	-23
Active?	N	N	Y	Y	Y	Y
Transpassive?	N	N	Y	Y	Y	Y
Epp-GrphOCP (mV)	138	84	0	0	0	0
Eb-GrphOCP (mV)	223	200	0	0	0	0
Gen&PitCorr?	N	N	Y	Y	Y	Y
Ipit (Amps/cm2)	4.0E-6	4.8E-6				
MPYpit Galv. (mpy)	47	57				
MPYpit Steel (mpy)	37	44				

* Types: 1 - passive, 2 - psedo-passive, 3 - active

Table F.2. CONTINUED.

Description of Measurement or Interpreted Value	CFM_S6.9_CL	CFM_S3.6_CL	CC_S2.9_CL	CC_S6.7_CL	RAP_S1.8_CL	RAP_S4.3_CL
Corr Rate (mpy)	36.0	26.7	5.09	18.15	30.8	65.2
E (I=0) (mV)	-686.8	-715.5	-578.4	-602.3	-622.8	-583.6
Ba (mV/decade)	432	409	282	654	361	766
Bc (mV/decade)	226	146	260	182	207	467
B, Tafel Const.	148	108	135	142	132	290
Stern-Geary	64.4	46.7	58.7	61.8	57.1	126.0
Hysteresis (decade)	0.05	0.1	-0.25	-0.25	0.1	-0.3
OCP, SCE (mV)	-630	-633	-557	-574	-576	-559
Epp (mV)	-615	-662	-578	-564	-621	-582
Eb (mV)	-496	-474	-578	-564	-621	-582
Erp (mV)	-561	-569	-439	-428	-550	-450
Graph OCP (mV)	-689	-716	-578	-600	-621	-582
Type (1,2,or 3)*	2	2	3	3	3	3
PasRegWidth (mV)	119	188	0	0	0	0
OCP-Erp (mV)	-69	-64	-118	-146	-26	-109
Pits Initiate?	Y	Y	N	N	Y	N
Pits Grow?	N	N	N	N	N	N
GrphOCP-OCP (mV)	-59	-83	-21	-26	-45	-23
GrphOCP-Erp (mV)	-128	-147	-139	-172	-71	-132
Calc Pit Rate?	N	N	N	N	N	N
Epp-OCP (mV)	15	-29	-21	10	-45	-23
Eb-OCP (mV)	134	159	-21	10	-45	-23
Active?	N	Y	Y	N	Y	Y
Transpassive?	N	N	Y	N	Y	Y
Epp-GrphOCP (mV)	74	54	0	36	0	0
Eb-GrphOCP (mV)	193	242	0	36	0	0
Gen&PitCorr?	N	N	Y	Y	Y	Y
Ipit (Amps/cm2)						
MPYpit Galv. (mpy)						
MPYpit Steel (mpy)						

* Types: 1 - passive, 2 - psedo-passive, 3 - active

Table F.2. CONTINUED.

Description of Measurement or Interpreted Value	CFM_S3.9_NCL	CFM_S4.9_NCL	CC_S2.7_NCL	CC_S6.3_NCL	RAP_S3.2_NCL	RAP_S3.7_NCL
Corr Rate (mpy)	1.17	1.176	0.669	0.928	2.17	0.520
E (I=0) (mV)	-447.4	-573.5	-289.5	-341	-568.8	-363.7
Ba (mV/decade)	975	792	516	787	295	710
Bc (mV/decade)	378	209	183	242	295	606
B, Tafel Const.	272	165	135	185	148	327
Stern-Geary	118.3	71.8	58.7	80.4	64.0	142.0
Hysteresis (decade)	-0.4	-0.3	-0.9	-0.8	0.2	-0.3
OCP, SCE (mV)	-415	-550	-224	-290	-551	-352
Epp (mV)	-379	-511	-14	-115	-493	-364
Eb (mV)	-321	-464	621	627	-393	-364
Erp (mV)	-211	-436	153	42	-479	-171
Graph OCP (mV)	-446	-571	-289	-339	-567	-364
Type (1,2,or 3)*	2	1	2	2	2	3
PasRegWidth (mV)	58	47	635	742	100	0
OCP-Erp (mV)	-204	-114	-377	-332	-72	-181
Pits Initiate?	N	N	N	N	Y	N
Pits Grow?	N	N	N	N	N	N
GrphOCP-OCP (mV)	-31	-21	-65	-49	-16	-12
GrphOCP-Erp (mV)	-235	-135	-442	-381	-88	-193
Calc Pit Rate?	N	N	N	N	N	N
Epp-OCP (mV)	36	39	210	175	58	-12
Eb-OCP (mV)	94	86	845	917	158	-12
Active?	N	N	N	N	N	Y
Transpassive?	N	N	N	N	N	Y
Epp-GrphOCP (mV)	67	60	275	224	74	0
Eb-GrphOCP (mV)	125	107	910	966	174	0
Gen&PitCorr?	N	N	N	N	N	Y
Ipit (Amps/cm2)						
MPYpit Galv. (mpy)						
MPYpit Steel (mpy)						

* Types: 1 - passive, 2 - psedo-passive, 3 - active

APPENDIX G

POTENTIAL READING PLOTS

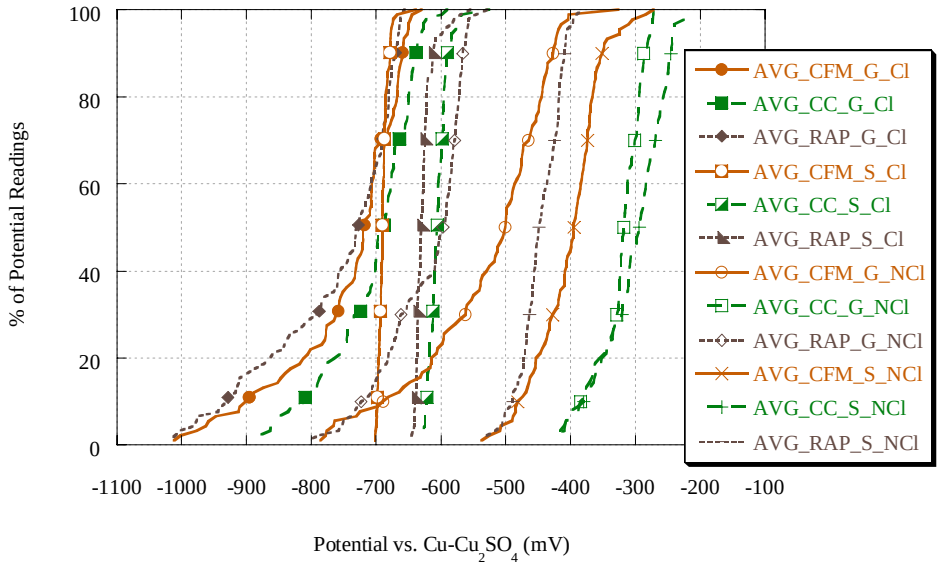

Figure G.1. Distribution of Avgerage Potential Readings for All LTT Groups.

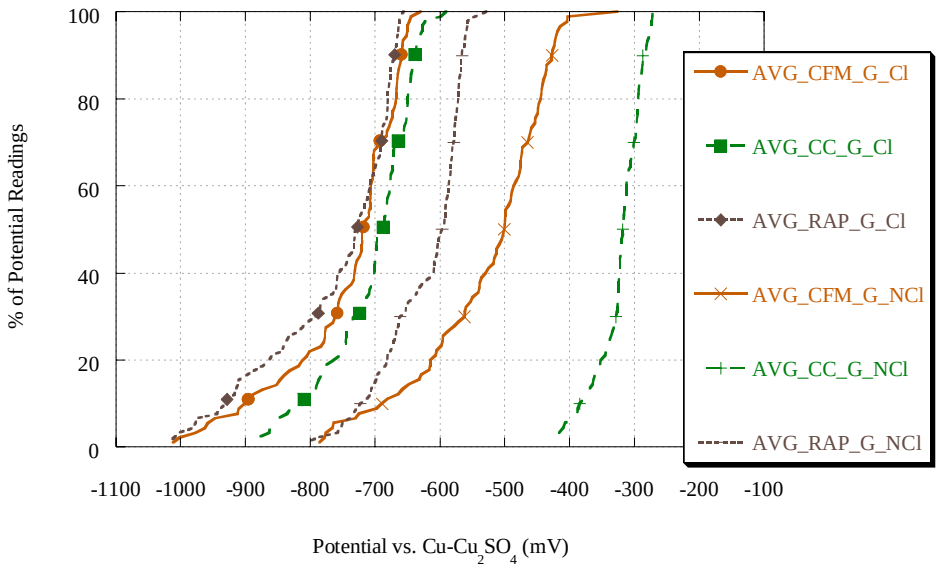

Figure G.2. Distribution of Avgerage Potential Readings for G LTT Groups.

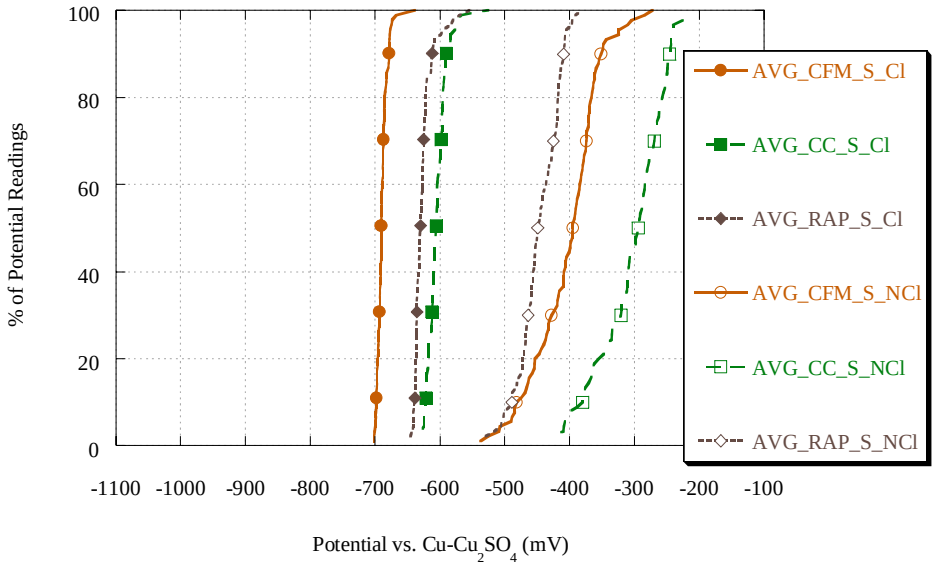

Figure G.3. Distribution of Avgerage Potential Readings for S LTT Groups.

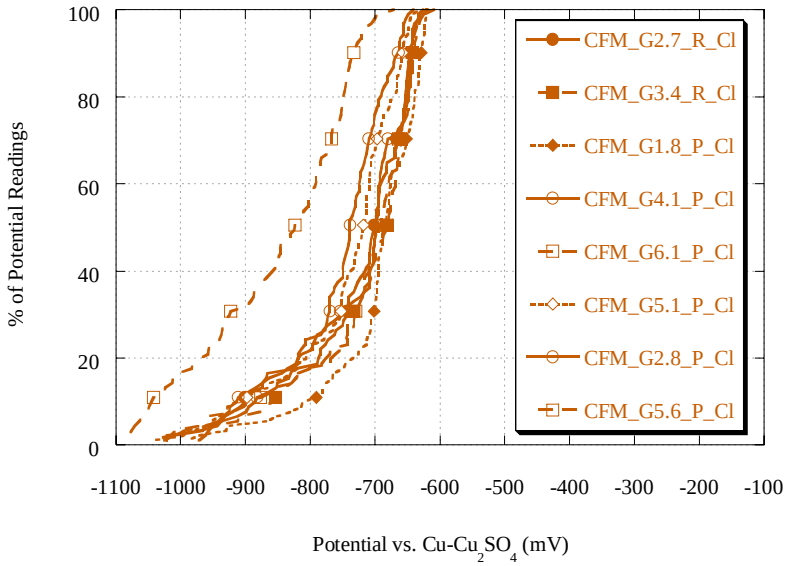

Figure G.4. Distribution of Potential Readings for CFM G CL LTT Samples.

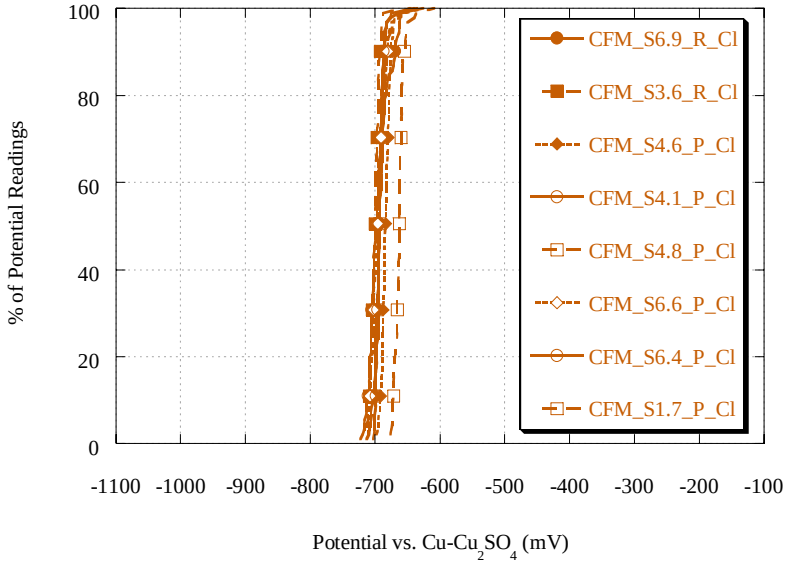

Figure G.5. Distribution of Potential Readings for CFM S CL LTT Samples.

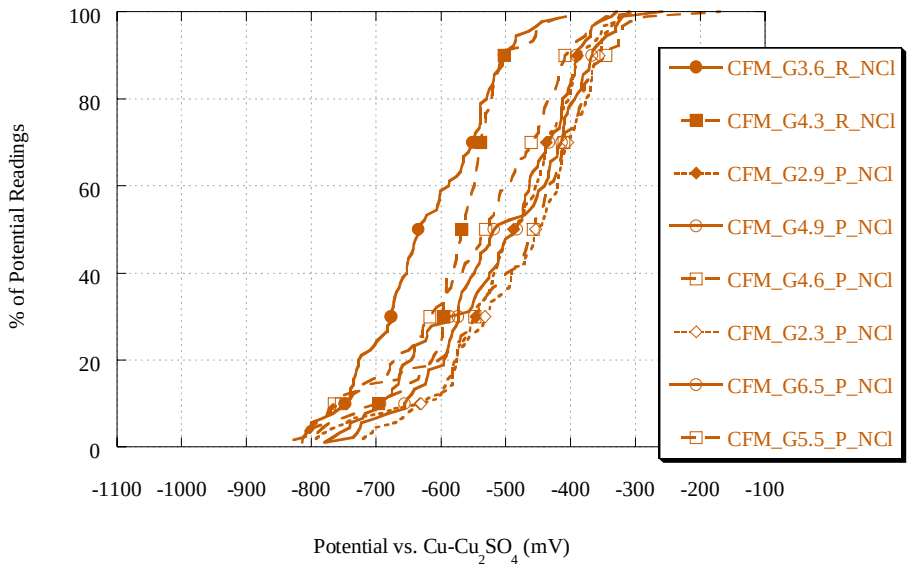

Figure G.6. Distribution of Potential Readings for CFM G NCL LTT Samples.

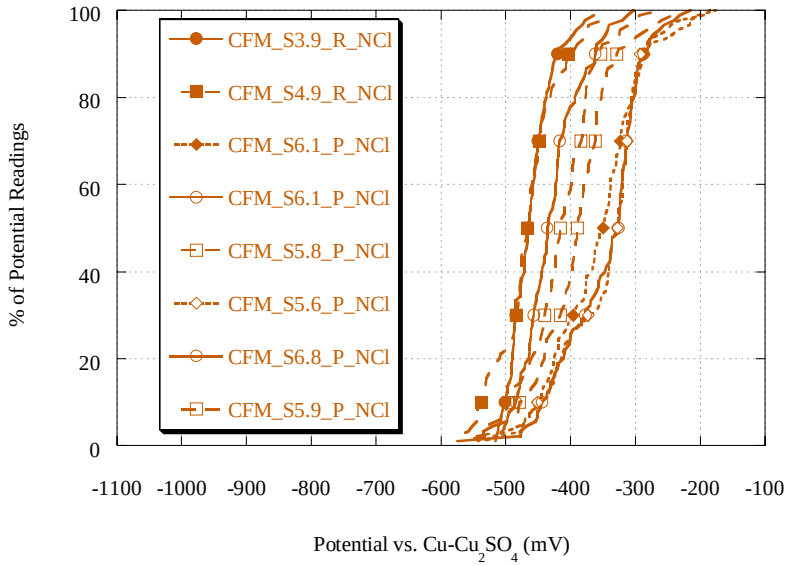

Figure G.7. Distribution of Potential Readings for CFM S NCL LTT Samples.

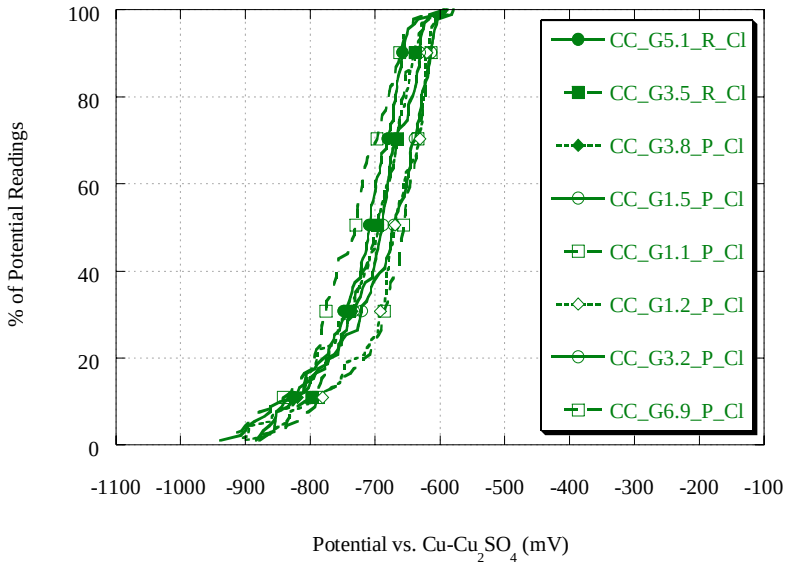

Figure G.8. Distribution of Potential Readings for CC G CL LTT Samples.

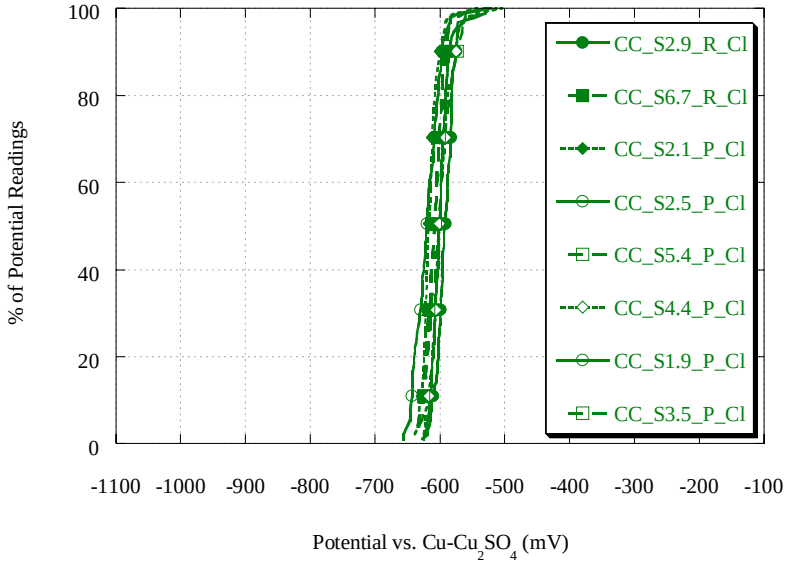

Figure G.9. Distribution of Potential Readings for CC S CL LTT Samples.

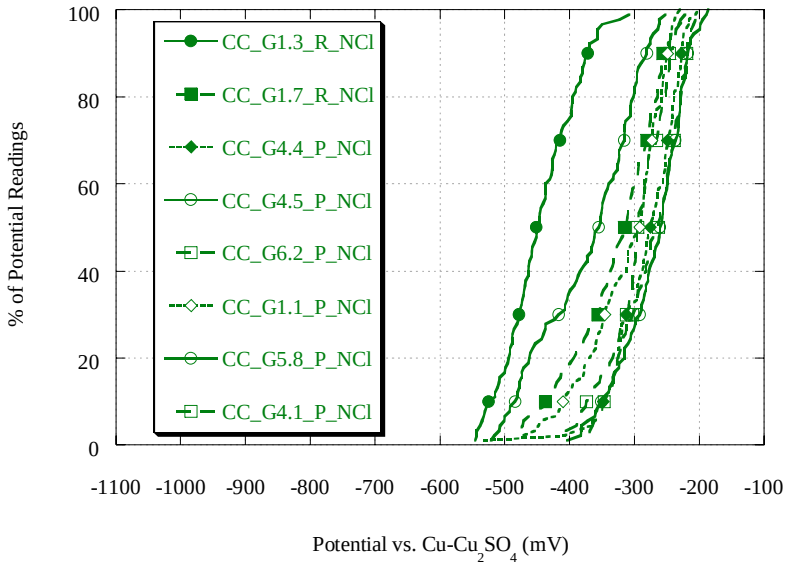

Figure G.10. Distribution of Potential Readings for CC G NCL LTT Samples.

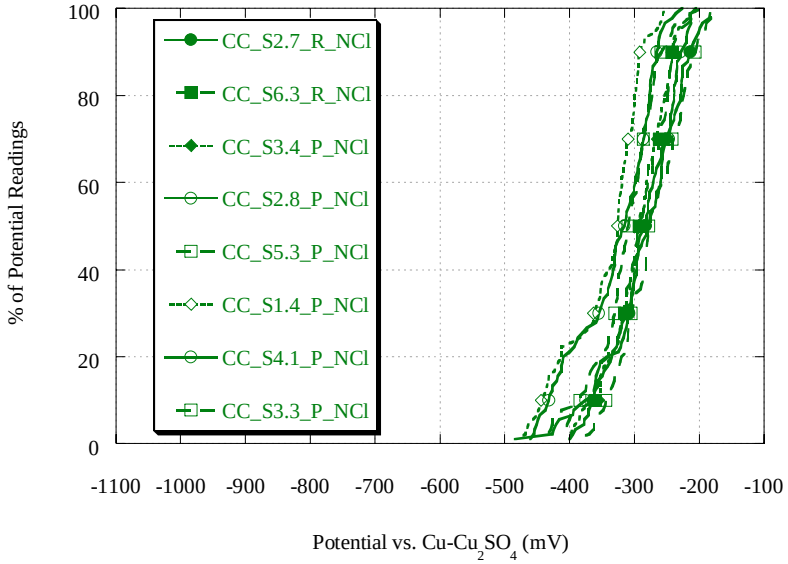

Figure G.11. Distribution of Potential Readings for CC S NCL LTT Samples..

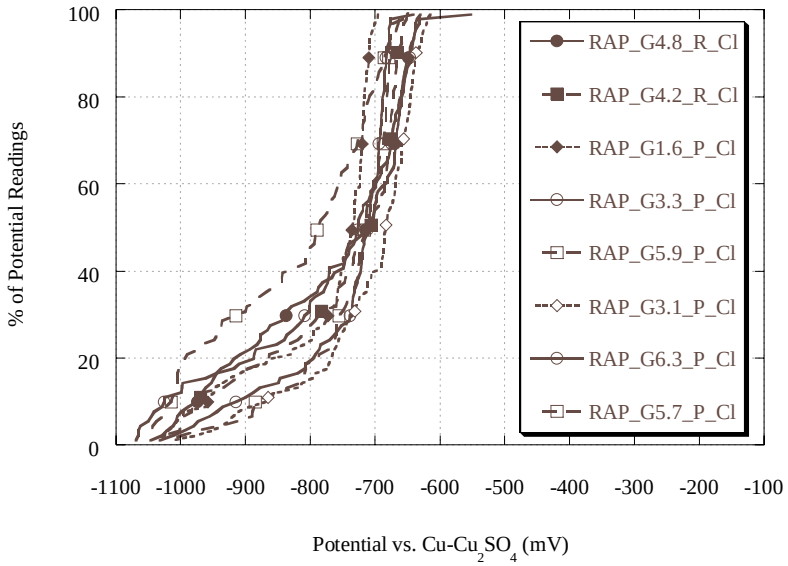

Figure G.12. Distribution of Potential Readings for RAP G CL LTT Samples.

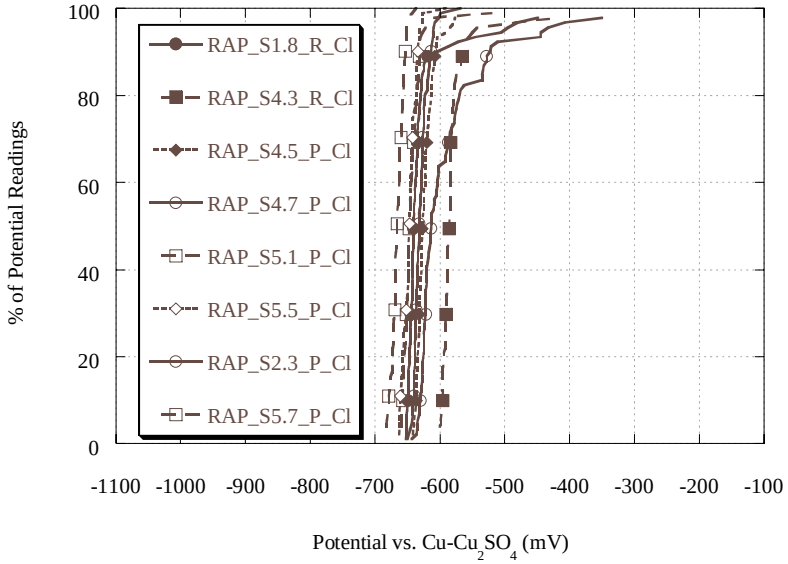

Figure G.13. Distribution of Potential Readings for RAP S CL LTT Samples.

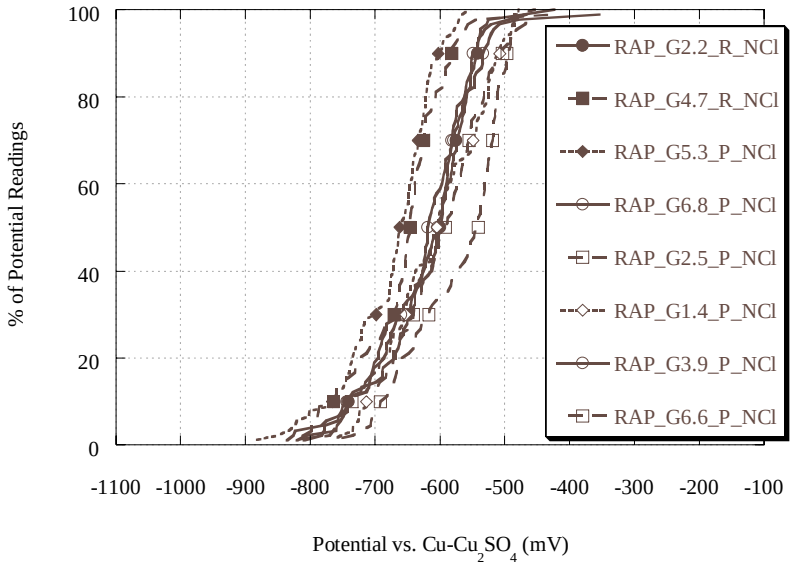

Figue G.14. Distribution of Potential Readings for RAP G NCL LTT Samples.

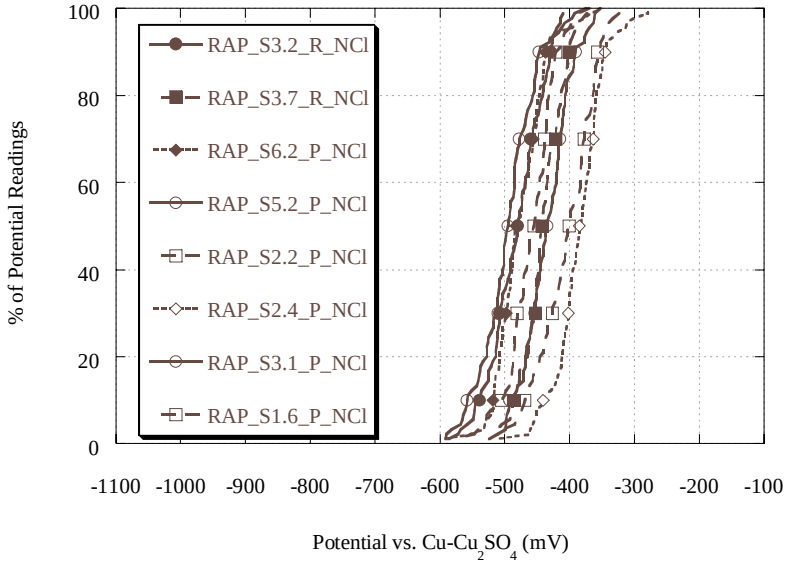

Figure G.15. Distribution of Potential Readings for RAP S NCL LTT Samples.

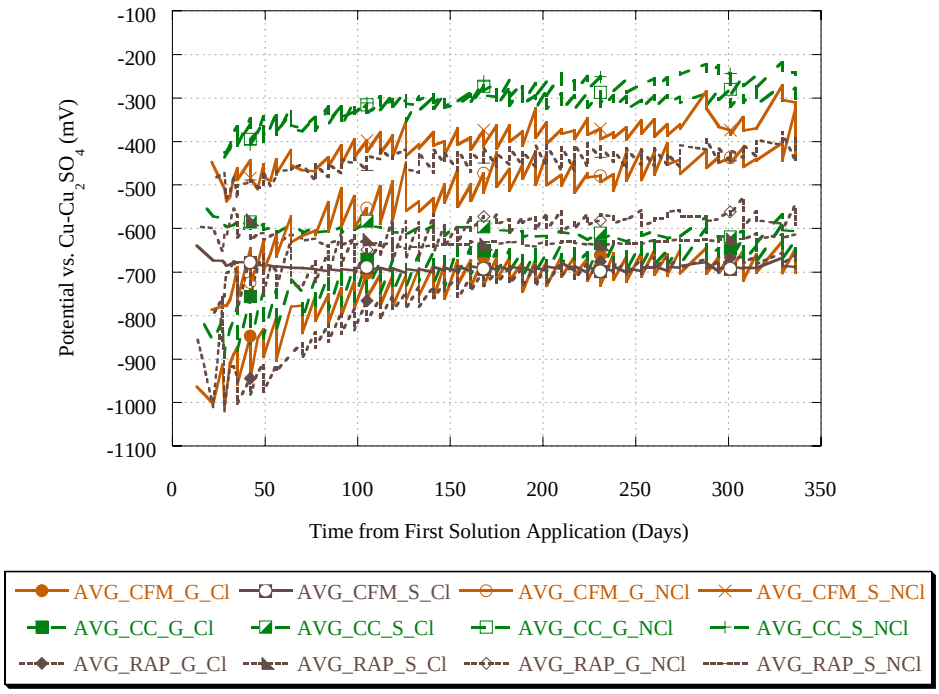

Figure G.16. Avgerage Potential Readings for all LTT Groups Over Time.

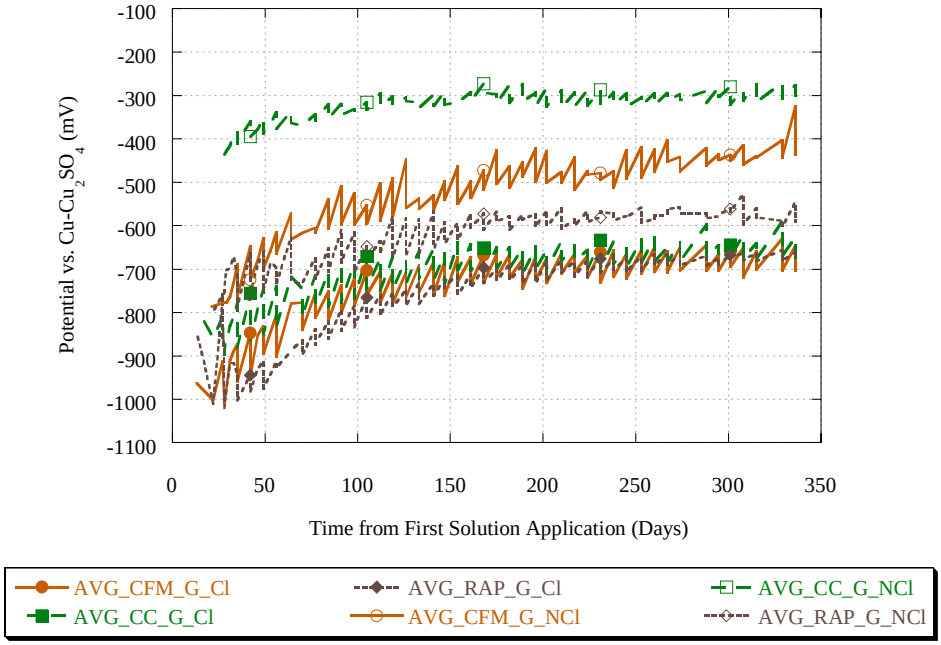

Figure G.17. Avgerage Potential Readings for G LTT Groups Over Time.

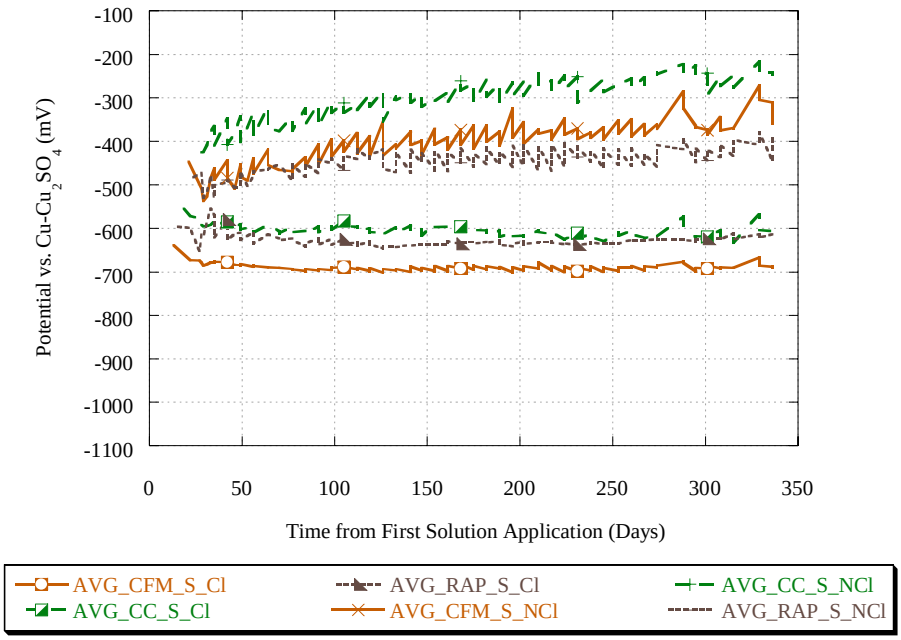

Figure G.18. Avgerage Potential Readings for S LTT Groups Over Time.

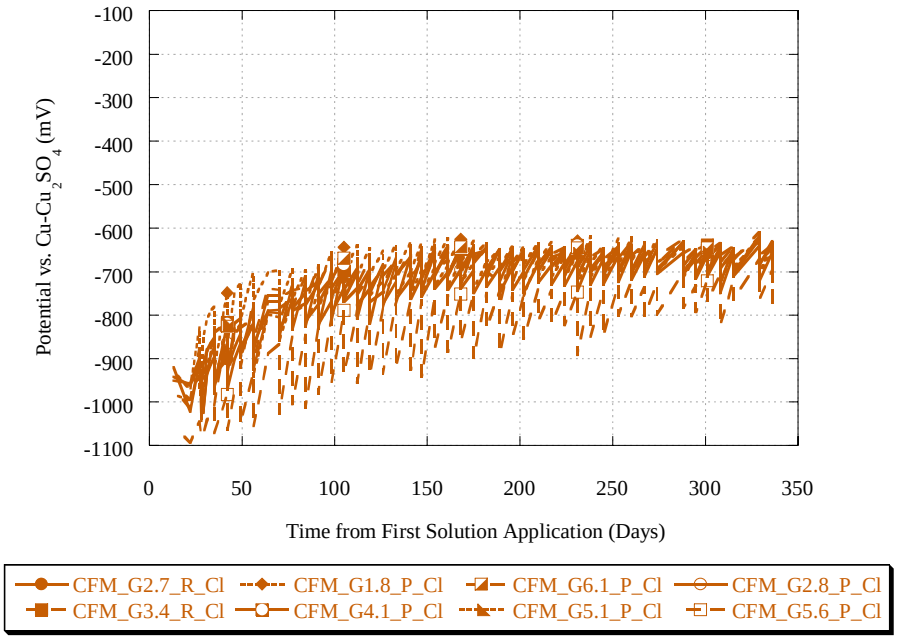

Figure G.19. Potential Readings for CFM G CL LTT Samples Over Time.

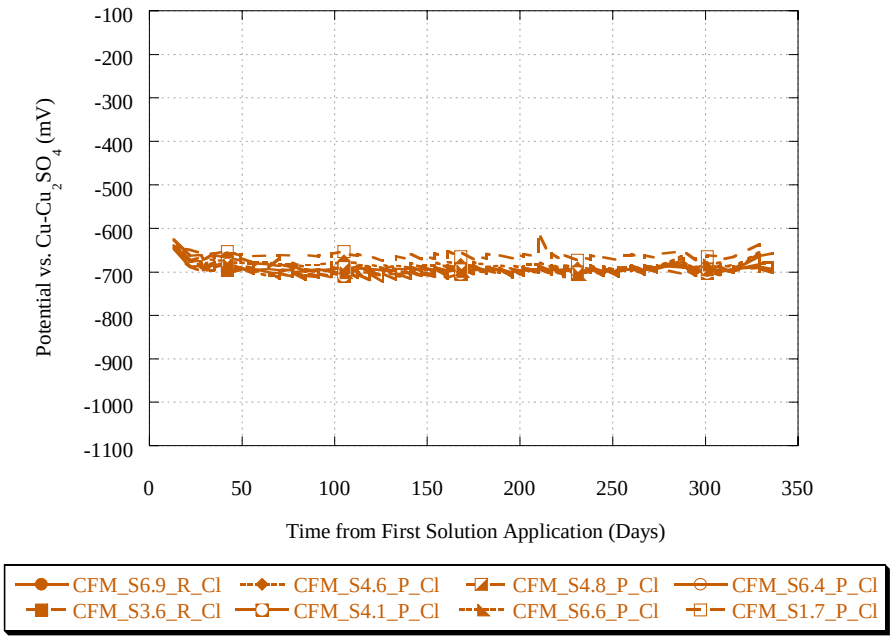

Figure G.20. Potential Readings for CFM S CL LTT Samples Over Time.

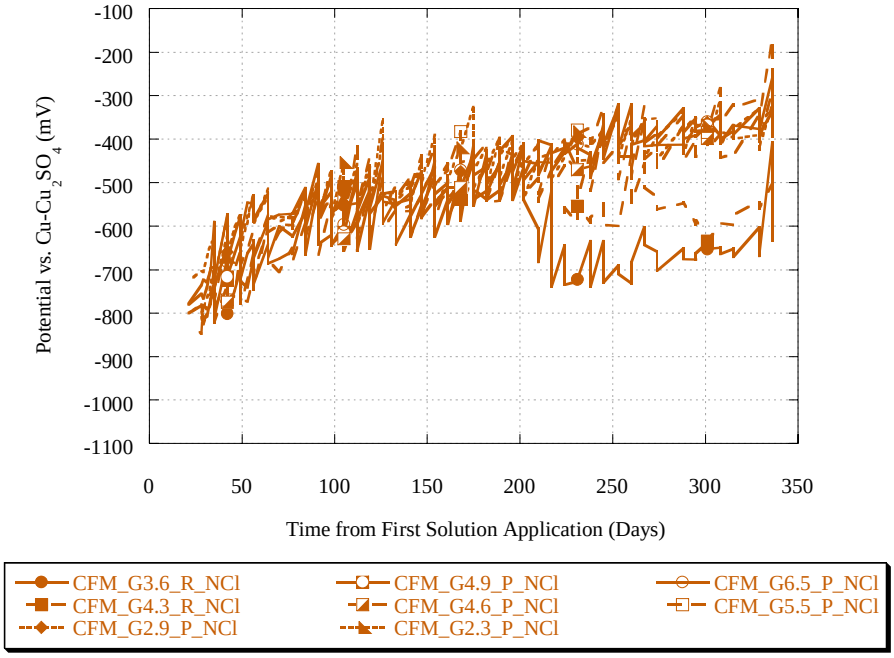

Figure G.21. Potential Readings for CFM G NCL LTT Samples Over Time.

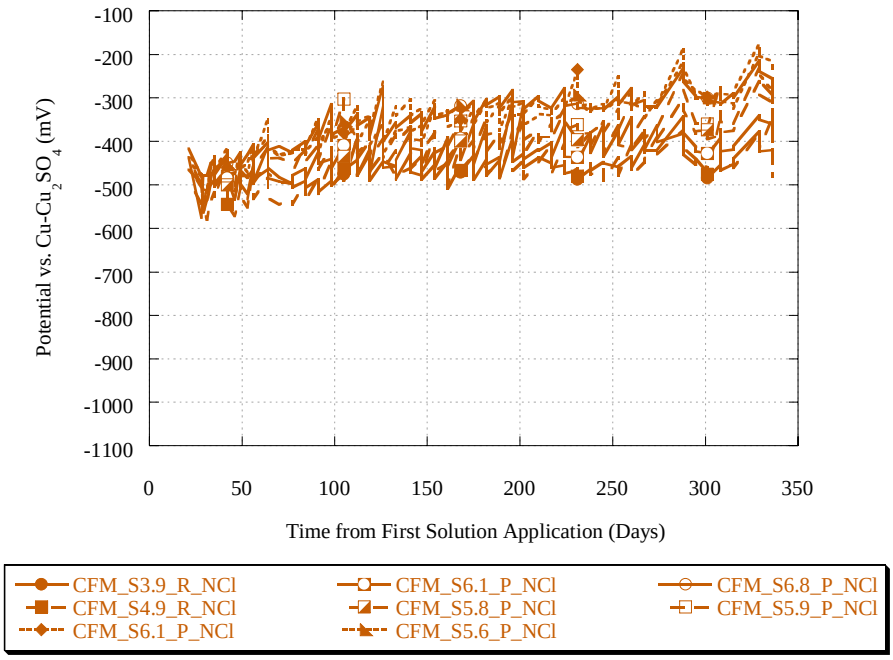

Figure G.22. Potential Readings for CFM S NCL LTT Samples Over Time.

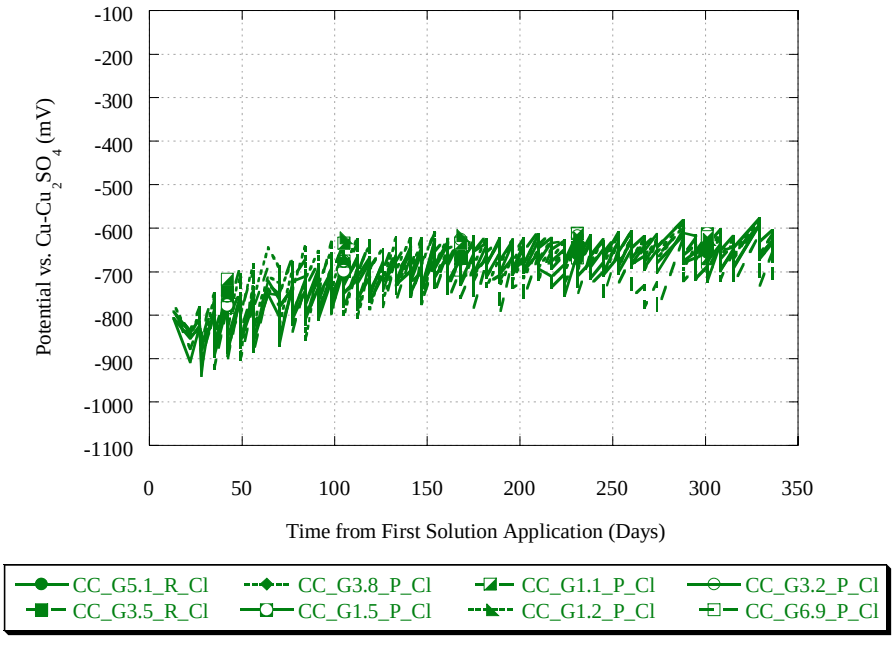

Figure G.23. Potential Readings for CC G CL LTT Samples Over Time.

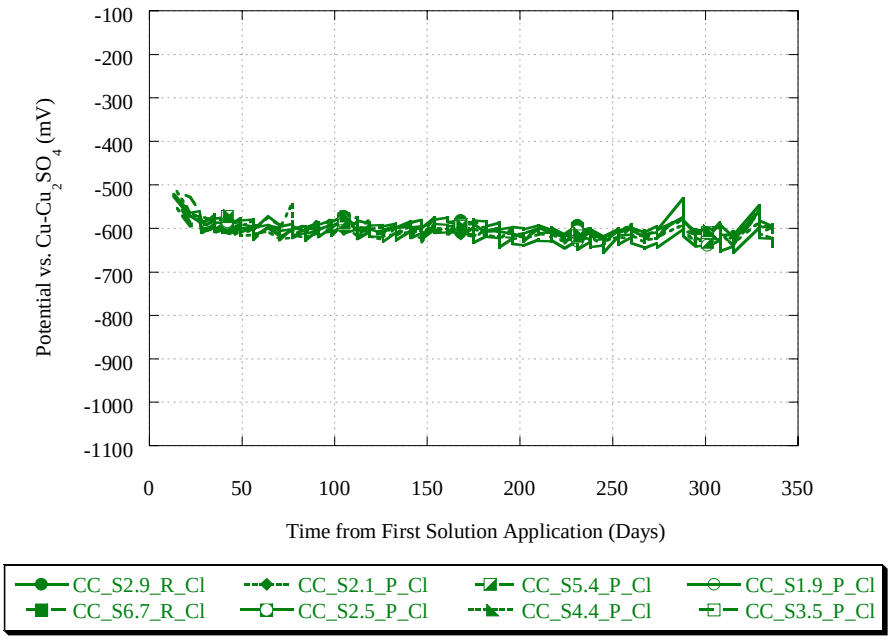

Figure G.24. Potential Readings for CC S CL LTT Samples Over Time.

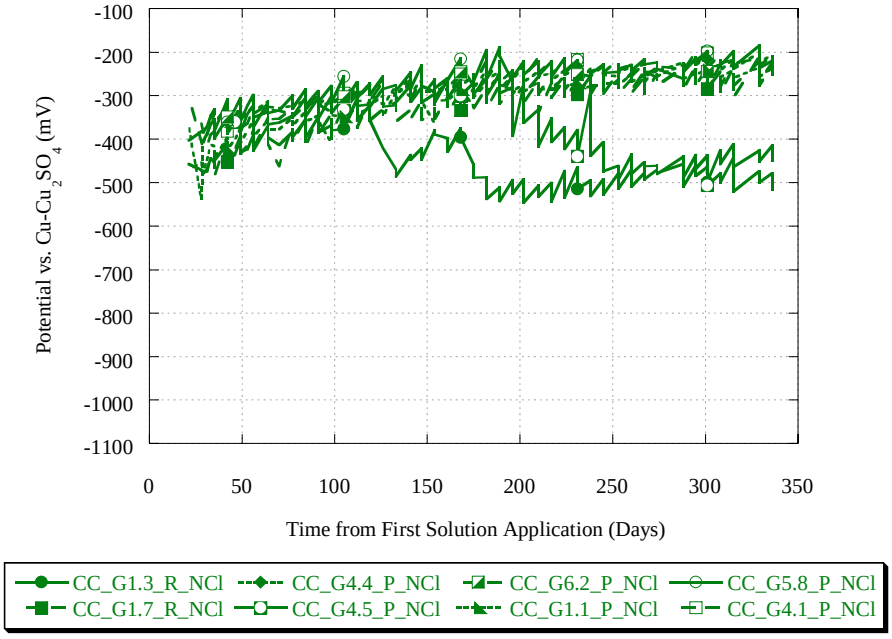

Figure G.25. Potential Readings for CC G NCL LTT Samples Over Time.

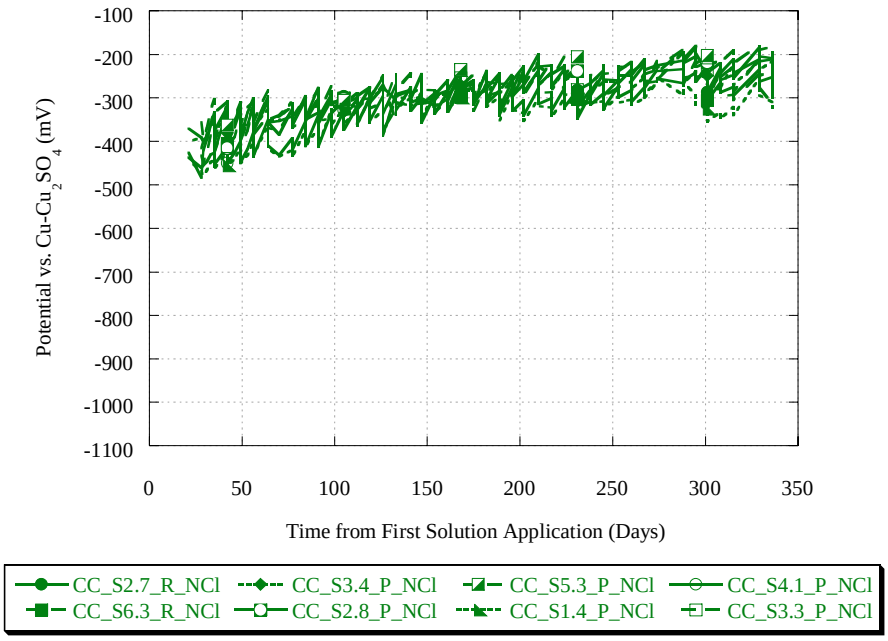

Figure G.26. Potential Readings for CC S NCL LTT Samples Over Time.

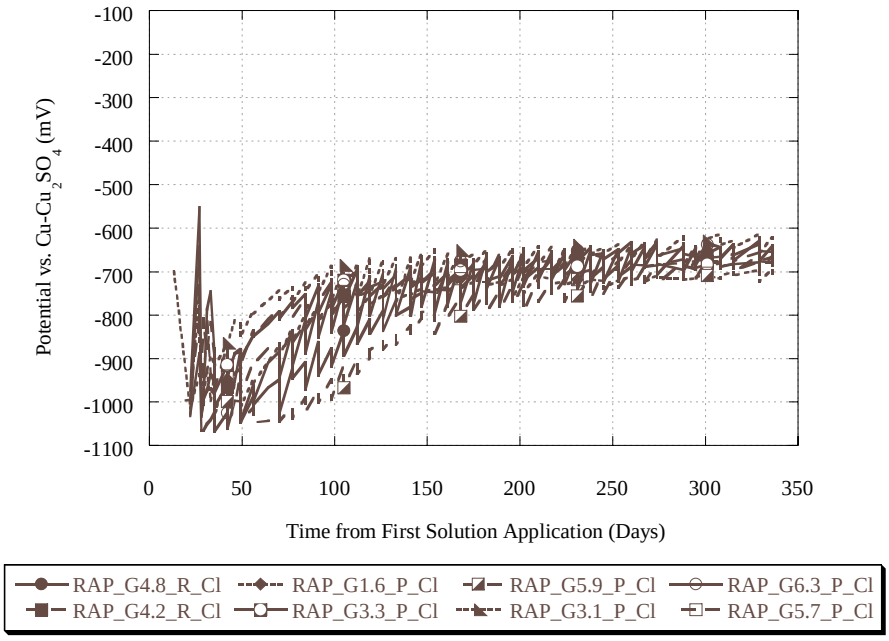

Figure G.27. Potential Readings for RAP G CL LTT Samples Over Time.

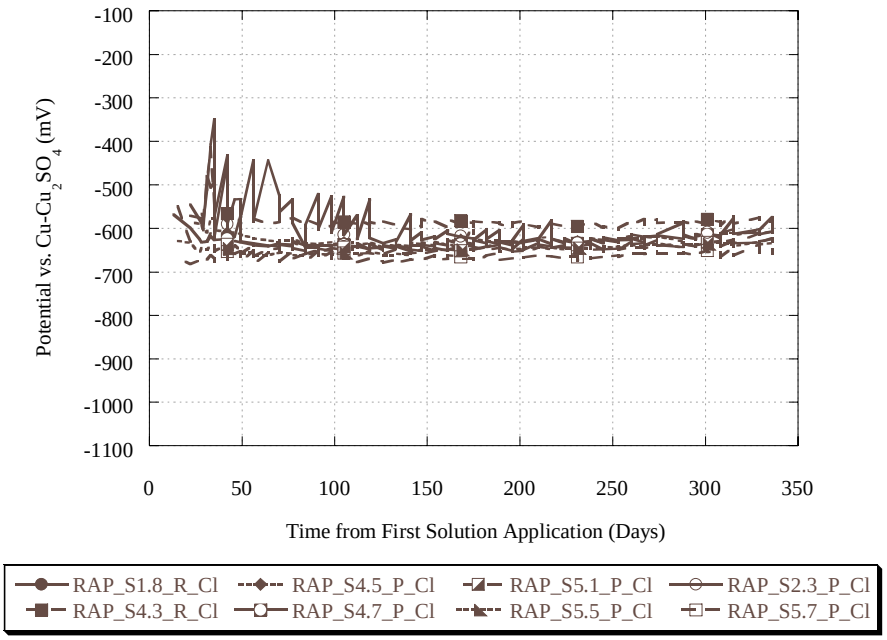

Figure G.28. Potential Readings for RAP S CL LTT Samples Over Time.

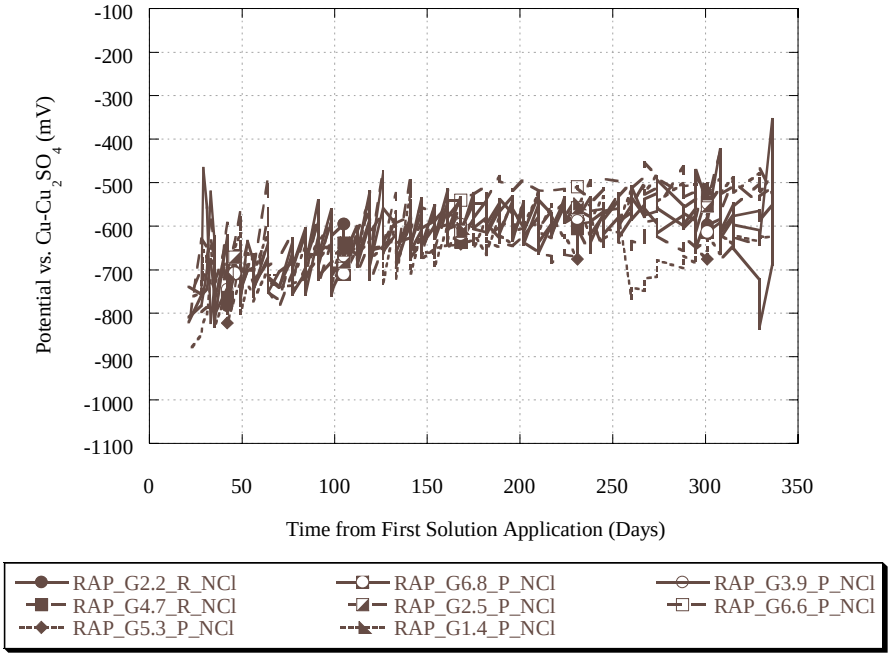

Figure G.29. Potential Readings for RAP G NCL LTT Samples Over Time.

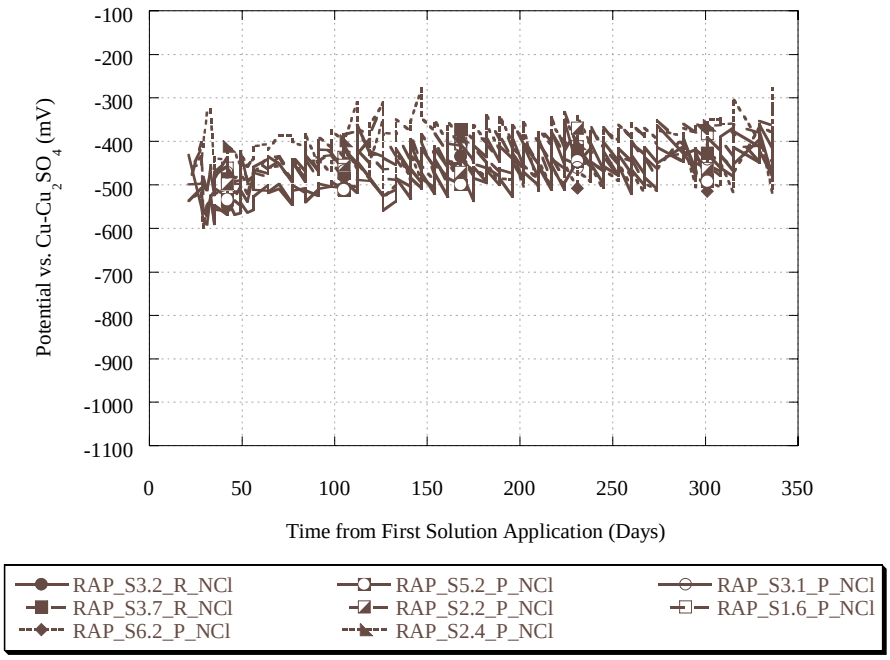

Figure G.30. Potential Readings for RAP S NCL LTT Samples Over Time.

APPENDIX H

LTT VALUES USED IN STATISTICAL ANALYSIS

Table H.1. LTT Values Used in Statistical Analysis.

Data Description	CFM_G2.7_CL	CFM_G3.4_CL	CFM_G1.8_CL	CFM_G4.1_CL	CFM_G6.1_CL	CFM_G5.1_CL
Sample Number	2.7	3.4	1.8	4.10	6.1	5.1
Backfill Type	CFM	CFM	CFM	CFM	CFM	CFM
Metal Type	G	G	G	G	G	G
Environment	CL	CL	CL	CL	CL	CL
Test Type	R	R	P	P	P	P
Measured Corr. Rate (mils/yr)	7.243	8.706	8.717	7.529	9.880	1.816
Estimated Corr. Rate (mils/yr)	53.0	10.24				
Density (lb/ft^3)	126	129	118	118	121	127
Resistivity (ohm-cm)	218.3	206.6	324.7	235.8	378.8	314.5
Chloride (mg/L)	1589.6	1652.6	1018.4	1333.7	729.78	997.42
Sulfate (mg/L)	1.363	1.42	1.425	0.011	1.041	3.675
Redox Potential (mV)	162	188.9	160.5	163.2	161.8	154.5
pH	10.06	9.79	10.12	10.16	10.28	10.23

Table H.1. CONTINUED.

Data Description	CFM_G2.8_CL	CFM_G5.6_CL	CC_G5.1_CL	CC_G3.5_CL	CC_G3.8_CL	CC_G1.5_CL
Sample Number	2.8	5.6	5.10	3.5	3.8	1.5
Backfill Type	CFM	CFM	CC	CC	CC	CC
Metal Type	G	G	G	G	G	G
Environment	CL	CL	CL	CL	CL	CL
Test Type	P	P	R	R	P	P
Measured Corr. Rate (mils/yr)	8.279	4.316	3.237	5.266	3.322	3.931
Estimated Corr. Rate (mils/yr)			17.80	18.38		
Density (lb/ft^3)	128	124	123	113	107	108
Resistivity (ohm-cm)	222.7	366.3	115.3	129.5	119.8	102.2
Chloride (mg/L)	1532.6	838.3	2763.9	2225.3	2555.6	3207.7
Sulfate (mg/L)	12.937	6.082	310.97	318.09	278.45	501.22
Redox Potential (mV)	173.9	171.5	19.7	-22.8	7.4	25.3
pH	9.90	9.94	11.61	11.59	11.69	11.35

Table H.1. CONTINUED.

Data Description	CC_G1.1_CL	CC_G1.2_CL	CC_G3.2_CL	CC_G6.9_CL	RAP_G4.8_CL	RAP_G4.2_CL
Sample Number	1.1	1.2	3.2	6.9	4.8	4.2
Backfill Type	CC	CC	CC	CC	RAP	RAP
Metal Type	G	G	G	G	G	G
Environment	CL	CL	CL	CL	CL	CL
Test Type	P	P	P	P	R	R
Measured Corr. Rate (mils/yr)	4.711	6.228	4.412	4.070	5.480	6.484
Estimated Corr. Rate (mils/yr)					98.4	174.1
Density (lb/ft^3)	119	107	113	118	111	114
Resistivity (ohm-cm)	115.7	117.1	105.0	108.8	170.9	190.5
Chloride (mg/L)	2684.9	2566.0	2684.7	3017.1	1908.1	1594.9
Sulfate (mg/L)	346.10	225.77	224.84	420.91	47.193	15.759
Redox Potential (mV)	20.6	11.0	7.8	28.0	84.1	85.9
pH	11.43	11.83	11.85	11.40	9.79	9.69

Table H.1. CONTINUED.

Data Description	RAP_G1.6_CL	RAP_G3.3_CL	RAP_G5.9_CL	RAP_G3.1_CL	RAP_G6.3_CL	RAP_G5.7_CL
Sample Number	1.6	3.3	5.9	3.10	6.3	5.7
Backfill Type	RAP	RAP	RAP	RAP	RAP	RAP
Metal Type	G	G	G	G	G	G
Environment	CL	CL	CL	CL	CL	CL
Test Type	P	P	P	P	P	P
Measured Corr. Rate (mils/yr)	4.358	9.774	5.427	6.944	9.721	8.653
Estimated Corr. Rate (mils/yr)						
Density (lb/ft^3)	115	116	117	113	119	114
Resistivity (ohm-cm)	178.6	190.1	198.0	247.5	298.5	233.6
Chloride (mg/L)	1962.4	1844.9	1593.2	1411.3	1013.8	1459.9
Sulfate (mg/L)	17.888	11.386	14.318	12.583	13.677	10.628
Redox Potential (mV)	78.3	140.9	88.5	97.1	63.2	82.4
pH	9.74	8.86	9.54	9.82	9.95	9.3

Table H.1. CONTINUED.

Data Description	CFM_G3.6_NCL	CFM_G4.3_NCL	CFM_G2.9_NCL	CFM_G4.9_NCL	CFM_G4.6_NCL	CFM_G2.3_NCL
Sample Number	3.6	4.3	2.9	4.9	4.6	2.3
Backfill Type	CFM	CFM	CFM	CFM	CFM	CFM
Metal Type	G	G	G	G	G	G
Environment	NCL	NCL	NCL	NCL	NCL	NCL
Test Type	R	R	P	P	P	P
Measured Corr. Rate (mils/yr)	1.068	1.656	0.865	0.267	0.748	1.634
Estimated Corr. Rate (mils/yr)	1.006	1.572				
Density (lb/ft^3)	115	120	117	110	113	112
Resistivity (ohm-cm)	15504	15038	17606	15083	16556	16667
Chloride (mg/L)	1.3363	11.305	2.342	1.1365	1.992	1.557
Sulfate (mg/L)	0.963	1.198	1.58	0.747	0.759	1.027
Redox Potential (mV)	176.1	187.8	195.1	185.8	202.7	196.2
pH	9.47	9.41	9.47	9.30	9.49	9.43

Table H.1. CONTINUED.

Data Description	CFM_G6.5_NCL	CFM_G5.5_NCL	CC_G1.3_NCL	CC_G1.7_NCL	CC_G4.4_NCL	CC_G4.5_NCL
Sample Number	6.5	5.5	1.3	1.7	4.4	4.5
Backfill Type	CFM	CFM	CC	CC	CC	CC
Metal Type	G	G	G	G	G	G
Environment	NCL	NCL	NCL	NCL	NCL	NCL
Test Type	P	P	R	R	P	P
Measured Corr. Rate (mils/yr)	1.367	1.538	1.250	0.684	0.353	1.517
Estimated Corr. Rate (mils/yr)			0.896	0.240		
Density (lb/ft^3)	110	111	115	111	109	106
Resistivity (ohm-cm)	16260	16340	924	796	1029	1435
Chloride (mg/L)	1.272	0.986	18.705	27.016	4.731	4.892
Sulfate (mg/L)	1.283	1.164	128.62	60.319	112.19	258.14
Redox Potential (mV)	192.7	200.2	15.0	18.8	17.8	80.9
pH	9.53	9.30	11.82	11.95	11.78	10.88

Table H.1. CONTINUED.

Data Description	CC_G6.2_NCL	CC_G1.1_NCL	CC_G5.8_NCL	CC_G4.1_NCL	RAP_G2.2_NCL	RAP_G4.7_NCL
Sample Number	6.2	1.10	5.8	4.1	2.2	4.7
Backfill Type	CC	CC	CC	CC	RAP	RAP
Metal Type	G	G	G	G	G	G
Environment	NCL	NCL	NCL	NCL	NCL	NCL
Test Type	P	P	P	P	R	R
Measured Corr. Rate (mils/yr)	0.288	1.528	0.128	0.214	0.288	0.363
Estimated Corr. Rate (mils/yr)					1.508	1.761
Density (lb/ft^3)	112	116	116	114	115	117
Resistivity (ohm-cm)	1206	672	1280	1416	7893	9506
Chloride (mg/L)	4.924	4.563	3.857	5.07	4.918	12.461
Sulfate (mg/L)	215.63	234.23	181.55	235.32	6.998	12.366
Redox Potential (mV)	47.0	37.5	47.1	69.5	236.4	208.6
pH	11.49	12.03	11.57	11.23	8.67	8.64

Table H.1. CONTINUED.

Data Description	RAP_G5.3_NCL	RAP_G6.8_NCL	RAP_G2.5_NCL	RAP_G1.4_NCL	RAP_G3.9_NCL	RAP_G6.6_NCL
Sample Number	5.3	6.8	2.5	1.4	3.9	6.6
Backfill Type	RAP	RAP	RAP	RAP	RAP	RAP
Metal Type	G	G	G	G	G	G
Environment	NCL	NCL	NCL	NCL	NCL	NCL
Test Type	P	P	P	P	P	P
Measured Corr. Rate (mils/yr)	0.929	0.801	0.961	0.320	0.598	0.331
Estimated Corr. Rate (mils/yr)						
Density (lb/ft^3)	117	114	111	111	114	115
Resistivity (ohm-cm)	11561	11186	13793	10395	11682	12346
Chloride (mg/L)	2.320	2.002	1.493	2.632	1.820	1.536
Sulfate (mg/L)	7.875	8.959	5.305	9.044	7.745	6.752
Redox Potential (mV)	235.6	228.1	241.0	239.8	239.9	243.6
pH	8.78	8.73	8.88	8.85	8.82	8.72

Table H.1. CONTINUED.

Data Description	CFM_S6.9_CL	CFM_S3.6_CL	CFM_S4.6_CL	CFM_S4.1_CL	CFM_S4.8_CL	CFM_S6.6_CL
Sample Number	6.9	3.6	4.6	4.1	4.8	6.6
Backfill Type	CFM	CFM	CFM	CFM	CFM	CFM
Metal Type	S	S	S	S	S	S
Environment	CL	CL	CL	CL	CL	CL
Test Type	R	R	P	P	P	P
Measured Corr. Rate (mils/yr)	4.857	4.677	5.238	3.485	4.006	4.807
Estimated Corr. Rate (mils/yr)	37.8	52.7				
Density (lb/ft^3)	99	111	107	129	115	114
Resistivity (ohm-cm)	38.9	120.6	170.6	359.7	359.7	179.5
Chloride (mg/L)	3987.5	3163.1	2136.1	1001.3	998.7	1972.6
Sulfate (mg/L)	6.692	4.022	6.570	3.707	2.966	1.223
Redox Potential (mV)	158.5	160.6	177.1	184.6	169.0	182.7
pH	9.21	9.37	9.43	9.65	9.48	9.55

Table H.1. CONTINUED.

Data Description	CFM_S6.4_CL	CFM_S1.7_CL	CC_S2.9_CL	CC_S6.7_CL	CC_S2.1_CL	CC_S2.5_CL
Sample Number	6.4	1.7	2.9	6.7	2.10	2.5
Backfill Type	CFM	CFM	CC	CC	CC	CC
Metal Type	S	S	S	S	S	S
Environment	CL	CL	CL	CL	CL	CL
Test Type	P	P	R	R	P	P
Measured Corr. Rate (mils/yr)	5.929	5.458	4.406	5.187	4.707	4.907
Estimated Corr. Rate (mils/yr)			3.79	41.2		
Density (lb/ft^3)	112	119	118	117	115	116
Resistivity (ohm-cm)	116.4	143.5	85.0	95.8	99.0	76.7
Chloride (mg/L)	3090.3	1923.7	3214.	3253.7	3260.2	3485.2
Sulfate (mg/L)	3.490	1.159	246.22	178.45	306.23	278.90
Redox Potential (mV)	180	160.4	16.9	-3.9	7.8	-18.9
pH	9.47	9.72	11.53	11.87	11.62	11.8

Table H.1. CONTINUED.

Data Description	CC_S5.4_CL	CC_S4.4_CL	CC_S1.9_CL	CC_S3.5_CL	RAP_S1.8_CL	RAP_S4.3_CL
Sample Number	5.4	4.4	1.9	3.5	1.8	4.3
Backfill Type	CC	CC	CC	CC	RAP	RAP
Metal Type	S	S	S	S	S	S
Environment	CL	CL	CL	CL	CL	CL
Test Type	P	P	P	P	R	R
Measured Corr. Rate (mils/yr)	5.828	4.838	4.206	4.767	8.843	8.703
Estimated Corr. Rate (mils/yr)					99.3	196.2
Density (lb/ft^3)	110	113	99.5	106	119	117
Resistivity (ohm-cm)	90.3	79.2	94.5	103.8	214.1	136.4
Chloride (mg/L)	3830.7	3262.5	3352.3	3038.1	1635.7	2534.1
Sulfate (mg/L)	452.92	157.12	121.99	219.46	22.712	11.423
Redox Potential (mV)	20.4	-65.3	-11.0	-4.8	115.1	106.2
pH	11.33	11.84	11.84	11.82	8.87	8.48

Table H.1. CONTINUED.

Data Description	RAP_S4.5_CL	RAP_S4.7_CL	RAP_S5.1_CL	RAP_S5.5_CL	RAP_S2.3_CL	RAP_S5.7_CL
Sample Number	4.5	4.7	5.1	5.5	2.3	5.7
Backfill Type	RAP	RAP	RAP	RAP	RAP	RAP
Metal Type	S	S	S	S	S	S
Environment	CL	CL	CL	CL	CL	CL
Test Type	P	P	P	P	P	P
Measured Corr. Rate (mils/yr)	7.801	7.901	8.262	7.641	7.911	7.661
Estimated Corr. Rate (mils/yr)						
Density (lb/ft^3)	111	105	106	119	118	116
Resistivity (ohm-cm)	230.9	156.0	232.0	239.8	162.1	181.8
Chloride (mg/L)	1379.08	2085.06	1516.10	1293.59	2184.10	1987.70
Sulfate (mg/L)	10.89	8.576	12.398	10.612	28.215	12.90
Redox Potential (mV)	108.0	115.4	77.3	79.6	141.7	118.6
pH	9.04	8.92	9.46	9.42	7.93	8.97

Table H.1. CONTINUED.

Data Description	CFM_S3.9_NCL	CFM_S4.9_NCL	CFM_S6.1_NCL	CFM_S6.1_NCL	CFM_S5.8_NCL	CFM_S5.6_NCL
Sample Number	3.9	4.9	6.10	6.1	5.8	5.6
Backfill Type	CFM	CFM	CFM	CFM	CFM	CFM
Metal Type	S	S	S	S	S	S
Environment	NCL	NCL	NCL	NCL	NCL	NCL
Test Type	R	R	P	P	P	P
Measured Corr. Rate (mils/yr)	1.322	1.243	0.882	1.076	1.142	1.026
Estimated Corr. Rate (mils/yr)		3.81	6.81			
Density (lb/ft^3)	122	120	113	116	122	109
Resistivity (ohm-cm)	14409	14903	16667	18692	16611	16611
Chloride (mg/L)	62.498	3.018	6.098	1.720	1.232	1.045
Sulfate (mg/L)	1.12	3.027	0.935	0.80	1.13	1.362
Redox Potential (mV)	172.4	169.3	177.2	185.9	186.0	182.9
pH	9.60	9.76	9.62	9.66	9.58	9.34

Table H.1. CONTINUED.

Data Description	CFM_S6.8_NCL	CFM_S5.9_NCL	CC_S2.7_NCL	CC_S6.3_NCL	CC_S3.4_NCL	CC_S2.8_NCL
Sample Number	6.8	5.9	2.7	6.3	3.4	2.8
Backfill Type	CFM	CFM	CC	CC	CC	CC
Metal Type	S	S	S	S	S	S
Environment	NCL	NCL	NCL	NCL	NCL	NCL
Test Type	P	P	R	R	P	P
Measured Corr. Rate (mils/yr)	0.901	1.038	0.919	0.737	0.775	0.921
Estimated Corr. Rate (mils/yr)			1.075	1.719		
Density (lb/ft^3)	112	122	115	103	111	113
Resistivity (ohm-cm)	19455	18215	811	959	956	1330
Chloride (mg/L)	0.601	1.934	62.255	5.061	8.118	4.439
Sulfate (mg/L)	0.695	0.8855	74.835	82.305	322.94	179.0
Redox Potential (mV)	212.8	210.2	8.0	26.6	65.6	47.4
pH	9.42	9.13	11.98	11.95	11.25	11.59

Table H.1. CONTINUED.

Data Description	CC_S5.3_NCL	CC_S1.4_NCL	CC_S4.1_NCL	CC_S3.3_NCL	RAP_S3.2_NCL	RAP_S3.7_NCL
Sample Number	5.3	1.4	4.10	3.3	3.2	3.7
Backfill Type	CC	CC	CC	CC	RAP	RAP
Metal Type	S	S	S	S	S	S
Environment	NCL	NCL	NCL	NCL	NCL	NCL
Test Type	P	P	P	P	R	R
Measured Corr. Rate (mils/yr)	0.863	1.044	0.831	1.058	1.322	1.162
Estimated Corr. Rate (mils/yr)					3.56	1.458
Density (lb/ft^3)	116	113	105	112	112	113
Resistivity (ohm-cm)	796	1488	1307	987	11614	9311
Chloride (mg/L)	5.485	5.294	3.058	3.002	45.811	2.330
Sulfate (mg/L)	53.739	191.67	158.44	93.465	7.853	12.708
Redox Potential (mV)	5.60	67.3	54.7	25.7	224.8	228.2
pH	11.94	11.39	11.54	11.90	8.75	8.57

Table H.1. CONTINUED.

Data Description	RAP_S6.2_NCL	RAP_S5.2_NCL	RAP_S2.2_NCL	RAP_S2.4_NCL	RAP_S3.1_NCL	RAP_S1.6_NCL
Sample Number	6.2	5.2	2.2	2.4	3.10	1.6
Backfill Type	RAP	RAP	RAP	RAP	RAP	RAP
Metal Type	S	S	S	S	S	S
Environment	NCL	NCL	NCL	NCL	NCL	NCL
Test Type	P	P	P	P	P	P
Measured Corr. Rate (mils/yr)	1.280	1.154	1.412	1.248	1.212	1.368
Estimated Corr. Rate (mils/yr)						
Density (lb/ft^3)	113	114	113	114	113	112
Resistivity (ohm-cm)	11494	10616	13228	5015	13228	13038
Chloride (mg/L)	4.096	2.039	1.4219	6.7102	6.710	1.417
Sulfate (mg/L)	7.387	8.947	15.515	34.895	6.290	5.493
Redox Potential (mV)	227.0	228.5	235.5	198.2	237.5	232.6
pH	8.71	8.56	8.84	8.51	8.82	8.87

VITA

Name:	Michael Watts Esfeller, Jr.
Address:	P.O. Box 114 Coden, AL 36523
E-mail Address:	mesfeller@hotmail.com
Education:	M.S., Civil Engineering, Texas A&M University, 2006 B.S., Civil Engineering, University of South Alabama, 2001